SYNTHETIC HOST DEFENSE PEPTIDES AS THERAPIES FOR SKIN INFLAMMATION AND BIOFILMS

by

Bing Wu

B.Sc., University of British Columbia, 2015

A THESIS SUBMITTED IN PARTIAL FULFILLMENT OF

THE REQUIREMENTS FOR THE DEGREE OF

DOCTOR OF PHILOSOPHY

in

THE FACULTY OF GRADUATE AND POSTDOCTORAL STUDIES

(MICROBIOLOGY AND IMMUNOLOGY)

THE UNIVERSITY OF BRITISH COLUMBIA

(Vancouver)

December 2021

The following individuals certify that they have read, and recommend to the Faculty of Graduate and Postdoctoral Studies for acceptance, the dissertation entitled:

Synthetic host defense peptides as therapies for skin inflammation and biofilms

submitted by Bing Wu in partial fulfillment of the requirements for

the degree of Doctor of Philosophy

in Microbiology and Immunology

Examining Committee:

Robert E. W. Hancock, Microbiology and Immunology, UBC
Supervisor

Kenneth Harder, Microbiology and Immunology, UBC
Supervisory Committee Member

Christopher Mark Overall, Oral Biolgical & Medical Sciences, UBC
University Examiner

Brett Finlay, Biochemistry and Molecular Biology; Microbiology and Immunology, UBC
University Examiner

Additional Supervisory Committee Members:

Stuart Turvey, Pediatrics, UBC
Supervisory Committee Member

Marc Horwitz, Microbiology and Immunology, UBC
Supervisory Committee Member

Abstract

Novel treatments for inflammatory skin disorders are of great demand as sterile inflammatory skin diseases such as psoriasis and atopic dermatitis are common, long-lasting, and detrimental to people's quality of life, yet have no cure. Skin biofilm infections caused by *Staphylococcus aureus* and *Pseudomonas aeruginosa* are intrinsically and adaptively resistant to antimicrobial agents but lack specific treatments. Natural and synthetic host defense peptides are known to exhibit beneficial biological functions including direct antimicrobial, antibiofilm, immunomodulatory and anti-inflammatory properties. Therefore, I proposed that anti-inflammatory peptide IDR-1002 and antibiofilm peptide DJK-5 could tackle skin inflammation by different underlying mechanisms. IDR-1002 was shown to have promising *in vitro* and *in vivo* anti-inflammatory effects. In an animal model, it dampened PMA-induced ear edema, proinflammatory cytokine and reactive oxygen and nitrogen species release and neutrophil recruitment by downregulating G-protein coupled receptors that recognize proinflammatory mediators. IDR-1002 also suppressed the IFN-γ pathway and an interferon regulatory factor-8-regulated network in PMA-induced inflammation. Similarly, lipidated peptidomimetics Pam-(Lys-βNspe)$_6$-NH_2 and Lau-(Lys-βNspe)$_6$-NH_2 were potent suppressors of PMA-induced sterile skin inflammation comparable to the non-steroidal anti-inflammatory drug indomethacin. To study biofilm skin infection, I established an air-liquid interface epidermal model and showed that DJK-5 significantly reduced 1-day and 3-day Methicillin-resistant *S. aureus* (MRSA) and *P. aeruginosa* biofilms. Using this *in vivo*-like humanized system as a screening platform allowed the identification of novel peptides D-3006 and D-3007 with superior antibiofilm activity and immunomodulatory potential. Skin with thermal wounds had increased susceptibility to MRSA biofilm infection, and DJK-5 treatment significantly reduced bacterial load, cytotoxicity, and pro-inflammatory cytokines. Combination treatment of DJK-5 with IDR-1002 further reduced cytotoxicity and skin inflammation. Transcriptomic analysis revealed that DJK-5 treatment restored skin barrier function, suppressed MRSA intracellular invasion, and dampened TNF-α signalling and transcription factors AP-1, c/EBPB and CREB, leading to reduced production of proinflammatory mediators such as cytokines, prostaglandins, and matrix metalloproteinases. Both IDR-1002 and DJK-5 returned skin to homeostasis by downregulating TNF-α and NF-κB signalling and their negative regulators, and upregulating TSC22D3, an important mediator of glucocorticoid anti-inflammatory effects. These data reveal the intrinsic promise of synthetic peptides in treating inflammation and biofilm infections.

Lay Summary

Skin is an essential protective barrier of the human body that is constantly challenged by environmental insults and microbial pathogens. Chronic inflammatory skin diseases such as psoriasis and atopic dermatitis and skin inflammation triggered by bacterial infections such as *Staphylococcus aureus* and *Pseudomonas aeruginosa*, continue to cause public health burdens due to the lack of effective treatments. This is even more problematic with the emergence of antimicrobial resistance and the insufficient development of novel antimicrobials. In this thesis, I demonstrated that synthetic host defense peptides could tackle skin inflammation by dampening harmful host immune responses and eliminating structured bacterial communities called biofilms that are the most common growth state in infections and highly recalcitrant to antibiotics.

Preface

A version of Chapter 3 has been published in **Wu, B. C.**, Lee, A. H. Y. & Hancock, R. E. W. Mechanisms of the Innate Defense Regulator Peptide-1002 Anti-Inflammatory Activity in a Sterile Inflammation Mouse Model. *The Journal of Immunology* **199**, 3592–3603 (2017). (https://pubmed.ncbi.nlm.nih.gov/28993516/) Reza Falsafi prepared the RNA-Seq libraries. Dr. Amy Lee performed the RNA-Seq analysis and edited the manuscript. Dr. Hamid Masoudi quantified immune cell populations in the H&E-stained specimens. Dr. Kelli Wuerth helped with establishing the mouse model. Dr. Robert E. W. Hancock supervised the project, provided guidance on the experiments and troubleshooting, and edited the manuscript. I designed and performed the experiments, analyzed the data and wrote the manuscript.

Content from Chapter 4 has been published in **Wu, B. C.**, Skovbakke, S. L., Masoudi, H., Hancock, R. E. W. & Franzyk, H. *In vivo* Anti-inflammatory Activity of Lipidated Peptidomimetics Pam-(Lys-βNspe)$_6$-NH_2 and Lau-(Lys-βNspe)$_6$-NH_2 Against PMA-Induced Acute Inflammation. *Front. Immunol.* **11**, (2020). Dr. Henrik Franzyk designed the peptidomimetics. Dr. Sarah L. Skovbakke performed *in vitro* investigations. Dr. Hamid Masoudi performed pathology scoring and quantification on the H&E staining samples. Dr. Robert E. W. Hancock supervised the project, provided guidance on the experiments and troubleshooting. I designed and performed the *in vivo* experiments and analyzed the data. All authors contributed to the interpretation of the data and writing, reviewing, and editing the manuscript.

Some content from Chapter 5 and Chapter 6 has been published in **Wu, B. C.**, Haney, E. F., Akhoundsadegh, N., Pletzer, D., Trimble, M. J., Adriaans, A. E., Nibbering, P. H., & Hancock, R. E. W. Human organoid biofilm model for assessing antibiofilm activity of novel agents. *NPJ Biofilms Microbiomes* **7**, 8 (2021). Dr. Evan F. Haney performed the scanning electron microscopy and the confocal microscopy on the skin biofilm model and reviewed and edited the manuscript. Noushin Akhoundsadegh helped with growing some batches of the organoid skin model. Dr. Daniel Pletzer and Michael J. Trimble generated bacterial strains and assisted with the confocal microscopy experiments. Alwin E. Adriaans and Dr. Peter H. Nibbering provided training and assistance with the ALI model. Dr. Robert E. W. Hancock supervised the project, provided guidance on the experiments and troubleshooting, and extensively edited the manuscript. I designed and performed the experiments, analyzed the data and wrote the manuscript.

All mouse experiments were performed according to the guidelines of the Canadian Council on Animal Care. The experimental protocols A15-0282 and A16-0169 on animal studies were

examined and approved by the University of British Columbia Animal Care Committee.

All experiments involving human surplus skin samples were performed under the approved protocol H18-00657 following the guidelines of the University of British Columbia Clinical Research Ethics Board. The surgical sites for samples collected were approved by the College of Physicians and Surgeons of British Columbia.

Table of Contents

List of Tables

List of Figures

List of Abbreviations

ANOVA	Analysis of variance
CXCL	C-X-C motif chemokine ligand
DC	Dendritic cell
DE gene	Differential expressed gene
ER	Endoplasmic reticulum
ERK	Extracellular signal-regulated kinases
FAK	Focal adhesion kinase
FPR	Formyl peptide receptor
GPCR	G protein-coupled receptor
H&E	Hematoxylin and eosin
hBD	Human β-defensin
HDP	Host defense peptide
HNP	Human neutrophil peptide
HPF	High power field
IDR	Innate defense regulator
IFN	Interferon
IL	Interleukin
ILC	Innate lymphoid cell
ILK	Integrin-linked kinase
IRF	Interferon regulatory factor
JNK	c-Jun NH2-terminal kinase
LB	Lysogeny broth
LPS	Lipopolysaccharide
LTA	Lipoteichoic acid
MAPK	Mitogen-activated protein kinase
MCP	Monocyte chemoattractant protein
MHC	Major histocompatibility complex
MMP	Matrix metalloproteinases
MRSA	Methicillin-resistant *Staphylococcus aureus*
NF-κB	Nuclear factor-κB
NLR	Nucleotide-binding and oligomerization domain-like receptor
NLRP	NOD, leucine-rich repeat and pyrin domaincontaining protein
NOD	Nucleotide-binding and oligomerization domain
NSAID	Nonsteroidal anti-inflammatory drugs
p38 MAPK	p38 family of kinases
PBS	Phosphate-buffered saline
PI3K	Phosphoinositide 3-kinase
PM1	Pam-(Lys-βNspe)$_6$-NH_2
PM2	Lau-(Lys-βNspe)$_6$-NH_2
PMA	Phorbol 12-myristate 13-acetate
(p)ppGpp	Guanosine penta or tetraphosphate
RLR	Retinoic acid-inducible gene I-like receptor
ROS	Reactive oxygen species
RNS	Reactive nitrogen species
SEM	Scanning Electron Microscopy

SSTI	Skin and soft-tissue infection
STAT	Signal transducer and activator of transcription
TEER	Transepithelial electrical resistance
TGF	Transforming growth factor
Th	T helper
TLR	Toll-like receptor
TNF	Tumor Necrosis Factor
T_{RM}	Tissue resident memory
TSB	Tryptic soy broth

Acknowledgements

First, I would like to thank my amazing supervisor Dr. Bob Hancock. During my undergraduate study, Bob provided me with the very first research opportunities and led me into the field of scientific research. It is a great honor for me to continue my graduate study in Bob's lab. Over the last 6 years of my PhD, Bob has given me extremely valuable guidance and support. I am truly amazed by his knowledge and passion in research.

I want to thank all of the heartwarming Hancock lab members. Especially Susan Farmer for organizing lots of fun lab events and for helping me with research ethics approvals. Special thanks to Dr. Evan Haney and Lauren Wilkinson who taught me fundamental research skills as my undergraduate mentors and continuously provided me with advice and inspiration during my PhD. I also would like to thank Dr. Evan Haney, Dr. Kelli Wuerth, Noushin Akhoundsadegh, Reza Falsafi, Manjeet Bains, Dr. Daniel Pletzer, Dr. Grace Choi and Dr. Michael Trimble for helping with various experiments and troubleshooting in their areas of expertise. Thanks to Dr. Amy Lee, Travis Blimkie and Dr. Bhav Dhillon for helping me with RNA-Seq data analysis and gaining an understanding of the big picture of my research.

I am grateful to Dr. Peter Nibbering, Alwin Adriaans and Anna de Breij for hosting my visit to their lab in Leiden, The Netherlands, and training me on the organoid skin model, which shaped my research in a more meaningful way. Thank you, Dr. Henrik Franzyk, Dr. Sarah Skovbakke and Dr. Hamid Masoudi for the collaboration on the peptidomimetic project, which added new perspectives to my research. I deeply appreciate Dr. Eric Pugash, Simone Robertson and other staff at Dr. Eric Pugash's clinic, Cambie Surgery Centre, False Creek Surgical Centre and Skinworks Surgery Centre for recruiting donors and collecting surplus skin samples for the *ex vivo* skin experiments.

Special thanks to my committee members Dr. Stuart Turvey, Dr. Marc Horwitz and Dr. Kenneth Harder for their guidance and advice. Special thanks to Dr. Laura Sly for being an examiner in my comprehensive exam. Lastly, I greatly appreciate Darlene Birkenhead and Parvin Bolourani for helping with scholarships and visa applications as well as other essential aspects of graduate study.

Dedication

I dedicate this thesis to my parents and husband. I would not be able to accomplish anything in my research and in my life without their love and support.

Chapter 1: Introduction

1.1 Inflammatory skin diseases and demands for novel therapeutics

Chronic sterile inflammatory skin diseases such as psoriasis and atopic dermatitis greatly impair patients' quality of life creating severe social, emotional and financial burdens. Patients with chronic inflammatory skin conditions are at a higher risk of depression and anxiety [1,2]. Additionally, individuals with psoriasis are at a greater risk of developing comorbid non-communicable diseases such as cardiovascular diseases, Crohn's disease and rheumatoid arthritis [3] while children with atopic dermatitis reported a higher prevalence of asthma, hay fever and food allergy [4]. Treatments for such inflammatory diseases can be lifelong, costly, accompanied by side effects and provide only temporary symptomatic relief without hope for a complete cure.

On the other hand, the emergence of antibiotic resistance poses a global public health concern leading to prolonged illness, increased treatment failure, and elevated rates of disability and mortality[5]. Drug-resistant infections are estimated to be responsible for 700,000 deaths per year globally and could potentially reach 10 million annually in 2050 if no action is taken [6]. *Pseudomonas aeruginosa* and *Staphylococcus aureus* are ranked critically and highly important respectively in the WHO global priority list of antibiotic-resistant bacteria [7] and are also common pathogens causing skin and soft tissue infections (SSTIs) [8]. *S. aureus* is the most commonly isolated bacterium from chronic wound infections found in 88–93.5% of chronic venous leg ulcers causing excessive inflammation and delaying wound healing and the re-epithelialization process [9]. Bacteria including *P. aeruginosa* and *S. aureus* can form multicellular biofilms that are 10 to 1000-times more resistant to conventional antibiotics when compared to planktonic bacteria [10]. A study found that all 160 *S. aureus* isolates from patients with skin infections were capable of biofilm formation suggesting that biofilm formation is a universal behaviour of *S. aureus* skin infections [11]. Since the clinical pipeline of new antimicrobials is dry and there is currently no treatment specifically targeting biofilm infections, effective treatments for skin infections are also highly demanded.

1.2 Anatomy of human skin

Human skin is the largest organ of the human body with a total area of 1.6-1.8 m^2 accounting for about 15% of the total adult body weight [12]. The essentiality of skin is beyond its function as a physical barrier between the external environment and internal organs since it also provides immune protection, regulates body temperature and water balance, and supplies hormones and neurotransmitters [13]. Human skin consists of 3 layers: the epidermis, dermis, and hypodermis (Figure 1).

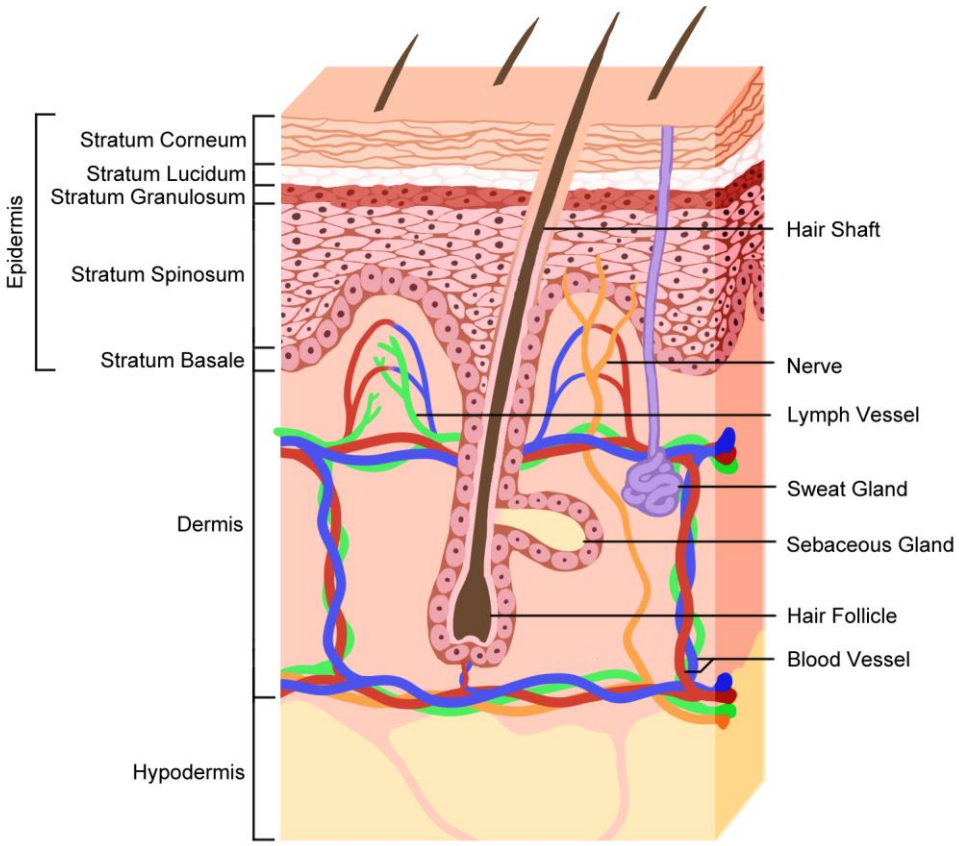

Figure 1. The anatomy of human skin.
Human skin consists of three layers: the epidermis, dermis and hypodermis and multiple skin appendages providing physical barriers, thermoregulation, nutrients and oxygen supply and sensory functions.

1.2.1 Epidermis anatomy

The epidermis is made up of predominately keratinocytes and other cell types including pigment-producing melanocytes and immune cells such as Langerhans cells and T cells [13]. The epidermis can be characterized into 4-5 layers: stratum corneum, stratum lucidum, stratum granulosum, stratum spinosum and stratum basale. Stratum corneum, the most superficial layer, consists of corneocytes, which are terminally differentiated keratinocytes [14]. Stratum lucidum is a thin and translucent layer of epidermis, present only in the thickest portion of the skin such as the palms of the hands. Stratum granulosum comprises layers of cells packed with dense basophilic keratohyalin granules containing keratin filament bundles and associated proteins (e.g. loricrin, filaggrin, and trichohyalin) [15]. The stratum granulosum also carries lamellar granules containing lipids and hydrolytic enzymes, which get secreted onto the cell surface forming a waterproof barrier[16]. Underneath the stratum granulosum, the stratum spinosum is comprised of cells 8-10 layers deep that are interconnected with desmosomes specialized for cell-to-cell adhesion [13]. Likewise, the bottom

layer of epidermis, the stratum basale, is also connected by desmosomes and anchored to basement membrane (a highly specialized extracellular matrix structure) through hemidesmosomes. Stratum basale undergoes continuous mitosis producing keratinocytes migrating and differentiating into upper layers of the epidermis [17].

1.2.2 Barrier function of the epidermis

The formation of a barrier by the epidermis is supported by stratified cell layers as well as inter- and intra-cellular scaffolds. Keratinocytes produce intermediate filament-forming proteins called keratins that are important epithelial cytoskeleton components providing mechanical strength and also having implicated functions in cell signalling, stress responses and apoptosis [18,19]. The structural integrity of the epidermis is supported by cell-cell adhesion involving desmosomes, adherens junctions and tight junctions. Desmosomes are transmembrane protein complexes connected to intracellular keratin filament networks linking adjacent cells in the stratum granulosum, stratum spinosum and stratum basale and providing strong intercellular adhesion [20]. Modified desmosomes called corneodesmosomes are present in the stratum corneum, and play an important role in the regulation of desquamation [21]. Adherens junctions are cadherin based intercellular junctions linking to F-actin cytoskeleton. E-cadherin is the prominent type of cadherin expressed in all layers of the epidermis whereas P-cadherin is mainly found around hair follicles [22]. The third type of intercellular junction, tight junctions, is localized to cell-cell borders of the stratum granulosum separating the apical membrane domains from the basolateral side and restricting the traffic of ions and proteins through intercellular space [21]. Tight junctions are formed by transmembrane proteins claudins, occludin and junctional adhesion molecules. The tight junction complexes are connected to the actin cytoskeleton through intracellular scaffold proteins such as zonula occludens proteins [23]. Together the differentiated keratinocytes and the tight mechanical adhesion between these cells protect the skin from routine and extreme environmental insults.

1.2.3 Dermis anatomy

The dermis, connected to the epidermis through the basement membrane, is mainly made up of fibroblasts embedded in an extracellular matrix providing physical strength, flexibility and elasticity. Extracellular matrix is a three-dimensional scaffold interwoven with multiple components including the fiber-forming structural molecules (e.g. collagen, fibrin and elastin) creating a framework of rigid proteins, nonfiber-forming structural molecules (e.g. proteoglycans and glycosaminoglycans) regulating osmosis, and matricellular proteins (e.g. osteopontin, osteonectin

and fibulins) modifying cell matrix signalling [24]. Fibroblasts produce essential matrix components such as collagen, elastin and dermal glycosaminoglycans, and the extracellular matrix in turn regulates fibroblast migration, senescence, and differentiation [25]. The dermis can be categorized into two layers. The papillary dermis is the upper layer closely connected to the epidermis through basement membrane. Human papillary dermis has irregular finger-like projections extending into the epidermis and interacts with the rete ridge projections from the epidermis. These junction structures increase the surface area of epidermis and dermis connections, and thus provide better anchoring, increased resistance to shear forces and enhanced nutrient transportation [26]. The papillary dermis is composed of a loose meshwork of thin collagenous fibers (mean 38 μm) interspersed with elastic fibres whereas the underneath reticular dermis is made up of large diameter collagen fibres (mean 80 μm) connected with elastic fibres [26]. The dermis also contains a variety of innate and adaptive immune cells (discussed in section 1.3 - Skin immune system).

1.2.4 Hypodermis anatomy

The hypodermis, also called superficial fascia, is the deepest layer of the skin, which mainly consists of fibroblasts, adipocytes and macrophages. This skin layer is rich in proteoglycan and glycosaminoglycans giving rise to mucus-like appearances. Adipocytes in the hypodermis are grouped in lobules and spaced by fibrous septa and skin appendages [26]. Fat deposits in the hypodermis are regulated by hormones such as leptin, insulin, testosterone and estrogen as well as genetic factors. The hypodermis provides structural support, energy storage, insulation and shock absorption [27].

1.2.5 Skin substructures

Skin houses multiple appendages or substructures such as sweat glands, hair follicles, sebaceous glands, blood vessels and sensory neurons [17]. Sweat glands serve a thermoregulatory function via evaporative heat loss. Eccrine sweat glands, distributed across the skin, are the most abundant in the human body. The eccrine sweat is composed of a complex aqueous mixture of chemicals including micronutrients (e.g. sodium chlorite, potassium, calcium) and non-micronutrient components (e.g. lactate, urea, antibodies, host defense peptides (HDPs) and cytokines) [28]. Such sweat-gland products can be distributed by skin hairs. In addition, hairs also function as a protective covering, regulate body temperature and enhance sensation. The hair follicles begin at the surface of epidermis and extend into dermis. The sebaceous glands, closely associated with hair follicles, are holocrine glands that secrete a lipid-rich sebum providing a hydrophobic barrier for the hairs [29]. Blood vessels provide nutrients and oxygen supply and aid in thermoregulation. The vascular system in the

skin consists of two plexuses, one is located between the papillary and reticular layers of the dermis and the other lies between the dermis and subcutaneous tissues. The control of blood flow through vasodilation and vasoconstriction in response to warm or cold conditions helps to effectively maintain normal body temperature [13]. Nerve endings transmit sensation such as pain, temperature and pressure beyond the skin's surface. Free nerve endings are the most common type of nerve endings in the skin responding to pain, temperature variations and light touch. They are unencapsulated branching terminations of sensory fibers that lie near blood vessels and extend into the middle of the epidermis[30].

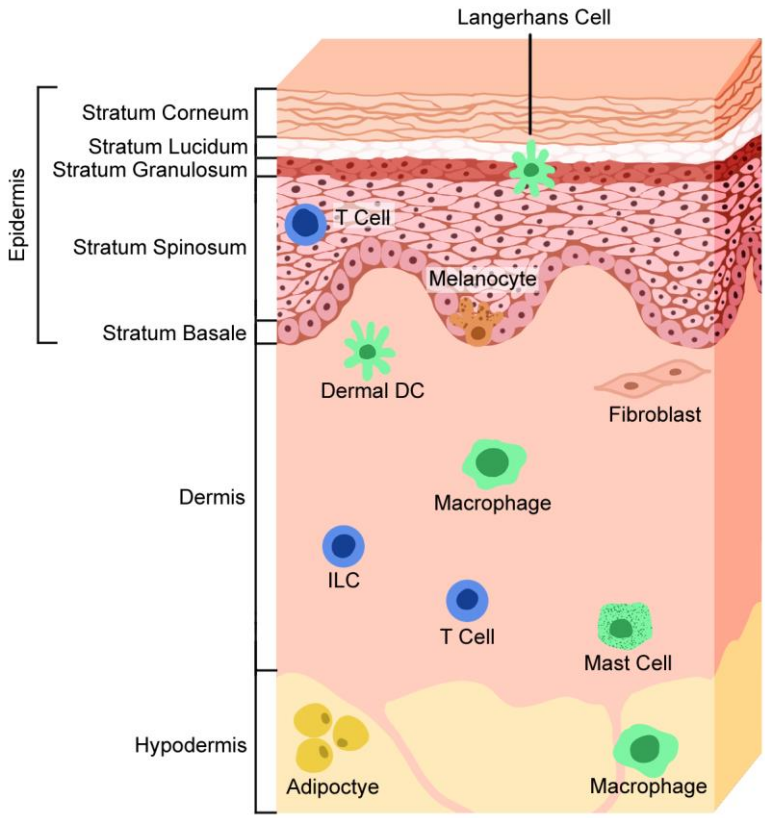

Figure 2. Human skin system under homeostasis.
Human skin is populated by multiple immune cells including Langerhans cells and T cells in the epidermis and dermal DCs, macrophages, mast cells, T cells and innate lymphoid cells in the dermis.

1.3 Skin immune system

Human skin immunity consists of a variety of innate and adaptive immune cells which, together with HDPs and cytokines that these cells produce, function to protect against environmental and microbial insults. Under homeostasis, the epidermis harbours Langerhans cells and tissue resident T cells, and the dermis is populated by dermal dendritic cells (DCs), macrophages, mast cells, T cells and innate lymphoid cells (ILCs) (Figure 2) [31].

1.3.1 Langerhans cells

Langerhans cells, characterized by high expression of class II major histocompatibility complex (MHC) and the presence of langerin$^+$ (CD207$^+$) Birbeck granules, share a common precursor with tissue-resident macrophages [27]. Unlike tissue macrophages, however, Langerhans cells have the ability to migrate to skin-draining lymph nodes and present antigen to naïve T cells. Langerhans cells, located in the stratum spinosum, can sample the environment by extending and retracting dendrites between keratinocytes without damaging the tight junction barrier [32]. Langerhans cells can also induce proliferation of skin regulatory T cells and function to maintain tolerance during homeostasis, while promoting the proliferation of effector T cells and memory T cells under inflammatory conditions [33,34].

1.3.2 Epidermal tissue resident Tcells

Also found in the epidermis, are non-circulating tissue resident memory T cells (T_{RM}) cells persisting at sites of previous infections which contribute to long-term local immune surveillance. Besides the skin, T_{RM} can also be found in the lungs and intestines. Inflammatory stimuli such as type I interferon (IFN), Tumor Necrosis Factor (TNF)-α, Interleukin (IL)-33 and IL-12 can promote the differentiation of T_{RM} while IL-7 and IL-15 produced within the hair follicles are essential for T_{RM} maintenance [35]. Upon sensing danger, T_{RM} can release IFN-γ and other pro-inflammatory cytokines, which recruit immune cells to the site of infection [35]. For example, a population of CD103$^+$, CD69$^+$, CD8$^+$ T_{RM} with low CD62L and low CD122 expression (phenotypically distinct from lymphoid memory T cells) have been shown to protect against herpes simplex virus reinfection [36]. The majority of T cells in human skin are αβ T cells with 1–10% γδ T cells. The unconventional γδ T cells have immunologic features of both the innate and adaptive immunity and can respond rapidly to inflammatory stimuli without MHC-restricted antigenic specificity [37,38].

1.3.3 Dermal dendritic cells

Dermal DCs are heterogeneous groups of cells typically found in the upper portion of the reticular dermis that can migrate to skin-draining lymph nodes and prime adaptive immune responses[27]. Humans have two types of conventional myeloid DCs. Conventional DC1 cells (CD141$^+$, CD11c^{low}, CD11b^{low}) are capable of cross presentation, priming T helper (Th)-1, and natural killer responses. Conventional DC2 cells (CD1c$^+$, CD11c$^+$, CD11b$^+$) are potent IL-12 producers and have been shown to activate a wide range of adaptive components including Th-1, Th-2, Th-17 and CD8$^+$ T cells [39]. During inflammatory conditions, other subtypes of DCs such as

Plasmacytoid DCs and monocyte-derived DCs can be recruited into the skin.

1.3.4 Macrophages

Skin macrophages reside in the deeper dermis and hypodermis and play essential roles in phagocytosis of foreign and damaged cells, inflammation, wound healing, hair follicle regeneration, etc [40]. Dermal macrophages come from two distinct sources: self-renewing skin resident macrophages derived from prenatal yolk sac, and circulating monocytes homing to tissues in a CCR2-dependent manner [41]. Macrophages exhibit plasticity and versatility depending on the environmental trigger. The M1 polarized macrophages in response to IFN-γ and TNF-α stimulation can improve phagocytic and microbicidal activities and produce pro-inflammatory mediators such as IL-1, IL-6 and nitric oxide [42]. In contrast, the alternatively activated M2 macrophages polarized in response to macrophage colony-stimulating factor, IL-4 and IL-13 secrete IL-10 and Transforming growth factor (TGF)-β. M2 macrophages can be divided into M2a, M2b, M2c and M2d subgroups and are involved in parasitic infection, resolution of inflammation and wound healing [43].

1.3.5 Mast cells

Mast cells are located in the papillary and reticular dermis and have cytoplasmic granules containing histamine, sulfated proteoglycans, serotonin, tryptase and chymase [27]. During helminth infections, the high-affinity IgE receptors on mast cell surfaces are crosslinked via IgE-antigen complexes leading to the release of granules contents and cytokines (e.g. IL-4 and IL-5) promoting a Th-2 type immune response [44]. Mast cells can also participate in pathogen recognition through Toll-like receptors (TLRs) and produce proinflammatory mediators without degranulation [45]. Ironically, mast cells are also known for their pathogenic role in allergic reactions and chronic inflammatory diseases such as atopic dermatitis [46,47].

1.3.6 Dermal T cells

The resident and recirculating T cell populations in dermis are complex, including memory T cells (e.g. $T_{RM,}$ central memory T cells and effector memory T cells), regulatory T cells and effector T cells. The vast majority (about 80%) of T cells in the adult human dermis are $CD69^+$ $T_{RM,}$ and the minority (about 20%) are $CD69^-$ recirculating T cells [48]. In contrast to the epidermis, both $CD4^+$ and $CD8^+$ T_{RM} cells in the dermis are $CD103^-$ which, compared to $CD103^+$ T_{RM} cells, are less robust in producing cytokines such as IFN-γ, TNF-α and IL-22, but have greater proliferation capacity in response to stimulation such as anti-CD3 and anti-CD28 antibodies or heat-killed extracts of *Candida albicans* or *S. aureus* [48]. Recirculating memory T cells can be classified into two subgroups based on

the expression of CCR7, which controls homing to secondary lymphoid organs [49,50]. CCR7- effector memory T cells express high levels of β1 and β2 integrins and readily home to inflamed tissues whereas $CCR7^+$ central memory T cells express lymph-node homing receptors [49,50]. $Foxp3^+$ and $CD4^+$ regulatory T cells are well known for their protective role in autoimmune reactions [51]. An early influx of regulatory T cells in the neonatal skin can mediate immune tolerance of commensal microbes [52]. In adulthood, the homing of regulatory T cells from the peripheral circulation to skin is dependent on the expression of CCR4, CCR6, CD103 and the cutaneous lymphocyte antigen [51]. Regulatory T cells have also been shown to facilitate wound healing by suppressing IFN-γ production and proinflammatory macrophage accumulation [53].

1.3.7 Innate lymphoid cells

Skin-resident ILCs are the innate counterpart of adaptive Th cells and have essential functions in maintaining skin barrier function and homeostasis, but are also involved in chronic inflammatory skin diseases [54]. Based on their cytokine profiles and transcription factors, ILCs are classified into three groups. Group 1 ILCs including natural killer cells and group 1 innate lymphoid cells (ILC1) that express transcription factor T-bet, produce IFN-γ, granzymes and perforins, and promote type 1 immunity [55]. Group 2 ILCs are type 2 cytokine producers (e.g. IL-4, IL-5 and IL-13). Skin resident ILC2s express the skin-homing markers cutaneous lymphocyte antigen and CCR10, and produce type 2 cytokines (e.g. IL-4, IL-5 and IL-13) [56]. Group 3 ILCs including lymphoid tissue inducers and ILC3s are capable of producing Th-17 and Th-22 cytokines[57]. The main subtype of ILC3 in healthy human skin does not express natural cytotoxicity receptors while an increased number of ILC3 expressing natural cytotoxicity receptors have been reported in lesional skin and the peripheral blood of psoriasis patients [56].

1.4 Skin commensal

Healthy human skin is populated with beneficial bacteria, fungi and viruses with *Propionibacterium*, *Corynebacterium* and *Staphylococcus spp.* among the top bacterial species [58]. Commensal microbes can function as a barrier preventing pathogen colonization. For example, a subset of *Staphylococcus epidermidis* strains expressing the serine protease glutamyl endopeptidase can inhibit *S. aureus* biofilm formation [59]. Commensal microbes also modulate skin immunity and play essential roles in keratinocyte differentiation, skin cytokine and HDP production and induction of local regulatory T cells [60]. However, skin commensals such as *S. epidermidis* can also cause infections upon colonizing medical implants or in individuals with an impaired skin barrier [61,62].

1.5 Skin and soft-tissue infections

SSTIs involve microbial invasion and infection of the skin and underlying fascia, subcutaneous tissue and muscle [8,63,64]. SSTIs are common yet serious issues that afflicted 3.2 million people in the USA in 2012 at an aggregated cost of $15 billion [65]. In North America, *S. aureus* (45.9%), *P. aeruginosa* (10.8%) and *Enterococcus* species (8.2%) are among the leading causes of community-acquired SSTIs [8]. Current treatment regimens for SSTIs often include topical (e.g. mupirocin and retapamulin) and systemic (e.g. ciprofloxacin, cefazolin and linezolid) use of broad-spectrum antibiotics [64,66], which likely contribute to the growing problem of antibiotic resistance while demonstrating poor efficacy. For example, prolonged Vancomycin therapy has been shown to select for heteroresistance in isogenic *S. aureus* isolates *in vivo* by promoting gradual accumulation of mutations leading to increasing Vancomycin minimal inhibitory concentrations [67].

1.5.1 *S. aureus* in SSTIs

S. aureus persistently colonizes about 15% of adult's skin without causing infections, but if it travels to the wrong locations such as deeper layers of skin it can lead to invasive infections and/or toxin-mediated diseases [68]. *S. aureus* are commonly associated with chronic conditions such as atopic dermatitis [69], diabetic foot ulcers [70], and nosocomial infections in burn victims [71]. *S. aureus* expresses a variety of virulence factors that facilitate skin infections including adhesins for host cell attachment (e.g. clumping factor B and fibronectin-binding proteins), enzymes that promote tissue invasion (e.g. hyaluronidase), toxins that lyse host immune cells (e.g. phenol-soluble modulins), and factors that allow evasion of immune cell recognition (e.g. protein A) [72].

The emergence of methicillin-resistant *S. aureus* (MRSA) was associated with a dramatic increase in SSTIs in recent years [73]. Methicillin resistance is conferred by horizontal transfer of a mobile genetic element *mec*, which encodes penicillin-binding protein 2a with a lower affinity for β-lactams [74]. MRSA strains such as community-acquired MRSA USA300 and healthcare-associated MRSA CC30 account for recent outbreaks in North America [75]. In particular, USA300 carries the arginine catabolic mobile genetic element that provides resistance to HDPs, allowing survival at low-pH environments found on skin [75,76].

1.5.2 *P. aeruginosa* in SSTIs

P. aeruginosa is an opportunistic pathogen that is the most common cause of respiratory infections and is frequently associated with neutropenia, cystic fibrosis, chronic bronchiectasis, severe burns and chronic wounds [77]. *P. aeruginosa* can also cause a range of superficial to deep skin

infections and manifestations such as the green nail syndrome (chloronychia), folliculitis, toe web infections, bacteremia associated skin lesions and rare but life-threatening gangrenous cellulitis [78]. Major virulence factors impacting the outcomes of *P. aeruginosa* infections include flagella and type IV pili allowing motility, attachment, and colonization of host cells, type II secretion system-encoded toxins and hydrolytic enzymes (e.g. exotoxin A and elastase), type III secretion systems-encoded toxins (e.g. exoenzymes ExoS, ExoT, ExoU) modulating host immune responses, and quorum sensing systems that regulate virulence gene expression and biofilm formation [79]. *P. aeruginosa* is also notorious for its remarkable capacity to resist antibiotics such as aminoglycosides, quinolones and β-lactams due to especially intrinsic and adaptive resistance mechanisms [80].

1.6 Bacterial biofilms

Besides intrinsic and acquired antibiotic resistance, bacterial pathogens such as *S. aureus* and *P. aeruginosa* can adapt to challenging environments by forming structured surface-associated multicellular communities called biofilms. Bacteria within biofilms are 10 to 1000-times more resistant to conventional antibiotics compared to planktonic bacteria and have been identified as major players in chronic infections [10].

1.6.1 Biofilm formation

The formation of biofilms from planktonic cells entails highly regulated events in response to "stressful" environmental cues such as insufficient nutrient levels. The initial attachment is reversible and can be interrupted by local hydrodynamic forces. To facilitate firm attachment, *S. aureus* produces surface adhesins such as the microbial surface component recognizing adhesive matrix molecules (e.g. clumping factors and fibronectin binding proteins) while *P. aeruginosa* makes use of extracellular adhesive appendages such as flagella and pili [81].

As more bacteria cells adhere more tightly to surfaces, they are connected by self-made extracellular polymeric substances (which make surface association essentially irreversible) and form colonial aggregates. As biofilms grow and mature, they can establish a three-directional structure that promotes bacterial nutrient acquisition and cell-cell communication, as well as providing protection against host immune responses and antibiotics [82]. The biofilm extracellular matrix is predominately composed of high hydrated polysaccharides, DNA, proteins, lipids and, when relevant, host factors[81]. In *S. aureus*, the polysaccharide intercellular adhesin produced from the *icaADBC* operon is essential for biofilm formation under anaerobic conditions and its production is also regulated by other factors such as glucose, ethanol, osmolarity, temperature and antibiotics [9]. Some *S. aureus* strains form

biofilm independent of the polysaccharide intercellular adhesin by utilizing other proteins such as protein A, biofilm-associated protein and fibronectin-binding proteins [9]. In *P. aeruginosa,* exopolysaccharides such as Psl/Pel and alginate are important for initiation of biofilm formation and the stability of biofilm structures [83]. Extracellular DNA, essential for both *S. aureus* and *P. aeruginosa* biofilm formation also provides biofilm structural support and allows for horizontal gene transfer among competent sister bacteria [84].

In response to depletion of nutrients and oxygen (or an increase in nutrients), build-up of waste products and nitric oxide, and other signals including those involved in quorum sensing, bacteria can disperse from a mature biofilm and return to the planktonic state [85]. Dispersed cells typically have lower intracellular cyclic di-guanosine monophosphate concentrations and can display distinct transcriptome and physiology, increased virulence and altered antibiotic susceptibilities in comparison with their biofilm counterparts [85–87].

1.6.2 Biofilm resistance to antimicrobial agents

Multiple antimicrobial resistance mechanisms have been linked to the highly recalcitrant nature of biofilms, and their relative contribution to resistance likely depends on the type of biofilms and treatment. A major contributing factor to high resistance observed in biofilms is the adaptive changes in gene expression as a result of the altered growth state associated with biofilm formation and/or external stresses [88,89]. For instance, in *P. aeruginosa* biofilm, a MerR-type transcriptional activator BrlR activates genes encoding ATP-binding cassette transport systems (PA1874-77) and multiple multidrug efflux pump genes, which are responsible for resistance to multiple classes of antibiotics [90]. Other examples of adaptive resistance genes preferentially expressed in *P. aeruginosa* biofilms include the type VI secretion system gene *tssC1,* two-component regulator PA0756–57 and the *ndvB* gene which encodes a glucosyltransferase required for the biosynthesis of periplasmic glucans that sequester antibiotics [91,92].

Another example of resistance mechanisms related to gene expression is the influence of metabolism. Since most antibiotics target actively growing bacteria, the slow growth rate and reduced metabolic rate at the base of static biofilms under nutrient limiting conditions can result in antibiotic resistance [93,94]. Indeed, nutrient depletion and other stress conditions can induce the bacterial stringent response, a broadly conserved bacterial stress response signalled by alarmines guanosine penta or tetraphosphate ((p)ppGpp), that affects up to a third of bacteria transcriptome and has broad effects on bacteria metabolism and physiology including slowing down cell division [95]. The stringent response has been shown to promote antibiotic tolerance in biofilms by reducing levels of oxidant

stress in bacterial cells [96]. Stringent response can also enhance antibiotic resistance dissemination by integron-mediated acquisition and exchange of antibiotic resistance genes [97]. Furthermore, the stringent response regulates antibiotic-tolerant persister formation [98].

In addition, bacteria heterogeneity, based on distinct microenvironments from the surface to inner parts of biofilms due to oxygen, nutrient and pH gradients, also contributes to resistance [81]. In a *Staphylococcus* colony biofilm model, subpopulations of bacteria can grow aerobically or fermentatively, become dormant or die, and have stratified patterns of DNA and protein synthetic activities [99]. In particular, the metabolically-inactive persister cells within biofilms exhibit tolerance to antibiotics without undergoing genetic changes and are proposed to be partly contributed to the recalcitrance of chronic infections by reseeding biofilms upon cessation of antibiotic treatment in the clinical setting [81,100].

Bacterial pathogens within biofilms can utilize quorum sensing systems to develop antimicrobial resistance and activate virulence [101]. For example, the *las* and *rhl* quorum sensing systems in *P. aeruginosa* control the expression of superoxide dismutase and catalase genes, which mediate biofilm susceptibility to hydrogen peroxide [102]. Quorum sensing systems can also influence the expression of efflux pumps leading to multidrug resistance [103].

Finally, in selected instances, the biofilm extracellular matrix can act as a barrier preventing the penetration of antimicrobial agents. The ability of the biofilm matrix to reduce antibiotic penetration might be due to the ionic interactions between antibiotics and the matrix. For example, *P. aeruginosa* biofilm sequesters the positively-charged antibiotic tobramycin while allowing the neutral antibiotic ciprofloxacin to penetrate [104]. In addition, bacteria factors secreted into the matrix can deactivate antibiotics. For example, *Klebsiella pneumonia* biofilms prevent ampicillin penetration by producing the ampicillin-degrading enzyme β-lactamase that is concentrated within the biofilm community [105].

1.7 Inflammation

Inflammation is a vital part of the body's first line of defense. A controlled inflammatory response can protect against foreign invaders, eliminate damaged cells, and initiate tissue repair [106]. Signs of skin inflammation include redness, swelling, heat and pain reflecting coordinated processes of inflammatory mediator production, vascular permeability increases and immune cell recruitment. Failure to resolve acute inflammation can lead to prolonged (chronic) inflammation lasting for several months to years. Chronic inflammation underlies the pathogenesis of most human diseases including Alzheimer's, asthma, atherosclerosis, chronic obstructive pulmonary disease and rheumatoid arthritis

to name a few [107–111].

1.7.1 Initiation of inflammation

Inflammation can be triggered by microbes (e.g. bacteria, viruses and fungi) and microbial products. The initiation of inflammation involves the recognition of loosely-conserved microbial signature molecules present in pathogens (sometimes referred to as pathogen-associated molecular patterns) through germline-encoded pattern recognition receptors that are widely expressed by immune and non-immune cells. There are five major types of pattern recognition receptors, namely, TLRs, Retinoic acid-inducible gene I-like receptors (RLRs), C-type lectin receptors, Nucleotide-binding and oligomerization domain (NOD)-like receptors (NLRs), and AIM2-like receptors [112]. TLRs are transmembrane receptors located at the cellular (TLR-1,2,4,5,6,10) or endosomal (TLR-3,7,8,9) membranes that sensing distinct microbial signatures. For example, among others, TLR-4 recognizes lipopolysaccharide (LPS), TLR-3 binds to double strand viral RNA, and TLR-2 recognizes lipoteichoic acid (LTA) and lipopeptides. Upon ligand binding through the leucine-rich repeat motifs on the extracellular or luminal side, TLRs usually multimerize and can induce cytoplasmic signal transduction through their TIR domain [113]. RLRs such as RIG-I and MDA5 are cytosolic RNA sensors that induce the production of IFN and the antiviral response [114]. C-type lectin receptors are calcium-dependent carbohydrate-binding proteins expressed by a variety of innate immune cells such as DCs, monocytes, macrophages and neutrophils. For example, ligand binding of CD207 on Langerhans cells triggers the antigen internalization, degradation and subsequent antigen presentation [115]. NLRs are also cytosolic receptors that contain a conserved central NACHT domain and in most cases C-terminal leucine-rich repeat motifs for ligand binding. NLRs such as NOD1 and NOD2 recognize bacterial peptidoglycan fragments leading to enhanced activation of nuclear factor-κB (NF-κB) and mitogen-activated protein kinases (MAPKs). Some NLRs such as NOD, leucine-rich repeat and pyrin domain containing protein (NLRP)1 and NLRP3 form multiprotein complexes called inflammasomes, which contain the inflammatory protease caspase-1 response for processing of inflammatory cytokines IL-1β and IL-18 [116]. Similarly, double stranded DNA sensing AIM2-like receptors also form inflammasomes and result in IL-1β or IFN production[117].

Inflammation induced by stimulants of non-microbial origin, such as irritants (sometimes called damage-associated molecular patterns) or alarmines that can be released from damaged cells and tissues, is referred to as sterile inflammation [118]. These stimulants can originate from intracellular sources (e.g. nuclear proteins, mitochondrial formylated peptides, ATP and uric acid) and

extracellular components (e.g. hyaluronan) [119]. These sterile inflammatory stimuli can be recognized by pattern recognition receptors such as TLRs and NLRs and additional alternative receptors such as integrin, CD44 and RAGE [119]. For example, the nuclear protein high-mobility group box 1 that participates in the pathogenesis of both acute and chronic kidney and hepatic inflammation, can activate both TLR2/4 and RAGE [120,121]. Many pathogenic sterile stimuli such as cholesterol crystals in atherosclerosis, silica particles in lung fibrosis and β-amyloid peptides in Alzheimer's disease have been reported to activate the NLRP3 inflammasome and IL-1β production [122].

1.7.2 Inflammatory signalling pathways

Activation of the pattern recognition receptors and other receptors by microbial signatures or irritants initiates intracellular inflammatory signalling pathways, which conduct the pathogen or danger signals from extracellular environments or cytoplasm to the nucleus leading to expression of proinflammatory genes. Most TLRs, except TLR3 and endocytosed TLR4, recruit the adaptor protein MyD88. MyD88 and a group of serine/threonine kinases- IRAKs- form a Myddosome complex, which induces the ubiquitin ligase TRAF6 activation. Activated TRAF6 promotes K63-linked polyubiquitylation of itself, IRAK1 and the TAK1 protein complex. TAK1 then activates two central pro-inflammatory pathways, the NF-κB and the MAPK pathways [123,124], among others. In the case of TLR-3 and endocytosed TLR-4, the adaptor protein TRIF is engaged followed by TRAF6 and TRAF3 recruitment, which activates TAK1 complex and leads to the activation of NF-κB and MAPKs, among others. TRAF3 can also activate transcription factor IFN regulatory factor (IRF)-3 and the expression of type I IFN genes [123]. It is worth mentioning that although this description makes it sound like these pathways have identical outcomes (NF-κB/MAPK activation), there are in fact profound differences in the consequences of activation by different ligands likely due to the involvement in inflammation of multiple other pathways (e.g. JAK-STAT, the PI3K, Src family kinases, Ras, TRIF-IRF and protein kinase C pathways, etc.) and various modulators including anti-inflammatory modulators.

NF-κB is a family of transcription factors including p50 (NF-κB1), p52 (NF-κB2), p65 (RelA), RelB and c-Rel [125], with each of these having specific targets, properties and activation profiles. Pattern recognition receptors and inflammatory cytokines such as TNF-α and IL-1β activate canonical NF-κB signalling which involves the phosphorylation and subsequent degradation of IκBα by IκB kinase complex allowing the translocation of NF-κB from cytoplasm to the nucleus where it acts as transcription factors to induce inflammatory gene expression [126]. NF-κB activation induces the production of thousands of proteins including prominently proinflammatory cytokines (e.g. IL-

1β, IL-6 and TNF-α) and chemokines (e.g. monocyte chemoattractant protein (MCP)-1), and upregulation of cell adhesion molecules (e.g. VCAM-1 and ICAM-1). In particular, NF-κB is required for the expression of both NLRP3 and pro-IL-1β, which primes NLRP3 inflammasome formation [127]. Secondary stimuli such as microbial components or signals indicating mitochondrial stress and lysosome damage (e.g. extracellular ATP, reactive oxygen species (ROS) and ionic flux) further lead to NLRP3 inflammasome activation [128]. NF-κB signalling also regulates immune cell survival and functions such as macrophages M1 polarization, neutrophil apoptosis and DC maturation[127].

MAPKs are serine/threonine kinases that include 3 subfamilies: the extracellular signal-regulated kinases (ERK), the c-Jun NH_2-terminal kinases (JNKs), and the p38 family of kinases (p38 MAPKs) [129]. To transduce intracellular signals, a MAPK kinase kinase, a MAPK kinase and a MAPK consecutively phosphorylate the downstream kinase and eventually lead to the activation of various target transcription factors, thereby modulating cellular processes such as cell survival, metabolism, stress response and inflammation [130]. For example, after TRAF-6 activation during the MyD88-dependent TLR signalling, two MAPK pathways: TAK1-MKK4/7-JNK and MEKK1-MKK3/6-p38 MAPK are activated [124]. These MAPKs promote the activation of transcription factors such as CREB, c/EBPβ and AP-1, and induce the expression of proinflammatory cytokines, chemokines and cell adhesion molecules similar to NF-κB [124]. MAPK pathways can be differentially regulated during sterile inflammation and bacteria infection. In a study for preterm birth, both LPS and water-soluble cigarette smoke extract induced inflammation and IL-8 production in fetal membranes [131]. Water-soluble cigarette smoke triggered greater ROS production and activated p38 MAPK, JNK, c-Jun and cellular senescence whereas LPS activated signal transducer and activator of transcription (STAT) 1, supressed ERK-1 and produced IL-8 through NF-κB activation [131].

Cytokines and chemokines are essential inflammatory mediators that function to communicate and coordinate immune cell function and trafficking. Cytokine signalling involves Janus family tyrosine kinases that are constitutively associated with cytokine receptors. Upon cytokine binding, Jak kinases increase in activity and phosphorylate cytokine receptors and the recruited STAT transcription factors [132]. STATs then undergo dimerization and nucleus translocation to regulate transcription of inflammatory genes [132]. Chemokines direct the migration of immune cells by engaging the rhodopsin-like family of G protein–coupled receptors (GPCRs) on the cell surface leading to the activation of phospholipase C and phosphoinositide 3-kinase (PI3K). Two second messenger molecules produced from activated phospholipase C (inositol-trisphosphate and diacylglycerol) can trigger calcium mobilization and activate protein kinase C respectively [133]. It is

worth mentioning that phorbol 12-myristate 13-acetate (PMA), the trigger of sterile skin inflammation in Chapter 3 and 4, activates protein kinase C by mimicking diacylglycerol [134]. These signalling events can trigger a diverged downstream signalling network depending on the cytokine and cell type engaged. For example, in neutrophils, diacylglycerol and protein kinase C activation through CXCL1 signalling contribute to the assembly of NADPH oxidase complex and subsequent ROS production [135]. In addition, PI3K activation through CXCL1/CXCL2 promotes neutrophil degranulation, adhesion and chemotaxis through ERK and phosphokinase signalling [136]. Other proinflammatory mediators such as histamines, leukotrienes, prostaglandins and platelet-activation factors also bind to GPCRs causing arteriolar dilation and leukocyte recruitment [137,138].

1.7.3 Acute inflammation

Acute skin inflammation is a fast reacting and well-coordinated process (Figure 3). Keratinocytes and local immune cells produce a variety of proinflammatory mediators and initiate acute inflammation within minutes after microbial invasion or sterile tissue injury. Nitric oxide, produced by nitric oxide synthase in response to increased calcium flux and inflammatory cytokines (e.g. TNF-α and IL-1β), causes vascular smooth muscle relaxation [139]. Keratinocytes upregulate human β-defensins (hBD) 2-4 leading to histamine and prostaglandin production. Prostaglandins produced by phospholipases and cyclooxygenases also contribute to vasodilation and can sensitize nociceptors to pain-inducing mediators such as bradykinin and histamine [137]. In the meantime, fluid exudation and tissue edema happen as the results of proinflammatory mediators (e.g. prostaglandins, histamine, bradykinin, complements and platelet-activating factors) increasing the permeability of capillaries and facilitating the migration of immune cells and soluble mediators into the site of inflammation [139]. HDPs can also function as immune cells chemoattractants and direct their recruitment. Activated endothelial cells increase the expression of adhesion molecules (e.g. E-selections, P-selections, VCAM-1 and ICAM-1), which bind to leukocytes integrins (e.g. LFA-1 and Mac-1) and L-selectins mediating the rolling, adhesion and diapedesis processes [138].

Neutrophils are the first populations recruited to the inflammation site arriving within 20 minutes [140]. Their migration follows the gradients of chemoattractants, primarily IL-8 and Leukotriene B4 in the endothelium, and fMLF and anaphylatoxin C5a in the peripheral tissues [141]. Activated neutrophils clear evading microbes and prevent pathogen dissemination through phagocytosis, release of granule contents (e.g. elastase, myeloperoxidase, defensins, lactoferrin and matrix metalloprotease 9) and formation of neutrophil extracellular traps [142]. In addition, neutrophils are capable of producing ROS, cytokines and chemokines (e.g. IL-17, IFN-γ, IL-8, MCP-1 and MIP-

1α), which recruit and modulate other immune cells such as monocytes, DCs and natural killer cells [143]. For example, neutrophils expressing IL-12, MIP-1α, TLR-2, TLR-4, TLR-5, TLR-8, and promoting macrophage activation have been observed in intravenous MRSA-infected mice, whereas neutrophils expressing IL-10, MCP-1, TLR-2, TLR-4, TLR-7, and TLR-9 are isolated from methicillin-sensitive *S. aureus* infection [144].

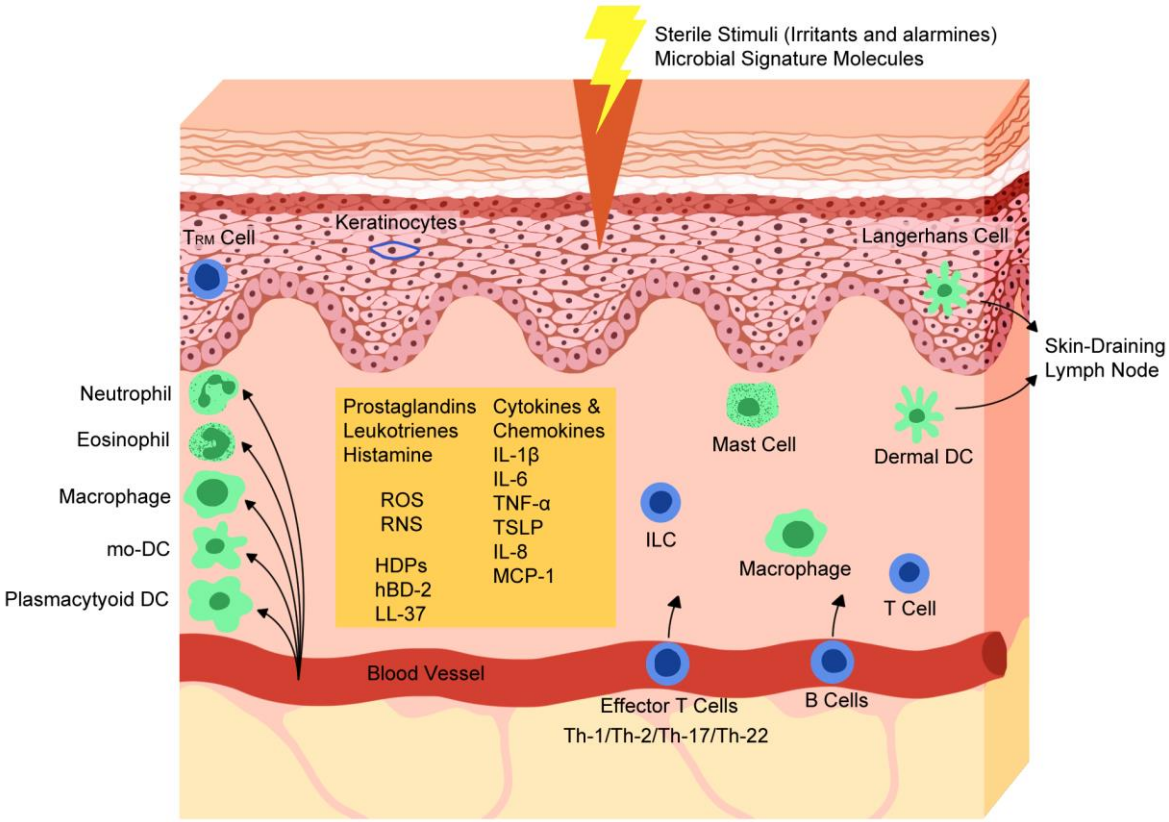

Figure 3. Acute skin inflammatory response.
Acute skin inflammation is triggered upon contact with skin sensing sterile stimuli and/or microbial signature molecules. Keratinocytes and local immune cells such as tissue resident memory T cells (T_{RM}), mast cells, tissue resident macrophages and innate lymphoid cells (ILCs) produce proinflammatory mediators and HDPs causing vasodilation and directing the recruitment of other immune cells such as neutrophils, eosinophils, macrophages, monocytes-derived dendritic cells (mo-DCs) and plasmacytoid DCs to the site of inflammation. Recruited immune cells also produce proinflammatory mediators amplifying the inflammatory response. Langerhans cells and dermal DCs become activated and migrate to skin-draining lymph nodes where they direct T cell or B cell responses.

In response to sterile skin injury, dermal DCs change from random motion to directional migration towards the site of injury with an increase in cell velocity over a span of 50 minutes [145]. Upon antigen uptake, both Langerhans cells and dermal DCs mature and migrate to adjacent lymph nodes, while upregulating MHCII and costimulatory receptor molecules such as CD86, CD80, CD83, and CD40 [146]. The migration of DCs to lymph nodes depends on CXCR4 and CCR7 expression and

happens within hours, peaking at 1-3 days post antigen exposure [147]. It is also known that functions of DCs in inflammation go beyond T cell priming. In the spleen, a group of DCs serve as the major source of TNF-α and inducible nitric oxide synthase within the first 48 hours of intracellular *Listeria monocytogenes* infection and provide early antimicrobial defense [148]. In addition, plasmacytoid DCs specialized for antiviral immunity can rapidly produce type I and III IFNs upon sensing intracellular viral nucleic acids through TLR activation [149].

Within the first 8 - 24 hours, chemokines such has MCP-1 and MCP-3 can recruit proinflammatory monocyte populations ($CD14^{++}CD16^{-}$ classical monocytes and $CD14^{++}CD16^{+}$ intermediate monocytes in humans and $CD11b^{+}CD115^{+}Ly6C^{high}$ monocytes in mice) to the site of inflammation where the majority differentiate into macrophages or DCs and some maintain monocyte features with the ability to migrate to the draining lymph nodes [150]. During inflammation, both monocyte-derived macrophages and tissue resident macrophages differentiate into an M1-like phenotype and remove pathogens or harmful stimuli by phagocytosis, production of reactive oxygen/nitrogen species (ROS/RNS), proinflammatory cytokines, and antimicrobial peptides and present antigens [151].

Under inflammatory conditions, various effector T cells can be recruited to the skin and their activation depend on specific antigen, co-stimulatory signals and the cytokine milieu. In brief, intracellular pathogens and viral infections trigger IFN-γ and IL-12 production, which upregulate T-bet expression and promotes Th-1 cell production. Extracellular pathogens induce Th-2 responses, involving IL-4, IL-5 and IL-13 production and B-cell class switching [152]. IL-17-producing Th-17 cells function in anti-bacterial and antifungal responses [153,154] and IL-22-producing Th-22 cells can induce the production of antimicrobial peptides and promote keratinocyte proliferation [155].

Acute inflammation is self-limiting followed by coordinated resolution once the inflammatory triggers are successfully removed. Depletion of cytokines and chemokines lead to the attenuation of leukocyte recruitment. In addition, chemokine CXCL-8 binding to the atypical chemokine receptor-1 lacking the ability to trigger G-protein-dependent signalling cascades can prevent neutrophil migration [156]. Resolution mediators such as lipoxin A_4, resolvin E1 and annexin A1 render neutrophils unresponsive to agonists and initiate neutrophil apoptosis, leading to phagocytosis by macrophages[157]. Efferocytosis induces macrophage reprograming from the proinflammatory M1 to an IL-10 and TGF-β secreting M2 phenotype [158]. Finally, egress of immune cells to the lymphatic vasculature instructs the adaptive immune response and induces tissue repair leading to homeostasis[159].

1.7.4 Chronic inflammation

Failure to resolve acute inflammation can lead to long-lasting chronic inflammatory conditions. Excessive sterile inflammation leads to the pathological consequences of non-communicable diseases. According to the World Health Organization, non-communicable diseases accounted for 74% of deaths globally in 2019 [160]. In particular, cardiovascular diseases, chronic obstructive pulmonary disease, Alzheimer's disease and diabetes mellitus are among the top 10 causes of death at the global level, responsible for more than 20 million deaths in total in 2019 [160]. On the other hand, chronic diseases of infectious etiology pose a threat to the well-being of worldwide populations and create heavy health burdens [161]. Bacterial pathogens such as *P. aeruginosa, S. aureus, Helicobacter pylori* and *Escherichia coli* can evade or overcome the host immune system causing persistent infection and inflammation through intracellular growth and formation of biofilms, small colony variants and persisters [162]. For example, chronic bacterial infections, especially *Haemophilus influenzae* (32.3%) and *P. aeruginosa* (30.1%), lead to deterioration of lung function as well as longer and more frequent hospital visits in bronchiectasis and cystic fibrosis patients [163].

Chronic inflammation is of complex etiology and pathophysiology, making research study and therapeutic development challenging. Psoriasis and atopic dermatitis are both chronic skin conditions that serve as paradigms for studying pathogenic mechanisms of chronic skin inflammation. Psoriasis, affecting 2% of the world population, is characterized by formation of raised and sharply edged plaques on the skin and inflammation of the joints (psoriatic arthritis) with a strong genetic predisposition [164]. Genome-wide association studies found that multiple loci within the MHC confer increased risk of psoriasis [165]. In psoriatic skin, keratinocytes overexpress host defense peptides such as LL37, β-defensins and S100 proteins, which activates type I IFN producing plasmacytoid DCs and start the development of the psoriatic plaque [166,167]. In addition, activation of Th-17 cells in psoriatic skin by IL-23 producing DCs leads to the secretion of IL-17A, IL-17F and IL-22. These Th-17 cytokines are responsible for key histological features in psoriasis such as epidermal hyperplasia and recruitment of inflammatory cells [168]. Patients with psoriasis have also been shown to have an increased number of circulating Th-17 cells in their peripheral blood [169,170]. The long-persisting and fast reacting T_{RM} also contribute to the immunopathogenesis. The $CD4^+$ and $CD8^+$ T_{RM} are major sources of IL-17A and IL-22 contributing to the relapse of psoriatic lesions in the same locations [171–173].

Atopic dermatitis is the most common chronic inflammatory skin disease affecting about 13% of children and 7-10% of adults in the United States [174]. Genetic predisposition, epidermis disruption and immune response dysregulation are considered to be the major factors of atopic dermatitis

pathophysiology [175]. Mutation of human filaggrin, particularly homozygous mutations, increases the risk of disease onset, persistency and associated infections [176]. Impaired epidermal keratinocytes produce proinflammatory cytokines such as IL-1β, thymic stromal lymphopoietin (TSLP), IL-6 and IL-25 leading to Langerhans cell and dermal DC activation promoting a Th-2 response. Cytokines produced by Th-2 cells such as IL-4, IL-5 and IL-33 contribute to abnormal keratinocyte differentiation and dysregulation of HDP production [175]. In the atopic dermatitis skin lesions, there is an increase in the percentage of mast cells expressing TNF-α, IL-4 and IL-6 and a decrease in the mast cell chymase activity resulting in an impaired degradation of proinflammatory cytokines [46,47]. *S. aureus* that colonizes more than 90% of atopic dermatitis patients, secrets δ-toxin and induces the degranulation of mast cells [177]. Elevated numbers of ILC2 with high expression of ST2, IL-17RB and TSLP-R have also been observed in the skin lesion suggesting a pathogenic role [178]. Interestingly, Th-17 cells have been reported in the acute skin lesions and blood of atopic dermatitis patients highlighting the complexity of the underlying disease mechanisms [179]. The transition from acute to chronic phases of atopic dermatitis happens around day 3 and the chronic phase is driven by Th-1, Th-22 and Th-17 responses [180].

1.7.5 Treatments and limitations

Current treatment options for chronic inflammatory skin disorders include nonsteroidal anti-inflammatory drugs (NSAID) blocking cyclooxygenases and alleviating the pain and swelling caused by inflammation, corticosteroids exerting anti-inflammatory, antiproliferative, and local vasoconstrictive effects through downregulation of proinflammatory cytokines, calcineurin inhibitors blocking pathogenic T cell activation by inhibiting IL-2 production, and phototherapy-induced keratinocyte apoptosis after exposing the skin to controlled amounts of natural or artificial light [181,182]. In addition, biologics target specific immune pathways based on the understanding of disease immunopathology. For example, biologics inhibiting TNF-α, p40IL-12/23, and IL-17 are approved by the US Food and Drug Administration to treat psoriatic arthritis, and anti IL-4/IL-13, anti IL-22, anti IL-31, anti TSLP and IgE directed therapy are approved for treating moderate to severe atopic dermatitis [181,183].

Despite the availability of different treatment options, there is currently no cure for many chronic inflammatory disorders such as psoriasis and atopic dermatitis. Common side effects include skin irritation, burning, pruritus and edema. Long-term usage of glucocorticoids increase the risk of musculoskeletal adverse effects such as osteoporosis and adverse gastrointestinal effects, such as gastritis, ulcer formation, and bleeding [184]. Targeted biologic drugs can be costly due to complex

manufacturing, transportation and storage. For example, the IL-4 receptor antagonist dupilumab costs approximately $37,000 per patient per year representing a significant burden to patients and the healthcare system [185]. Moreover, the use of immune suppression as a common therapeutic strategy can lead to higher risk of infectious diseases. Therefore, immune modulators that dampen excessive inflammation without compromising appropriate immune responses to infections can serve as superior therapeutic solutions.

1.8 Host defense peptides and their synthetic analogs

HDPs, also known as antimicrobial peptides, are evolutionarily conserved, short (12-50 amino acids) and positively charged (+2 to +9) peptides broadly belonging to four structural groups: α-helical linear peptides, β-sheet peptides with disulfide bridges, cyclic peptides and peptides with extended flexible loop structures [186]. Synthetic analogs of naturally occurring HDPs such as innate defense regulator (IDR) peptides have improved activities and low cytotoxicity. HDPs and derivatives exert a variety of biological effects ranging from direct antimicrobial activity to antibiofilm and immunomodulatory functions [187].

According to the the Antimicrobial Peptide Database, about 140 HDPs from a variety of body sites (e.g. skin, eyes, ears, mouths, gut and urinary tract) have been identified in man [188,189]. Human skin produces a variety of HDPs, such as the cathelicidin LL-37, defensins and dermcidin, in resident skin cells (e.g. keratinocytes, sebocytes, eccrine glands, and mast cells) as well as recruited inflammatory cells (e.g. neutrophils, natural killer cells, monocytes and macrophages) [190]. LL-37, the only cathelicidin in humans, is α-helical and becomes active upon cleavage by serine proteinase 3 from its precursor protein hCAP18 [191]. Defensins have β-sheet structures and can be subcategorized based on the connectivity of their three disulfide bridges. Human neutrophil peptide (HNP)-1, -2 and -3 are α-defensins mainly produced by neutrophils, and hBD-1 to 4 can be produced by skin keratinocytes. Dermcidin is constitutively secreted and distributed to the skin surface in sweat [192]. Besides HDPs, human skin also produces cationic proteins such as lactoferrin, histones and lysozymes, which have weak antimicrobial activities either per se or after cleavage [186].

1.8.1 Immune modulation by HDPs

Although traditionally termed antimicrobial peptides, HDPs are strongly antagonized by physiological concentrations of salts and anionic polymers such as glycosaminoglycans and extracellular DNA [193,194]. In contrast, under physiological conditions and in animal models of infection, HDPs and IDR peptides exhibit a wide variety of immunomodulatory functions such as

induction of chemotaxis, modulation of inflammation, regulation of immune cell polarization and cytokine profiles, adjuvanticity and promotion of adaptive immunity [187,193]. This has led to the proposal that regulation of the immune system is the major function of such peptides. Other biological functions of HDPs include anti-cancer effects, promotion of wound healing, stimulation of angiogenesis and regulation of the microbiota [187]. HDP and their synthetic derivatives collectively display these diverse biological effects by regulating immune signalling networks.

Healthy human skin constitutively expresses some HDPs at low levels including hBD-1, produced by keratinocytes and sweat gland ducts, and LL-37 produced by mast cells and macrophages [195]. Some HDPs are also induced or upregulated by infection or sterile inflammation, while degranulation of phagocytic cells, especially neutrophils and macrophages, can substantially increase local concentrations, especially in inflammatory situations. For example, *S. aureus*, *S. epidermidis*, *E. coli*, and *P. aeruginosa* can induce hBD-2 expression in keratinocytes [196]. HDPs act as chemoattractants for immune cells both through the upregulation of chemokines and at higher concentrations directly. For example, β-defensins can direct the migration of immature-dendritic cells and memory T-cells through chemokine receptor CCR6 activation [197]. LL-37 is chemoattractive to neutrophils, monocytes, and T cells by activating G-protein-coupled receptors [198].

HDPs and synthetic analogs can modulate immune cell functions and thereby affect various aspects of inflammatory responses. For example, LL-37 promotes the antimicrobial function of neutrophils by inducing the generation of reactive oxygen species and release of HNP 1-3 [199]. LL-37 also induces neutrophil chemokine IL-8 production by activating p38 MAPK and ERK pathways [199]. IDR-1018 drives macrophage differentiation towards an intermediate M1-M2 state, enhancing anti-inflammatory functions while maintaining certain pro-inflammatory activities important to the resolution of infections [200]. It has been shown that hBD-2, hBD-3 and hBD-4 can induce the expression of cytokines (e.g. IL-6, IL-10) and chemokines (e.g. MCP-1, CCL-20, CCL-5) in human primary keratinocytes through the activation of GPCR and phospholipase C signaling pathways [201]. Synthetic peptides such as IDR-1018 and IDR-1002 can enhance chemokine induction while suppressing potentially harmful inflammatory cytokines [202–204]. In addition, hBDs upregulate keratinocyte migration and proliferation through the activation of the epidermal growth factor receptor, STAT1 and STAT3 [201]. Similarly, LL-37 promotes keratinocyte migration in an epidermal growth factor receptor and STAT3 dependent manor [205]. Defensins such as HNP-1 and -4 and hBD 2-4, as well as LL-37, have been shown to induce histamine release from mast cells [192]. Both HDPs (e.g. LL-37 and hBD2) and synthetic peptides (e.g. IDR-1 and IDR-1002) can control inflammation in animal models of sepsis [186,193]. In particular, the infection resolving and anti-inflammatory effects

of IDR-1002 have been demonstrated in several studies (summarized in the Chapter 3 Introduction). It is worth mentioning that depending on the cell type and stimuli, HDPs exhibit a mixture of or bias towards pro- or anti-inflammatory effects. For example, LL-37 can direct macrophage differentiation towards the M1 phenotype and induce inflammasome activation and type 1 IFN production [206]. Conversely, LL-37 suppresses TLR agonist-induced inflammation by a complex mechanism involving multiple points of intervention (e.g. inhibiting specific proinflammatory genes and reducing nuclear translocation of NF-κB subunits p50 and p65) [207].

HDP and IDR peptides can also bridge the innate and adaptive immunity by directing recruitment, phagocytosis and upregulating co-stimulatory molecules of antigen-presenting cells such as macrophages and DCs and thereby influence the polarization of lymphocyte responses[186,193]. This ability to boost and shape immune response makes peptides ideal vaccine adjuvants. Indeed, hBD3 has been shown to improve vaccine formulations by enhancing cellular uptake of nucleic acids [208]. IDR-1002 can enhance IgG1/IgG2 humoral immune responses in a vaccine formulation against Mycoplasma bovis disease [209].

1.8.2 Direct antimicrobial activity

Traditionally, HDPs and their derivatives have been recognized for their modest broad-spectrum antimicrobial activities against bacteria, fungi, viruses, and parasites. However, as mentioned above, the direct antimicrobial activity of most HDPs is greatly impaired in the presence of physiological concentrations of divalent cations and polyanions found in the blood, organs, mucosa and body fluids, suggesting an alternative role of HDPs, such as immunomodulation under physiological conditions [210]. For example, in medium of low ionic strength, LL-37 is active (MIC 1-30 μg/ml) against a variety of Gram-positive and Gram-negative bacteria but has no killing activity against *S. aureus* or *S. typhimurium* in tissue culture medium at concentrations as high as 100 μg/ml[211]. Synthetic peptides generated from computer-aided design and active structural analogs of natural animal peptides (e.g. synthetic peptide PV5 derived from horseshoe crab polyphemusins) exhibit protective roles in animal models [212,213]. Nevertheless, the local release of HDPs *in vivo* (e.g. through degranulation of neutrophils or entrapment in neutrophil NETs) could lead to high enough local concentrations that they might be effective in killing bacteria.

The mechanism of HDP activity is complex and not fully understood. While it is generally accepted that peptides adopt specific active structures upon interacting with biological membranes and this is a precursor to their antibacterial effects, accumulated evidence suggests that peptide structural plasticity and flexibility allows them to interact differentially with multiple cellular targets

and exhibit activity against a broad range of microorganisms [187]. Some peptides are proposed to exhibit antimicrobial activity through interactions between positively charged HDPs and negatively charged bacterial membrane with the amphipathic nature of HDPs being essential for their membrane-destabilizing properties leading to subsequent bacterial leakage and death [186]. Other peptides translocate across the membrane and target intracellular processes such as DNA or RNA synthesis and protein synthesis or folding [186]. Conversely, hBD-3 mediates killing by inhibiting cell wall synthesis in *S. aureus* and results in localized lesions and protrusions of bacterial cytoplasmic contents [214]. Synthetic peptide DP7, designed by a machine-learning method, interferes with MRSA amino acid biosynthesis [215].

1.8.3 Antibiofilm activity

The most recently described activity of certain HDPs is antibiofilm activity and it was demonstrated that LL-37 had preferential activity against *P. aeruginosa* biofilms, acting at one sixteenth the MIC for free swimming planktonic bacteria [216]. Since then, other natural HDPs such as indolicidin, hBD-2, hBD-3 and Protegrin 1 have been demonstrated to have antibiofilm activity against both Gram-positive and Gram-negative species such as *S. aureus*, *Acinetobacter baumannii*, *Burkholderia thailandensis* and *P. aeruginosa* [217,218]. Many synthetic peptides including 1037, IDR-1018, DJK-5, P10, NRC-16 and BMAP27-melittin, to name a few, also exhibit promising and preferential antibiofilm effects [10]. In particular, peptides IDR-1018 and DJK-5 have broad-spectrum activity in both biofilm inhibition and eradication [219–221]. Antibiofilm peptides are generally speaking those HDPs and synthetic analogs that have antibiofilm effects at concentrations lower than their MIC and there is no obligate overlap in the structure-activity relationships between antibiofilm and direct antimicrobial activities of peptides, suggesting distinct mechanisms of action between antibiofilm peptides and those targeting planktonic bacteria [187,217].

The antibiofilm mechanisms of HDPs and derivatives involve targeting one or multiple stages of biofilm formation and regulation. As a potentially universal mechanism IDR-1018 and DJK-5 target the bacterial stringent response, required for biofilm formation, by binding and targeting the degradation of (p)ppGpp [221,222]. It has also been suggested that LL-37 inhibits *P. aeruginosa* surface attachment, interferes with quorum sensing and stimulates twitching motility, which inhibit biofilm maturation and promotes disassembly of biofilm structures [216]. Hepcidin 20 reduces the extracellular matrix mass of *S. epidermidis* biofilm [223], and 1018 and DJK-5 both stimulate dispersal of biofilms[221,222]. In addition, DJK-5 supresses phenol soluble modulin production in *S. aureus* which may be involved in biofilm formation [220].

1.9 Conclusion

Knowing the great potential of natural HDPs, researchers have made continuous efforts to manipulate the biophysical characteristics of natural HDPs and select for synthetic sequences with improved antimicrobial, antibiofilm and anti-inflammatory activity. Approaches for activity optimization include targeted substitutions to enhance certain properties (amphipathicity, charge etc.), examining activities of truncated versions of larger peptides, identifying novel peptides using a synthetic combinatorial library technology, and combining SPOT synthesis (peptide array) and standard fluorenyl methoxy carbonyl chemistry to perform systematic point substitutions of active peptides (a relatively simple and inexpensive way to generate a library of cellulose-tethered peptides for screening) [224]. Computational approaches such as Quantitative structure–activity relationship modeling can help to predict the peptide efficacy *in silico* using structural descriptors based on their primary sequences and the physicochemical interrelationships of individual amino acids along the peptide chain [187]. Since HDPs are inherently susceptible to proteolytic degradation, different approaches for conferring increased stability have been explored: e.g., incorporation of non-natural amino acids, L- to D-amino acid substitution, cyclization, modification of the termini, and formulation using drug delivery systems [224]. Alternatively, peptidomimetics with their pharmacophore mimicking a natural peptide while maintaining the desired biological effects also confer stability against proteolysis [225].

Several synthetic HDPs (e.g. IDR-1002 and DJK-5) or peptidomimetics (e.g. Pam-(Lys-βNspe)$_6$-NH_2 and Lau-(Lys-βNspe)$_6$-NH_2) obtained from such optimization approaches have shown promising *in vitro* and/or *in vivo* effects, but their efficacy in skin inflammation had not yet been shown. I hypothesized that synthetic HDPs and peptidomimetics could be used to treat sterile inflammation and biofilm-associated skin disorders. The anti-inflammatory and antibiofilm mechanisms of these peptides were proposed to involve modulation of multiple signal transduction pathways such as chemokine, IL-1, TNF-α and IFN signalling cascades, which are regulated by essential transcription factors such as IRF-8, NF-κB and AP-1. In additon, I proposed that sterile skin inflammation could be treated by synthetic peptides or peptidomimetics that directly dampen host inflammatory responses, while skin inflammation induced by biofilm infections could be treated by antibiofilm peptides that target the pathogen and eradicate the biofilms while combining with immunomodulatory peptides to resolve associated inflammation (Figure 4).

My goals were to: (1) Investigate the anti-inflammatory activity and underlying mechanisms of IDR-1002 in sterile skin inflammation (Chapter 3); (2) Study the anti-inflammatory effect of peptidomimetics Pam-(Lys-βNspe)$_6$-NH_2 and Lau-(Lys-βNspe)$_6$-NH_2 in PMA-induced skin

inflammation (Chapter 4); (3) Establish and characterize *in vivo*-like air liquid interface skin biofilm models to serve as biologically relevant platform for novel peptide screening (Chapter 5); and (4) Use the skin organoid model to study the antibiofilm and anti-inflammatory effects of DJK-5 and IDR-1002 against MRSA biofilm associated with thermally injured skin (Chapter 6).

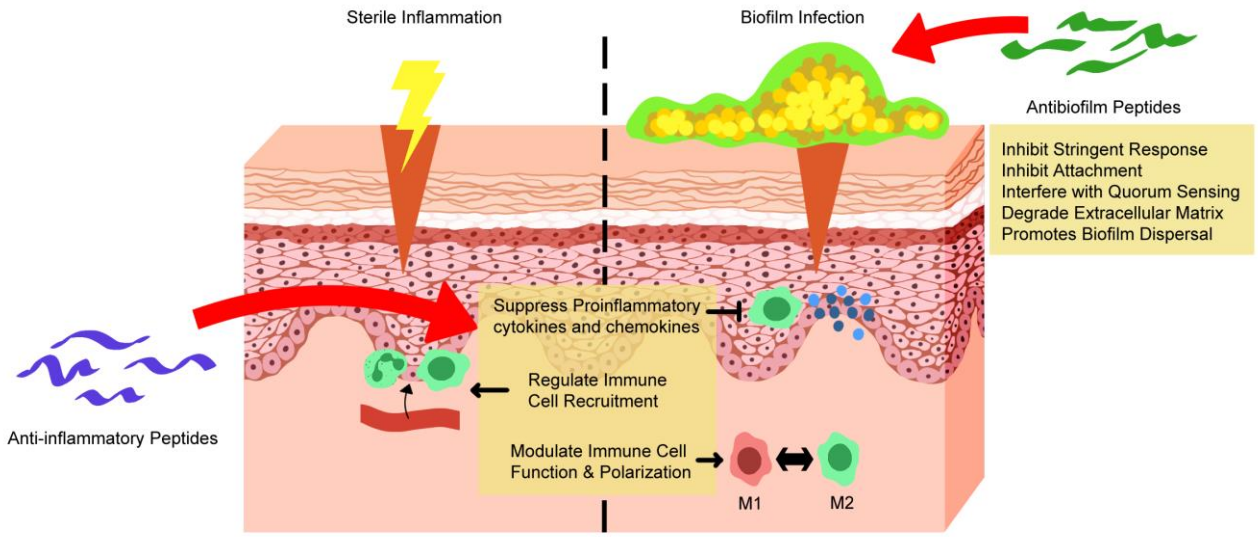

Figure 4. Synthetic HDPs as treatment for sterile skin inflammation and biofilm skin infections. In sterile inflammation, synthetic HDPs dampen host inflammatory responses. In biofilm associated skin inflammation, synthetic HDPs eradicate biofilm and modulate host immune response.

Chapter 2: Material and Methods

2.1 Peptides and peptidomimetics synthesis

Peptide IDR-1002 (VQRWLIVWRIRK-NH_2) and DJK-5 (*VQWRAIRVRVIR-NH_2*; all D amino acids) and other peptides used in this study (listed in Table 2) were synthesized using solid-phase 9-fluorenylmethoxy carbonyl chemistry and purified to ~95% using reverse-phase high-performance liquid chromatography. Peptide DJK-5 was synthesized by CPC Scientific (Sunnyvale, CA) and all other peptides were obtained from GenScript (Piscataway, NJ). Peptide identity was confirmed by mass spectrometry. Peptidomimetics Pam-(Lys-βNspe)$_6$-NH_2 (PM1) and Lau-(Lys-βNspe)$_6$-NH_2 (PM2) were prepared by a solid-phase synthesis methodology involving assembly of dimeric and/or tetrameric building blocks on a Rink amide resin by using PyBOP as a coupling reagent as earlier reported [226,227]. On the day of the experiment, the peptides or peptidomimetics were diluted to the appropriate working concentration. Stock peptide solutions were subjected to no more than three freeze/thaw cycles.

2.2 RAW 264.7 cell culture and *in vitro* IDR-1002 anti-inflammatory activity study

RAW 264.7 cells (passage number 3 to 15) were maintained in the Dulbecco's modified Eagle's medium supplemented with 10% heat-killed fetal bovine serum (Invitrogen), 2 mM L-glutamine, 100 units/ml penicillin and 100 μg/mL streptomycin at 37°C and 5% CO_2. One milliliter of 2x10^5 cells/ml RAW 264.7 cells was seeded into each well of a 24-well plate (Costar 3524) and rested for 12 hours before treatment. RAW 264.7 cells were then treated with 5-100 ng/ml *P. aeruginosa* PAO1 LPS, 5-50 μg/ml *S. aureus* LTA and 50-500 μg/ml *Saccharomyces cerevisiae* zymosan with or without 25 μg/ml IDR-1002 in fresh media. Culture supernatants were harvested 24 hours post-treatment for measuring cytotoxicity using the Lactate dehydrogenase assay, the production of nitric oxide using the Griess assay, and levels of TNF-α and IL-6 by sandwich ELISA kits (eBioscience), according to the manufacturer's instructions. The *in vitro* experiments were repeated 5 times.

2.3 RAW 264.7 cell cytotoxicity

The cytotoxicity of the LPS, LTA and zymosan treatments with or without 25 μg/ml IDR-1002 against RAW 264.7 cells was measured using the Cytotoxicity Detection Kit (Roche Diagnostics) according to the manufacturer's instructions. RAW 264.7 cell supernatants were collected and assessed 24 hours post-treatment. Supernatants of untreated RAW 264.7 cells or RAW 264.7 cells lysed with 2% Triton X-100 were used as negative (0% toxicity) or positive (100%

toxicity) controls respectively.

2.4 RAW 264.7 cell nitric oxide production

Griess reagent (modified) was purchased from Sigma-Aldrich. Equal volumes (100 μl) of 1x Griess reagent were mixed with Griess standards or RAW 264.7 cell supernatant harvested 24 hours post-treatment in duplicates. The absorbance at 540 nm was determined by a microplate reader (PowerWave 340) after 15 minutes incubation at room temperature.

2.5 Mice

All mouse experiments were performed according to the guidelines of the Canadian Council on Animal Care. CD-1 female mice (5 weeks old) were purchased from Charles River Laboratories (Wilmington, MA). The mice were maintained at a controlled room temperature (22 ± 2°C) and humidity (40−60%) under a 14-hour light and 10-hour dark cycle for at least 1 week before the experiments. Standard housing and animal care were provided by the Modified Barrier Facility at the University of British Columbia. Experimental and control mice were co-housed, and mice were divided randomly among different treatment groups on the days of the experiments.

2.6 PMA-induced mouse ear inflammation model

CD-1 female mice (6–7 weeks old) were anesthetized under 2-5% isoflurane for 10-15 minutes. To induce inflammation, 20 μl of 125 μg/ml PMA (i.e. 2.5 μg total; Sigma-Aldrich) dissolved in acetone was applied topically onto both ears of mice and allowed to air-dry. After PMA was fully absorbed, 20 μl of peptide IDR-1002 (30 mg/ml or 15 mg/ml in 50% ethanol) or peptidomimetic PM1 or PM2 (30 mg/ml or 10 mg/ml in 50% ethanol), or the positive anti-inflammatory control indomethacin (30 mg/ml or 15 mg/ml in acetone; Sigma-Aldrich*)* was applied topically onto one ear of each mouse. The contralateral ear was given the same volume of the vehicle/solvent (20 μl of 50% ethanol for mice given IDR-1002 or peptidomimetic, and 20 μl of acetone for mice given indomethacin). Mice were euthanized 6 hours or 24 hours post-PMA treatment for sample collection. The ear thickness was measured using a digital caliper. Ear biopsies (5 mm in diameter) were cut out using disposable biopsy punches (VWR), weighed and homogenized in 600 μl of Tissue Extraction Reagent I supplemented with protease inhibitor cocktails and phosphatase inhibitor cocktails 2 (Sigma-Aldrich), and then centrifuged at 13000 rpm for 20 minutes at 4°C to collect the supernatant. Blood samples were obtained by cardiac puncture in 1.5 ml microcentrifuge tubes without any anticoagulant. The blood tubes were incubated undisturbed at room temperature

for 30 minutes to allow clotting, and then each tube was centrifuged at 2000 rpm for 10 minutes, followed immediately by supernatant (serum) collection. IL-6, MCP-1 and CXCL-1 levels in mice ear tissue and serum were quantified from 5-23 mice per peptide concentration by ELISA.

2.7 *In vivo* imaging

2.7.1 Reactive oxygen and nitrogen species

The reactive oxygen and nitrogen species production was visualized following a modified protocol from van der Plas *et al.* [228]. In brief, mice were injected subcutaneously with the luminescence probe L-012 (Wako Chemicals; 25 mg/kg) dissolved in 50% phosphate-buffered saline (PBS), 5.5 hours post-PMA treatment. Mice were then imaged using the IVIS Spectrum (Caliper Life Sciences) 20-30 minutes post-injection under 2% isoflurane anesthesia. Images were acquired using the Living Image version 3.1 (Caliper Life Sciences) with 45 seconds exposure time.

2.7.2 Neutrophils recruitment

To detect neutrophils, mice were injected with the Neutrophil-Specific, NIR fluorescence probe (Kerafast; 0.1 μmol/kg) intravenously 3 hours post-PMA treatment and imaged using the IVIS Spectrum (Caliper Life Sciences) 3 hours post-injection under 2% isoflurane anesthesia. Images were acquired using the Living Image version 3.1 (Caliper Life Sciences) under auto-exposure with fluorescent filter setting 745 nm for excitation and 800 nm for emission.

2.8 Histology assessment of mouse ear tissue

Ear biopsies (5mm in diameter) were collected 6 hours post-treatment and fixed in 10% neutral-buffered formalin solution (Sigma-Aldrich) for 36-48 hours and then stored in 70% ethanol at room temperature. Hematoxylin and eosin (H&E) Staining of ear tissue cross sections (3-6 biological replicates) was conducted by Wax-it Histology Services Inc. (Vancouver, BC). The numbers of immune cells per high power field (HPF) (400-fold magnification) and the ear edema scores in the stained specimens were quantified by an independent pathologist in a blinded manner. The ear edema scores were assigned (0: no edema, 1: mild, 2: moderate, and 3: severe) based on the degree of increase in dermal interstitial fluid.

2.9 Bacterial strains and growth conditions

Bacterial strains used in the human skin organoid model include USA300-LAC [229] (referred to as MRSA), and a luminescent MRSA strain SAP149 [230] (referred to as MRSA-*lux*), *P. aeruginosa* strain PAO1 [231] and a luminescent strain of *P. aeruginosa* [232] (PAO1-*lux*). Bacteria strains used for

confocal microscopy imaging included *S. aureus* USA300-LAC transformed with a pKK22 plasmid expressing a far-red fluorescent protein (MRSA-FarRed) as well as *P. aeruginosa* PAO1 transformed with an mCherry expressing plasmid, pMCh-23 (PAO1-mcherry) [233]. All *S. aureus* strains were grown overnight in Tryptic soy broth (TSB) containing 1% D-glucose at 37°C with shaking at 180 rpm, sub-cultured to mid-exponential growth phase in TSB 1% D-glucose. Bacteria were harvested and resuspended in sterile PBS to a concentration of 2 x 10^8 CFU/ml before seeding onto the skin surface. All *P. aeruginosa* strains were grown in Lysogeny broth (LB) under the same conditions as mentioned above, subcultured in LB medium and resuspended in PBS at 2 x 10^8 CFU/ml before seeding.

2.10 Generation of fluorescently tagged MRSA and PAO1 strains

The 742-bp eqFP650 far-red fluorescent gene was excised from plasmid pSFRFPS1 via *Asc*I restriction sites and transferred onto *Asc*I-digested plasmid pKK22, yielding pKK22.eqFP650, and transformed into DH5αλpir. After confirmation of the correct orientation of the gene, the plasmid was transformed into *S. aureus* RN4220 as described below. Successful transformants were verified by assessing fluorescent yield with a Synergy H1 96-well microtiter plate reader (BioTek Instruments) at wavelengths of 605 nm (excitation) and 670 nm (emission). The plasmid was re-isolated from RN4220 and transformed into USA300-LAC and transformants were verified via plasmid extraction and fluorescence measurements.

2.10.1 Plasmid transformation of MRSA

Overnight cultures of *S. aureus* RN4220 or USA300-LAC were diluted to an optical density of 0.5 and incubated at 37ºC with shaking for 30 minutes. One ml was transferred into microcentrifuge tubes and harvested by centrifugation. All centrifugation steps were done at room temperature at 6,200 g for 5 minutes. Preparation of electrocompetent cells was done as previously described [234]. Briefly, cells were washed twice with equal volume of autoclaved water, followed by one wash with 1/5 and one wash with 1/10 the volume 10% glycerol. Subsequently, the final pellet was resuspended in 100 µl 500 mM sucrose and cells incubated with 2 µg DNA for 15 minutes at room temperature. DNA was transformed using a Gene Pulser (Bio-Rad) at 2.3 kV, 100 Ω, 25 µF. Cells were recovered in TSB for one hour at 37ºC and spread on Tryptic soy agar plates with 15 µg/ml Trimethoprim overnight at 37ºC. Successful plasmid transformants were confirmed via plasmid isolation (Qiagen) and restriction enzyme digest. Plasmids were isolated from overnight cultures that were first pelleted and re-suspended in buffer P1 (Qiagen) containing 10 µl Lysostaphin (5 mg/ml stock), and further

incubated at 37ºC for 30 minutes before following the manufacturer's instructions.

2.10.2 Plasmid transformation of *P. aeruginosa*

Plasmid pMCh-23 was transformed into electrocompetent *P. aeruginosa* PAO1 as previously described [235]. Briefly, cells were washed in 300 mM sucrose and electroporation of 500 ng plasmid DNA was carried out at 2.5 kV, 25 μF, 200 Ω, using the Gene Pulser Electroporater (Bio-Rad). Transformants were selected on LB agar plates containing 50 μg/ml gentamicin. The mCherry expression in PAO1 was confirmed via fluorescence measurements at 580 nm (ex) and 610 nm (em).

2.11 Microscopic characterization of bacterial biofilm associated with N/TERT skin

2.11.1 H&E staining

The filter insets containing N/TERT skin and MRSA or *P. aeruginosa* biofilm were sandwiched between two foam biopsy pads (ThermoFisher Scientific) in a tissue embedding cassette (Sigma-Aldrich), fixed in 10% neutral-buffered formalin for 24 hours, then transferred to 70% ethanol for storage. H&E staining was performed by Wax-it Histology Services Inc. and images were analyzed using the Aperio ImageScope software v12.4.0.5043 (Leica Biosystems).

2.11.2 Scanning Electron Microscopy (SEM)

Following MRSA-*lux* and PAO1-*lux* biofilm formation and DJK-5 treatment, the skin inserts were transferred to a fresh 12 well plate, washed twice with PBS and submerged in 10% neutral-buffered formalin to fix the skin samples. The following day, the formalin was decanted and the fixed samples were washed in fresh buffer, dehydrated through a graded ethanol series (30, 50, 70, 80, 90, 95, 100%) and critical-point dried (Tousimis Autosamdri 815B) over a period of 24 hours. Samples were sputter-coated (Cressington 208HR) with 10nm AuPd. All SEM samples of 1-day old biofilms on skin were prepared twice, while samples of 3-day old biofilms and burned skin were prepared once. Images shown are representative of the 3 to 10 images collected for each sample. SEM images were collected on a Hitachi S2600 Variable Pressure SEM (Hitachi, Ltd.) or a Hitachi S-4700 Field Emission SEM (Hitachi, Ltd.).

2.11.3 Confocal Laser Scanning Microscopy

Skin bacterial biofilms were grown for 24 hours using either MRSA-FarRed or *P. aeruginosa* PAO1-mCherry. The samples were rinsed with DPBS and then stained for 10 minutes with CellMask Green plasma membrane stain (Thermo Fisher Scientific) according to the manufacturer's instructions. Samples were then fixed for 10 minutes in 10% formalin followed by three rinses in

DPBS. All samples were stored at 4°C and imaged within one week of harvesting. Confocal imaging was performed on a Zeiss LSM 800 Microscope equipped with a 20x/0.8 Plan-APOCHROMAT objective (Carl Zeiss Canada Ltd.). Images were captured with the Zen software package (v2.6) and Z-stack images were analyzed in the Fiji software package [236].

2.12 N/TERT keratinocyte cell culture

N/TERT keratinocyte cells were kindly provided by Dr. Peter Nibbering (Leiden University Medical Center), Dr. Ivan Litvinov (McGill University) and Dr. Anna Mandinova (Massachusetts General Hospital), with permission from Dr. James Rheinwald (Harvard Medical School). N/TERT cells were maintained below 40% confluency in Keratinocyte-SFM medium supplemented with 25 μg/ml Bovine Pituitary Extract, 0.2 ng/ml human recombinant Epidermal Growth Factor 1-53 and 0.3 mM $CaCl_2$ (Thermo Fisher Scientific) at 37°C and 7.3% CO_2. Culture medium was refreshed every 2-3 days until ready for passage.

2.13 Generation of the N/TERT epidermal skin

Skin models were established using a modification of described methods [237]. Briefly, 3 x 10^5 N/TERT cells in 400 μl DermaLife K Keratinocyte Complete Medium (Lifeline Cell Technology) with LifeFactors (5 μg/ml rh Insulin LifeFactor, 6 mM L-Glutamine LifeFactor, 1 μM Epinephrine LifeFactor, 5 μg/ml Apo-Transferrin LifeFactor, 0.5 ng/ml rh TGF-α LifeFactor, 0.4% Extract P LifeFactor, 100 ng/ml Hydrocortisone Hemisuccinate LifeFactor) were seeded onto each filter insert (ThinCert™ Cell culture insert, Greiner bio-one) in a 12-well ThinCert™ Plate (Greiner bio-one) holding 4.1 ml/well DermaLife K Keratinocyte Complete Medium with LifeFactors below each filter. Medium was refreshed every second day until N/TERT cells reached confluency in 3-4 days. Culture medium both on top and below the filter were then switched to the skin differentiation medium: DMEM/Ham's F-12/CnT-Prime 3D Barrier Media in a 3:1:4 ratio supplemented with 0.1 μg/ml hydrocortisone, 0.125 μg/ml isoproterenol, 0.25 μg/ml bovine insulin, 26.5 pM selenious acid, 5 mM L-serine, 5 μM L-carnitine, 1.6 mg/ml BSA, 25 μM palmitic acid, 15 μM linoleic acid and 7 μM arachidonic acid. Medium on top of the filters was removed the next day to allow air-exposure, which induced differentiation and stratification of the epidermis. After 2-3 days, linoleic acid concentration was increased to 30 μM. The skin samples were cultured for 10 days at air-liquid interface at 37°C and 7.3% CO_2 with medium being refreshed every 2-3 days.

2.14 Biofilm growth and peptide treatment in the N/TERT epidermal skin model

2.14.1 Antibiofilm activity of DJK5

To establish biofilm on the N/TERT epidermal skin, 1 x 10^6 CFU (5 µl of 2 x 10^8 CFU/ml) MRSA or PAO1, or luminescent MRSA-*lux* or PAO1-*lux*, or fluorescently tagged MRSA-FarRed or PAO1-mcherry resuspended in PBS were seeded in the center of the skin model and cultured at 37°C and 7.3% CO_2. One day or three days after inoculation, 30 µl of 0.1% (1 mg/ml) or 0.4% (4 mg/ml) DJK-5 peptide was added on top of the biofilm for 4 hours. To visualize biofilms, skin samples seeded with luminescent bacteria were imaged using the ChemiDoc Imaging System (Bio-Rad) before and after peptide treatment. To quantify bacterial counts, skin samples, together with the filter inserts, were excised using a disposable scalpel (VWR), sonicated in 1.5 ml PBS for 5 minutes, vortexed, serially diluted, and plated on LB agar plates. The cut-off of the Y-axis in Figure 17-19,21-22 indicates the detection limit of CFU count while bars indicate the geometric mean of recovered CFU.

2.14.2 Screening for novel antibiofilm peptides

One million (5 µl of 2 x 10^8 CFU/ml) luminescent MRSA-*lux* or PAO1-*lux* resuspended in PBS were seeded in the center of the skin model and cultured at 37°C and 7.3% CO_2 for 24 hours to establish skin biofilm. One day after inoculation, 30 µl of 0.1% (1 mg/ml) peptides listed in Table 2 was added on top of the biofilm for 4 hours. Thirty microliters of antibiotics fusidic acid or gentamicin at 0.1%, 0.5% or 2% were used as positive antibiofilm controls for MRSA-*lux* or PAO1-*lux* biofilm, respectively. To qualitatively determine peptide efficacy, bioluminescence from skin biofilm was imaged using the ChemiDoc Imaging System (Bio-Rad) before and after peptide or antibiotics treatment. Bacterial burden on each skin sample was quantified by serial dilution and plating on LB agar plates.

2.15 MRSA USA300 thermal wounding epidermal skin model

Thermal damage was created by applying a digital soldering iron (FX888D, American Hakko Products, Inc.) to 10-day air-liquid interface skins at 100°C for 4 seconds. The skin filter inserts were transferred to 12-well plates (Sigma-Aldrich) containing 800 µl/well fresh culture medium prior to bacterial infection. MRSA biofilm was established by seeding 2 x 10^6 CFU in 5 µl PBS on top of the thermally damaged skin and cultured at 37°C and 5% CO_2 for 24 hours. DJK-5 peptide (30 µl of 0.4%) alone or in combination with 0.01%, 0.1% or 0.4% 1002 was administered on top of the pre-formed biofilm. Skin samples were collected 24 hours post peptide treatment for colony count. Culture supernatants below the skin filter inserts were harvested for measuring cytotoxicity by the

Lactate dehydrogenase assay using a Cytotoxicity Detection Kit (Roche Diagnostics), according to the manufacturer's instructions. Untreated skin samples or skin samples treated with 5% Triton X-100 was used as negative (0% toxicity) or positive (100% toxicity) control, respectively. Culture supernatants were also used to measure IL-1β and IL-8 production using ELISA kits from eBioscience.

2.16 MRSA USA300 thermal wounding *ex vivo* skin model

The surplus human skin experimental protocol (H18-000657) was approved by the UBC Clinical Research Ethics Board and the College of Physicians and Surgeons of British Columbia. Healthy breast surplus skin samples (3-5 mm in thickness) were collected from consenting healthy donors (age 19-45) post-breast reduction surgery. Skin was rinsed 3 times with PBS and cut into 8 mm biopsies. The apical side of the skin was thermally injured with a digital soldering iron at 150°C for 10 seconds. A reservoir for infection and treatment was created by building a barrier surrounding the skin containing the burn wound with a light-curing dental liquid dam (Ultradent), followed by 4 seconds of Ultraviolet light fixation. Skin with treatment reservoir was cultured at the air-liquid interface on a metal wire rack with 3.2 ml of the skin differentiation medium (full ingredients listed in 2.13) underneath. MRSA biofilm was established by seeding 2 x 10^6 CFU USA300 in 3 µl TSB with 1% glucose on top of the thermal damaged skin and cultured at 37°C and 5% CO_2 for 24 hours. Skin biofilm was treated with 5 µl 0.1% or 0.4% DJK-5, D-3006, D-3007 or fusidic acid (Sigma-Aldrich) for 4 hours and then collected for colony count and H&E staining by Wax-it histology Inc.

2.17 RNA extraction

2.17.1 PMA-induced mouse ear inflammation model

Mouse ear biopsies (5 mm in diameter) were taken from fifteen mice 6 hours post-treatment, including: 1) five vehicle control mice (20 µl acetone and 20 µl 50% ethanol); 2) four PMA-treated mice (20 µl 125 µg/ml PMA and 20 µl 50% ethanol); and 3) six PMA and IDR-1002 co-treated mice (20 µl 125 µg/ml PMA and 20 µl 30 mg/ml IDR-1002). Ear biopsies were harvested and immediately submerged in 800 µl RNA*later* RNA stabilization solution (ThermoFisher Scientific) and stored at -80°C until RNA isolation. Total RNA from each sample was extracted using the RNeasy Mini Kit (Qiagen) following manufacturer's protocol. For quality control, 1 µl of each sample was run on the Agilent 2100 Bioanalyzer using the Eukaryotic Total RNA Nano Chip (Agilent Technologies).

2.17.2 MRSA USA300 thermal wounding epidermal skin model

N/TERT epidermal skin was collected from 4 treatment groups, namely: 1) untreated skin control; 2) burned skin control (skin thermally challenged at 100°C for 4 seconds); 3) burned skin with MRSA biofilm (burned skin spotted with 2 x 10^6 CFU MRSA USA300 for 24 hours then treated with 30 µl PBS for 24 hours); and 4) burned skin with MRSA biofilm and DJK-5 treatment (burned skin with 24 hours MRSA USA300 biofilm then treated with 30 µl of 0.4% DJK-5 for 24 hours). Skin models were excised from the ThinCert™ Cell culture insert (Greiner bio-one) using a disposable scalpel and immediately submerged in 800 µl RNA*later* RNA stabilization solution (ThermoFisher Scientific), stored at 4°C overnight and then transferred to -80°C until RNA isolation. To harvest enough RNA for RNA-Seq analysis, three skin models with the same treatment were pooled into one sample before RNA extraction. Total RNA was extracted from four pooled samples per treatment group using the RNeasy Micro Kit (Qiagen) following the manufacturer's protocol. For quality control, 1 µl of each sample was run on the Agilent 2100 Bioanalyzer using the Eukaryotic Total RNA Nano Chip (Agilent Technologies).

2.18 RNA-Seq library preparation

To construct libraries, 1-2 µg of each RNA sample was used. Poly-A tailed RNA enrichment was done using the Magnetic mRNA Isolation Kit (New England Biolabs). Complementary DNA library preparation was done using the Kapa Stranded Total RNA Kit (Kapa Biosystems). In brief, mRNAs were enzymatically fragmented followed by first and second strand complementary DNA synthesis. Overhangs were repaired and adenylated to produce blunt ends and unique indices were ligated onto the 5' end. DNA libraries were amplified by polymerase chain reaction followed by cleaning and size selection using the AMPure XP kit (Agencourt). DNA samples were quantified using the Quant-iT™ dsDNA Assay Kit (ThermoFisher Scientific) and normalized to 4 nM.

2.19 RNA-Seq analysis

2.19.1 PMA-induced mouse ear inflammation model

Mouse RNA-Seq libraries were sequenced on HiSeq 2500 sequencer (Illumina) using the High Output mode at the University of British Columbia Sequencing Centre. Sequenced data quality control was performed using FastQC v0.11.5 and MultiQC v0.8.dev0 [238]. Sample libraries were then aligned to mouse genome Ensembl GRCm38 [239] using STAR v2.5 [240]. The median of uniquely mapped reads was about 6 million/sample. A read count table was generated using HTSeq-count v0.6.1p1 [241] and genes that had lower than 10 counts were removed. Differential expression analysis

was performed using DESeq2 v1.14.0 [242]. Pathway enrichment was carried out using Sigora v2.0.1 [243] and network analysis was done by NetworkAnalyst [244]. The genes in various inflammatory pathways were downloaded from InnateDB [245]. In RNA-Seq analysis, the cut-off used for differentially expressed genes was set to be at ≥ ±2-fold with a p-value adjusted for multiple testing of ≤0.05. Statistical analysis for pathway enrichment was performed by the hypergeometric test and corrected for multiple comparisons by Bonferroni's method with a p-value cut-off of ≤0.001.

2.19.2 MRSA USA300 thermal wounding skin model

N/TERT skin RNA-Seq libraries were sequenced on a HiSeqX sequencer (Illumina) at Canada's Michael Smith Genome Sciences Centre (GSC) at BC Cancer Agency. Sequenced data quality control was performed using FastQC [246] v0.11.8 and MultiQC v1.8 [238]. Sample libraries were then aligned to the human reference genome, Ensembl GRCh38 v98 [239] using STAR v2.7.3a[240]. Uniquely mapped reads had a minimum of 12.3 million, median of 29.5 million, and a maximum of 47.6 million. A read count table was generated using HTSeq-count v0.11.2 [241] and genes that had fewer than 10 counts across the four biological replicates were removed. Differentially expressed (DE) gene analysis was performed using DESeq2 v1.28.1, and DE genes were included if they had an absolute fold change value of ≥ 1.5 and adjusted p-value ≤ 0.05 [242]. Reactome [247] pathway enrichment of DE genes was performed using Sigora v3.0.5, with significance defined as a Bonferroni-corrected p-value ≤ 0.001 [243]. Network analysis was done by uploading genes and their respective fold change values to NetworkAnalyst for construction of protein-protein interaction networks [244].

2.20 Statistical analysis

Statistical significance was determined using GraphPad Prism Version 8.0.2. Unless otherwise stated, comparison between two groups was performed using the Student's unpaired *t*-test, and comparison among multiple groups was performed using the one-way analysis of variance (ANOVA) followed by Dunnett's multiple comparisons test. For analyzing bacterial colony counts, non-parametric tests were used. Specifically, comparisons between two groups were determined using the Mann-Whitney test, and comparisons among multiple groups were performed using the Kruskal–Wallis test with Dunn's multiple comparisons test. Statistical significance was reported using the following cut-offs: * p-value ≤ 0.05; ** p-value ≤ 0.01; *** p-value ≤ 0.001; **** p-value ≤ 0.0001.

Chapter 3: IDR-1002 as Treatment for Sterile Skin Inflammation

3.1 Introduction

Dysregulated inflammation is a well-known pathological factor at the root of many human disorders and represents a major threat to human health and welfare [248]. HDPs and IDRs possess encouraging therapeutic potential due to their ability to modulate the immune response to increase protective immunity while dampening inflammation [193,194].

Peptide IDR-1002 was initially selected from a library of bactenecin derivatives based on its enhanced ability to induce chemokines from human peripheral blood mononuclear cells, which correlated with protection against *S. aureus* and *E. coli* infections *in vivo* [249]. IDR-1002 was also able to effectively dampen proinflammatory cytokine induction in response to inflammatory agonists *in vitro* [202,250,251]. Previous research has demonstrated that IDR-1002 can significantly suppress LPS-mediated neutrophil degranulation and the release of ROS [252]. IDR-1002 can also control immune-mediated inflammation in synovial fibroblasts, a key cell type in rheumatoid arthritis, by dampening the IL-1β response while promoting IL-1Ra and IL-10 production [250]. The suppressive effect of IDR-1002 on IL-1β-induced inflammation is achieved in part by down-regulating the activation of p50 NF-κB, JNK and p38 MAPK [250]. The dual effect of IDR-1002 has also been observed in LPS-stimulated macrophages where the peptide dampens the inflammatory response by inhibiting NF-κB nuclear translocation while activating p38 MAPK/ERK1/2–MSK1-dependent CREB phosphorylation [251]. IDR-1002 thus represents a potential anti-inflammatory and anti-infective therapeutic candidate due to its ability to dampen excessive inflammation without compromising the ability of the immune system to fight infections. Despite the promising anti-inflammatory activities of IDR-1002 observed during bacterial infection, its role in controlling sterile inflammation has not been well characterized *in vivo*. The aim of Chapter 3 was to study the anti-inflammatory effect and underlying meshiams of IDR-1002 in sterile skin inflammation.

3.2 IDR-1002 peptide dampened LPS, LTA and zymosan-induced inflammatory responses in RAW 264.7 cells

Initial studies on the anti-inflammatory effect of IDR-1002 were carried out *in vitro* using RAW 264.7 murine monocyte/macrophage cells challenged with TLR4 agonist LPS and TLR2 agonists LTA and zymosan. LPS and LTA triggered TNF-α, IL-6 and nitric oxide production in a dose-dependent manner whereas zymosan only induced a TNF-α response 24 hours post-stimulation (Figure 5a-c).

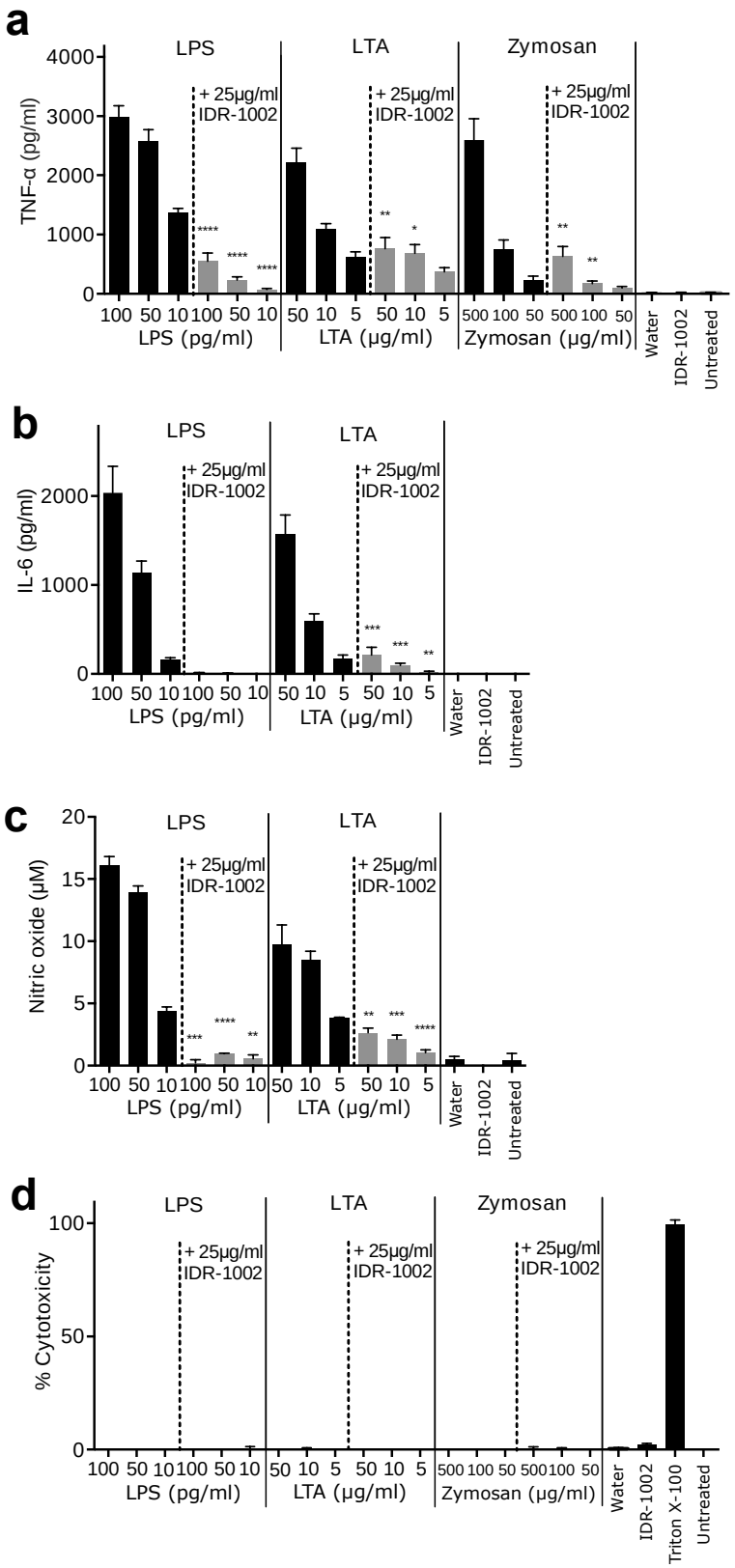

Figure 5. IDR-1002 dampened LPS, LTA and zymosan-induced inflammatory responses in RAW 264.7 cells.

RAW 264.7 cells were treated with different concentrations of LPS, LTA and zymosan in the absence

or presence of 25 μg/ml IDR-1002. Culture supernatants were harvested 24 hours post-treatment. The concentrations of TNF-α (**a**) and IL-6 (**b**) were determined by ELISA, and the concentration of nitric oxide (**c**) was quantified by the Griess assay. (**d**) Cytotoxicity was determined using the lactate dehydrogenase assay. Supernatants from untreated RAW 264.7 cells or RAW 264.7 cells lysed with 2% Triton X-100 were used as negative (0% toxicity) or positive (100% toxicity) controls, respectively. Data shown was an average of 5 independent replicates and error bars were calculated as the standard error of the mean. Statistical analysis comparing peptide treated or untreated RAW 264.7 cells challenged with the same concentration of each stimulus was performed using Student's unpaired t test (* $p \leq 0.05$; ** $p \leq 0.01$; *** $p \leq 0.001$; **** $p \leq 0.0001$).

The addition of 25 μg/ml IDR-1002 led to significant suppression of LPS, LTA (at 50 and 10 μg/ml) and zymosan (at 500 and 100 μg/ml) induced TNF-α production. IDR-1002 also significantly dampened IL-6 and nitric oxide production triggered by LPS and LTA. In particular, 25 μg/ml IDR-1002 completely abolished the LPS-induced IL-6 response. Neither the stimuli nor peptide treatment were cytotoxic towards RAW 264.7 cells as determined using the Lactate Dehydrogenase assay (Figure 5d).The anti-inflammatory activity of IDR-1002 occurred at even lower concentrations and 5 μg/ml caused a 77% decrease in LPS-stimulated TNF-α production by RAW 264.7 cells, consistent with previous data on human cells [202]. These results confirmed and extended previous data [202,250,251] indicating that IDR-1002 peptide effectively suppressed sterile inflammatory responses *in vitro*. PMA was also tested as an inflammatory stimulus, however this agent was quite toxic *in vitro*, and did not trigger TNF-α, IL-6 and nitric oxide production within the concentration range (≤ 1 μg/ml) that was non-toxic to RAW 264.7 cells.

3.3 IDR-1002 suppressed the production of pro-inflammatory cytokine and chemokines *in vivo*

To investigate the anti-inflammatory activity of IDR-1002 on sterile inflammation *in vivo*, I utilized the well-established PMA-induced mouse ear inflammation model. The topical administration of 20 μl 125 μg/ml PMA onto the ears of female CD-1 mice caused a strong inflammatory reaction as revealed by a nearly 3-fold increase in ear thickness and biopsy weight when compared to ears treated with vehicle control or peptide control. PMA also triggered strong production of proinflammatory cytokine IL-6 [243 ± 71 pg/ml (mean ± SD)], and chemokines MCP-1 (1718 ± 474 pg/ml) and CXCL-1 (849 ± 286 pg/ml) in the ear tissue. The effect of IDR-1002 treatment was evaluated by applying 0.6 mg/ear or 0.3 mg/ear peptide topically onto one ear of each mouse immediately after PMA challenge. Matching doses of the nonsteroidal anti-inflammatory drug indomethacin were used as positive controls, while the addition of vehicles (solvents) served as negative controls and were also applied topically after PMA treatment.

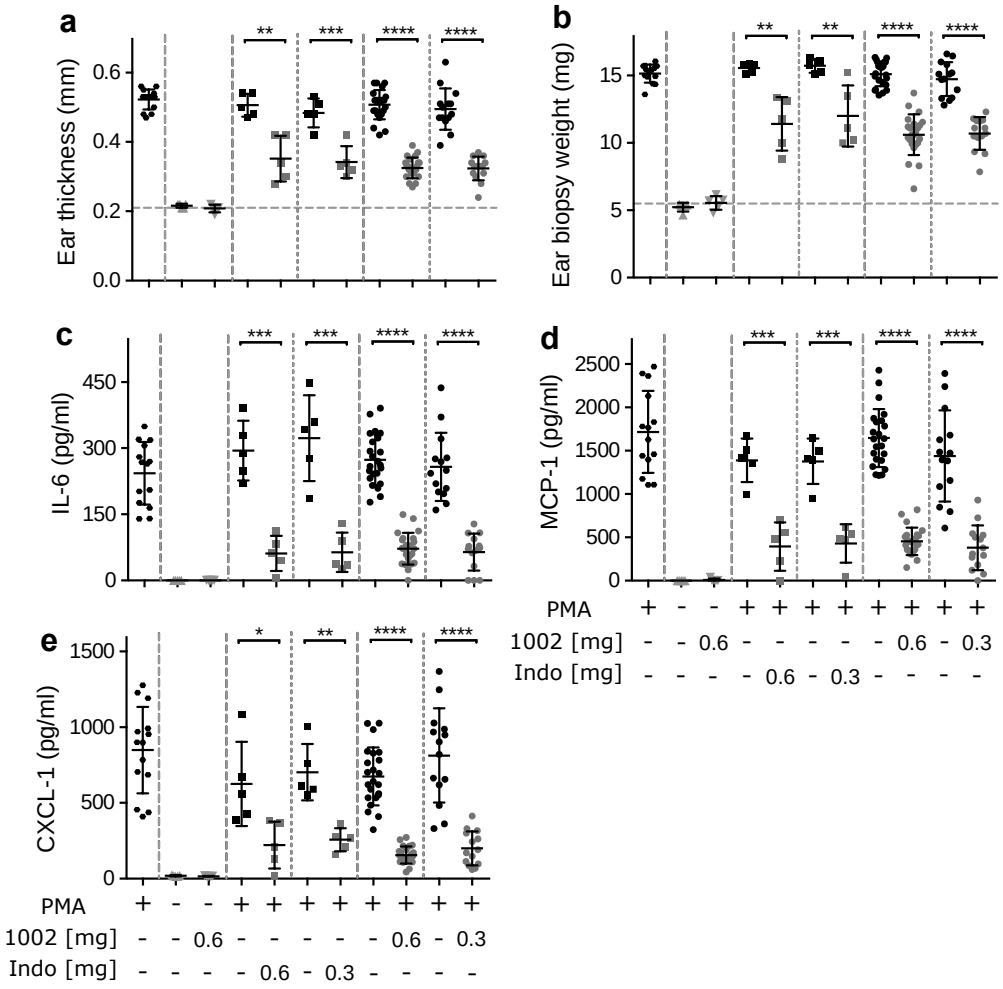

Figure 6. IDR-1002 suppressed PMA-induced ear edema and the production of pro-inflammatory cytokine and chemokines in PMA-inflamed ear tissue.
Ears of CD-1 mice were treated topically with 20 μl of 125 μg/ml PMA. Either 0.6 mg/ear or 0.3 mg/ear IDR-1002 was administered onto one ear of each mouse immediately after PMA treatment. Indomethacin (Indo) at a dose of 0.6 mg/ear or 0.3 mg/ear was used as positive anti-inflammatory control and was also applied topically onto one ear of each mouse post-PMA treatment. The contralateral ears were given the same volume of the vehicle/solvent. Mice were euthanized 6 hours post-PMA treatment and increases in ear thickness (**a**) and ear weight (**b**) were quantified. Ear biopsy was collected and homogenized for IL-6 (**c**), MCP-1 (**d**) and CXCL-1 (**e**) measurement using ELISA. Student's unpaired t test (* $p \leq 0.05$; ** $p \leq 0.01$; *** $p \leq 0.001$; **** $p \leq 0.0001$).

At 6 hours post-treatment, IDR-1002 significantly ($p<0.0001$) suppressed the increase in ear thickness and ear weight induced by PMA to an extent equivalent to that by the positive control indomethacin (Figure 6a-b). Peptide treatment also consistently and significantly ($p<0.0001$) dampened the production of IL-6, MCP-1 and CXCL-1 in the ear tissue (Figure 6c-e). PMA caused only modest changes in serum cytokine levels and neither indomethacin nor peptide IDR-1002 significantly altered the cytokine levels in mouse serum at 6 hours (Appendix Figure A1a, c, e).

The anti-inflammatory effect of IDR-1002 on ear inflammation was also measured at 24 hours

post PMA-treatment (Figure 7). IDR-1002 treatment led to suppression of ear tissue edema almost to the level of the vehicle-treated control suggesting resolution of inflammation within 24 hours (Figure 7a-b). In addition, peptide treatment completely inhibited the production of IL-6, MCP-1 and CXCL-1 in the ear tissue (15 mice per peptide concentration; Figure 7c-e). Similar to the 6-hour treatment, IDR-1002 by itself did not significantly alter cytokine and chemokine levels in the mouse serum 24 hours post-PMA treatment (Figure A1b, d, f). These results indicated that a single IDR-1002 topical treatment suppressed PMA-induced acute inflammation by downregulating proinflammatory cytokine production at early stages of inflammation and resolving local inflammation within 24 hours.

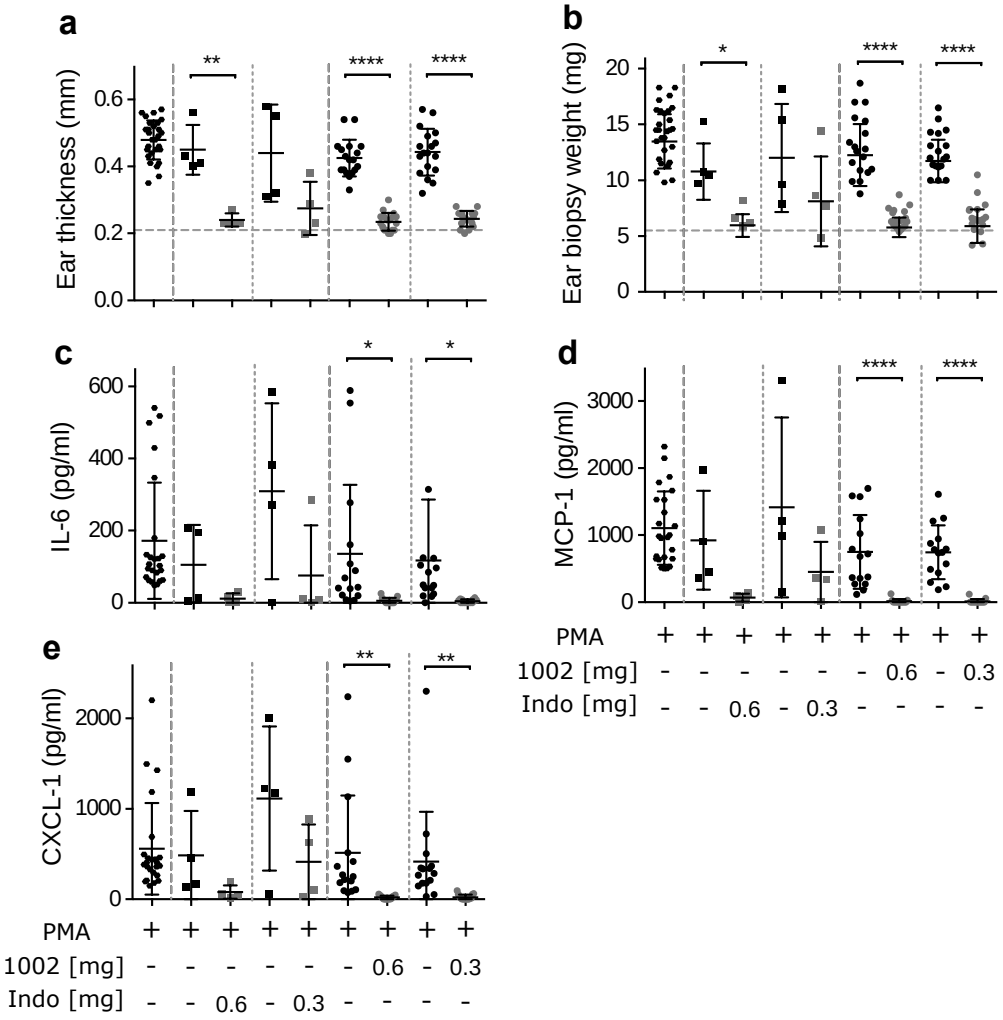

Figure 7. By 24 hours, IDR-1002 almost completely suppressed PMA-induced ear edema and the production of pro-inflammatory cytokine and chemokines in PMA-inflamed ear tissue.
Ears of CD-1 mice were treated as mentioned in Figure 6. Mice were euthanized 24 hours post-PMA treatment and increases in ear thickness (**a**) and ear weight (**b**) were quantified. Ear biopsy was collected and homogenized for IL-6 (**c**), MCP-1 (**d**) and CXCL-1 (**e**) measurement using ELISA. Student's unpaired t test (* $p \leq 0.05$; ** $p \leq 0.01$; **** $p \leq 0.0001$).

3.4 IDR-1002 dampened the production of ROS/RNS and attenuated neutrophil infiltration *in vivo*

The overproduction of ROS and RNS can induce oxidative and nitrosative stress responses, which contribute a variety of pathological processes including inflammatory diseases [253]. I investigated whether PMA triggered these responses and whether IDR-1002 could dampen ROS/RNS production by subcutaneous injection of a luminescent probe L-012 that allows the visualization of ROS/RNS [228,254]. PMA led to potent induction of local ROS/RNS production (Figure 8a) while administration of vehicle or IDR-1002 on the contralateral ear led to no induction of these species. IDR-1002 treatment at both doses (0.6 mg/ear and 0.3 mg/ear) dampened the production of ROS/RNS in the PMA-inflamed ear tissue as shown by substantially diminished luminescence signals after *in vivo* imaging (Figure 8a).

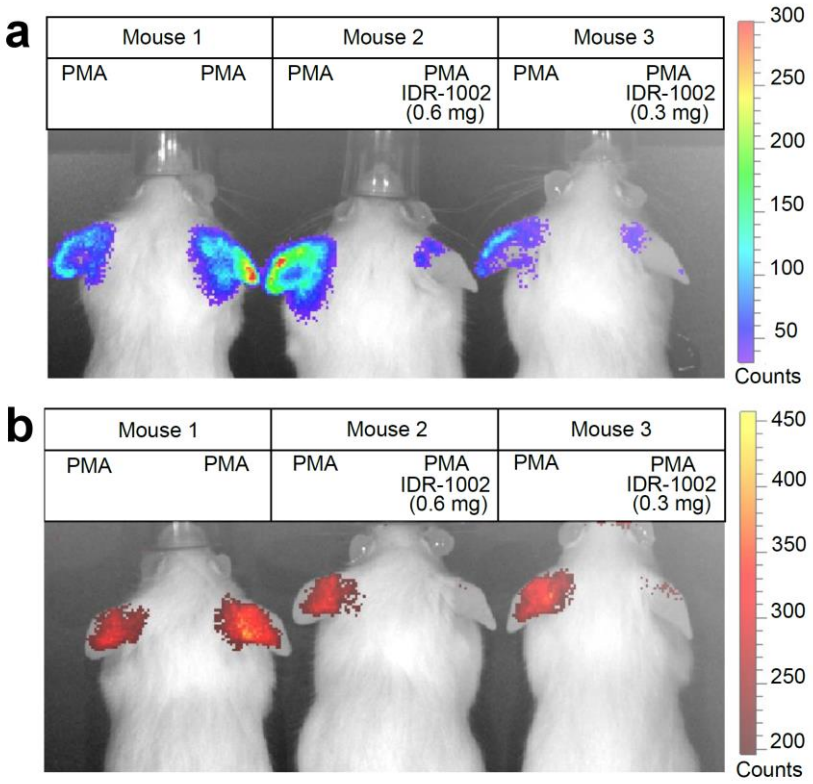

Figure 8. IDR-1002 dampened the production of reactive oxygen and nitrogen species and attenuated neutrophil infiltration in the PMA-inflamed ear tissue.
Ears of CD-1 mice were treated topically with IDR-1002 and/or 20 µl of 125 µg/ml PMA. *In vivo* imaging was performed 6 hours post-treatment. To visualize reactive oxygen and nitrogen species production, mice were injected with the luminescent probe L-012 (Wako Chemical; 25 mg/kg) subcutaneously and imaged using the IVIS Spectrum 20-30 minutes post-injection (**a**). To detect neutrophil recruitment, mice were injected with the Neutrophil-Specific, NIR fluorescent probe (Kerafast; 0.4 mg/kg) intravenously and imaged using the IVIS Spectrum (**b**).

Since neutrophils are one of the dominant cell types mediating acute PMA-induced inflammation and a major source of ROS [255,256], I also monitored neutrophil levels by *in vivo* imaging using the NIR fluorescent probe, a cyanine7-conjugated, polyethylene glycol-modified hexapeptide that binds specifically to the formylpeptide receptor of neutrophils [257]. PMA caused a strong local (ear tissue) neutrophil influx after 6 hours, which was almost completely attenuated by peptide treatment (Figure 8b).

3.5 IDR-1002 reduced PMA-induced ear edema and modulated immune cell composition *in vivo*

Since increases in ear thickness, weight and redness were triggered by topical PMA treatment, H&E staining was used to further study ear edema and the effect of IDR-1002 on tissue structure and immune cell composition (Figure 9).

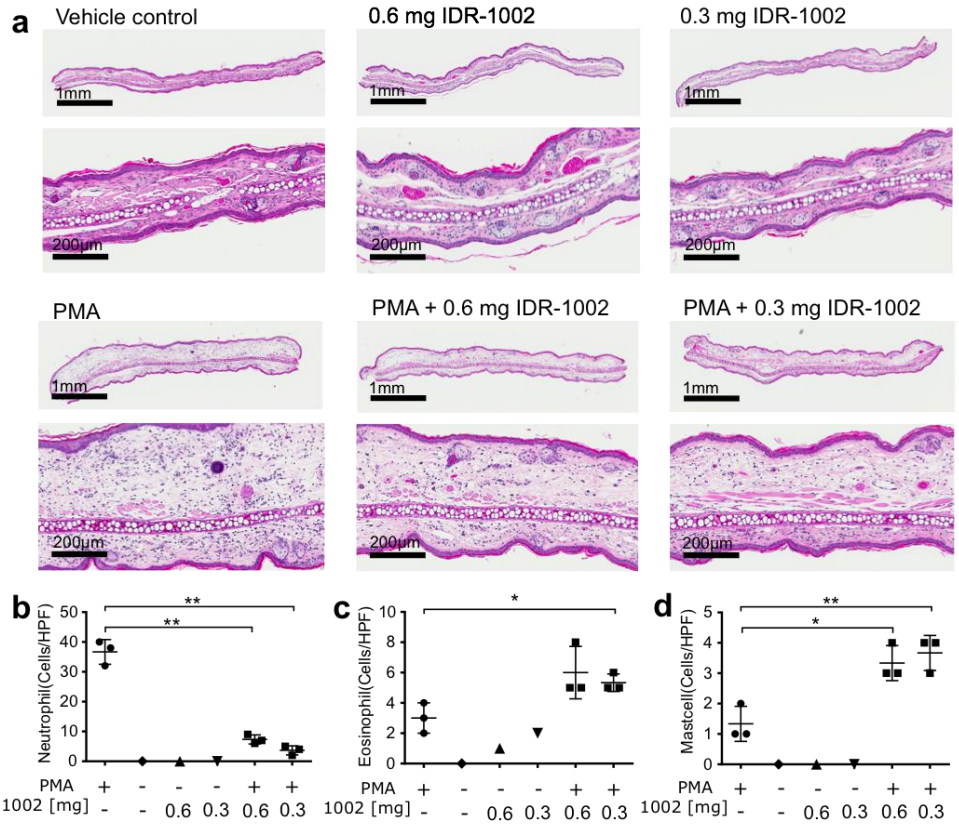

Figure 9. IDR-1002 reduced PMA-induced ear edema and attenuated neutrophil recruitment in the PMA-inflamed ear tissue.
Ears of CD-1 mice were treated topically with IDR-1002 and/or 20 μl of 125 μg/ml PMA. Mice were euthanized 6 hours post-PMA treatment and ear biopsy were collected and fixed in 10% neutral buffered formalin. H&E staining was performed on ear tissue cross sections by Wax-it Histology Services Inc. (**a**). The numbers of immune cells per high power field (HPF) in the stained specimens (**b-d**) were quantified by a pathologist.

Compared to administration of the vehicle control or IDR-1002 alone, PMA treatment resulted in substantial thickening of the ear due to a massive recruitment of immune cells and accumulation of interstitial fluid in the dermal layer of the ear tissue. The suppressive effects of IDR-1002 on inflammation were seen by decreases in immune cell density and relative ear thickness (Figure 9a). The stained sections were scored by an independent pathologist. Consistent with the *in vivo* imaging results (Figure 8b), peptide treatment significantly decreased the number of neutrophils present in the PMA-treated ear tissue by up to 10-fold (Figure 9b). Interestingly, under inflammatory conditions, IDR-1002 treatment resulted in a nearly two-fold increase in eosinophils (Figure 9c) and a 2.5-fold increase in mast cells (Figure 9d). While these increases were modest (cf. eosinophilic esophagitis where the eosinophil counts can range from 1 to above 400 per HPF [258]), I was concerned that the appearance of these cells was associated with an allergic reaction. Therefore, I examined the levels of histamine in mouse ear tissue and serum. No significant changes of histamine levels were observed 15 minutes, 1 hour and 6 hours post-peptide treatment (Figure A2).

3.6 RNA-Seq analysis of IDR-1002 suppression of PMA-induced inflammation

To gain a more comprehensive understanding of the anti-inflammatory mechanism of IDR-1002, RNA-Seq analysis was performed on RNA samples extracted from mouse ear tissue at 6 hours post-treatment with vehicle, PMA alone or PMA followed immediately by IDR-1002. Genes were considered differentially expressed if they had an expression change of ≥±2-fold with an adjusted p-value ≤0.05. Pathway enrichment analysis using Sigora v2.0.1 [243] considered only those over-represented pathways with an adjusted p-value ≤0.001. PMA treatment induced tremendous transcriptomic changes with 2,270 upregulated genes and 2,048 downregulated genes as compared to vehicle control. The top upregulated pathways compared to vehicle control were inflammatory pathways involved in cytokine signalling (adjusted p-value 1.63×10^{-195}), especially IFN-γ (1.47×10^{-153}), TNF (4.28×10^{-21}) and IL-1 (6.62×10^{-17}) signalling, GPCR signalling such as class A/1 rhodopsin-like receptor cascade (1.88×10^{-63}) and chemokine receptor activation (3.50×10^{-150}), hemostasis (1.66×10^{-65}) and various receptor tyrosine kinases and TLR signalling pathways (Figure 10). Among these pathways, TNF-α and IL-1 responses have well-established roles in mediating sterile inflammation [118,259,260]. In addition, the IFN-γ pathway and integrin-mediated cell adhesion process were previously found to be essential for PMA-induced inflammation [261–264]. Pathways downregulated by PMA included those involved in WNT ligand biogenesis, trafficking (1.89×10^{-6}), and signalling (2.92×10^{-6}), which are known to orchestrate cell proliferation, differentiation and migration during skin organogenesis [265,266].

Figure 10. Pathways dysregulated by PMA-induced sterile inflammation with or without IDR-1002 treatment.
Pathway enrichment was carried out using Sigora v2.0.1. Statistical analysis was performed by hypergeometric test and multiple comparisons were corrected by Bonferroni's method with a p-value cut off ≤0.001. Red circles indicate upregulated pathways and green circles indicate downregulated pathways.

To characterize the mechanism of action of IDR-1002 on PMA-induced inflammation, I compared PMA challenge and IDR-1002 treatment to PMA challenge alone, and observed significant downregulation of chemokine receptors ($4.95x10^{-99}$) in the class A/1 rhodopsin-like GPCR family ($9.12x10^{-45}$), cytokine signalling ($7.58x10^{-21}$) especially IFN-γ ($3.15x10^{-38}$), and pattern recognition receptor cascades such as C-type lectin receptors ($2.60x10^{-13}$), TLR1-2 heterodimer ($4.21x10^{-5}$), and TLR10 ($3.30x10^{-5}$) (Figure 10). Consistent with the *in vivo* imaging and histology results indicating

that IDR-1002 attenuated PMA-induced immune cell infiltration, the signalling pathway involved in leukocyte extravasation (cell surface interactions at the vascular wall $4.57x10^{-71}$) was also substantially downregulated by IDR-1002. In contrast, genes function in WNT signalling ($4.32x10^{-4}$) were upregulated in the PMA-inflamed ear treated with IDR-1002 compared to PMA alone.

3.7 IDR-1002 downregulated a variety of class A/1 rhodopsin-like receptors functioning in inflammation

Class A/1 rhodopsin-like receptors are the major family of GPCRs and play important roles in the sensing and cellular communication processes of inflammation [267]. Therefore, I further probed the effect of IDR-1002 on the expression of chemokines and their receptors during sterile inflammation. PMA and IDR-1002 combined treatment compared to PMA challenge downregulated chemokine receptors and their ligands for neutrophils (e.g. Cxcr1, Cxcr2, Cxcl1, Cxcl2, Cxcl3 and Cxcl5), eosinophils (e.g. Ccl11), monocytes (e.g. Ccl7) and other chemokines attracting multiple cell types (e.g. Ccl3 and Ccl5) (Figure A3). In addition, class A/1 rhodopsin-like receptors recognizing other proinflammatory mediators such as prostaglandins (e.g. Ptger2 and Ptgir), histamine (e.g. Hrh2), platelet activating factor (e.g. Ptafr) and anaphylatoxin C3a (e.g. C3ar1) were also downregulated by IDR-1002. These results were consistent with the hypothesis that IDR-1002 acted by attenuating the migration and accumulation of inflammatory cells and controlled vascular endothelial permeability by modulating the expression of class A/1 rhodopsin-like receptors.

3.8 IDR-1002 dampened inflammation by suppressing an Irf8-regulated network

Irf8 is a transcription factor restricted primarily to hematopoietic cells, that often acts by associating with other transcription factors to modulate key inflammatory responses, including the IFN-γ response, TLR signalling and the expression of inducible nitric oxide synthase [268,269]. Comparing PMA and IDR-1002 combined treatment to PMA challenge, Irf8 was identified to be one of the central hubs in the zero-order protein-protein interaction network, interacting with 28 other transcriptionally dysregulated proteins (27 of which were upregulated by PMA and suppressed in the presence of IDR-1002 treatment) (Figure 11). These interactors included Tlr4, Tnf and Nlrp3, each of which play central roles in inflammatory signalling and cytokine production, as well as proteins involved in the recruitment (e.g. Ccl5, Ccl6 and Itga5) and function (e.g. Slc11a1/Nramp, Csf3r, and Ncf1) of inflammatory cells including macrophages and neutrophils [270–273]. Each of these 28 protein interactors have been previously shown to have Irf8 binding sites and are regulated by Irf8 and its transcription factor partners [274–277]. For example, Irf8 works in cooperation with transcription factors

Irf1, NFκB and PU.1 to promote chemokine Ccl5 expression in response to IFN-γ and LPS [275]. Irf8 and Irf1 are also involved in IFN-γ-induced TNF-α expression [277]. Furthermore, Irf8 participates in the transcriptional regulation of the LPS-induced TLR4 cascade and the cross-talk between TLR4 signalling and the IFN-γ response [268,276]. Since Irf8 plays a critical role in upregulating inflammation in cooperation with various transcription factors, I propose that IDR-1002 acts to control a variety of inflammatory responses by suppressing the induction of Irf8 and its target genes such as Ccl5, TNF and TLR4. These results thus provided key insights to the anti-inflammatory mechanism of IDR-1002.

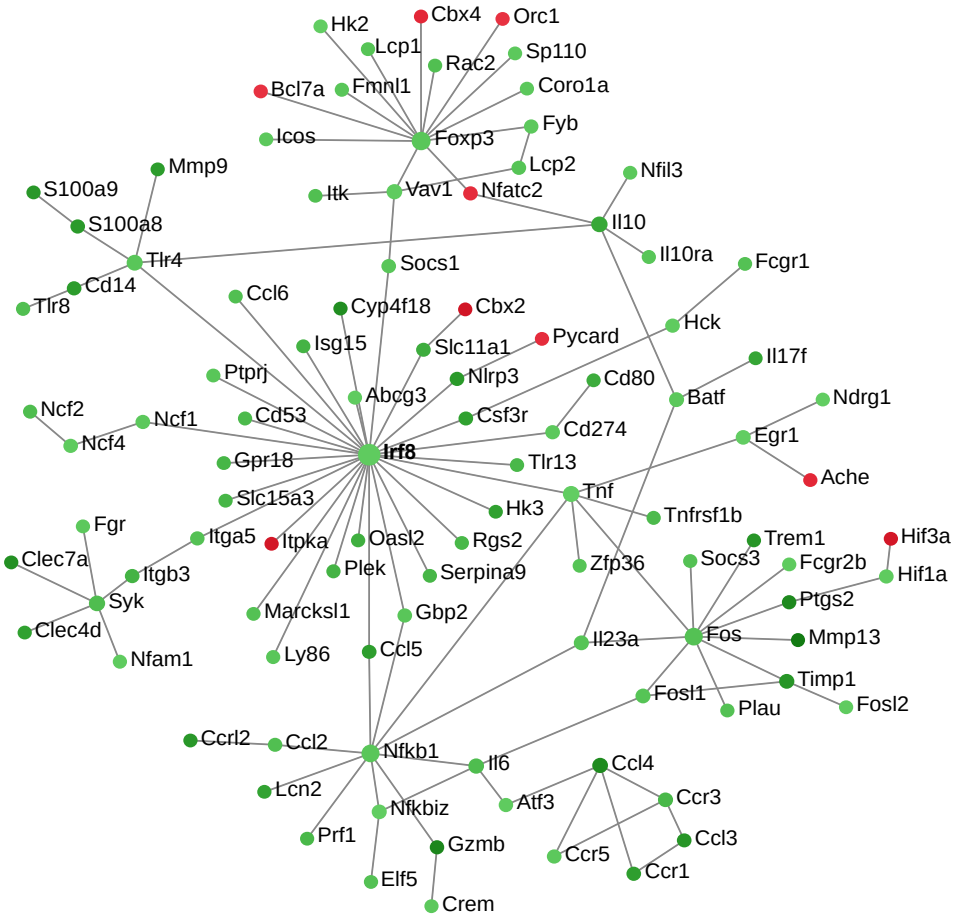

Figure 11. Network analysis of IDR-1002 suppression of PMA-induced ear inflammation. Zero order protein-protein interaction network comparing PMA and IDR-1002 combined treatment to PMA challenge alone using NetworkAnalyst. Red nodes denote upregulation and green nodes denote downregulation.

3.9 Discussion

Peptide IDR-1002 has been demonstrated to promote *in vivo* protective innate immunity to infections, dampen proinflammatory cytokine responses to inflammatory agonists and promote protective adaptive immunity as a component of adjuvant formulations [202,204,249–252]. Here I

investigated the ability of IDR-1002 to antagonize sterile inflammation.

The *in vitro* studies were carried out using mouse monocytic RAW 264.7 cells where I showed that IDR-1002 significantly suppressed LPS and LTA-induced TNF-α, IL-6 and nitric oxide production as well as the zymosan-induced TNF-α response (Figure 5a-c) without harming RAW 264.7 cell membrane integrity (Figure 5d). Previous studies showed that IDR-1002 reduced the LPS-induced inflammation in human peripheral blood mononuclear cells [202]. The observation here that IDR-1002 reduced TLR4 and TLR2 agonist-induced inflammation was consistent with this finding and extended the scope of inflammatory agonists that IDR-1002 could antagonize.

To further investigate the anti-inflammatory activities of IDR-1002 *in vivo*, I used the PMA-induced mouse ear inflammation model, a well-established model for screening the activities of many anti-inflammatory drugs [278]. PMA treatment induced strong inflammatory responses as observed by increases in ear thickness, ear weight and proinflammatory cytokine production locally (in ear tissue) and, to a limited extent, systemically (in serum). Topical IDR-1002 treatment suppressed proinflammatory cytokine production in the PMA-inflamed ear tissue at 6 hours post-treatment (Figure 6) and completely inhibited PMA-induced IL-6, MCP-1 and CXCL-1 production locally within 24 hours (Figure 7). This anti-inflammatory effect was comparable to the NSAID indomethacin. Critically, indomethacin acts via a completely different mechanism i.e., through potent, nonselective inhibition of the enzyme cyclooxygenase, thereby limiting the production of prostaglandins. In addition, indomethacin is a potent anti-inflammatory agent with many serious side effects. For example, indomethacin increases the risk of cardiovascular thrombotic events, gastrointestinal ulceration and skin rashes [279,280]. In particular, neutrophils and reactive oxygen species have been reported to play crucial roles in the development of indomethacin-induced gastric mucosal injury [281]. IDR-1002 peptide was previously shown to modulate neutrophil degranulation, adhesion and ROS production *in vitro* [252]. Using *in vivo* imaging techniques, I was able to monitor real-time ROS/RNS levels. The imaging results showed that IDR-1002 could effectively dampen the production of ROS/RNS, likely by attenuating neutrophil infiltration (Figure 8). The reduction of the neutrophil population in the PMA-inflamed ear tissue was confirmed by a histology study where peptide treatment significantly decreased the number of neutrophils per HPF (Figure 9). Interestingly, although H&E staining indicated an increase in the eosinophil and mast cell density, this was not accompanied by increases in histamine release (Figure A2), a deleterious effect observed for several other HDPs including hBD-2 and LL-37 [282]. Together, these results demonstrate a potential advantage of IDR-1002 as an anti-inflammatory drug candidate.

Using RNA-Seq analysis, the global transcriptomic changes were studied, avoiding bias towards specific pathways and oversimplification of the biological outputs. Pathway analysis revealed that multiple pathways were significantly upregulated in the PMA treated ear tissue (Figure 10). These include IFN-γ, TNF and IL-1 cascades, which are at the core of many autoinflammatory and autoimmune disorders such as systemic lupus erythematosus, rheumatoid arthritis and atherosclerosis [283–286]. TLR signalling, known to initiate and perpetuate nonmicrobial inflammatory responses triggered by sterile stimuli, was also upregulated by PMA treatment [118,119]. Differential gene expression analysis revealed that most of the genes were downregulated by IDR-1002 under PMA-induced inflammatory conditions. These genes belonged to many of the inflammatory pathways upregulated in response to PMA such as the chemokine-receptors-binding-chemokine pathway, cell surface interactions at the vascular wall, class A/1 rhodopsin-like receptors and IFN-γ signalling (Figure 10). A key limitation of this approach is that the gene expression occurred in the diverse population of cells in the ear and could not be accurately associated with any particular cell type. An estimate of the changes in ear tissue cell populations was obtained by the frequency of appearance of cell markers in the RNA-Seq dataset (Table A1). Comparing PMA and IDR-1002 combined treatment to PMA challenge alone, I observed a significant decrease in macrophage or monocyte, DC, neutrophil and natural killer cell markers, and an increase in mast cell markers. However, these apparent changes in cell numbers were insufficient to fully explain the large number and, in some instances, high fold-changes of genes differentially regulated by IDR-1002 treatment. Therefore, the anti-inflammatory effect of IDR-1002 was likely achieved by modulating both functions and numbers of the ear tissue cell populations. RNA-Seq analysis was perfomed 6 hours post-PMA challenge because a consistent anti-inflammatory effect of IDR-1002 was observed at this time point (e.g. reducing ear edema, pro-inflammatory cytokines and ROS/RNS levels). However, since some immune cells such as monocytes often arrive at the site of tissue inflammation after 8-24 hours [150], the choice of this early time point might overlook certain aspects of inflammation.

Topical application of PMA onto mouse ears is known to provoke prostaglandin and leukotriene biosynthesis, which leads to increased vascular permeability and evokes infiltration of inflammatory cells including neutrophils [255,287,288]. Comparing IDR-1002 treated to untreated PMA-inflamed ear tissue, there was substantial suppression of a variety of class A/1 rhodopsin-like receptors, the largest group of GPCRs, including but not limited to receptors for neutrophils, prostaglandins, histamine, platelet activating factor and anaphylatoxin (Figure A3). Previous studies have shown that IDR peptides can interact with GPCRs on the cell surface and thereafter modulate

immune cell functions [193]. In particular, IDR-1002 can enhance chemokine production and promote neutrophil infiltration in response to bacterial infections [249]. Results from current studies suggest that during sterile inflammation, control of GPCR expression, especially suppression of the expression of chemokine and chemokine receptors, might be an essential aspect of the anti-inflammatory mechanism of the IDR-1002 peptide. This highlights the ability of IDR-1002 to differentially modulate the immune response depending on the inflammatory triggers. Furthermore, the pathway mediating the leukocyte extravasation process was among the top pathways downregulated by IDR-1002 treatment (Figure 10) including many leukocyte adhesion molecules from the selectin family and the integrin family. These results supported the observation that IDR-1002 attenuated neutrophil infiltration and effectively dampened PMA-induced ear inflammation.

IFN regulatory factors constitute a family of transcription factors and play essential roles in host defense and inflammation [289,290]. Irf8 is expressed in macrophages, DCs, and T and B lymphocytes [291,292]. Irf8 was previously shown to be essential in the differentiation and functions of macrophages and DCs, generation of a Th-1 response in response to IFN-γ, and protection against intracellular pathogens including *Mycobacterium tuberculosis, Salmonella* Typhimurium and *Helicobacter pylori* [274,292–296]. Comparing IDR-1002 and PMA combined treatment to PMA challenge alone revealed that Irf8 was a major hub in the protein-protein interaction network, interacting with 28 other dysregulated gene products involved in both innate and adaptive immunity. Many of these Irf8-interactors play a role in disorders with inflammatory etiology. For example, Irf8 participates in the transcriptional regulation of TLR-4 signalling in murine lungs during endotoxemia [276]. Irf8 and Stat1 have been shown to mediate the cross-talk between LPS-induced TLR-4 signalling and the IFN-γ response, both of which are key processes contributing to the early stages of atherosclerosis and plaque development [268]. Furthermore, regulation by Irf8 of Ccl5, Isg15, Cd274, Oasl2, and Slc15a3, and Gbp2 expression, was previously found to drive pathological inflammation during cerebral malaria [297]. These results support the possibility that by suppressing the key transcription factor Irf8, IDR-1002 could potentially control a variety of inflammatory responses mediated by Irf8 target genes such as Ccl5, TNF-α and TLR-4. Since there is currently no clinical development of anti-inflammatory agents targeting Irf8 [268], these results also highlight the value of IDR-1002 as a novel therapeutic candidate for combating inflammatory diseases. IDR-1002 can modulate multiple signaling transduction pathways by acting on cell surface receptors as well as intracellular targets. MAPKs, PI3K, and the NF-κB signaling pathway have all been shown to be essential for IDR-1002 activity [249]. A previous study demonstrated that sequestosome-1/p62 is the key intracellular target of

IDR-1 [298]. IDR-1002 could potentially interact with similar targets to those used by IDR-1 [249]. In particular, overexpression of sequestosome-1/p62 has been shown to inhibit Irf8 activities and modulate NF-κB activation, which in turn attenuates cytokine expression in macrophages [299].

Chapter 4: Lipidated Peptidomimetics Pam-(Lys-βNspe)$_6$-NH$_2$ and Lau-(Lys-βNspe)$_6$-NH$_2$ as Treatment for Sterile Skin Inflammation

4.1 Introduction

Neutrophils constitute the most abundant circulating immune cells that are rapidly recruited to sites of inflammation (e.g. induced via PMA stimulation), where they are major contributors to the local production and release of reactive oxygen and nitrogen species (i.e., ROS/RNS) as I observed in Chapter 3 in ear tissue models. Formyl peptide receptors (FPRs) belong to the class of G-protein-coupled receptors with seven transmembrane domains [300]. In neutrophils, FPRs are involved in both initiation of inflammatory responses (e.g. assembly and activation of NADPH-oxidase leading to ROS production) and resolution of inflammation, which make FPRs ideal targets for therapeutic intervention [301–306]. The subtype FPR1 recognizes the prototypical bacteria- and damage-associated N-formylated peptide agonists leading to subsequent induction of pro-inflammatory responses, whereas FPR2 recognizes a diverse range of structurally distinct ligands (including lipids, N-formylated and non-formylated peptides as well as small molecules), and it is involved in both pro-inflammatory and inflammation-resolving processes [300,303,307].

Under physiological conditions, HDPs preferentially modulate innate immune responses by affecting immune cell differentiation, activation, and trafficking, thereby linking innate and adaptive immunity. Many of these immunomodulatory functions of HDPs are mediated though FPRs resulting in the attenuation of sterile and pathogen-induced inflammation as well as promotion of wound healing [194,210,302,308]. Thus, continuous efforts have been devoted to development of HDPs and synthetic mimetics as beneficial therapies [10,309,310]. Peptidomimetics comprise peptide-like molecules with altered backbones that retain side chains similar to those of natural peptides [225]. Peptoid oligomers and hybrids with a high content of α- or β-peptoid residues have been found to possess proteolytic stability [310–313]. Examples include the immunomodulatory compounds Pam-(Lys-βNspe)$_6$-NH$_2$ (PM1) and Lau-(Lys-βNspe)$_6$-NH$_2$ (PM2) that are lipidated peptidomimetics consisting of alternating α-amino acids and β-peptoid residues (Figure 12) [314–316].

Initially, PM1 was identified from a library of α-peptide/β-peptoid oligomers due to its ability to attenuate, in primary human leukocytes, the production of pro-inflammatory cytokines in response to stimulation with bacterial membrane components including LPS and LTA at concentrations of 60 nM and 0.85 μM, respectively [314] (Table 1). *In vitro* cellular assays on primary human neutrophils demonstrated that PM1 (at 50 nM) inhibits the release of ROS, neutrophil degranulation, and increases in cytosolic Ca^{2+} concentration upon stimulation with the FPR2-selective peptide agonist

WKYMWM [315]. Interestingly, the analogue PM2, with a four-carbon shorter lipid tail, possesses similar anti-inflammatory properties, albeit at 2- to 4-fold higher concentrations than PM1 [315]. Importantly, PM2 proved to be a subtype-selective antagonist of the orthologous mouse receptor, Fpr2, while PM1 antagonized both Fpr1 and Fpr2 signalling [316]. Thus, PM2 constitutes the first FPR2 antagonist displaying cross-species selectivity and potency, and thus can be a convenient tool for elucidating the specific regulatory roles of FPR2 via mouse models of infection and inflammation (Table 1). The aim of Chapter 4 was to perform the first *in vivo* study of peptidomimetics PM1 and PM2 and explore their anti-inflammatory effects using the PMA-induced acute sterile inflammation mouse model.

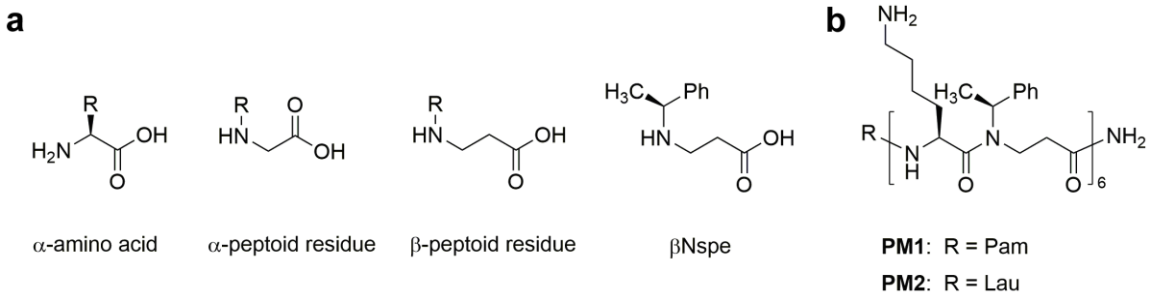

Figure 12. Chemical structures of peptoid residues (a) and peptidomimetics (b).

Table 1. Overview of *in vitro* immunomodulatory activities reported for peptidomimetics PM1 and PM2 (stated as IC50 values).

Characteristic	PM1 (μM)	PM2 (μM)	Reference
Lipopolysaccharide neutralization	0.06 (0.04-0.08)	0.13 (0.08-0.21)	[314]
Lipoteichoic acid neutralization	0.85 (0.5-1.43)	1.84 (1.20-2.82)	[314]
Leukocyte viability	24 (19-30)	27 (18-40)	[314]
HepG2 viability	28 (23-37)	24 (14-42)	[314]
Human FPR2 inhibition	0.05 (0.04-0.07)	0.18 (0.14-0.24)	[315]
Mouse Fpr2 inhibition	+++	0.40 (0.16-0.97)	[316]
Mouse Fpr1 inhibition	++	-	[316]

+++ = very potent; ++ = potent; – = inactive.

4.2 Peptidomimetics PM1 and PM2 dampened PMA-induced ear edema and reduced tissue pro-inflammatory cytokine and chemokine levels

To induce acute ear inflammation, PMA was applied topically to both ears of CD-1 mice. The *in vivo* anti-inflammatory activity of the peptidomimetics was tested by treating one of the PMA-

inflamed ears with peptidomimetic PM1 or PM2, while the contralateral ear was given the solvent as a control. The ear tissue challenged with PMA started to show signs of inflammation, including swelling and redness after about 2 hours post-PMA application. These symptoms of inflammation were postponed 3-4 hours in ears treated with PM1 and PM2. Consistent with the previous IDR-1002 study (Chapter 3) [317], I observed a ~3-fold increase in ear biopsy weight and significant induction of MCP-1, CXCL-1 and IL-6 in the ear tissue 6 hours post-PMA challenge (Figure 13). At the dosages of 0.2 mg/ear and 0.6 mg/ear both peptidomimetics PM1 and PM2 significantly suppressed PMA-induced increases in ear biopsy weight (Figure 13a,e). Topical PM1 (Figure 13b-d) and PM2 (Figure 13f-h) treatment, at both tested dosages, also significantly decreased MCP-1, CXCL-1 and IL-6 concentrations when compared to those in ears challenged with PMA alone. The anti-inflammatory activity was comparable for both peptidomimetics when applying 0.6 mg/ear and with a matching dose of indomethacin. Application of peptidomimetics alone did not trigger any indications of inflammation. To further study whether topical treatment with peptidomimetics PM1 and PM2 exerted a systemic immunomodulatory effect beyond the ear tissue, I measured serum cytokine levels (Figure A4). However, most of these cytokine levels were not affected by the peptidomimetics or indomethacin, with the exception of PM1 giving rise to a decreased serum CXCL-1 concentration upon topical application of 0.6 mg/ear (Figure A4b). Together these results infer that HDP mimics PM1 and PM2 both were capable of effectively reducing PMA-induced ear inflammation and the effects of both peptidomimetics and indomethacin were largely local within the ear tissue.

4.3 PM1 and PM2 attenuate neutrophil recruitment into inflamed ear tissue

To evaluate histologic alterations and inflammatory cell distribution in response to PMA challenge and the treatment with peptidomimetics, H & E staining was performed on tissue biopsies (Figure 14a). In comparison to the sample from the vehicle control tissue, the cross section of ear tissue challenged with PMA exhibited a substantial expansion in the dermal thickness due to increased interstitial fluid. Upon treatment with PM1 or PM2, I observed a prominent decrease in the inflammatory immune cell density and a modest reduction of the dermal thickness. Ear edema scoring revealed that PMA-stimulated ear tissue had moderate to severe edema.

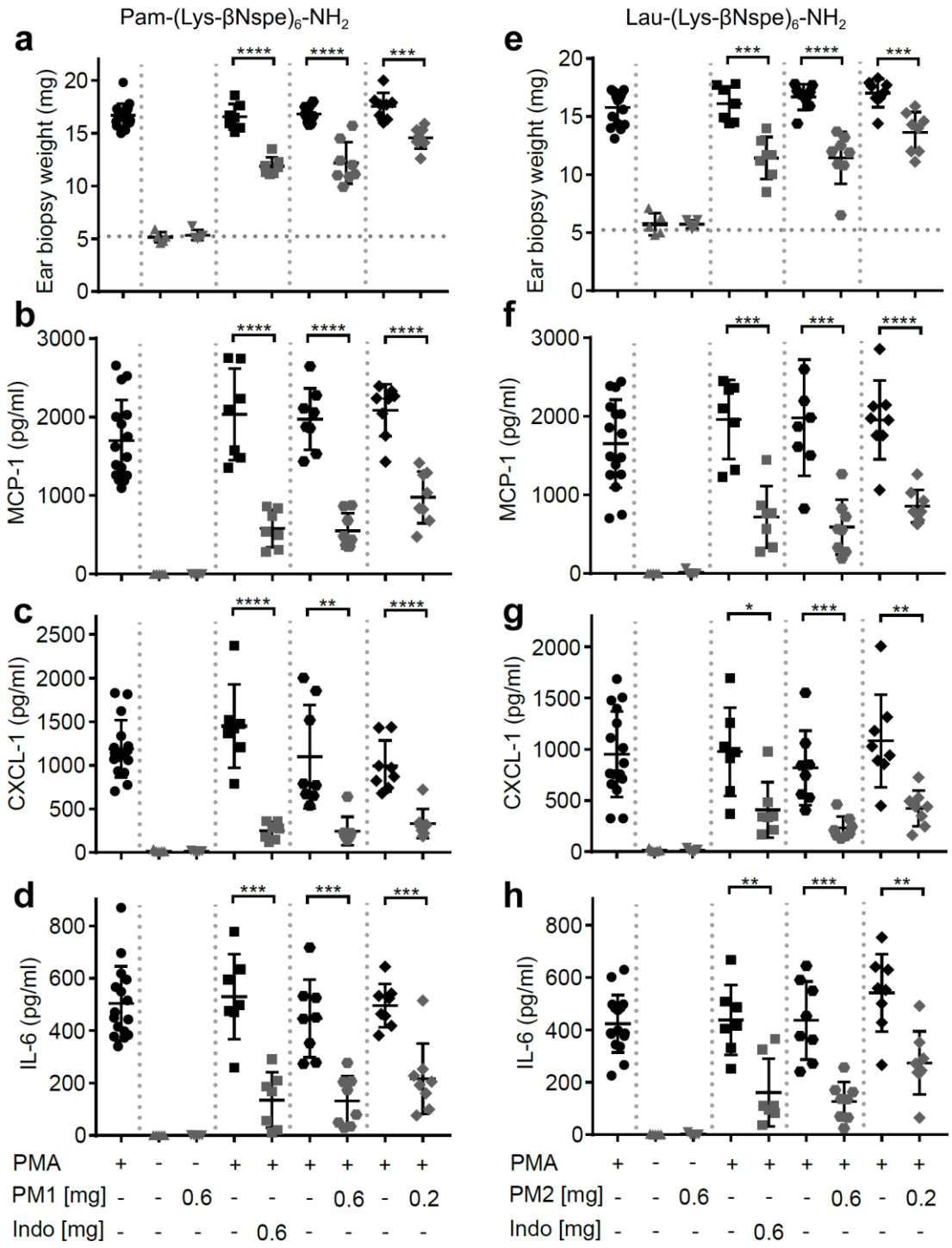

Figure 13. Peptidomimetics PM1 and PM2 reduced PMA-induced ear edema and the production of proinflammatory chemokines MCP-1 and CXCL-1 and cytokine IL-6 in PMA-inflamed ear tissue.

PMA (20 µl of 125 µg/ml solution) was applied topically onto CD-1 female mice ears. Indomethacin (Indo) or peptidomimetic Pam-(Lys-βNspe)$_6$-NH$_2$ (PM1; **a-d**) or Lau-(Lys-βNspe)$_6$-NH$_2$ (PM2; **e-h**) at 0.6 or 0.2 mg/ear was given topically to one ear of each mouse after PMA being absorbed. The contralateral ear was given 20 µl of vehicle. Mice were euthanized 6 hours post-treatment and ear

biopsies (5 mm in diameter) were harvested for measuring weight (**a,e**) and MCP-1 (**b,f**), CXCL-1 (**c,g**) and IL-6 (**d,h**) levels by ELISA. Each condition was repeated with a total of five to eight mice in four independent experiments. Error bars indicate Mean ± SD. Statistics: *$p \leq 0.05$, **$p \leq 0.01$, ***$p \leq 0.001$, ****$p \leq 0.0001$, Student's unpaired t-test.

Comparable to indomethacin, PM1 or PM2 treatment significantly decreased ear edema scores reducing the symptoms to moderate on average (Figure 14b). Topical PMA challenge also triggered a marked, predominantly neutrophilic inflammatory infiltration in the ear tissue (Figure 14c). I also observed significant, but less pronounced, increases in the number of monocytes (Figure 14d) and lymphocytes (Figure 14f), and a minor elevation in eosinophil density (Figure 14e). Treatment with PM1 or PM2 both effectively dampened neutrophil infiltration. PM2 decreased neutrophil counts from an average of 91 cells/HPF to about 10 cells/HPF and 12 cells/HPF for ears to which 0.6 mg and 0.2 mg PM2 were administered, respectively (Figure 14c). Compared to PMA-inflamed ears, PM1 and PM2 treatment did not affect the number of monocytes and eosinophils, but increased the lymphocyte count slightly. These results show that topical treatment with these peptidomimetics can reduce PMA-induced ear edema by preventing excessive influx of neutrophils.

4.4 PM1 and PM2 reduced the release of ROS/RNS from PMA-challenged ear tissue

Next I monitored the levels of ROS/RNS, since neutrophil degranulation and the production of ROS/RNS is closely associated with acute inflammatory processes, and an excessive production of these may contribute considerably to the severity of acute inflammation [253,256]. Thus, I injected mice subcutaneously in the back with the luminescent probe L-012 that has high sensitivity toward ROS/RNS and demonstrates enhanced luminescence when binding to these species [254]. Subsequently, the mice were subjected to analysis using an *in vivo* imaging system, 6 hours post-treatment. Figure 15 shows *in vivo* imaging results from three independent experiments. Topical PMA stimulation induced strong ROS/RNS release with some variations among individuals (Figure 15a). Treatment with PM1 at both 0.6 and 0.2 mg/ear almost completely inhibited ROS/RNS production in the ear tissue (Figure 15a), whereas PM2 had a slightly less potent inhibitory effect, being somewhat more effective at the higher dosage (Figure 15b). Again, the inhibitory effect on ROS/RNS release was comparable for both peptidomimetics and the positive anti-inflammatory control indomethacin.

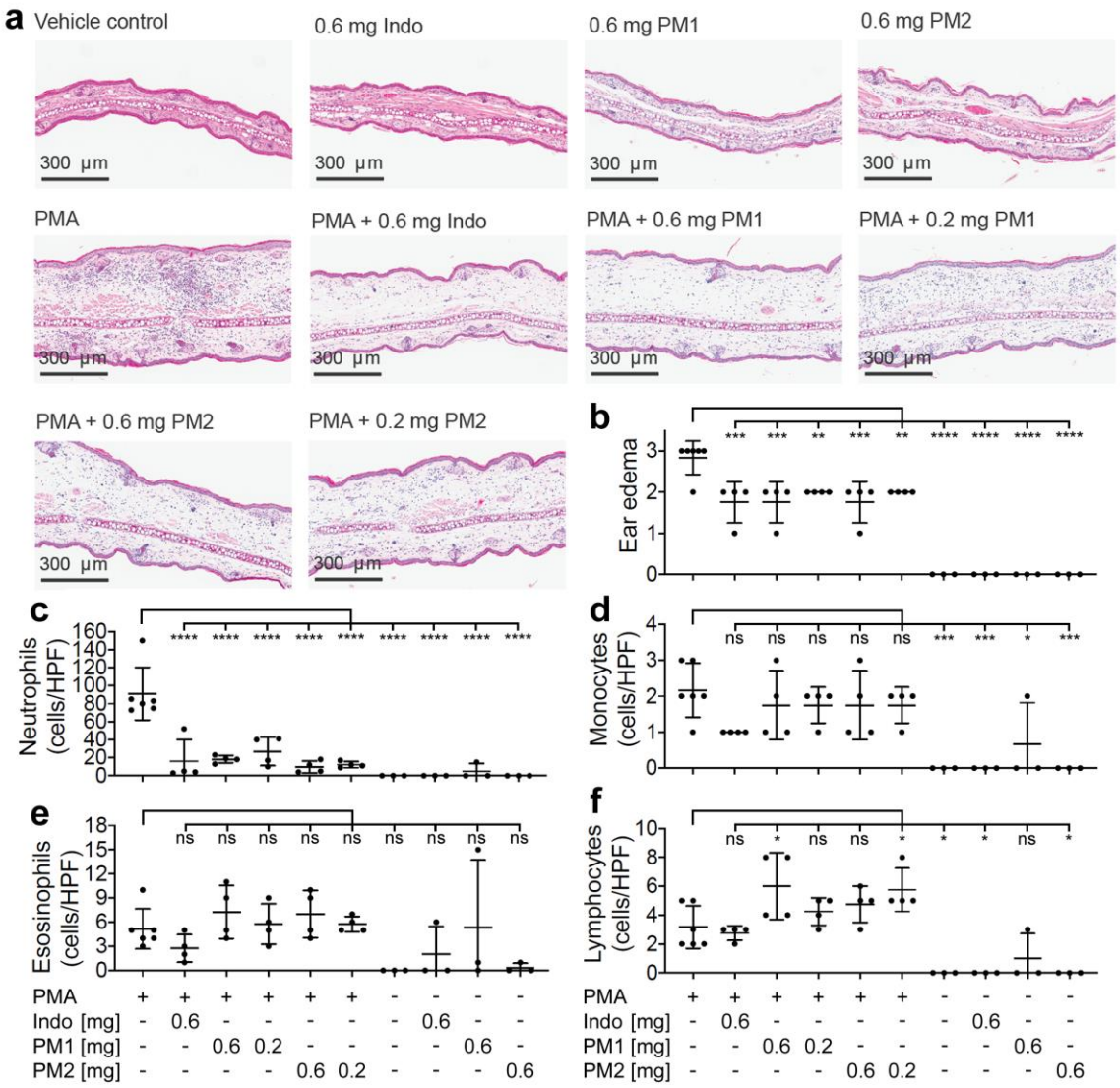

Figure 14. Peptidomimetics PM1 and PM2 suppressed neutrophil infiltration in the ear tissue. (**a**) A representative image of H & E stained ear tissue biopsies from a total of three to six biological replicates (three independent experiments) per treatment group is shown. (**b**) Ear edema pathology scores (0: no edema, 1: mild, 2: moderate and 3: severe) were assigned. The number of each type of immune cells present in the stained specimen was determined (cells/HPF): (**c**) neutrophils, (**d**) monocytes, (**e**) eosinophils, and (**f**) lymphocytes. Error bars indicate Mean ± SD. Statistics: *$p \leq 0.05$, ***$p \leq 0.001$, ****$p \leq 0.0001$, one-way ANOVA, Dunnett's multiple comparisons test.

4.5 Discussion

Peptidomimetics PM1 and PM2 belong to the class of α-peptide/β-peptoid hybrids with improved proteolytic stability and bioavailability when compared to that of natural HDPs, while retaining beneficial *in vitro* anti-inflammatory properties including suppression of neutrophil activation and attenuation of pro-inflammatory cytokine production in response to stimulation with bacterial membrane components [314–316,318].

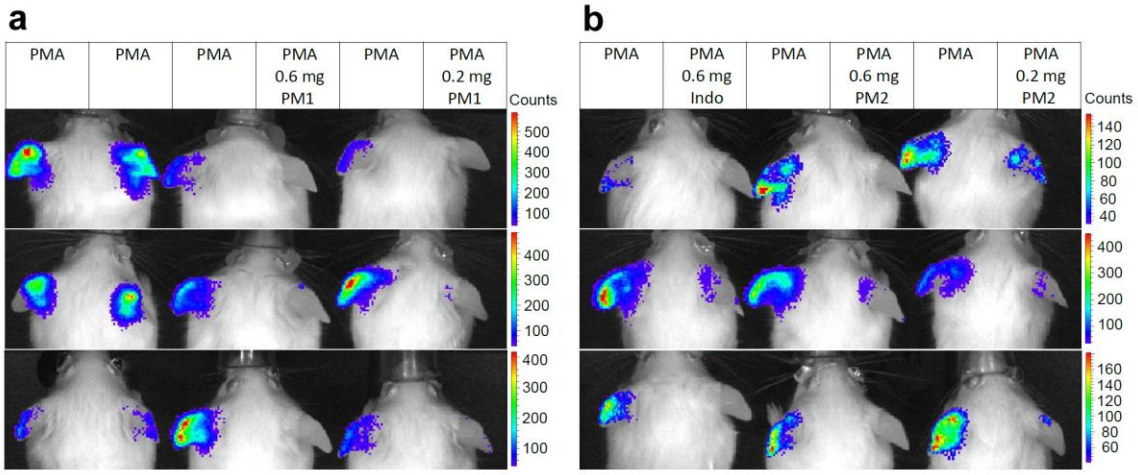

Figure 15. Peptidomimetics PM1 and PM2 attenuated release of ROS/RNS from PMA-challenged ear tissue.
Ears of CD-1 mice were stimulated with PMA and the right ear of each mouse was treated with vehicle control (50% acetone), 0.6 mg PM1 or 0.2 mg PMA respectively (**a**) or 0.6 mg indomethacin, 0.6 mg PM2 or 0.2 mg PM2 respectively (**b**). At 5.5 hours post-treatment, CD-1 mice were injected subcutaneously with 25 mg/kg L-012 luminescent probe. ROS/RNS levels in ear tissue were visualized by imaging mice with an *in vivo* imaging system 20–30 minutes post-probe injection under 2% isoflurane anaesthesia. Three biological replicates from three independent experiments were included per treatment group.

Here I examined the potential of PM1 and PM2 as modulators of PMA-induced sterile inflammation *in vivo* and demonstrated that treatment with PM1 or PM2 effectively reduced PMA-induced ear edema and the production of MCP-1, CXCL-1 and IL-6 within the ear tissue to an equivalent extent of that of the NSAID indomethacin positive control (Figure 13). Importantly, I observed similar cytokine levels in the PMA-treated negative control ears when comparing mice given only PMA on both ears with mice that had a peptidomimetic applied to one ear and PMA on the other, indicating that topical treatment with a peptidomimetic on one ear did not affect the cytokine levels in the contralateral ear. In addition, both peptidomimetics and indomethacin had only minor effects on the serum cytokine levels (Figure A4). Therefore, the anti-inflammatory effect of these peptidomimetics appears to be localized to the ear tissue when applied topically. It is worth mentioning that treatment with PM1 or PM2 was well-tolerated by mice, since I did not observe any signs of piloerection, hunching, extensive scratching or decreased activity for any mice given topical treatment (up to 30 mg/mL) of these two peptidomimetics.

H & E staining showed that the majority of inflammatory cells being recruited to the PMA-inflamed ear tissue were neutrophils, and that treatment with PM1 or PM2 resulted in a prominent reduction in the neutrophil count (Figure 14), which led to a major decrease in the amount of ROS/RNS accumulated in the ear tissue (Figure 15). In previous studies it was found that pre-

incubation of neutrophils with PM1 or PM2 inhibits FPR2-induced ROS production, but not PMA-stimulated ROS secretion from neutrophils *in vitro* [315,316]. A different outcome in the *in vivo* model was expected since neutrophils are not abundant in healthy skin. Thus, in this *in vivo* ear inflammation model, it did not appear likely that a high number of neutrophils would become directly activated by PMA. In Chapter 3, RNA-Seq transcriptomic analysis showed that topical PMA challenge in mouse ears activates cytokine signalling, especially IFN-γ, TNF-α and IL-1β as well as chemokine signalling via the class A/1 rhodopsin-like receptor family, and via TLR signalling pathways [317]. Therefore, PM1 and PM2 could potentially interfere with these early processes locally, leading to suppression of neutrophil recruitment and activation.

One limitation of using the PMA-induced mouse ear inflammation model (Chapter 3 and Chapter 4) for evaluating the anti-inflammatory efficacy resides in the intrinsic differences in the structural and cellular components of human and mouse skin. For example, human skin has thicker epidermis and dermis and lower hair follicle density when compared to that of the mouse skin [31]. These differences can affect the adsorption of peptides or peptidomimetics. In addition, skin immunity differs in human and mouse. For instance, Langerhans cells and $CD8^+$ T cells are the major immune cell types in the epidermis of human skin, as compared to dendritic epidermal T cells which are more predominant in mouse epidermis [31,319]. Therefore, the favourable anti-inflammatory effect observed in mouse skin needs to be confirmed in relevant human skin systems. Indeed, I stimulated the N/TERT human epidermal skin model (described in Chapter 5 and Chapter 6) with PMA but no significant inflammatory effect was triggered, likely due to the lack of skin immune cells in this model.

One of the main anti-inflammatory mechanisms of PM1 and PM2 *in vitro* is mediated through inhibition of FPR2/Fpr2 in human and mouse neutrophils [315,316]. Besides neutrophils, FPR2 is also expressed by a variety of immune cells (e.g., monocytes/macrophages, natural killer cells, DCs and T cells) and non-immune cells (e.g., keratinocytes, intestinal epithelial cells, endothelial cells, and synovial fibroblasts), and they participate in infection responses, pathogenesis of inflammation and cancer [305]. The detailed functions of FPR2 in skin inflammation have not been well-characterized to date. Activation of FPR2 by PSMα peptides leads to cytokine release, neutrophil chemotaxis and activation during *S. aureus* skin infections [320–322]. In sterile skin wounds, mouse Fpr1 and Fpr2 have been reported to mediate early neutrophil infiltration into the dermis prior to the production of neutrophil-specific chemokines such as CXCL-1 and CXCL-2 through recognition of FPR ligands produced at the site of injury [323]. Also, Fpr1 has been shown to mediate neutrophil accumulation at

sites of injury-induced sterile inflammation via recognition of mitochondria-derived formylated peptides [324–326]. Consistent with these reports, treatment with PM1 or PM2 dampened the initiation of sterile skin inflammation, suppressed ear edema, reduced local cytokine levels and attenuated neutrophil infiltration. In particular, PM1, an antagonist of both Fpr1 and Fpr2 (Table 1), had a better inhibitory effect on local ROS/RNS production when compared to PM2, which is Fpr2-selective (Figure 15). It is likely that the topical PMA challenge resulted in the release of FPR ligands from damaged cells such as keratinocytes, endothelial cells, and Langerhans cells in the skin as well as neutrophils and monocytes being recruited to the inflammatory site, and that the effects of PM1 and PM2 in this experimental setting were mediated by Fpr antagonism. Nevertheless, PM1 and PM2 also potently inhibited *in vitro* cytokine secretion induced by stimulation with agonists for TLR-2 and TLR-4. This would occur through cell-dependent mechanisms targeting monocytes and neutrophils [314], indicating that PM1 and PM2 might also inhibit cytokine secretion by TLR-expressing skin-resident cells such as macrophages and Langerhans cells. Further studies are needed to elucidate the detailed molecular mechanism(s) and targeted cell types behind the *in vivo* anti-inflammatory effects exerted by PM1 and PM2.

Chapter 5: Human organoid biofilm model for assessing antibiofilm activity of novel agents

5.1 Introduction

Knowing that synthetic HDPs and peptidomimetics have promising anti-inflammatory effects in sterile skin inflammation, I proceeded to study another major aspect of common skin problems: bacterial biofilm infections and associated skin inflammation. There has been considerable discussion concerning the antibiotic resistance threat as resistance and multi-drug resistance rises and insufficient new antibiotics are being discovered [327]. However, of similar or even greater concern are biofilm infections since not a single drug has been approved for use against such infections, despite the fact that biofilms represent 65% and 80% of all microbial and chronic human infections respectively [328,329].

Currently the treatment of biofilm infections often involves surgical debridement and the use of combinations of antibiotics developed for free swimming (planktonic) bacteria [330,331]. However, this is problematic because biofilms are adaptively multi-drug resistant, and can rapidly recover from surgical debridement [330]. Therefore, I proposed that synthetic peptide-based therapeutics that directly target the bacteria within a biofilm would be advantageous for future management of biofilm infections. Among the most effective peptides identified to date is a D-enantiomeric peptide DJK-5, which exhibits broad-spectrum antibiofilm activity against bacterial pathogens [219214]. It can eradicate oral biofilms [332], inhibit *P. aeruginosa* biofilms in a lung epithelial model [333], and reduce abscess size and bacterial burden in a murine cutaneous infection model [334]. These demonstrated antibiofilm effects make DJK-5 an attractive peptide candidate to test for efficacy against biofilm-associated skin infections.

Another enormous limitation in managing biofilm infections is the lack of convenient testing models due to the difficulty of recapitulating the clinical features of such infections [335]. There are no standardized *in vitro* biofilm tests like the minimal inhibitory concentration assays implemented by the Clinical and Laboratory Standards Institute. Therefore, the aims of Chapter 5 were to adapt air-liquid interface skin models to provide *in vivo*-like, humanized systems for (1) studying skin biofilm infections, and (2) screening novel antibiofilm therapeutics.

5.2 Characterization of bacterial biofilms on N/TERT epidermal skin surface

The morphology and architecture of 24-hour bacterial skin biofilms was assessed by histological H&E staining, scanning electron microscopy and confocal laser scanning microscopy. Histological analysis of the N/TERT epidermal skin cross-section revealed a stratified skin structure

8-10 cells deep (Figure 16a left).

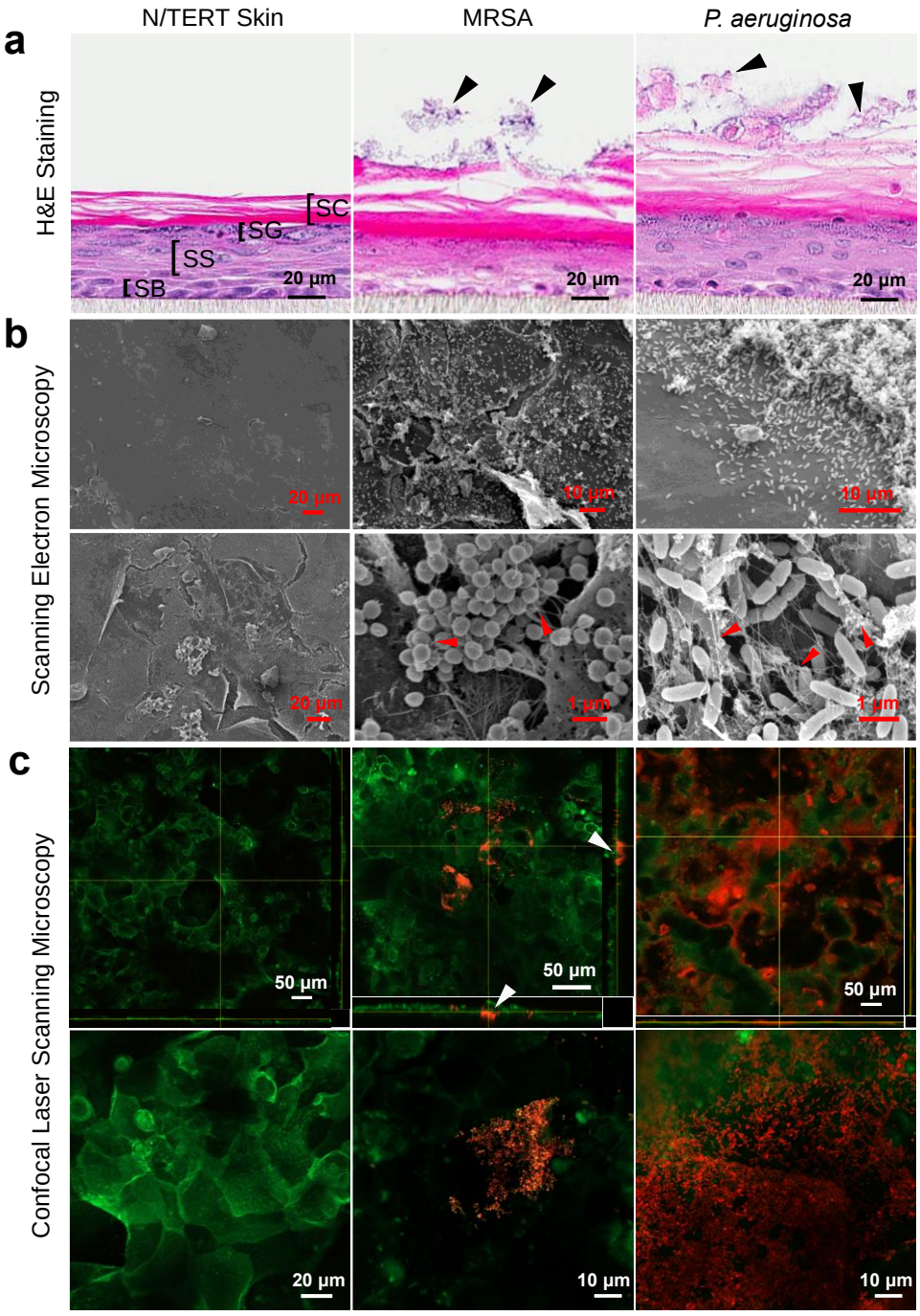

Figure 16. Microscopic characterization of MRSA and PAO1 biofilms on N/TERT skin.
(**a**) Control skin and skin infected with one million MRSA (USA300-LAC) or PAO1 biofilms were visualized with H&E staining 24 hours after seeding. Cross sections of skin layers corresponding to the stratum corneum (SC), stratum granulosum (SG), stratum spinosum (SS), and stratum basale (SB) were readily visible. MRSA and PAO1 biofilms on skin are indicated with arrows. (**b**) Control skin and 1-day MRSA-*lux* (MRSA SAP149) or PAO1-*lux* biofilm surface structures were imaged by SEM. Arrows indicate filamentous material resembling bacterial extracellular matrix interconnecting the MRSA and PAO1 biofilm. (**c**) Control skin or skin spotted with fluorescently tagged MRSA-

FarRed or PAO1-mCherry was stained with CellMask™ Green Plasma Membrane Stain and visualized using confocal microscopy 24 hours after infection. Arrows indicate MRSA-FarRed bacteria clusters penetrated underneath the surface of SC. Each of the bottom images in (**c**) is a zoomed-in region of the orthographic projection shown above.

Differentiated layers, including the stratum corneum, stratum granulosum, stratum spinosum and the basal cell layer, were readily distinguished above the cell culture filter insert (Figure 16a). When spotted with one million bacteria, clear aggregates could be observed on the skin surface 24 hours after seeding, consistent with the formation of adhered biofilms [336].

SEM imaging was performed to gain insights into the architecture of the skin surface structure. Untreated skin revealed some regions with smooth surfaces and other regions with rougher morphology, although the possibility that these were artifacts of fixation could not be ruled out (Figure 16b). The addition of Gram-positive MRSA to the skin resulted in small clusters of cells dispersed across the skin surface of the inoculation site. The application of Gram-negative *P. aeruginosa* resulted in a dense mat of adhered bacterial cells that completely covered the skin surface. High magnification images showed that MRSA and PAO1 biofilms were each inter-connected by thin filamentous extracellular matrices.

To gain further insights into the organization of the skin biofilms and their penetration into the underlying layers, confocal microscopy was performed using engineered MRSA and PAO1 bacterial strains expressing red fluorescent proteins (Far-red fluorescent protein and mCherry respectively) coupled with a membrane-specific fluorescent dye, CellMask™ Green Plasma Membrane Stain. This allowed for visual discrimination between cells within the biofilms and the membranes of the skin cells (Figure 16c). Staining of uninfected skin with the membrane specific dye revealed layers of distinct and elongated keratinocytes at the surface of the differentiated skin. Based on the depth of staining, it appeared that the CellMask™ Green dye only penetrated the top few cell layers of the skin corresponding to the upper layers of the stratum corneum seen in the H&E-stained samples. Application of fluorescently labeled MRSA to the skin surface and growth for 24 hours resulted in small microcolonies of bacteria present on the skin surface, as well as regions where bacterial aggregates had penetrated underneath the surface layer of epidermal cells (indicated by arrows). In contrast, fluorescently tagged PAO1 appeared as a dense mat of bacterial cells covering the entire surface of the skin.

5.3 Effect of DJK-5 peptide treatment on skin associated MRSA biofilm

To establish discrete, confined biofilms on top of the skin, MRSA or MRSA-*lux* strains were

spotted on the surface of the epidermis. In the case of the MRSA-*lux* strain, 24 hours after infection the area of biofilm colonization was visualized by imaging luminescence, which indicates actively metabolizing bacteria (Figure 17a). Biofilms treated with vehicle control had no obvious change in luminescence intensity and often spread to the edge of the filter insert. Treatment with DJK-5 at a low dosage (0.1%, 30 μg total peptide) reduced the area of colonization, while a high dosage (0.4%, 120 μg) completely abolished the luminescence. SEM images showed that, in contrast to untreated bacterial cells, MRSA-*lux* cocci treated with DJK-5 were enlarged and had rough surfaces sprinkled with small debris clusters, suggesting that DJK-5 treatment affected bacteria within the biofilm, causing damage to the bacterial cell wall and membrane. DJK-5 treatment also led to an apparent reduction in the string-like material, which I concluded above might be bacterial biofilm matrix (Figure 17b). It is not clear whether this reduction in biofilm matrix is due to a direct effect of DJK-5 on the matrix or peptide enhancement of natural biofilm dispersal [21]. DJK-5 treatment significantly reduced viable bacteria on the skin in a dose-dependent manner. The geometric mean of MRSA-*lux* bacteria decreased from 1.3×10^8 CFU/skin for untreated samples to 1.6×10^6 CFU/skin and 2.1×10^4 CFU/skin for 0.1% DJK-5 and 0.4% DJK-5 treated skin samples respectively (Figure 17c). Similar effects were seen for non-luminescent MRSA biofilms on skin surfaces treated with DJK-5 (Figure 17d). To visualize skin and MRSA biofilm structures, H&E staining was performed on MRSA colonized skin samples four hours post-DJK-5 treatment (Figure 17e). MRSA infected skin had clusters of bacteria attached to the surface, which also caused thickening and damage to the underlying stratum corneum. In peptide-treated samples, the bacteria on the skin surface were much less prominent and the damage to the stratum corneum was reduced (Figure 17e). Although viable bacteria were recovered from biofilms treated with 0.4% DJK-5, minimal bacterial clusters in H&E stained samples may reflect an insensitivity of this method in visualizing biofilms, especially when most bacteria were dead.

Since the luminescence signal correlated with the bacterial colony count recovered from each skin sample, this feature was used as a simple way of monitoring the progression of biofilm growth over time by imaging the luminescence from the biofilm every 24 hours following the initial inoculation. We found that most MRSA-*lux* biofilms could be maintained on the skin surface for about 3 days without breaching the skin barrier which otherwise would result in overgrowth of bacteria in the medium under the cell culture insert (Figure 17f, raw data shown in Figure A5a). Measurement of transepithelial electrical resistance (TEER) and FITC-dextran permeability confirmed that the skin organoids formed tight barriers, even after 1-3 days of biofilm formation,

while after longer periods of incubation with biofilms these assays confirmed disruption of skin integrity due to bacterial penetration (Figure A6).

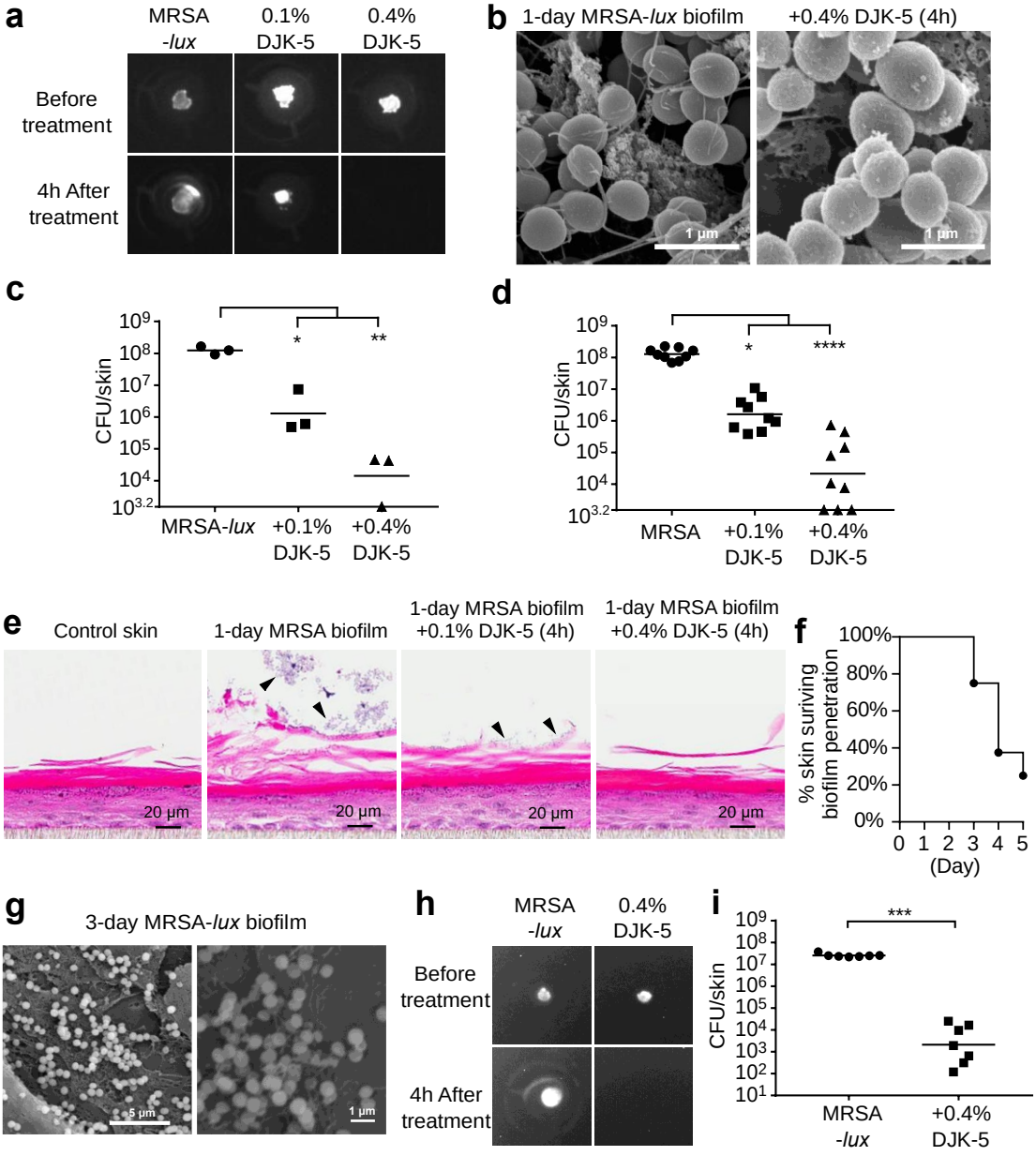

Figure 17. DJK-5 peptide reduced 1-day and 3-day pre-established MRSA biofilm on skin surface.

Skin biofilms were established by seeding one million MRSA (USA300-LAC) or MRSA-*lux* (MRSA SAP149) on top of the skin. Twenty-four hours post-infection, vehicle control or DJK-5 peptide at a dosage of 0.1% (30 μg) or 0.4% (120 μg) was administered on top of the skin. Four hours post-treatment, DJK-5 peptide reduced luminescence from skin colonized with MRSA-*lux* (**a**) and decreased total bacteria recovered from skin infected with MRSA-*lux* (**c**) and MRSA (**d**). Biofilm structures for MRSA-*lux* with or without DJK-5 treatment were visualized by SEM (**b**) and H&E staining (**e**). For the long-term study, MRSA-*lux* biofilm was imaged every 24 hours after initial inoculation, (**f**) shows the number of days that a confined biofilm can be maintained on top of skin

without bypassing the skin barrier resulting in bacterial growth in the culture medium below the filter insert (raw data shown in Figure A5**a**). MRSA-*lux* 3-day biofilm was visualized by SEM (**g**) and treated with 0.4% DJK-5 for 4 hours, which reduced luminescence (**h**) and CFU recovered (**i**) compared to untreated samples. Statistical significance (* $P \leq 0.05$; ** $P \leq 0.01$; *** $P \leq 0.001$; **** $P \leq 0.0001$) was determined using the Kruskal–Wallis test, Dunn's multiple comparisons test (**c,d**), or the Mann-Whitney test (**i**). Geometric mean of CFU count from 3-9 biological replicates was indicated in (**c,d,i**).

Visualization of the 3-day MRSA-*lux* biofilm by SEM revealed similar aggregates of MRSA-*lux* cells to those observed with 1-day biofilms (Figure 17g). Interestingly, DJK-5 was similarly effective at diminishing 3-day MRSA-*lux* biofilm when compared to 1-day biofilm. DJK-5 applied to the 3-day biofilms at a concentration of 0.4% successfully eliminated bacterial luminescence (Figure 17h) and significantly reduced bacterial load by 4 log orders of magnitude (Figure 17i) within 4 hours of treatment. Since the growth of biofilms were generally tolerated by the skin, it is worth noting that, at the end of the 3-day infection, MRSA-*lux* did not induce any increased cytotoxic effects or significant IL-1β and IL-8 release when compared to the uninfected control (Figure A7a-c).

5.4 Effect of DJK-5 peptide treatment on skin associated *P. aeruginosa* biofilms

I further studied whether DJK-5 could eradicate Gram-negative *P. aeruginosa* PAO1 biofilms associated with N/TERT epidermal skin. Here, I tested DJK-5 at 0.4% only since this concentration showed superior antibiofilm effects against MRSA. PAO1 biofilm treated with 0.4% DJK-5 for four hours resulted in an evident reduction in the luminescence signal, whereas biofilms given vehicle control led to an increase in the area of colonization (Figure 18a), possibly due to increased growth or additional lubrication/substrate to promote colony expansion/mobility. The surface of DJK-5 treated PAO1 cells formed numerous tube-like bleb structures and the shape of PAO1 cells transformed from rods to ovals, indicative of severe outer membrane damage, disruption in cell elongation and a loss of shape maintenance[337] (Figure 18b). DJK-5 treatment exerted similar antibiofilm effects against the luminescent and untagged strains of PAO1. The geometric mean of recovered PAO1-*lux* bacteria declined from 8.9×10^7 CFU/skin in control samples to 1.9×10^2 CFU/skin in peptide treated skin (Figure 18c), while non-luminescent PAO1 went down from 1.3×10^8 CFU/skin to 4.9×10^3 CFU/skin upon DJK-5 treatment (Figure 18d). H&E staining revealed that colonization of the skin surface with PAO1 led to increased thickness in the stratum corneum and the appearance of PAO1 biofilm aggregates were mostly observed in the middle to upper layers of the stratum corneum (Figure 18e).

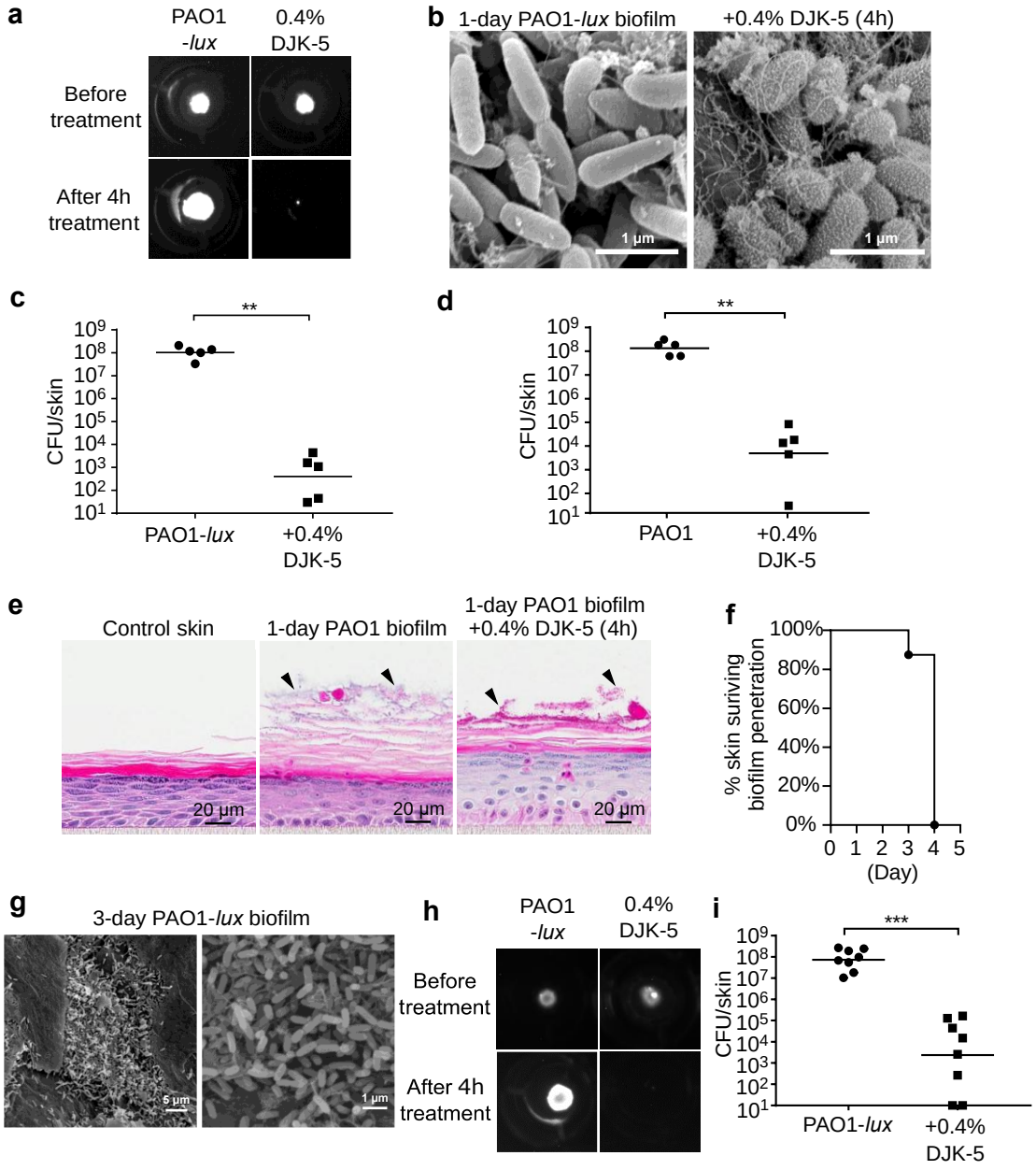

Figure 18. DJK5-peptide diminished *P. aeruginosa* PAO1 1-day and 3-day skin biofilm.
Biofilms of PAO1 or its luminescent version (PAO1-*lux*) were seeded on the skin for 24 hours then treated with 0.4% (120 µg) DJK5 peptide for 4 hours. Luminescence signals from colonized PAO1-*lux* were imagined using the ChemiDoc Imaging System (**a**). Biofilm structures were visualized by SEM (**b**). Colony counts from skin samples infected with the luminescent (**c**) and non-luminescent (**d**) PAO1 was determined. Histological analysis of the biofilm structures was performed by H&E staining (**e**). The number of days that skin barrier withstood biofilm growth was monitored (raw data shown in Figure A5**b**) (**f**). PAO1-*lux* 3-day biofilm was imaged by SEM (**g**) and treated with 0.4% DJK-5 for 4 hours, which reduced luminescence signals (**h**) and colony count (**i**). Statistical significance (** $P \leq 0.01$; *** $P \leq 0.001$) was determined using the Mann-Whitney test (**c,d,i**). Geometric mean of CFU count from 5-8 biological replicates was indicated in (**c,d,i**).

Following DJK-5 treatment, these clusters of PAO1 were diminished in size and this was accompanied by a reduction in stratum corneum thickness. Similar to MRSA, the skin barrier could endure the growth of PAO1 biofilm for about 3 days (Figure 18f, raw data shown in Figure A5b), and bacterial penetration coincided with substantial decrease in TEER measurements and increased permeability to FITC-dextran (Figure A6). The 3-day PAO1-*lux* biofilm structure was analyzed by SEM and similar clusters of PAO1-*lux* cells were observed (Figure 18g). DJK-5 demonstrated a comparable antibiofilm efficacy on 3-day PAO1-*lux* biofilm, where peptide treatment eliminated the luminescence signal after 4 hours (Figure 18h) and significantly decreased bacterial burden (Figure 18i). Again, no significant changes in toxicity and immune responses were triggered by PAO1-*lux* biofilms by day 3 (Figure A7d-f).

5.5 N/TERT skin model as a versatile platform for screening novel antibiofilm and anti-inflammatory peptides

After characterizing the biofilm skin organoid model, I used this platform to screen novel peptides and select for peptides with superior antibiofilm activity when compared to DJK-5. The one-day MRSA-*lux* (Figure 19a) and PAO1-*lux* (Figure 19b) skin biofilm system was used to screen the activity of several synthetic HDPs (Table 2) at a peptide concentration of 0.1%.

Table 2. Synthetic host defense peptides screened

Peptide	Enantiomeric Form	Sequence (all peptides amidated)
IDR-1002 (1002)	L	VQRWLIVWRIRK
DJK-5	D	VQWRAIRVRVIR
IDR-1018 (1018)	L	VRLIVAVRIWRR
HH2	L	VQLRIRVAVIRA
2008	L	RRWIVKVRIRRR
2009	L	KWRLLIRWRIQK
3002	L	ILVRWIRWRIQW
3006	L	IWLRLKVVLKRK
RI-3006	RI	KRKLVVKLRLWI
D-3006	D	IWLRLKVVLKRK
3007	L	VLKIKVKIWVVK
RI-3007	RI	KVVWIKVKIKLV
D-3007	D	VLKIKVKIWVVK

This approach revealed differential antibiofilm efficacies among the evaluated peptides that could be qualitatively assessed based on the luminescence (representative images shown in Figure 19 bottom panel) or quantified by recovering CFUs following peptide treatment.

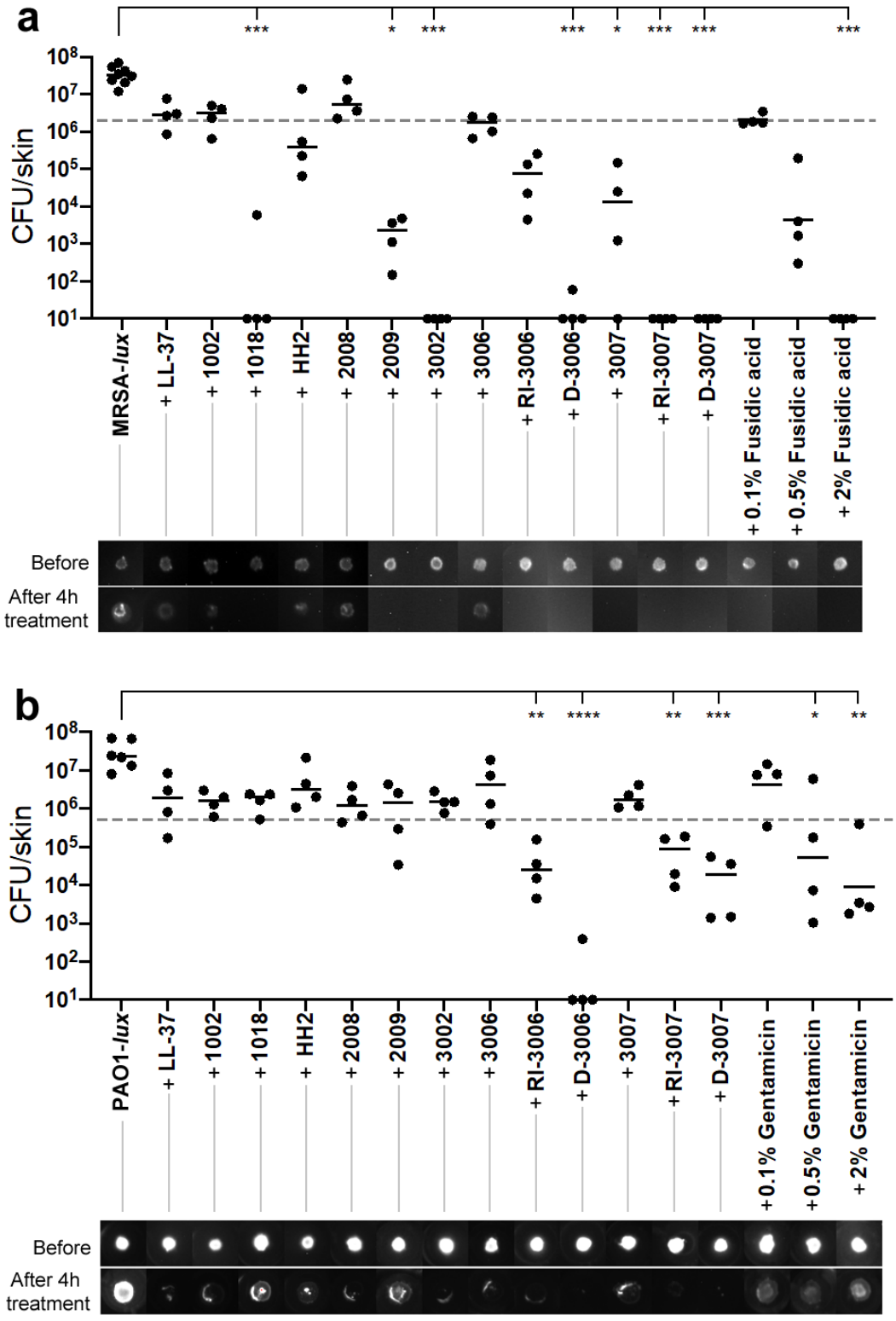

Figure 19. Novel peptides D-3006 and D-3007 had superior antibiofilm activity against MRSA and *P. aeruginosa* biofilm.

One day pre-established MRSA-*lux* (**a**) or PAO1-*lux* (**b**) biofilm was treated topically for 4 hours with 0.1% of various synthetic HDPs, or 0.1%-2% fusidic acid or gentamicin. Colony count recovered from each skin sample was determined with a representative luminescence image shown below.

Dashed lines indicate the antibiofilm activity of 0.1% DJK-5. Statistical significance (* $p \leq 0.05$; ** $p \leq 0.01$; *** $p \leq 0.001$; **** $p \leq 0.0001$) comparing peptide treated skins to MRSA-*lux* or PAO1-*lux* control was performed using the Kruskal–Wallis test, Dunn's multiple comparisons test. Geometric mean of colony count from 4-8 biological replicates was indicated.

Several peptides including RI-3006, D-3006, RI-3007 and D-3007 were identified to have superior activity as compared to DJK-5 in eradicating both MRSA and PAO1 biofilms whereas peptides 1018, 3002 and 3007 were more effective against MRSA skin biofilm (Figure 19). Notably, at the same concentration, all of the above peptides out-performed fusidic acid and gentamicin, which are topical antibiotics often prescribed for superficial Gram-positive and Gram-negative skin infections, respectively [338,339].

In order to use the epidermal skin model to study the immunomodulatory perspective of the peptides, I first attempted to stimulate N/TERT skin with LPS, LTA, Poly(I:C), zymosan A or PMA, from either the apical or basal side of the skin. Interestingly, only Poly(I:C) elicited an inflammatory response when challenged from the basal side of the skin. Similarly, monolayer N/TERT cells only had substantial IL-8 and IL-6 production in response to Poly(I:C) stimulation. Using these systems, I further investigated two of the peptides with leading antibiofilm activity, D-3006 and D-3007. Interestingly, these two novel peptides also exhibited immunomodulatory properties, as demonstrated by their ability to suppress Poly(I:C) induced IL-8 and IL-6 responses in a dose-dependent manner in monolayer N/TERT keratinocytes from as low as 0.2 μg/ml (Figure 20a-b). D-3006 and D-3007 also dampened the IL-8 and IL-6 production when N/TERT skin was simulated with Poly(I:C) from the basal side (Figure 20c-d). It is worth mentioning that D-3006 and D-3007 did not induce any cytotoxicity in either monolayers or skin at the concentrations tested, as measured by the LDH assay (not shown). Together these results show that the N/TERT human organoid skin model can be used as an *in-vivo* like platform for developing novel antibiofilm and anti-inflammatory peptides such as D-3006 and D-3007.

5.6 Antibiofilm activity of D-3006 and D-3007 in an *ex vivo* human skin MRSA biofilm model

To further validate the antibiofilm effect of D-3006 and D-3007 under more representative conditions, I established an air-liquid interface model using human breast surplus skin, by using thermal injury (see Chapter 6) as an additional tool to assist in biofilm establishment (Figure 21).

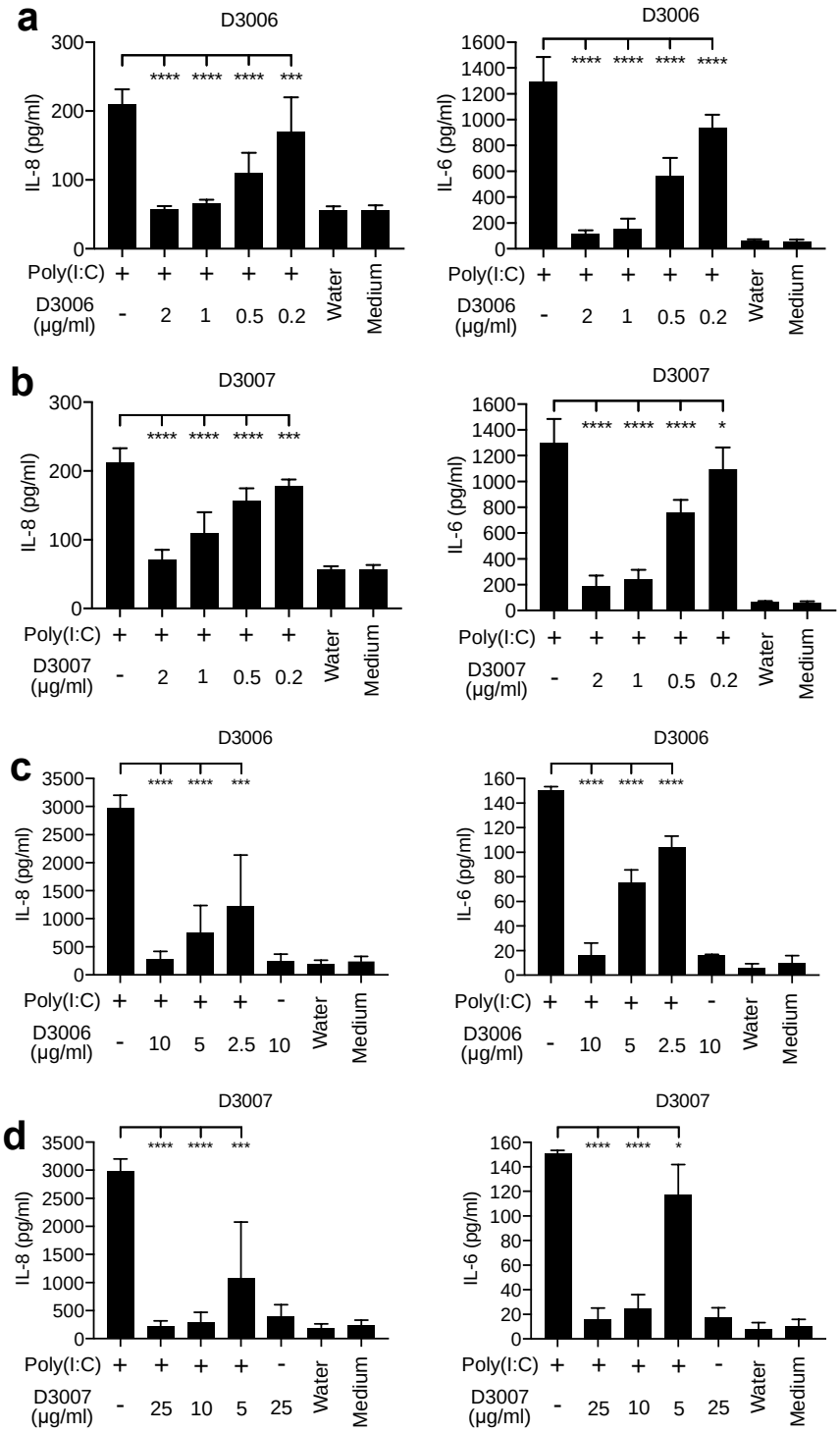

Figure 20. Novel peptides D-3006 and D-3007 had promising anti-inflammatory effect in Poly(I:C)-induced inflammation.

Monolayer N/TERT cells grown in 96-well plates stimulated with 400 ng/ml Poly(I:C) (**a-b**) or N/TERT skin stimulated with 20 µg/ml from the basolateral side (**c-d**) were treated with peptide D-3006 or D-3007 for 24 hours. Culture supernatant in 96-well plates (**a-b**) or culture medium below the skin (**c-d**) were used to determine IL-8 and IL-6 production by ELISA. Statistical significance of 3 independent experiments determined with one-way ANOVA, Dunnett's multiple comparisons test (* $p \leq 0.05$; ** $p \leq 0.01$; *** $p \leq 0.001$; **** $p \leq 0.0001$).

Compared to the N/TERT skin, this model contained both epidermis, dermis and immune cells. H&E staining of human skin cross sections showed this structural complexity with the epidermal rete ridges extending into the dermis, a characteristic of human skin (Figure 21a).

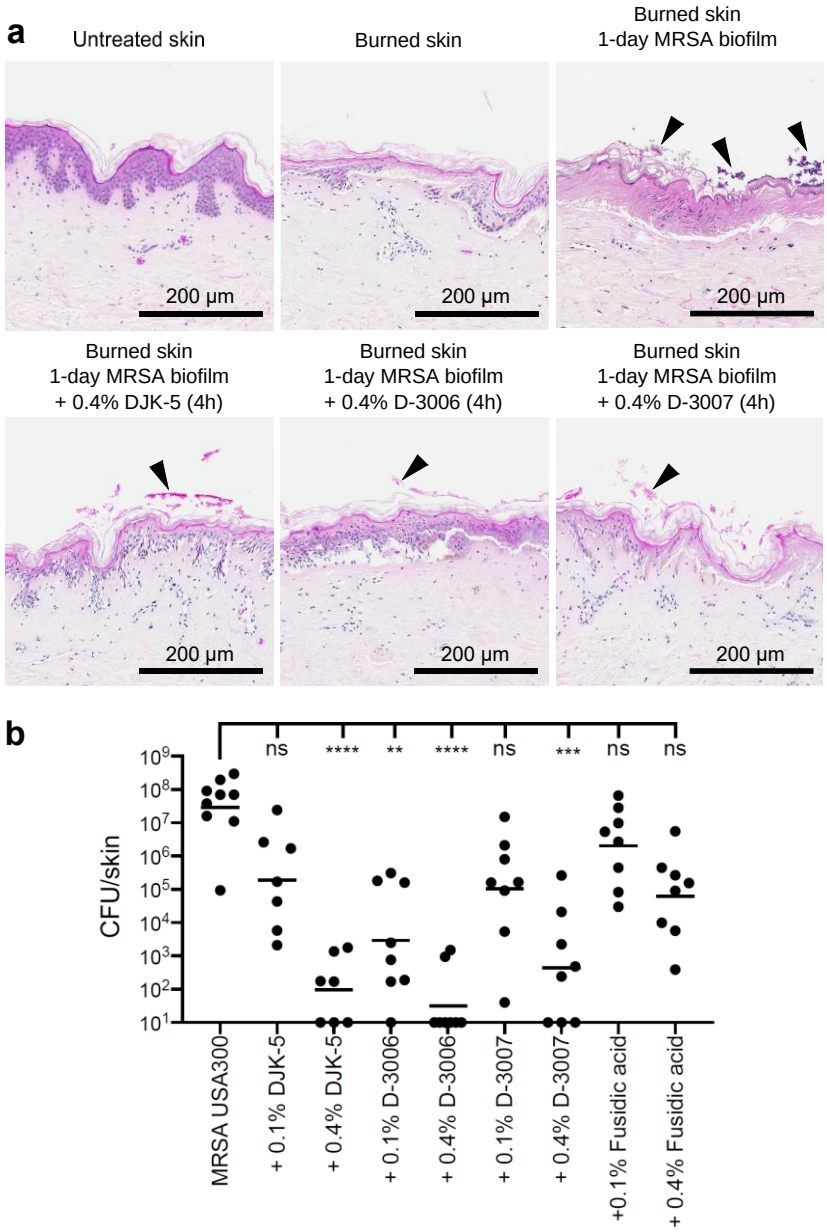

Figure 21. Antibiofilm activity of D-3006 and D-3007 in the *ex vivo* human skin MRSA biofilm model.

Human surplus skin obtained post-breast reduction surgery was thermally challenged at 150°C for 10s and cultured at air-liquid interface. Two million MRSA (USA300-LAC) were spotted on top of the burned skin and cultured for 24 hours, followed by 4 hours topical peptide treatment. Skin cross section was visualized by H&E (arrows indicate MRSA biofilm) (**a**). Colony count recovered from each skin sample was determined (**b**). Statistical significance (* $p \leq 0.05$; ** $p \leq 0.01$; *** $p \leq 0.001$; **** $p \leq 0.0001$) comparing peptide treated skins to MRSA control was performed using the

Kruskal–Wallis test, Dunn's multiple comparisons test. Geometric mean of colony count from 3 donors (7-9 replicates per conditions) was indicated.

The surface of this *ex vivo* skin was thermally injured at 150°C for 10s before MRSA infection to facilitate biofilm colonization. This thermal injury caused a large number of epidermal cells to lose their circular appearance and severely damaged the integration of the epidermis, causing it to separate from the dermis, while no major alterations in the dermis were observed (Figure 21a). Consistent with the observations of MRSA biofilm in the N/TERT skin model, one-day MRSA USA300-LAC biofilm appeared as purple clusters associated with the epidermis, and the remaining biofilms or debris were stained pink after peptide treatments (Figure 21a). Colony counts recovered after 4 hours peptide treatment showed that all peptides retained the antibiofilm activity in the *ex vivo* skin model (Figure 21b). DJK-5 and D-3007 had comparable efficacy in reducing the CFU by about 2 and 5 log orders of magnitude at 0.1% and 0.4% respectively. D-3006 had the most potent antibiofilm effect reducing the geometric mean to 33 organisms at 0.4%. All three peptides especially at 0.4% had superior activity compared to fusidic acid. Together these results confirmed the antibiofilm effect of D-3006 and D-3007 observed in the N/TERT skin model and demonstrated their potential as treatment for real human skin biofilm infections. Future studies are required to understand other perspectives of these two peptides such as aggregation property, *in vivo* toxicity and the mechanisms of action.

5.7 Discussion

There is increasing concern that the favourable results from *in vitro* screening and animal studies of novel drug compounds do not predict the outcomes of trails [340,341]. This problem drives the search for more informative experimental systems that are more representative of the *in vivo* conditions encountered during administration to man [342]. Organoids represent one of the most exciting tools for understanding disease pathology and testing novel drug toxicities and efficacies[342,343]. They have the added benefits of reducing the use of animals in pre-clinical testing and replacing *in vivo* infection models with an ethical alternative that better reflects human disease[344].

Here, I adapted an air-liquid interface human epidermal skin model as an *in vivo*-like screening tool for novel agents against biofilm infections such as MRSA and *P. aeruginosa*. The use of luminescently-tagged bacteria allowed for parallel activity comparison as well as monitoring the progression of the biofilm. Using multiple microscopic approaches, I further discovered that MRSA biofilm on the skin surface appeared as small aggregates of cells (Figure 16). This is consistent with the morphology of WT MRSA biofilm grown on a static inanimate surface where the clusters reflect

the characteristic waves of biofilm detachment and regrowth controlled by quorum-sensing and surfactant molecules [345]. In comparison, *P. aeruginosa* tended to form a more continuous dense mat on the skin surface. Colonization by both species resulted in thickening of the stratum corneum and the epidermal skin barrier could tolerate the growth of these biofilms for about 3 days without an increase in cytotoxicity (Figure A7). Upon treatment with the antibiofilm peptide, DJK-5, I observed a membrane blebbing effect in PAO1 cells (Figure 18), which is a common phenomenon also seen in other Gram-negative bacteria when treated with host defense peptides. For example, time and concentration dependent membrane blebbing has been observed in *E. coli* cells treated with two peptides BP100 and PepR [346]. This is likely due to the polycationic nature of host defense peptides that can disrupt the anionic outer membrane of Gram-negative bacteria.

Topical DJK-5 treatment had broad-spectrum antibiofilm activity reducing luminescence intensity and colony count of both MRSA and PAO1 biofilms (Figure 17-Figure 18). Since luminescence correlates with bacterial survival [347], this suggests that DJK-5 was directly killing the bacterial cells within the biofilms. Importantly, the DJK-5 concentrations used here were less than the concentration of current topical antibiotics (e.g. 1-2% mupirocin, fusidic acid or gentamicin cream or ointment) used in clinical settings [348,349]. In addition to the uprising antibiotic resistance issue, the recalcitrant nature of biofilm makes currently available antibiotic treatments insufficient. MRSA strains that are sensitive to mupirocin treatment in their planktonic state or during very early biofilm formation can become highly mupirocin resistant in established biofilms [350,351]. For example, 2% mupirocin ointment, Bactroban, is largely inactive against a 24-hour biofilm of the mupirocin-sensitive MRSA (strain LUH14616) [41] and sub-inhibitory concentrations of mupirocin have been shown to promote MRSA surface attachment and biofilm formation [352]. Together, these data underscore the inherent challenge in treating biofilm-associated infections in the clinic and highlight the value of the biofilm-based epidermal model in evaluating potential therapeutics for efficacy. In contrast to mupirocin, DJK-5 was equally effective against 3-day biofilms when compared to 1-day biofilms. This is likely because synthetic host defense peptides such as DJK-5, instead of targeting metabolically-active bacteria, function to promote the degradation of the stringent response mediator (p)ppGpp, which is necessary for biofilm initiation and maintenance[221,222]. Therefore DJK-5 represents a viable therapeutic candidate for treating recalcitrant and long-term biofilm infections.

Using the N/TERT skin biofilm system, I identified several novel peptides including D-3006 and D-3007 that have superior activity when compared to DJK-5 in eradicating both MRSA biofilm and PAO1 biofilm (Figure 19). Interestingly, for both D-3006 and D-3007 peptides, the RI-form

peptide exhibited improved antibiofilm activity as compared to their L-form counterparts, and the D-form peptides were the most potent against skin biofilms. This observation was consistent with several other peptides previously studied in our lab, where the D-form of the peptides had enhanced inhibitory effect against *P. aeruginosa* biofilm formation *in vitro* [219]. For example, DJK-1, DJK-2, DJK-3, DJK-4, DJK-5 and DJK-6 all had superior antibiofilm activity as compared to their L-form counterparts. In particular, DJK-5 at 10 μg/ml had 99.7% biofilm inhibition against *P. aeruginosa* whereas LJK-5 was largely inactive [219]. Although it is well accepted that D-form peptides have increased resistance to proteolytic degradation, the relationships between peptide amino acid chirality and their biological activities are complex and not yet fully understood. The differences in peptide activity could potentially be due to the introduction of D-amino acids altering peptide secondary structures and their tendency for self-assembly [353].

The results of the *ex vivo* human skin model largely confirmed the antibiofilm effects of D-3006 and D-3007 against MRSA biofilm and their superior activity when compared to fusidic acid (Figure 20). However, neither D-3006 nor D-3007 showed as much improvement, when compared to DJK-5, as that observed in the N/TERT skin model (where they were about 6 log-fold more effective in reducing biofilm CFU at 0.1% peptide). The differences in peptide efficacy observed could potentially be because of the *ex vivo* human skin adding the structural complexity such as dermis and skin appendages and immune cells. For example, $CD14^+$ or $CD1c^+$ monocytes/macrophages, $CD11c^+$ DCs, $CD56^+CD3^-$ natural killer cells, $CD4^+$ T cells, $CD8^+$ T cells and $CD19^+$ B cells have been previously isolated from *ex vivo* skin samples [354,355]. In addition, the CFU count from the *ex vivo* skin model had more variations reflecting donor variability. Nevertheless, D-3006 was found to be most active in both models.

It is worth mentioning that the *ex vivo* skin model is not suitable for screening a large number of peptides due to limited donor availability. Also, the skin dermis tends to retain dyes used in standard lab assays such as the lactate dehydrogenase assay and the MTT assay making it difficult for toxicity testing. Therefore, both skin biofilm models have their merits and drawbacks and the N/TERT skin biofilm model serves as a simple, easily accessible and bio-relevant model for developing novel antibiofilm agents. Another major limitation of both air-liquid interface skin models is that these static culture systems make it difficult to study dynamic processes such as nutrient exchange and immune cell migration. Future experiments can implement other systems such as the microfluidic skin-on-chip technology where skin is constructed in the presence of fluid flow under controlled microenvironments that closely mimic the mechanical force and biochemical gradients

encountered by natural human skin [356].

Chapter 6: Treating MRSA biofilm and inflammation in thermally damaged skin with antibiofilm peptide DJK-5

6.1 Introduction

Bacterial biofilms associated with damaged skin due to burns, physical injury and diseases such as atopic dermatitis and non-healing ulcers in diabetic patients are difficult to treat as a result of defects in immune function and structural integrity of the skin [357,358]. Biofilms colonizing wounds can impede wound healing [359] and cause hyper-inflammatory [360] responses that are detrimental to the host. In particular, *S. aureus* and *P. aeruginosa* biofilms are among the most common in burn and chronic wounds [70,361]. Laboratory study of wound infections can be difficult since *in vivo* biofilm-infected burn wound models are often complex, of limited relevance, ethically-challenging to implement, and performed in animals that do not reflect conditions of the human skin [362,363]. For example, the skin structures of common lab animals (e.g. mice and rats) are inherently different from human skin [364,365] and wound healing in mice occurs primarily through wound contraction while humans heal through re-epithelialization and granulation [363]. The use of a closer mimic (e.g. porcine skin) is often costly and requires specialized facilities [366]. Therefore, an easily accessible human skin model mimicking burned or damaged conditions would be favorable for studying biofilm wound infections.

In the previous chapter, I observed that 3-day *S. aureus* and *P. aeruginosa* biofilms on the N/TERT skin surface triggered minimal host immune responses when skin maintained a functional barrier. To study whether biofilm infections elicit stronger host immune responses in damaged skin, and whether an impaired skin barrier affects biofilm growth and peptide efficacy, I developed a thermally-challenged MRSA biofilm skin model in this Chapter. The aims of Chapter 6 were to: (1) Use transcriptomics coupled with bioinformatics analyses to explore skin epithelium responses to MRSA biofilm infection and DJK-5 treatment; (2) Compare gene expression between PMA-induced sterile inflammation and bacterial biofilm-triggered inflammation; and (3) Analyze common anti-inflammatory pathways and networks that were modulated by IDR-1002 and DJK-5 in the two types of inflammation.

6.2 DJK-5 reduced MRSA biofilm on thermally injured skin and suppressed skin cytotoxicity and inflammation

N/TERT skin was thermally challenged using a digital soldering iron set to 100°C for 4 seconds prior to establishing MRSA biofilm. Thermal challenge severely injured the epidermis,

especially the stratum granulosum and stratum spinosum layers, while the presence of MRSA biofilm further damaged the surface stratum corneum layer of the skin (Figure 22a). Biofilm-infected burned skin that was treated with DJK-5 had a clear reduction in colonizing bacteria (Figure 22a). SEM imaging indicated that burning of the skin did not cause major changes in the surface of the stratum corneum (Figure 22b). MRSA biofilm colonized the surface and some gaps in between skin cracks (Figure 22b). Topical treatment of the MRSA biofilm on the burned skin with 0.4% DJK-5 peptide for 24 hours significantly reduced the bacterial burden on the burned skin by 2,000-fold, decreasing the bacterial load from 7.8×10^8 CFU/skin to 3.2×10^5 CFU/skin (Figure 22c).

I further characterized the cellular immune responses of biofilm-infected burned skin by assaying the growth medium underneath the cell culture inserts. MRSA colonization of burned skin triggered 47% skin cytosolic lactate dehydrogenase release, while DJK-5 treatment significantly decreased cytotoxicity induced by the MRSA biofilm to only 15% (Figure 22d). MRSA infection also induced pro-inflammatory IL-1β and IL-8 production from thermally damaged skin, both of which were significantly suppressed by treatment with DJK-5 (Figure 22e, f). Compared to control skin, skin that was thermally damaged and treated only with DJK-5 (no biofilm) caused non-significant (~5%) increase in observed cytotoxicity (Figure A8a) and slightly increased IL-8 production (Figure A8b), suggesting that neither burning of the skin nor peptide treatment, per se, triggered a large change in the overall cytotoxicity or immune response. Furthermore, normal skin with established MRSA-*lux* or PAO1-*lux* biofilm and treated with vehicle control (water) for 24 hours (Figure A8c-f), also exhibited only minimal cytotoxic effects (Figure A8e) and an approximately 2-fold induction in IL-8 levels (Figure A8f). Overall, these results demonstrate that burning of the skin increase the susceptibility and severity of the biofilm infection. I also attempted infecting the thermally damaged skin with the strain PAO1, however, *Pseudomonas* consistently penetrated through the damaged skin resulting in growth in the skin culture medium under the cell culture insert within 24 hours of inoculation (not shown).

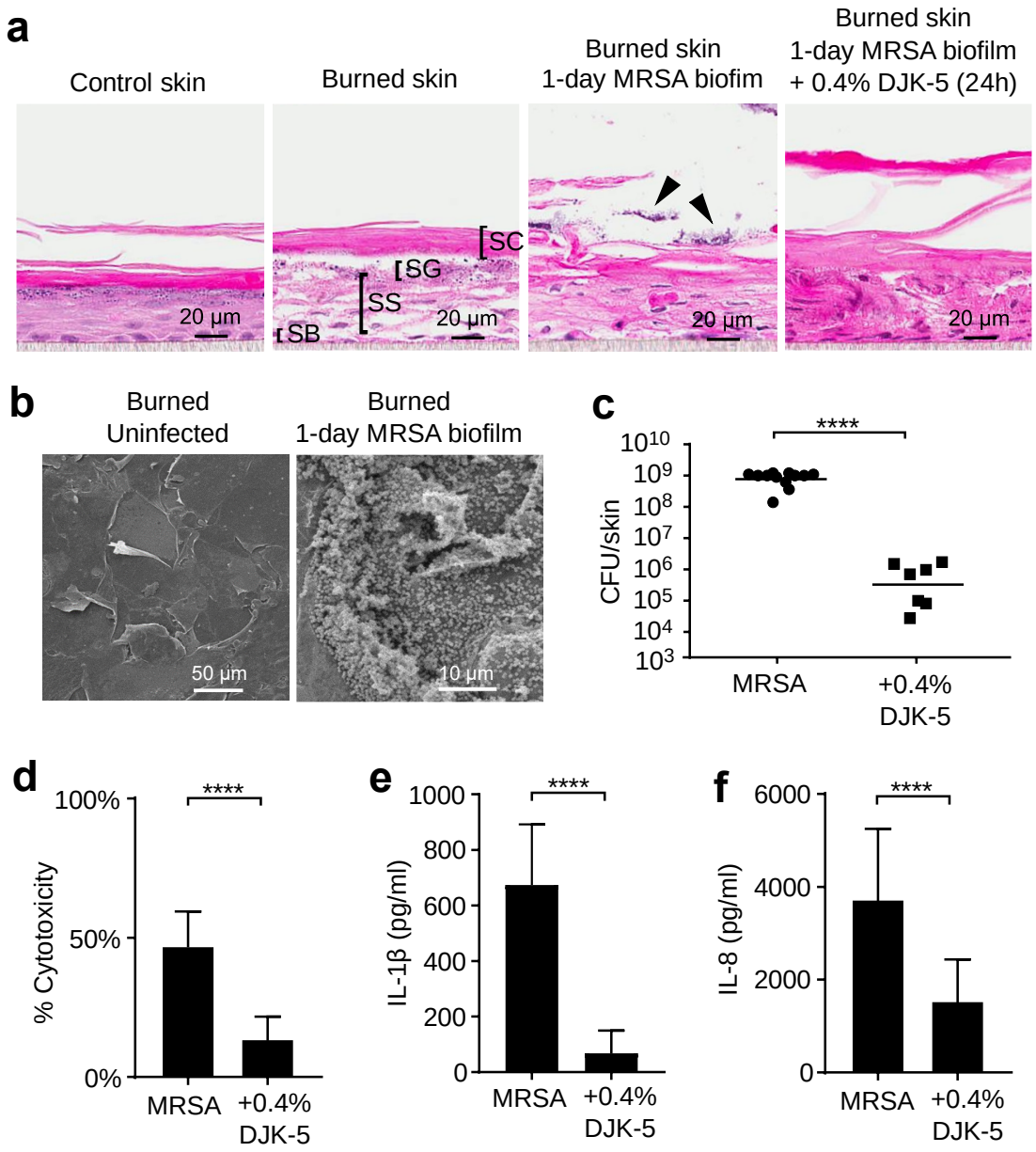

Figure 22. DJK-5 reduced MRSA biofilm, cytotoxicity and pro-inflammatory cytokine production in a thermal burn skin model.

Skin samples were subjected to thermal wounding for 4 seconds at 100°C. One million MRSA (USA300-LAC) was then spotted on top of the burned skin and cultured for 24 hours. Cross sections of epidermal layers corresponding to the stratum corneum (SC), stratum granulosum (SG), stratum spinosum (SS), and stratum basale (SB) were visualized by H&E (arrows indicate MRSA biofilm) (**a**). (**b**) The burned skin and biofilm on top were visualized by SEM. (**c**) DJK-5 peptide in PBS at a dose of 0.4% (120 µg) or - as control - PBS was subsequently applied topically for 24 hours. Samples were collected for bacterial counts (bars indicate geometric mean). (**d**) Culture supernatants below the filter inserts were used for measuring cytotoxicity by the lactate dehydrogenase assay. The amount of IL-1β (**e**) and IL-8 (**f**) in the medium below the filter inserts was quantified by ELISA. Error bars indicate mean with SD in (**d-f**). Statistical significance was calculated using the Mann-Whitney test (**c**) or the student's unpaired t test (**d-f**) from 7-12 biological replicates (**** $P \leq 0.0001$).

6.3 Combining antibiofilm peptide DJK-5 and anti-inflammatory peptide IDR-1002

To investigate whether anti-inflammatory peptides IDR-1002 could further improve antibiofilm activity and reduce skin inflammation, I tested a combination treatment of DJK-5 and IDR-1002 against MRSA biofilm established on burned skin. The effect of 0.4% IDR-1002 treatment alone on MRSA biofilms was marginal, resulting in only a 17-fold reduction in bacterial count compared to untreated biofilms (Figure 23a). This was to be expected since this peptide exhibits relatively weak direct antimicrobial and antibiofilm effects *in vitro* [367]. Moreover, combining 0.4% DJK-5 treatment with IDR-1002 at 0.01%, 0.1% or 0.4% did not significantly enhance antibiofilm effects compared to DJK-5 treatment alone (Figure 23a). However, despite its weak antibiofilm activity, IDR-1002 treatment resulted in significant decreases in cytotoxicity and release of pro-inflammatory IL-1β from MRSA-infected burned skin. When, compared to DJK-5 single treatment, combination treatment with both DJK-5 and IDR-1002 further reduced MRSA-induced cytotoxicity and IL-1β production (Figure 23b, c). The combined treatment caused a non-significant decrease in IL-8 release (Figure 23d), indicating the maintenance of this protective chemokine. Overall, these results demonstrated the potential of employing a multi-pronged strategy to combat recalcitrant skin biofilm infections using synthetic HDPs by simultaneously targeting both the pathogen and promoting a beneficial immune response.

6.4 Effect of DJK-5 treatment on MRSA biofilm infected thermally-injured skin transcriptome

To understand the impact of MRSA infection and DJK-5 treatment on the host immune response, RNA-Seq analysis was performed on total mRNA samples extracted from thermally-challenged skin infected with 24 hours MRSA biofilm, followed by 24 hours DJK-5 treatment and burned skin controls. When comparing other treatment groups to burned skin, genes were considered differentially expressed (DE), if they had ≥ 1.5 absolute fold changes, with an adjusted p-value ≤0.05. MRSA biofilm infection of burned skin led to large transcriptomic changes with 4,366 up-regulated gene and 4,879 down-regulated genes when compared to burned skin control (Figure 24). DJK-5-treated, MRSA-infected burned skin had a substantial number of DE genes when compared to MRSA biofilm infected skin (4485 up-regulated and 3941 down-regulated). This appeared to be largely due to the reversal of the inflammation and skin damage caused by MRSA biofilm infection, since comparing DJK-5-treated, MRSA-infected burned skin to the burned control revealed very few DE genes (182 up-regulated and 8 down-regulated Figure 24). Thus DJK-5 treatment shifted the overall skin transcriptome closer to homeostasis without infection.

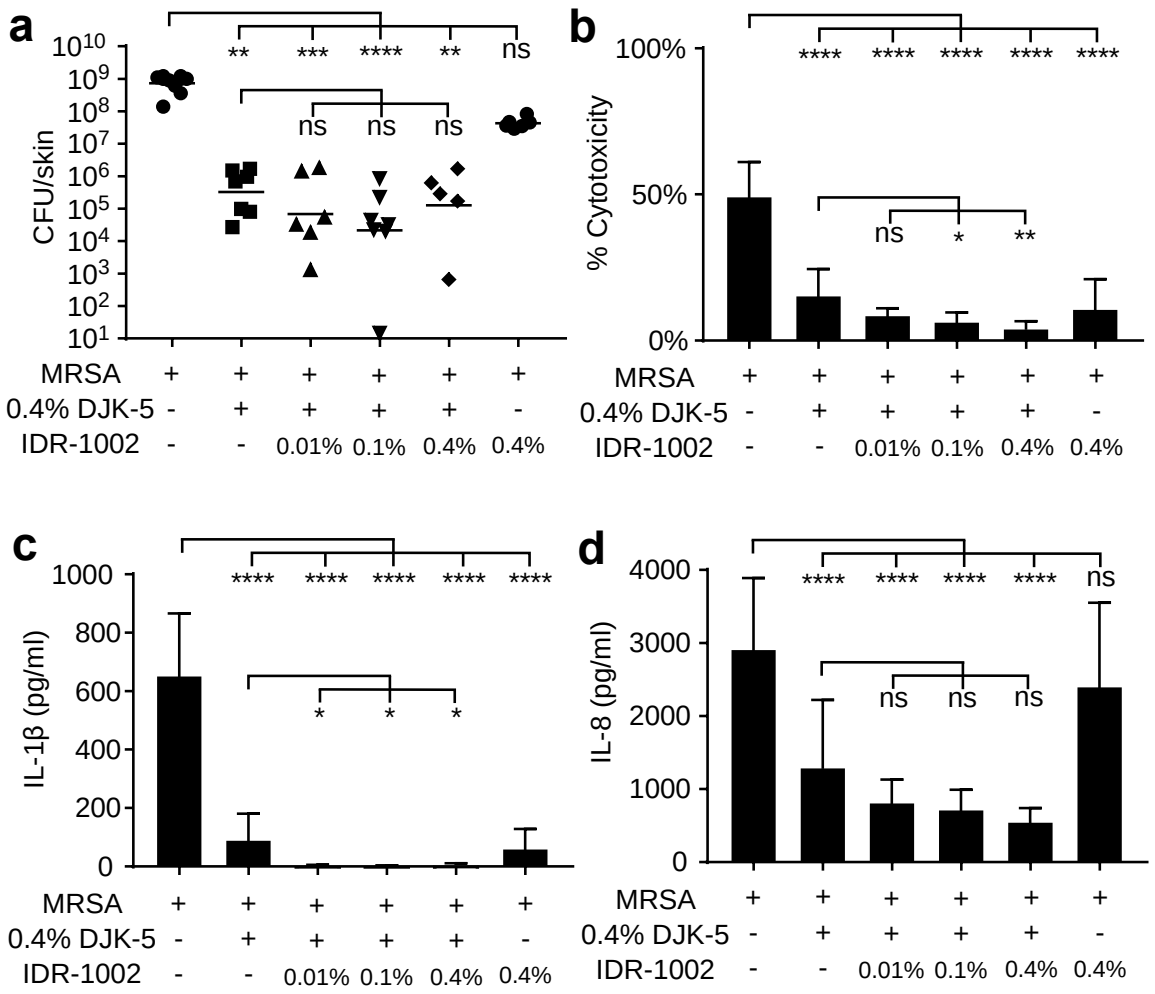

Figure 23. Peptides IDR-1002 and DJK-5 combined treatment further dampened MRSA induced cytotoxicity and IL-1β production in the thermal damaged skin model.
MRSA USA300LAC biofilms were established on top of thermally-damaged skin. DJK-5 alone or in combination with 0.01%, 0.1% or 0.4% IDR-1002 (3 μg, 30 μg or 120 μg) was added on top of skin biofilms for 24 hours. Skin samples were harvested for bacterial counts (bars indicate geometric mean) (**a**), and culture supernatant was used to determine cytotoxicity by the lactate dehydrogenase assay (**b**) and anti-inflammatory activity by ELISA (**c, d**). Error bars indicate mean with SD in (**b-d**). Statistical significance from 5-12 biological replicates in each condition was determined using the Kruskal–Wallis test, Dunn's multiple comparisons test (**a**) or one-way ANOVA, Dunnett's multiple comparisons test (**b-d**) (* $P \leq 0.05$; ** $P \leq 0.01$; *** $P \leq 0.001$; **** $P \leq 0.0001$).

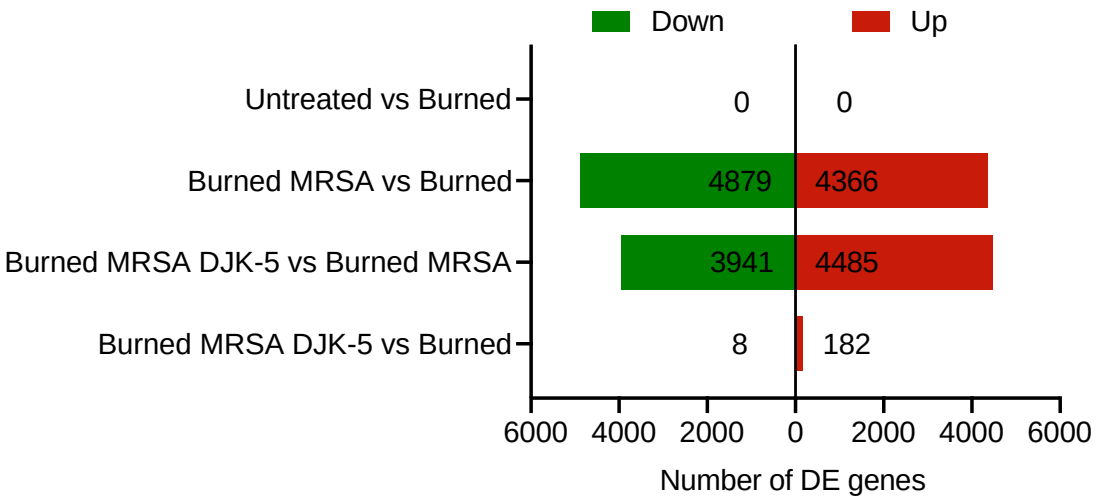

Figure 24. Differential expression analysis of MRSA biofilm infected thermally-injured skin treated with topical DJK-5.
One-day MRSA USA300LAC skin biofilms associated with thermally-damaged skin were treated with vehicle control or DJK-5 peptide at a dosage of 0.4% (120 μg) for 24 hours. To collect sufficient RNA, three skin samples with the same treatment were pooled into one sample and after RNA extraction and conversion to cDNA sequenced on a HiSeqX sequencer (Illumina). Differential expression (DE) analysis was performed using DESeq2 v1.28.1 [242], and significance was determined based on adjusted p-value ≤0.05 and fold change ≥ ±1.5.

Pathway enrichment analysis using Sigora [243] revealed the differential influence of MRSA infection and DJK-5 treatment on the burned skin, ranging from effects on the skin surface barrier function and inflammatory immune responses, to metabolic state changes (Figure 25). MRSA biofilm infection greatly impaired the formation of cornified envelope (layers of terminally differentiated, dead keratinocytes atop the skin; $p<2.78\text{x}10^{-239}$), which is responsible for maintaining the skin barrier function and the mechanical stability of individual cells in the epidermal tissue [272]. DJK-5 treatment remarkably eliminated the large change to this pathway with a significance value approaching 0, indicating a protective role in restoring barrier function. In addition, DJK-5 also promoted cilium assembly ($2.1\text{x}10^{-36}$) which is maintained by intra-flagellar transport ($5.08 \text{ x } 10^{-40}$) and involves signalling by the WNT ($1.3\text{x}10^{-10}$), Hedgehog ($2.7\text{x}10^{-8}$) and Notch ($9.0\text{x}10^{-4}$, downregulated) pathways. Primary cilia are known to play essential roles in skin morphogenesis, keratinocyte stratification and epidermal stress responses [368,369]. MRSA biofilm upregulated pathways involved in cell junction organization and skin extracellular matrix organization promoting the synthesis of collagen ($4.5\text{x}10^{-47}$), and interactions of elastic fibres ($8.3\text{x}10^{-13}$) and integrin ($1.4\text{x}10^{-8}$), reflecting the infected skin sensing increased external stress elicited by MRSA colonization. In particular, MRSA infection upregulated the senescence-associated secretory phenotype (SASP, $2.5\text{x}10^{-11}$), a

response signifying critical levels of cellular damage and tissue dysfunction triggered by external or internal insults, which is known to contribute to a variety of age-related diseases and chronic inflammation [370,371]. Pathways related to cell sensing of damage/stress such as DNA damage, oxidative stress and oncogenic signalling were upregulated in the MRSA biofilm-infected burned skin (e.g. oxidative stress induced senescence, $3.1x10^{-4}$; signalling by RAS mutants, $3.7x10^{-8}$; oncogenic MAPK signalling, $3.9x10^{-9}$) and restored to nearly normal in the skin given DJK-5 treatment (e.g. oxidative stress induced senescence, 7.39×10^{-5}; signalling by RAS mutants, $9.4x10^{-4}$; oncogenic MAPK signalling, $7.7x10^{-5}$). Notably, DJK-5 treatment strongly promoted DNA repair function ($1.1x10^{-75}$) including double stranded breaks ($1.7x10^{-9}$), abasic site ($3.3x10^{-12}$) and mismatch repair ($2.2x10^{-5}$), which were all downregulated in MRSA biofilm infected skin.

In the burned skin, MRSA biofilm infection provoked inflammatory responses including multiple interleukin pathways, such as IL-6 ($1.7x10^{-19}$), IL-1 ($2.0x10^{-12}$), IL-4 and IL-13 ($1.4x10^{-42}$), as well as NLRP3 inflammasome activation ($9.6x10^{-5}$), and upregulated type II ($2.4x10^{-12}$) IFN response (Figure 25). MRSA-infected skin also upregulated multiple pathways integrating intracellular signals including Rho GTPases ($1.1x10^{-274}$) which coordinate cell cycles and cell migration, and tyrosine kinases ($1.2x10^{-160}$) and the JAK-STAT pathway ($9.5x10^{-27}$) which functions in cytokine signalling (e.g. IL-6, IL-4 and IL-13). Skin treated with DJK-5 showed a reversal of these patterns in regulation of cytokine and signalling transduction, when compared to untreated MRSA biofilm, likely reflecting an overall dampened inflammatory state. In addition, MRSA biofilm induced death receptor signalling ($1.3x10^{-9}$) and apoptosis ($6.1x10^{-5}$) in burned skin, which has been proposed to be a beneficial host defense reaction during microbial infections [372]. Interestingly, DJK-5 treatment did not significantly interfere with this process at the transcriptomic level. MRSA infection upregulated pathways involving MHC I antigen presentation ($9.2x10^{-15}$) and ER-phagosome cross-presentation ($1.2x10^{-11}$) in the N/TERT skin cells, which typically detect intracellular, foreign or aberrant host proteins. Moreover, the Unfolded Protein Response ($7.4x10^{-7}$), a cytoprotective reaction in response to endoplasmic reticulum (ER) stress exerted by invading microorganisms was also activated in the MRSA infected burned skin [373]. This helps to partially explain the strong inflammatory response elicited in the burned skin by MRSA, which was largely absent in MRSA-infected intact skin, due to the thermal challenge damaging the skin barrier and host cell membrane, leading to increased susceptibility for MRSA invasion.

Pathway enrichment analysis also revealed a distinct metabolism profile (Figure 25). MRSA infected skin upregulated glycolysis ($2.9x10^{-11}$) and respiratory electron transport ($3.9x10^{-10}$)

reflecting an overall increase in ATP production in the burned skin during MRSA infection. For protein metabolism, MRSA biofilm infection promoted translation ($1.1x10^{-21}$) and protein phosphorylation (1.09×10^{-21}) but downregulated other post-translational modification processes including N-linked glycosylation ($2.7x10^{-10}$), methylation (8.5×10^{-6}), ubiquitylation (1.7×10^{-16}) and neddylation (3.2×10^{-20}). MRSA infected skin also demonstrated reduced metabolism of fatty acids ($2.2x10^{-62}$). By comparison, infected skin treated with DJK-5 showed an opposite pattern in metabolic regulation with reduced glycolysis ($3.7x10^{-19}$) and protein translation ($3.0x10^{-124}$), and increased fatty acid ($7.3x10^{-27}$) metabolism.

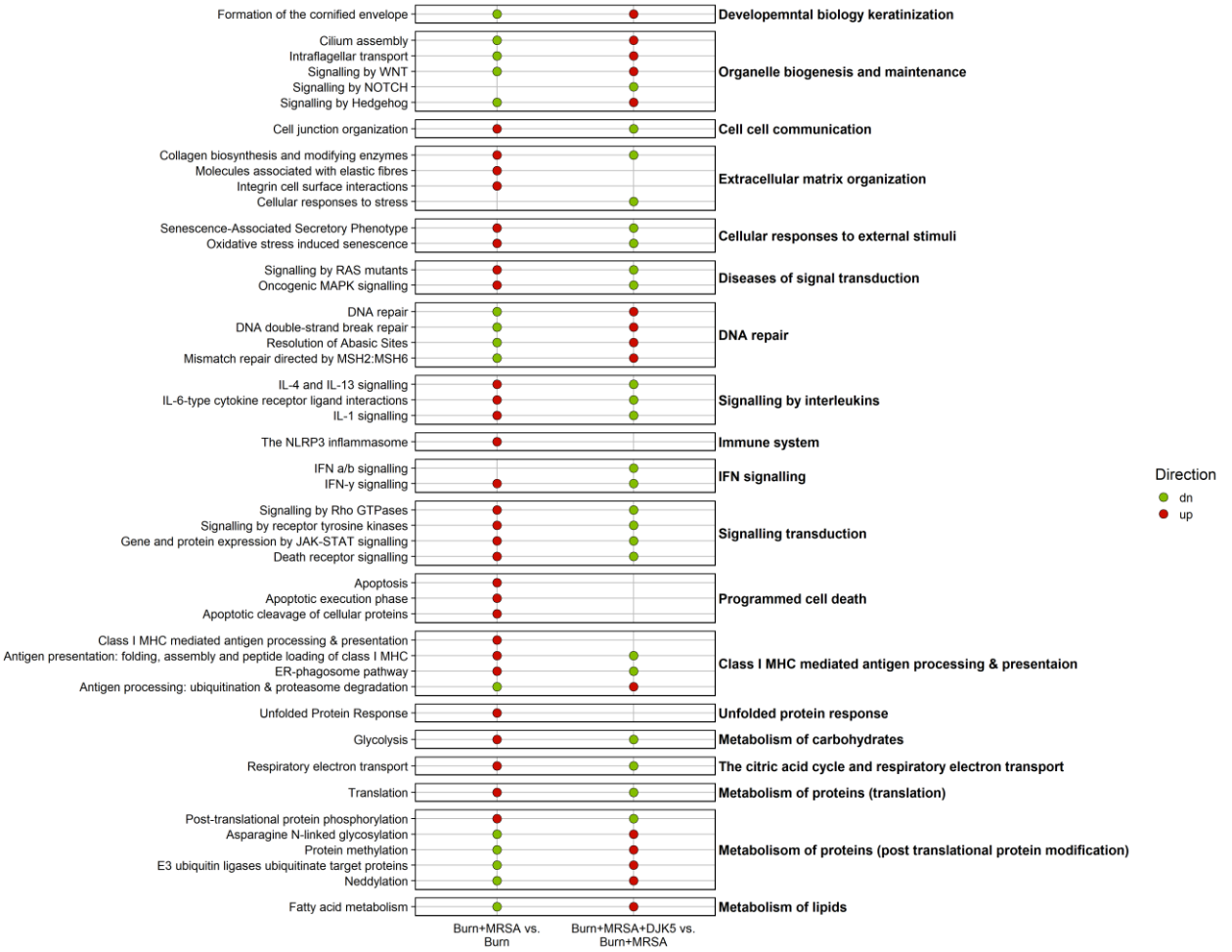

Figure 25. Selected pathways dysregulated by MRSA biofilm infection with or without DJK-5 treatment in thermally damaged N/TERT skin.
Pathway enrichment analysis using Sigora v3.0.5 considered the overrepresented pathways with an adjusted p-value <0.001. Red circles indicate upregulated pathways and green circles indicate downregulated pathways.

6.5 DJK-5 reduced MRSA invasion of N/TERT skin

Since pathway enrichment analysis revealed MHC I antigen presentation which was

consistent with a proportion of MRSA being internalized upon colonization, the mechanism of bacterial evasion was further studied. MRSA infection of thermally wounded skin upregulated multiple skin extracellular matrix genes such as collagen, fibronectin and laminin as well as their integrin receptors (Figure 26). Following fibronectin and integrin-mediated adhesion, MRSA infection upregulated multiple kinases such as the integrin-linked kinase (ILK), focal adhesion kinase (FAK) and Src kinase. Additionally, activation of the hepatocyte growth factor receptor MET lead to upregulation of downstream WAVE family proteins, which associate with an actin related protein 2/3 complex and function to enhance actin polymerization and internalization of MRSA.

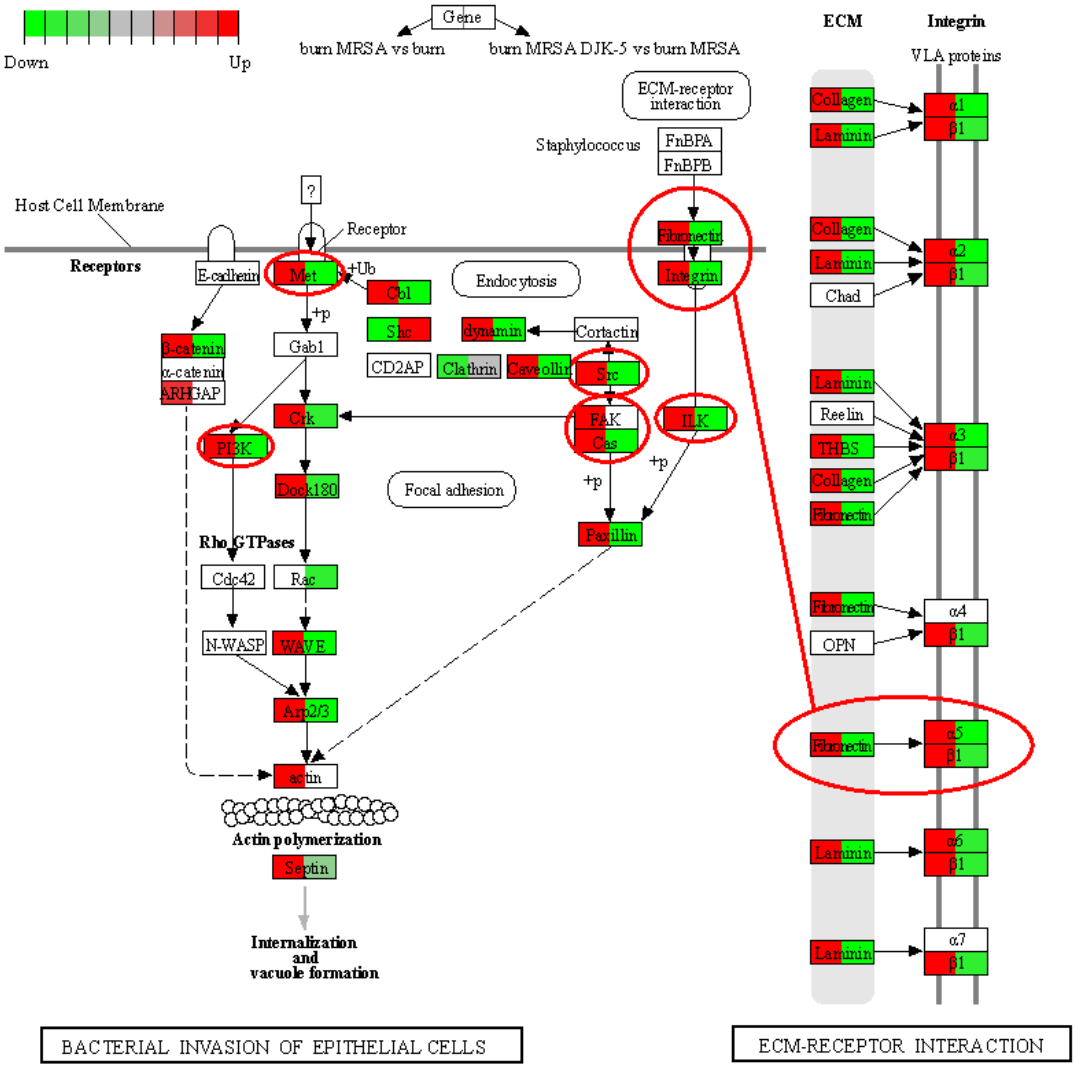

Figure 26. DJK-5 downregulated MRSA invasion of thermally damaged N/TERT skin. Modified KEGG Pathview graph of extracellular matrix-receptor interactions and bacterial invasion of epithelial cells. Left half of each gene compares MRSA infected burned skin to burned skin control and right half of each gene compares DJK-5 treated to untreated MRSA infection of burned skin. Red indicates upregulation and green indicates downregulation.

Conversely, DJK-5 treatment of biofilm infected burned skin led to downregulation of both

the fibronecin-integrin pathway and the MET pathway including the essential kinases (e.g. ILK, Src and PI3K), and resulted in reduced septin assembly. These results indicated that DJK-5 reduced MRSA intracellular invasion, in part by downregulating MRSA interaction with host cell adhesion molecules, intracellular kinases signalling cascades and MRSA mobilization of actin cytoskeleton.

6.6 DJK-5 dampened inflammation in MRSA biofilm infected skin through regulation of TNF-α signalling

NetworkAnalyst provides a method to display functional interactions of dysregulated genes as a protein-protein interaction network that reveals functional interactions (direct, biochemical and regulatory). Networks constructed using DE genes dysregulated by MRSA biofilm infection with or without DJK-5 treatment revealed tremendous complexity with more than 5,000 hubs (not shown), where hubs are key proteins that interact with many other dysregulated genes and are considered to be critical nodes in a network that both receive and disperse signals. The leading KEGG pathway functional enrichment of such a network involved the TNF-α, NF-κB, and MAPK pathways, which all take part in the TNF-α cascade. TNF-α signalling plays an important role in host defenses, inflammation, cell proliferation, and apoptosis [374]. In particular, TNF-α receptor 1 is critical for induction of skin inflammation by TNF-α [375]. Here, I observed that MRSA biofilm infection of thermally damaged skin upregulated MAPK pathways including MKK7-JNK and MKK3-p38 and downstream transcription factors AP-1, c/EBPB and CREB (Figure 27). Interestingly, DJK-5 treatment downregulated MRSA-induced MAPK kinases (MKK7, MKK3 and MEK) and transcription factors (AP-1, c/EBPB and CREB) expression without significantly altering MAPK expression. MRSA biofilm also activated NF-κB signalling including a component of the IκB kinase complex, IKKβ, IκBα and all NF-κB subunits. DJK-5 treatment downregulated NF-κB, together with decreased expression of other inflammation-related transcription factors AP-1, c/EBPB and CREB, and led to suppression of proinflammatory cytokines and chemokines (e.g. IL-1β, TNF-α, IL-8/CXCL-8, CXCL-2 and CCL-20), as well as enzymes for prostaglandin biosynthesis (e.g. PTGS2), matrix metalloproteinases (e.g. MMP3, MMP9 and MMP14), vascular endothelial growth factors (e.g. VEGFC), cell adhesion molecules (e.g. ICAM1) and genes that negatively regulate inflammation (e.g. BCL3, NFKBIA and SOCS3).

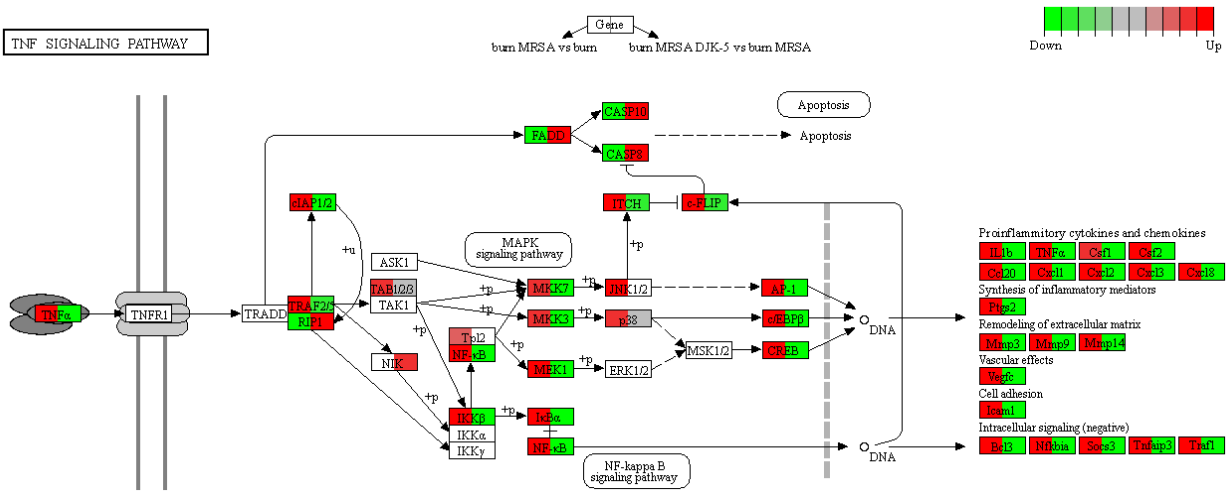

Figure 27. DJK-5 downregulated the TNF-α signalling pathway in MRSA biofilm induced skin inflammation.

Modified KEGG Pathview rendering of the TNF-α signalling pathway. Left half of each boxed gene compares MRSA infected burned skin to burned skin control and right half of each gene compares DJK-5 treated to untreated MRSA infection of burned skin. Red indicates upregulation and green indicates downregulation.

6.7 DJK-5 suppressed interleukin and interferon responses in MRSA biofilm skin inflammation

Pathway enrichment demonstrated that interleukins and interferons were major immune signalling cascades that were differentially expressed in response to DJK-5 treatment. Therefore, I further examined genes within these pathways. MRSA biofilm upregulated the IL-1 signalling cascade (e.g. IL1A, IL1B, IL1RN, IRAK2, TAB2, TAB3 and PELI1) (Figure 28a). Additionally, MRSA infection increased the expression of colony stimulating factor (CSF)-2, IL-6 and IL-7 receptors (e.g. IL6ST, IL6R, IL7R) but downregulated IL-18. DJK-5 treatment downregulated IL-1 and IL-6 signalling and suppressed MRSA biofilm-induced NF-κB (e.g. NFKB1, NFKB2 and RELA) and MAPK (e.g. MAP2K1, MAP3K3, MAP2K2) pathways. DJK-5 treatment also suppressed MRSA-induced sequestosome-1 expression, which plays roles in regulating TNF-α and NF-κB signalling and has been identified as an intracellular target of immunomodulatory peptides such as IDR-1 [298]. MRSA biofilm upregulated NOD1 but downregulated NOD2 expression, while DJK-5 treatment enhanced NOD2 and did not significantly alter pathogen sensing through NOD1. Upregulation of inflammation regulators in the negative feedback loops (e.g. SOCS1, SOCS3 and TNIP2) by MRSA biofilm infection were found for both interleukin and IFN pathways. MRSA upregulated IRF family transcription factors (IRF1, IRF2, IRF3, IRF6 and IRF9) regulating IFN responses but downregulated multiple types of IFN-stimulated genes (e.g. IFIT1-3, OAS1-2,

RNASEL, MX1-2 and GBP1,2,6) (Figure 28b-c). DJK-5 treatment reversed the expression pattern of IRFs and IFN-inducible genes returning skin to homeostasis.

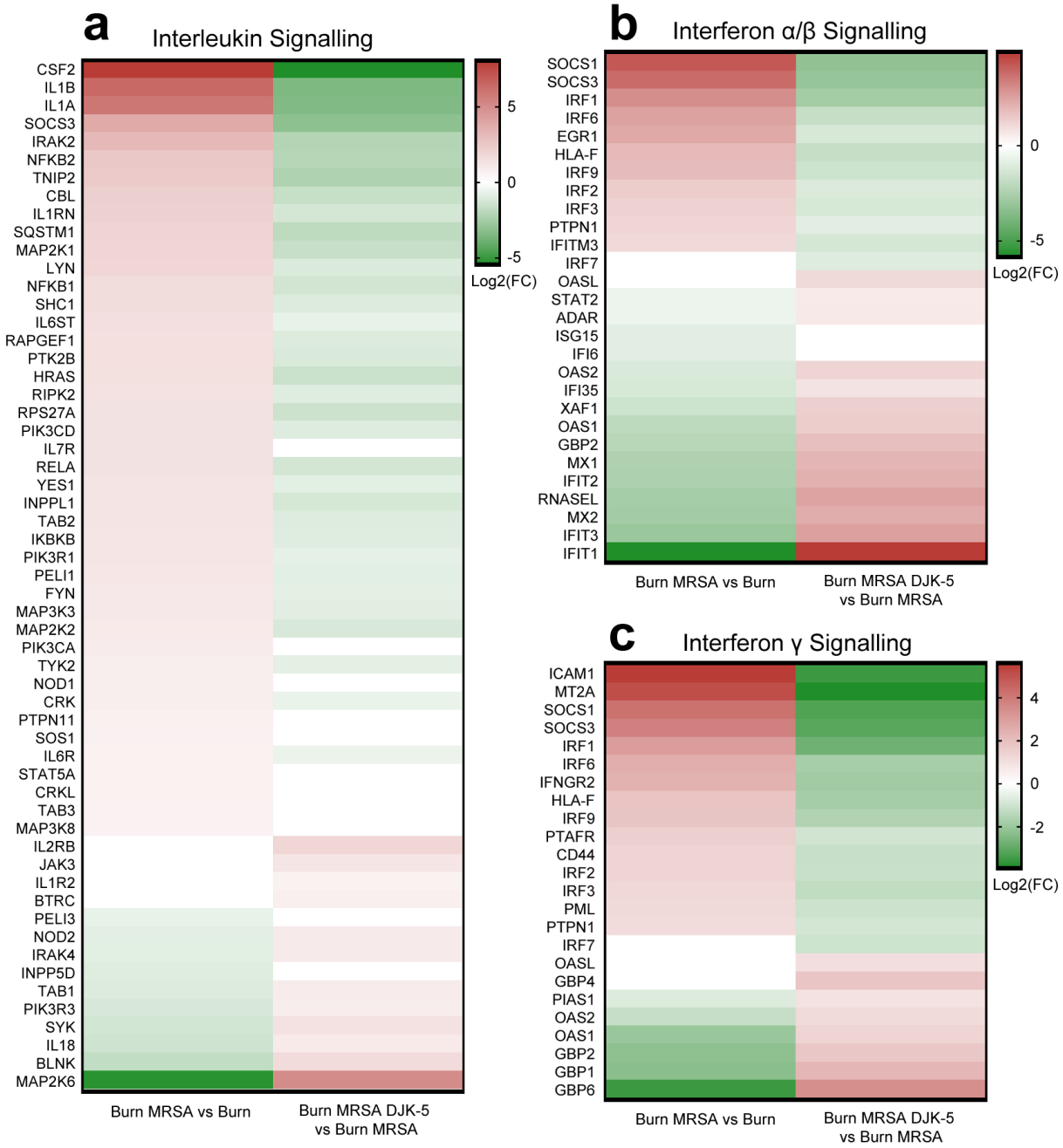

Figure 28. DJK-5 treatment downregulated interleukin and interferon responses in MRSA biofilm skin infection.

Heatmap of differentially expressed genes involved in the interleukin (**a**), interferon-α/β (**b**) and interferon-γ (**c**) signalling cascades in response to MRSA biofilm-induced skin inflammation with or without DJK-5 treatment. Genes from these pathways were downloaded from InnateDB. Color scale based on log2 fold change of DE genes with red indicating upregulation and green indicating downregulation.

6.8 Shared inflammatory mechanisms of PMA-induced sterile skin inflammation and MRSA biofilm skin infection

To study the common mechanisms driving both sterile skin inflammation (Chapter 3) and biofilm infection induced skin inflammation, I identified homologous genes that were differentially expressed in both studies. Comparing both types of inflammation, 910 shared DE genes were found to be commonly upregulated or downregulated by PMA challenge and MRSA biofilm infection. NetworkAnalyst of these DE genes (using their human homologs) revealed a zero-order protein-protein interaction network consisting of 285 hubs (Figure 29a). Major hubs with the most interactions were transcription factors (e.g. CEBPB, RELA, REL, NFKB1, HIF1A and ESR1), cytokines (e.g. TNF-α), receptor tyrosine kinases (e.g. EGFR), regulators orchestrating inflammatory responses (e.g. EGR1, SMAD3, NFKBIA and ARRB1) and genes involved in cellular response to DNA damage and ER stress (e.g. BRCA1).

Functional analysis using Reactome identified sub-networks directed by these major hubs that were involved in many inflammatory processes such as cytokine signalling in the immune system with the majority of these proteins (indicated with a blue highlight) also enriched in interleukin cascades (Figure 29b). Both PMA and MRSA biofilm-induced skin inflammation upregulated proteins essential for IL-1β signalling (e.g. FAS, TNIP2, IRAK2 and IL1B) and additional hubs (e.g. STAT5A, SYK and IL-4R) that were also involved in other interleukin cascades such as IL-2, IL-3, IL-4 and IL-13. This sub-network also contained proteins that participated in IFN responses with some being upregulated (e.g. EGR1, PTPN1 and IRF9) while others were downregulated (e.g. OAS1, IFIT3). Both types of skin inflammation led to NLRP3 activation (Figure 29c). In particular, proteins related to ER stress-induced NLRP3 activation (e.g. EIF2S1, ATF3 and ATF4) and regulators of NLRP3 inflammasome (e.g. MEFV and POP1) were upregulated. A similar subset of these proteins also functioned in the ER stress-induced unfolded protein response (Figure 29d). Functional analysis also identified a TLR signalling sub-network and the shared hubs belonging to proteins controlling multiple TLR cascades (e.g. RELA, MAPK11, IRAK2, PELI3, MAP2K6, NFKB1 and NFKBIA) rather than a specific TLR pathway (Figure 29e). Lastly, both PMA stimulation and MRSA biofilm modulated multiple extracellular matrix components (e.g. THBS1, TNC and LAMA1) and upregulated their integrin receptors (e.g. ITGA1, ITGA2 and ITGB1) and proteins involved in regulation and turnover of extracellular matrix (e.g. SMAD3 and MMP1).

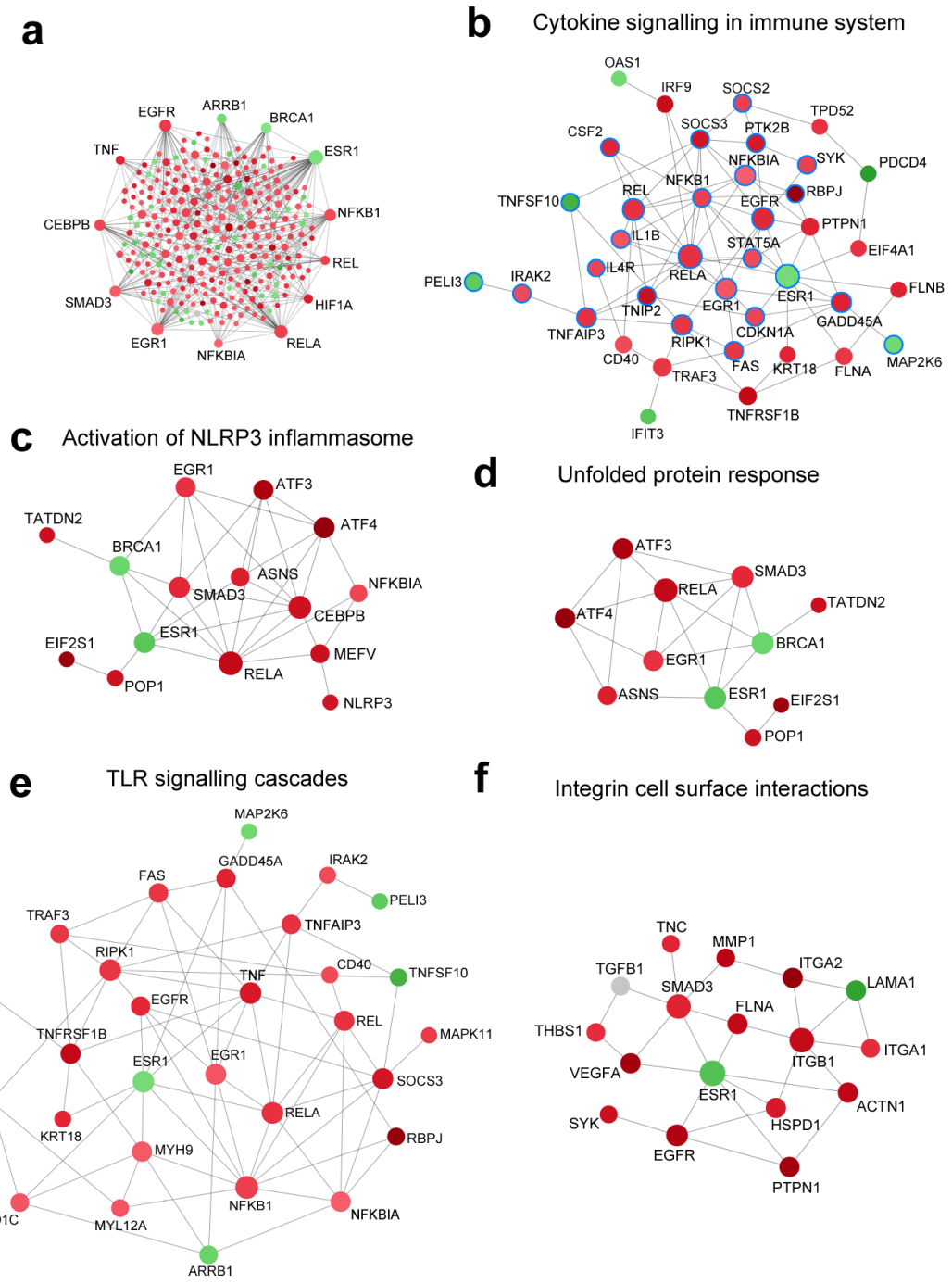

Figure 29. Shared inflammatory mechanisms of PMA-induced sterile skin inflammation and MRSA biofilm skin infection.

Zero order protein-protein interaction networks of shared and co-regulated DE genes comparing PMA-challenged mouse ear to control and burned MRSA biofilm infected N/TERT skin to control (**a**). Sub-networks (**b-f**) were generated by extracting hubs from the total network using the Reactome functional analysis in NetworkAnalyst. Red nodes denote upregulation and green nodes denote downregulation.

6.9 Synthetic host defense peptides IDR-1002 and DJK-5 dampened skin inflammation by downregulating TNF-α and NF-κB signalling and their negative regulators

To explore the common anti-inflammatory mechanisms of synthetic host defense peptides IDR-1002 and DJK-5, a protein-protein interaction network was constructed from shard DE genes that were regulated in the same directions in these two studies (Figure 30).

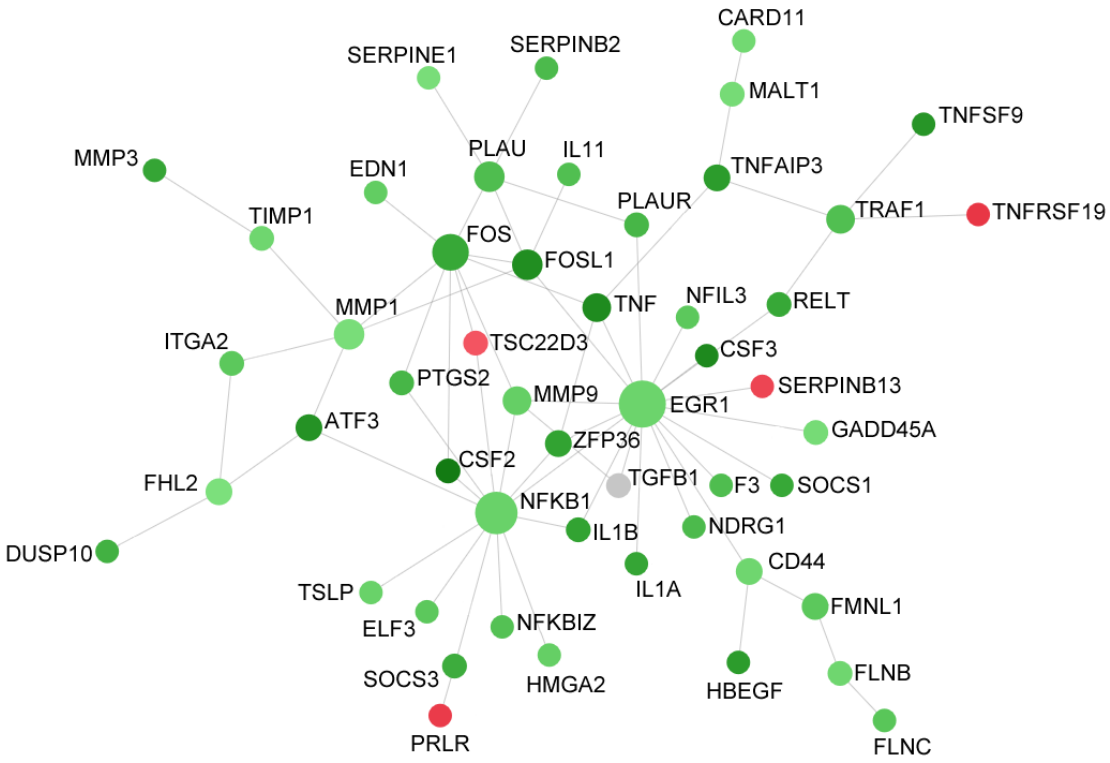

Figure 30. Shared anti-inflammatory mechanisms of synthetic HDPs IDR-1002 and DJK-5 in PMA-induced sterile skin inflammation and MRSA biofilm skin infection.
A zero-order protein-protein interaction network of shared and co-regulated DE genes comparing IDR-1002 treated PMA-induced sterile skin inflammation and DJK-5 treated MRSA biofilm skin infection. Red nodes denote upregulation and green nodes denote downregulation.

Major hubs downregulated by peptide treatment in both types of inflammation (Figure 30) were NFKB1, EGFR, TNF and the AP-1 transcription factor members FOS and FOSL1 downstream of TNF-α signalling. Peptide treatment also downregulated proinflammatory mediators such as cytokines (e.g. IL1A, IL1B, IL11, CSF2, CSF3 and TSLP), matrix metallopeptidases (e.g. MMP1, MMP3 and MMP9), prostaglandin synthase (e.g. PTGS2), and plasminogen activator and receptors (e.g. PLAU and PLAUR). Proteins involved in cell-cell interactions (e.g. CD44 and ITGA2) and cytoskeletal organization (e.g. FMNL1, FLNB and FLNC) were also downregulated by both peptide treatments. The dampened skin inflammation post-IDR-1002 and DJK-5 treatments was also

reflected by reduced expression of proteins that play regulatory roles in inflammation such as suppressors of cytokine signalling (e.g. SOCS1 and SOCS3), matrix metallopeptidases (e.g. TIMP1) and plasminogen activator (e.g. SERPINE1, SERPINB2) as well as regulators that were part of negative feedback loops of TNF-α, NF-κB and MAPK signalling (e.g. ZFP36, NFKBIZ, TNFAIP3 and DUSP10). Skin treated by both peptides upregulated an anti-inflammatory protein (e.g. TSC22D3) that suppressed AP-1 and NF-κB DNA-binding activities.

6.10 Discussion

Compared to MRSA biofilm in the absence of thermal skin damage, the bacterial burden recovered from thermally injured skin was nearly 10-fold higher (Figure 22). Since the epidermal barrier is crucial to confront and resist environmental stimuli (e.g. microbial colonization and changes in temperature, light and water) and to maintain internal homeostasis [376], the increase in bacterial burden could be due to an increase in MRSA colonization and invasion, and increased spreading across the surface of the skin and/or penetration into the deeper layers of the tissue. Therefore, this suggests that thermal challenge negatively impacted on the barrier properties of the skin, thereby increasing its susceptibility to MRSA infection. Consistent with this concept, in atopic dermatitis patients, *S. aureus* is able to more effectively penetrate lesional skin, when compared to non-lesional skin, as a result of impaired physical and antimicrobial barriers of the skin [377].

Host response to biofilm infections is complex and dynamic since bacterial signature molecules that are readily recognized by the host immune system can be hindered by extracellular polymeric substances and other components of biofilm extracellular matrix as the biofilm develops[378]. This is particularly complicated for *S. aureus* infections since this organism is capable of both intracellular and extracellular survival [379]. The inflammatory response also depends on the site of infection and types of immune cells present. Stratified keratinocytes in the skin epidermis are essential for skin barrier function, structural integrity and initiation of skin inflammation. However, their role in biofilm infection is not yet understood.

Consistent with the clinical features of biofilm wound infections [360], MRSA biofilm infection of burned N/TRERT skin caused enhanced cytotoxicity and IL-1β and IL-8 production (Figure 22), which was absent from MRSA infected intact skin (Figure A8). This indicated that host defense mechanisms of the skin were activated due to skin damage and the bacterial burden exceeded the threshold that intact skin could otherwise tolerate. Although H&E staining showed severe skin damage due to thermal injury (Figure 22), no DE genes were found when comparing burned skin to untreated skin (Figure 24). This is likely because the burned skin controls were collected 48 hours

post-thermal challenge for RNA-Seq analysis (together with samples in other experimental conditions), which was likely too late to capture the transcriptomic changes due to moderate thermal injury. Importantly, RNA-Seq analysis confirmed that MRSA biofilm elicited interleukin responses including strong IL-1α and IL-1β induction and NLRP3 activation (Figure 25). Additionally, TNF-α signalling, MAPK pathways including JNK, p38 MAPK and NF-κB signalling were major inflammatory pathways driving MRSA biofilm induced inflammation in N/TERT skin (Figure 27). Consistently, MRSA biofilm infections have been shown to enhance the expression of cytokines (e.g. IL-1α, IL-1β, IL-6, IL-8 and TNF-α) and antimicrobial proteins hBD-2, hBD-3 and RNAse7 in thermally wounded skin when compared to control human skin [380,381].

RNA-Seq results also revealed that MRSA biofilm modulated type I and II IFN responses and upregulated IRF transcription factors including IRF1, IRF2, IRF3, IRF6 and IRF9 (Figure 28). Although traditionally studied in the context of viral infections, IFN responses are also crucial players of inflammatory processes during bacterial infections regulating a diverse range of anti-bacterial host responses, mainly functioning through the induction of hundreds of IFN-stimulated genes [382]. *S. aureus* has been shown to upregulate type I IFN signaling in airway epithelial cells [383]. The role of IFN responses in skin biofilm infection to date is unclear. In keratinocytes, IRFs function to regulate growth and differentiation. For example, IFN-γ and IRF-1 inhibit keratinocyte proliferation [384]. All of IRF1, IRF2, IRF3, IRF6 and IRF9 have been identified in a protein-protein interaction network representing keratinocytes with low stem cell capabilities such as self-renewal and migration [385]. This is consistent with the conclusion that MRSA biofilm infection dysregulated epidermis formation. Interestingly, despite the upregulation of IRFs in MRSA biofilm infected skin, several types of IFN-stimulated genes were downregulated. This could due to the strong induction of negative regulators of IFN responses (e.g. SOCS-1 and SOCS-3), in part, as a result of bacteria interfering with the host response. Indeed, MRSA skin infection has been shown to gradually enhance SOCS-1 expression levels between 1- and 3-days post-infection and restrained skin host defenses as indicated by impaired bacterial clearance, macrophage antimicrobial effector functions, neutrophil recruitment and STAT-1 dependent production of proinflammatory cytokines [386]. Because Irf8 was identified to be a central hub downregulated by IDR-1002 in sterile skin inflammation, I compared expression of IRF/Irf family genes in both studies. PMA upregulated seven Irf members, namely, Irf1, Irf4, Irf5, Irf6, Irf7, Irf8 and Irf9, and only Irf8 was downregulated when IDR-1002 treatment was provided. In contrast, MRSA biofilm upregulated IRF1, IRF2, IRF3, IRF6 and IRF9 and DJK-5 treatment downregulated all these genes as well as IRF7. The lack of similarities in the expression of the IRF family genes is

expected since IRF8 is primarily expressed in immune cells and the N/TERT skin lacks these components.

The complex immune response triggered by MRSA biofilm was contributed to by skin recognizing MRSA surface antigens (e.g. LTA) and biofilm extracellular matrix components (e.g. exopolysaccharides and extracellular DNA) [387]. Additionally, many of the inflammatory genes in human epithelial keratinocytes that were induced by factors secreted from *S. aureus* biofilm identified in a previous study [388] were also upregulated by MRSA infected burned N/TERT skin (e.g. MCP1, IL8, CXCL1, IL1B, ILA, IL20, IL24, TNF, PTGS2, SMAD7, MMP1, DUSP1, NFKBIA, EFNA1, TNFAIP3. ADM, ZFP36, IFI27). The production of inflammatory cytokines and chemokines such as IL-1β and IL-8 indicated that MRSA penetrated into the deeper layers of the epidermal tissue since skin immune responses are dependent on the depth of tissue being impacted by the infection; thus natural HDPs such as hBD-2 and hBD-3 are upregulated in the upper epidermis, whereas pro-inflammatory cytokines such as IL-1β and IL-6 are mainly induced in the lower layers of the epidermis [389]. In contrast, MRSA intracellular invasion (Figure 26) helped to avoid triggering inflammation and other host defense mechanisms. *S. aureus* can be internalized and survive within keratinocytes without inducing cytotoxic effects or releasing the IL-33 danger signal [390].

Treating MRSA biofilm with DJK-5, especially in combination with the anti-inflammatory peptide 1002 (Figure 23), resulted in significant CFU reduction while also preventing excess tissue inflammation. In particular, the suppression of IL-1β production was both anti-inflammatory and also able to enhance the control of biofilm growth since IL-1β has been shown to promote *S. aureus* biofilm formation *in vitro* [391]. The strategy of combining an antibiofilm peptide with an anti-inflammatory peptide in treating skin biofilm infections, is appealing since prolonged inflammation, accompanied by heavy bacterial burden, tissue breakdown and necrosis, can adversely impact chronic wounds, given that sustained inflammation creates a proteolytic environment that prevents the progression of wound healing into the proliferation phase [392,393]. DJK-5 reduced the expression of MMPs (e.g. MMP3, MMP9 and MMP14) (Figure 27), a class of proteinases involved in extracellular matrix degradation and is associated with pathologic processes of chronic skin inflammation. All of MMP3, MMP9 and MMP14 have been found to accumulate in psoriatic plaques, cause cleavage of basement membrane and facilitate pathogenic T cell infiltration [394]. MMP9 induction also contributes to the activation of IL-1β and plasminogen, mediates skin damage and impairs wound healing [394]. Similarly in biofilm wound infection, the consequential excessive release of harmful MMPs prolongs the inflammatory response and fuels biofilm formation [395]. The suppressive effect on MMPs of DJK-

5 was mediated through downregulation of TNF-α signalling, NF-κB signalling, and signalling by multiple MAPK kinases (e.g. MKK7, MKK3 and MEK) and downstream transcription factors (e.g. AP-1, CEBPB and CREB). In addition to reducing MMP expression, suppression of these central inflammatory pathways by DJK-5 would result in dampening in many other aspects of inflammation including reducing cytokine, chemokine and prostaglandin production, potential reduction in blood vessel leakage and immune cell recruitment (Figure 27).

In addition to dampening skin inflammation, DJK-5 exhibited a protective role in preventing MRSA intracellular invasion. DJK-5 treatment suppressed MRSA biofilm-induced fibronectin and integrin expression in N/TERT epidermal skin (Figure 26). Interactions between *S. aureus* fibronectin-binding proteins (e.g. FnBPA and FnBPB) and host fibronectin and α5β1 integrins have been shown to mediate bacterial adhesion and invasion of non-professional phagocytic cells such as epithelial cells, endothelial cells and fibroblasts [396]. In addition, keratinocytes have been shown to increase the expression of fibronectin and α5β1 integrins upon wounding [397], providing more potential sites for MRSA attachment. DJK-5 treatment also downregulated several downstream kinases such as Src, FAK, and PI3K which have also been previously shown to be involved in *S. aureus* invading host cells [398–400]. Therefore, DJK-5 treatment reduced the susceptibility of MRSA infection in thermally damaged skin by reducing increases in bacteria adhesion and invasion. Interestingly, DJK-5 also suppressed of the expression of the receptor tyrosine kinase MET which navigates internalization of *Listeria monocytogenes* upon binding of bacterial surface protein InlB[401], suggesting a potential protective role against invasion of other bacterial species.

Although RNA-Seq provided an unbiased analysis of pathways and genes that were differentially expressed in response to MRSA biofilm infection and DJK-5 treatment at the RNA level (determined by sequencing of complementary DNA libraries), it is not known whether these changes in gene expression translate into changes at the protein level or corelate with changes in their biological functions. For future studies, it would be worthwhile to confirm the amount and activity of MMPs in the skin during MRSA biofilm infection with or without DJK-5. In addition, the number of intracellular MRSA can be compared before and after DJK-5 treatment to confirm the protective role of DJK-5 in reducing MRSA invasion.

Comparing MRSA biofilm skin inflammation (Chapter 6) with PMA-induced sterile skin inflammation (Chapter 3), pathways representing more diverse dysregulated biological functions were observed during MRSA biofilm infection, even though the N/TERT epidermal model was relatively simple when compared to the mouse model, which has a complete immune system

including local immune cells and the capacity for immune cell recruitment. This is expected due to the elevated complexity of host-microbial interactions during MRSA biofilm infection when compared to PMA stimulation. Both types of inflammation upregulated IL-1, IFN-γ and tyrosine kinase signalling. PMA-induced sterile inflammation also upregulated TLR pathways, GPCRs, C-type lectin receptors and impacted adaptive immunity, especially B cells (Figure 10). In comparison, skin inflammation elicited by MRSA biofilm upregulated additional interleukin pathways (e.g. IL-6, IL-4 and IL-13) and pathways involved in extracellular matrix organization, cellular response to external stimuli, apoptosis and MHC I antigen presentation (Figure 25). Both PMA and MRSA biofilm downregulated cilium assembly and WNT signalling in the skin. MRSA also impaired skin barrier functions, DNA repair and the skin metabolism (Figure 25). These results revealed the distinct pathological mechanisms driving the sterile inflammation when compared to MRSA biofilm induced inflammation. The comparison also highlights the essential role of IL-1 responses, which are critical for both types of skin inflammation. Indeed, overexpression of IL-1 has been shown to correlate with symptom exacerbation and disease progression of many skin disorders such as psoriasis, atopic dermatitis, neutrophilic dermatoses, skin phototoxicity, and skin cancer [402]. Pathway enrichment also showed that IDR-1002 dampened PMA-induced sterile inflammation by downregulating multiple immune pathways including IFN-γ, TLRs and class A/1 rhodopsin-like GPCR signalling (Figure 10). In comparison, DJK-5 treatment in the biofilm skin model had much broader effects on the skin barrier function, inflammatory responses and the metabolic state (Figure 25). These differences are likely because the anti-inflammatory activity observed in the PMA model was a direct immunomodulatory effect of IDR-1002 on mouse skin immunity whereas in the MRSA biofilm skin model, the transcriptomic changes reflect in part the reduction of MRSA biofilm and thus are a secondary effect of DJK-5 antibiofilm activity.

Analysis of coregulated genes in PMA- and MRSA biofilm-induced skin inflammation showed that transcription factors NF-κB (e.g. REL, RELA, NFKB1) and CEBPB, which either by themselves or together function to regulate cytokine signalling including IL-6, IL-8, IL-1, TNF-α, CSF and IFN responses [127,403], were major protein-protein interaction hubs underlying both types of inflammation. This is accompanied by downregulation of ESR1, which inhibits IL-6 expression by displacing NF-κB and associated coregulators from the IL-6 promoter [404]. Indeed, cytokine signalling, especially the IL-1 cascade, was identified as a sub-network based on co-regulated genes (Figure 29b). Interestingly, both types of inflammation also upregulated inflammatory regulators, and the repression by peptides of NF-κB activation (e.g. NFKBIA, TNIP2, TNFAIP3 and EGR1) and

cytokine receptor signalling via the JAK/STAT pathway (e.g. SOCS2 and SOCS3), suggested common mechanisms of the host to control excessive skin inflammation in response to MRSA biofilm and sterile stimuli. It is worth mentioning that upregulation of regulatory genes could be problematic depending on the pathological context. For example, SOCS3 is undetectable in the healthy skin but highly expressed in the epidermis of psoriatic skin where it suppresses the IFN-γ/TNF-α-induced apoptosis in human keratinocytes and contributes to peculiar thickening of the psoriatic epidermis [405]. In the case of bacterial infection, the over-expression of SOCS proteins has been linked to immune escape and exacerbation of disease [406]. For example, *L. monocytogenes* establishes prolonged infection in macrophages by enhancing SOSC3 expression and inhibiting IFN-γ signaling [407]. Therefore, treatment with synthetic host defense peptides IDR-1002 and DJK-5 were necessary to successfully control PMA- and MRSA biofilm-induced skin inflammation respectively. In addition, regulation of cytokine signalling for both types of skin inflammation elicited ER stress-induced UPR (Figure 29d) as shown by increased expression of EIF2S1 and downstream transcription factor ATF4, which in turn induced ATF3 and other stress genes. A subunit of hypoxia inducible factor, HIF1A, was identified as a major hub in both types of inflammation suggesting that the UPR was likely due in part to decreased oxygen availability in the cellular environment, which inhibits disulfide bond formation and impairs protein folding in the ER [408]. Similar hubs also mediated ER stress-induced activation of NLRP3 inflammasome (Figure 29c), which is the pathological basis of many diseases including bacterial infections and chronic sterile inflammatory diseases such as atherosclerosis [409,410]. Assembly of NLRP3 could be triggered by ER-stress induced ATF3, NF-κB activation, increased Ca^{2+} mobilization, ROS production and DNA damage [409].

Comparison of coregulated genes in response to IDR-1002 and DJK-5 treatment in both types of skin inflammation revealed that the anti-inflammatory effect involved a balanced downregulation of both proinflammatory mediators controlled by the TNF-α and NF-κB pathways and their negative regulators, suggesting that synthetic host defense peptides returned skin to hemostasis without having immunosuppressive effects. Major hubs in the protein-protein interaction network (Figure 30) such as NF-κB and AP-1 transcription factors play essential roles in skin physiology and pathology [411,412] including modulating inflammatory cytokine production, extracellular matrix remodelling and cell-cell communications. Multiple hubs downregulated by both peptides such as matrix metallopeptidases, plasminogen activators and transcriptional factor EGR1 can not only regulate extracellular matrix remodelling but also promote inflammation by modulating cytokine production or immune cell functions. For example, the plasminogen activator PLAU is a secreted serine protease

converting plasminogen to plasmin, which can in turn bind to multiple cell types triggering monocyte chemotaxis and cytokine production, neutrophil aggregation, platelet degranulation and endothelial cell arachidonate release [413]. EGR1 expression is elevated in the psoriatic skin lesions and has been identified to be a key regulator of IL-17A-induced psoriasin upregulation in psoriasis [414]. Interestingly, both peptide treatments upregulated the anti-inflammatory protein glucocorticoid-induced leucine zipper (TSC22D3). There is an inverse correlation between TSC22D3 expression and psoriatic lesions [415]. In addition, TSC22D3 mediates the therapeutic action of glucocorticoids, a treatment for psoriasis, by suppressing Th-17 responses and antagonizes multiple pro-inflammatory signaling pathways involved in psoriasis, including AP-1, NF-κB, STAT3, and ROR-γt [415]. These results demonstrate the therapeutic potential of both peptides in treating chronic inflammatory skin conditions.

Chapter 7: Conclusions and future directions

Skin forms a protective barrier that provides a first line of physical and immune defense. The intensive crosstalk among keratinocytes, fibroblasts, immune cells and the skin commensal bacteria are essential for maintaining immune hemostasis in the skin. Dysregulation of this equilibrium by sterile stimuli contributes to the pathogenesis of inflammatory skin diseases such as psoriasis and atopic dermatitis, which currently lack an effective cure. Biofilm skin infections caused by *S. aureus* and *P. aeruginosa* are recalcitrant, invasive and can elicit harmful inflammatory responses. The urgent issue of multiple antibiotic resistances and the adaptively resistant nature of biofilms demand development of new therapeutics. In my thesis, I demonstrated that synthetic HDPs and peptidomimetics provide such new solutions by targeting excessive skin inflammation and biofilm skin infections.

I showed that IDR-1002 suppressed LPS, LTA and zymosan-induced inflammatory responses *in vitro* using the RAW 264.7 cells. The effect of IDR-1002 peptide against sterile inflammation *in vivo* was investigated using the PMA-induced mouse ear inflammation model. IDR-1002 suppressed a variety of inflammatory responses including PMA-induced ear edema, the production of proinflammatory cytokines and ROS/RNS, and the recruitment of neutrophils into the inflamed tissue. I further explored the underlying mechanisms using systems biology approaches and showed that the *in vivo* suppressive effect of IDR-1002 on PMA-induced inflammation was contributed to by its ability to downregulate G-protein coupled receptors in the class A/1 rhodopsin-like receptor family. These included receptors recognizing central proinflammatory mediators such as chemokines, prostaglandins, histamine, platelet activating factor and anaphylatoxin. IDR-1002 also suppressed the IFN-γ pathway and an Irf-8-regulated network in PMA-induced inflammation. The overall transcriptomic changes were likely contributed by both shifts in cell populations and changes in the gene expression of individual cells. Due to the complexity of inflammation and the ability of synthetic HDPs to interact with multiple cellular targets, Irf-8 is likely to be critical, but not the only contributing factor. The relative contribution of Irf-8 could be confirmed in future experiments by specifically knocking down Irf-8 expression with small interfering RNA. Similarly, lipidated peptidomimetics Pam-(Lys-βNspe)$_6$-NH_2 and Lau-(Lys-βNspe)$_6$-NH_2 attenuated PMA-induced ear edema, proinflammatory cytokine and ROS/RNS release, and decreased neutrophil infiltration to a degree comparable to that of the NSAID indomethacin. These results revealed the promising *in vivo* anti-inflammatory effects of IDR-1002 and peptidomimetics Pam-(Lys-βNspe)$_6$-NH_2 and Lau-(Lys-βNspe)$_6$-NH_2 against acute sterile skin inflammation. To develop synthetic HDPs and

peptidomimetics as treatment for chronic skin inflammation, their efficacy and safety need to be tested in chronic inflammatory models. I attempted applying multiple dosages of PMA to mouse ear (5 times over 10 days) as it has been used as a model for psoriasis with a Th-17-like response [416]. However, although multiple dosages of PMA induced significant increases in ear edema compared to a single stimulation, a sustained inflammation was not triggered since reversal to minimal proinflammatory cytokine levels was detected within 24 hours after the fifth PMA challenge. Other clinically relevant chronic inflammatory models can be used in the future. For example, N/TERT skin can be supplemented with Th-1/Th-17 (TNF-α, IL-6, IL-1α, IL-17 and IL-22) cytokines or Th-2 (IL-4 and IL-13) cytokines during the final stage of the skin maturation to induce features of psoriasis and atopic dermatitis respectively [417]. Immune cells such as T cells can also be incorporated into skin equivalents to recapitulate clinical hallmarks of psoriasis and atopic dermatitis [418,419].

Although animal models are widely used to study human immunological responses and to test the activities of novel therapeutics, there is concern about whether animal models can truly reflect human immunology [420]. To provide a human organoid model for studying host-microbe interplay and enabling screening for novel antibiofilm agents, I developed a human epidermis organoid model with robust MRSA USA300 and *P. aeruginosa* PAO1 biofilm. Treatment of 1-day and 3-day MRSA and PAO1 biofilms with antibiofilm peptide DJK-5 significantly and substantially reduced the bacterial burden. Using this skin biofilm model as a screening platform, I identified novel peptides D-3006 and D-3007 with enhanced antibiofilm activities when compared to DJK-5, and substantially superior to fusidic acid and gentamicin, which are common prescriptions for skin infections formulated in cream or ointment [338,339]. The antibiofilm effect of D-3006 and D-3007 was confirmed in a new thermally burned *ex vivo* human skin model. In addition, D-3006 and D-3007 exhibited immunomodulatory potential dampening Poly(I:C) induced inflammation in monolayer N/TERT cells and the organoid skin model. Other important properties of D-3006 and D-3007 such as the *in vivo* toxicity, *in vivo* anti-inflammatory effect and the tendency of these peptides to form aggregrates in the presence of biological relevant concentrations of salts or serum as well as their mechanisms of action require further investigation. Together these results showed the utility of a biologically relevant, N/TERT cell derived, skin biofilm model that can be used as a platform for testing the antibiofilm and immunomodulatory effects of synthetic HDPs. This system provides a reliable and robust alternative to animal models of skin infections and should help bridge the gap between the discoveries of novel antibiofilm agents and their clinical applications.

Supplanting ethically-challenging animal burn models with the burned skin MRSA biofilm

model enabled the study of biofilm infections and associated skin damage and inflammation. I discovered that thermally wounded skin exhibited increased susceptibility to MRSA infection and topical treatment with DJK-5 effectively reduced MRSA bacterial burden and excessive skin inflammation. Combination treatment of DJK-5 and IDR-1002 further reduced cytotoxicity and pro-inflammatory cytokine production. DJK-5 treatment had broad effects on the MRSA biofilm infected skin transcriptome in promoting skin barrier function, dampening inflammation and modulating skin metabolism. The anti-inflammatory effects were mediated through downregulation of the TNF-α and NF-κB cascades and downstream transcription factors AP-1, c/EBPB and CREB, which resulted in the suppression of proinflammatory cytokines, especially IL-1, prostaglandin biosynthesis, MMPs, vascular endothelial growth factors and cell adhesion molecules. I also found that DJK-5 protected skin from MRSA intracellular invasion by downregulating genes involved in MRSA surface attachment and entry processes, including fibronectin, integrins, intracellular kinases (e.g. ILK, FAK and Src) and MRSA mobilization of actin cytoskeleton. Comparing PMA-induced sterile inflammation and MRSA biofilm skin infection, both types of inflammation upregulated proinflammatory cytokine signalling including IL-1β and NLRP3 activation, unfolded protein response, TLR signalling and integrin cell surface interactions as well negative regulators of NF-κB and cytokine signalling. Both DJK-5 and IDR-1002 treatments returned skin to hemostasis through balanced downregulation of proinflammatory mediators (e.g. cytokines, MMPs, prostaglandin synthase and plasminogen activators) controlled by the TNF-α and NF-κB pathways and genes in the negative feedback loops of these pathways. Since overexpression of negative inflammatory regulators is associated with bacterial immune escape and prolonged infections [406,407], the balanced suppression of both inflammatory pathways and their negative regulators by synthetic HDPs helped to explain how peptides can suppress harmful inflammation without compromising the ability of the immune system to fight infections. In addition, both peptides upregulated an anti-inflammatory protein TSC22D3, which mediates the therapeutic action of glucocorticoids, demonstrating the potential of IDR-1002 and DJK-5 in treating chronic skin disorders such as psoriasis.

In summary, this study investigated the anti-inflammatory properties of IDR-1002 in sterile skin inflammation and antibiofilm and anti-inflammatory effects of DJK-5 in biofilm skin infections. It also provided new insights into their mechanisms of action and revealed their therapeutic potential as treatments of skin inflammation. Formulation and delivery studies such as incorporating peptides into liposomal nanoparticles or loading peptides into wound dressings, are ongoing.

Bibliography

1. Schonmann, Y. *et al.* Atopic Eczema in Adulthood and Risk of Depression and Anxiety: A Population-Based Cohort Study. *J Allergy Clin Immunol Pract* **8**, 248-257.e16 (2020).
2. Sampogna, F., Tabolli, S., Abeni, D., & IDI Multipurpose Psoriasis Research on Vital Experiences (IMPROVE) investigators. Living with psoriasis: prevalence of shame, anger, worry, and problems in daily activities and social life. *Acta Derm Venereol* **92**, 299–303 (2012).
3. Boehncke, W.H., Boehncke, S., Tobin, A.M. & Kirby, B. The 'psoriatic march': a concept of how severe psoriasis may drive cardiovascular comorbidity. *Exp Dermatol* **20**, 303–307 (2011).
4. Silverberg, J. I. & Simpson, E. L. Association between severe eczema in children and multiple comorbid conditions and increased healthcare utilization. *Pediatr Allergy Immunol* **24**, 476–486 (2013).
5. World Health Organization. Antimicrobial resistance. https://www.who.int/news-room/fact-sheets/detail/antimicrobial-resistance (2020).
6. Bennani, H. *et al.* Overview of Evidence of Antimicrobial Use and Antimicrobial Resistance in the Food Chain. *Antibiotics (Basel)* **9**, 49 (2020).
7. World Health Organization. WHO publishes list of bacteria for which new antibiotics are urgently needed. https://www.who.int/news/item/27-02-2017-who-publishes-list-of-bacteria-for-which-new-antibiotics-are-urgently-needed (2017).
8. Ki, V. & Rotstein, C. Bacterial skin and soft tissue infections in adults: A review of their epidemiology, pathogenesis, diagnosis, treatment and site of care. *Can J Infect Dis Med Microbiol* **19**, 173–184 (2008).
9. Archer, N. K. *et al. Staphylococcus aureus* biofilms: properties, regulation, and roles in human disease. *Virulence* **2**, 445–459 (2011).
10. de la Fuente-Núñez, C., Cardoso, M. H., de Souza Cândido, E., Franco, O. L. & Hancock, R. E. W. Synthetic antibiofilm peptides. *Biochim. Biophys. Acta* **1858**, 1061–1069 (2016).
11. Kwiecinski, J., Kahlmeter, G. & Jin, T. Biofilm formation by *Staphylococcus aureus* isolates from skin and soft tissue infections. *Curr Microbiol* **70**, 698–703 (2015).
12. Kabashima, K., Honda, T., Ginhoux, F. & Egawa, G. The immunological anatomy of the skin. *Nat. Rev. Immunol.* **19**, 19–30 (2019).
13. Yousef, H., Alhajj, M. & Sharma, S. Anatomy, Skin (Integument), Epidermis. in *StatPearls* (StatPearls Publishing, 2021).
14. Matsui, T. & Amagai, M. Dissecting the formation, structure and barrier function of the stratum corneum. *Int Immunol* **27**, 269–280 (2015).
15. Freeman, S. C. & Sonthalia, S. Histology, Keratohyalin Granules. in *StatPearls* (StatPearls Publishing, 2021).
16. Muhammad, F. & Riviere, J. E. Chapter 21 - Dermal toxicity. in *Veterinary Toxicology (Second Edition)* (ed. Gupta, R. C.) 337–350 (Academic Press, 2012). doi:10.1016/B978-0-12-385926-6.00021-1.
17. Kolarsick, P. A. J., Kolarsick, M. A. & Goodwin, C. Anatomy and Physiology of the Skin. *Journal of the Dermatology Nurses' Association* **3**, 203–213 (2011).
18. Coulombe, P. A. & Omary, M. B. 'Hard' and 'soft' principles defining the structure, function and regulation of keratin intermediate filaments. *Curr Opin Cell Biol* **14**, 110–122 (2002).
19. Ramms, L. *et al.* Keratins as the main component for the mechanical integrity of keratinocytes. *Proc Natl Acad Sci U S A* **110**, 18513–18518 (2013).
20. Hatzfeld, M., Keil, R. & Magin, T. M. Desmosomes and Intermediate Filaments: Their Consequences for Tissue Mechanics. *Cold Spring Harb Perspect Biol* **9**, (2017).
21. Brandner, J. M. *et al.* Epidermal tight junctions in health and disease. *Tissue Barriers* **3**, e974451 (2015).

22. Sumigray, K. D. & Lechler, T. Cell adhesion in epidermal development and barrier formation. *Curr Top Dev Biol* **112**, 383–414 (2015).
23. Kirschner, N., Houdek, P., Fromm, M., Moll, I. & Brandner, J. M. Tight junctions form a barrier in human epidermis. *Eur J Cell Biol* **89**, 839–842 (2010).
24. Tracy, L. E., Minasian, R. A. & Caterson, E. J. Extracellular Matrix and Dermal Fibroblast Function in the Healing Wound. *Adv Wound Care (New Rochelle)* **5**, 119–136 (2016).
25. Menon, G. K., Dryer, L. & Kalafsky, R. Chapter 11 - Approaches to the Development of Cosmetic Products to Counter the Effects of Skin Aging. in *Skin Aging Handbook* (ed. Dayan, N.) 265–290 (William Andrew Publishing, 2009). doi:10.1016/B978-0-8155-1584-5.50015-6.
26. Wong, R., Geyer, S., Weninger, W., Guimberteau, J.-C. & Wong, J. K. The dynamic anatomy and patterning of skin. *Experimental Dermatology* **25**, 92–98 (2016).
27. Nguyen, A. V. & Soulika, A. M. The Dynamics of the Skin's Immune System. *Int J Mol Sci* **20**, (2019).
28. Baker, L. B. Physiology of sweat gland function: The roles of sweating and sweat composition in human health. *Temperature (Austin)* **6**, 211–259 (2019).
29. Martel, J. L., Miao, J. H. & Badri, T. Anatomy, Hair Follicle. in *StatPearls* (StatPearls Publishing, 2021).
30. Parvizi, J. & Kim, G. K. Chapter 153 - Nerve Endings. in *High Yield Orthopaedics* (eds. Parvizi, J. & Kim, G. K.) 315–316 (W.B. Saunders, 2010). doi:10.1016/B978-1-4160-0236-9.00164-4.
31. Pasparakis, M., Haase, I. & Nestle, F. O. Mechanisms regulating skin immunity and inflammation. *Nat. Rev. Immunol.* **14**, 289–301 (2014).
32. West, H. C. & Bennett, C. L. Redefining the Role of Langerhans Cells As Immune Regulators within the Skin. *Front. Immunol.* **8**, (2018).
33. Seneschal, J., Clark, R. A., Gehad, A., Baecher-Allan, C. M. & Kupper, T. S. Human Epidermal Langerhans Cells Maintain Immune Homeostasis in Skin by Activating Skin Resident Regulatory T Cells. *Immunity* **36**, 873–884 (2012).
34. Deckers, J., Hammad, H. & Hoste, E. Langerhans Cells: Sensing the Environment in Health and Disease. *Front Immunol* **9**, 93 (2018).
35. Behr, F. M., Chuwonpad, A., Stark, R. & van Gisbergen, K. P. J. M. Armed and Ready: Transcriptional Regulation of Tissue-Resident Memory CD8 T Cells. *Front Immunol* **9**, 1770 (2018).
36. Gebhardt, T. *et al.* Memory T cells in nonlymphoid tissue that provide enhanced local immunity during infection with herpes simplex virus. *Nat Immunol* **10**, 524–530 (2009).
37. Cruz, M. S., Diamond, A., Russell, A. & Jameson, J. M. Human αβ and γδ T Cells in Skin Immunity and Disease. *Front Immunol* **9**, (2018).
38. Khairallah, C., Chu, T. H. & Sheridan, B. S. Tissue Adaptations of Memory and Tissue-Resident Gamma Delta T Cells. *Frontiers in Immunology* **9**, 2636 (2018).
39. Collin, M. & Bigley, V. Human dendritic cell subsets: an update. *Immunology* **154**, 3–20 (2018).
40. Davies, L. C., Jenkins, S. J., Allen, J. E. & Taylor, P. R. Tissue-resident macrophages. *Nat Immunol* **14**, 986–995 (2013).
41. Krzyszczyk, P., Schloss, R., Palmer, A. & Berthiaume, F. The Role of Macrophages in Acute and Chronic Wound Healing and Interventions to Promote Pro-wound Healing Phenotypes. *Front. Physiol.* **9**, (2018).
42. Mosser, D. M. & Edwards, J. P. Exploring the full spectrum of macrophage activation. *Nat Rev Immunol* **8**, 958–969 (2008).
43. Atri, C., Guerfali, F. Z. & Laouini, D. Role of Human Macrophage Polarization in Inflammation during Infectious Diseases. *Int J Mol Sci* **19**, (2018).
44. Ryan, N. M. & Oghumu, S. Role of mast cells in the generation of a T-helper type 2 dominated

anti-helminthic immune response. *Biosci Rep* **39**, (2019).
45. Supajatura, V. *et al.* Differential responses of mast cell Toll-like receptors 2 and 4 in allergy and innate immunity. *J Clin Invest* **109**, 1351–1359 (2002).
46. Ilves, T. & Harvima, I. T. Decrease in chymase activity is associated with increase in IL-6 expression in mast cells in atopic dermatitis. *Acta Derm Venereol* **95**, 411–416 (2015).
47. Siiskonen, H. & Harvima, I. Mast Cells and Sensory Nerves Contribute to Neurogenic Inflammation and Pruritus in Chronic Skin Inflammation. *Front. Cell. Neurosci.* **13**, (2019).
48. Watanabe, R. *et al.* Human skin is protected by four functionally and phenotypically discrete populations of resident and recirculating memory T cells. *Sci Transl Med* **7**, 279ra39 (2015).
49. Sallusto, F., Lenig, D., Förster, R., Lipp, M. & Lanzavecchia, A. Two subsets of memory T lymphocytes with distinct homing potentials and effector functions. *Nature* **401**, 708–712 (1999).
50. Mackay, L. K. *et al.* The developmental pathway for CD103 + CD8 + tissue-resident memory T cells of skin. *Nat Immunol* **14**, 1294–1301 (2013).
51. Ali, N. & Rosenblum, M. D. Regulatory T cells in skin. *Immunology* **152**, 372–381 (2017).
52. Scharschmidt, T. C. *et al.* A Wave of Regulatory T Cells into Neonatal Skin Mediates Tolerance to Commensal Microbes. *Immunity* **43**, 1011–1021 (2015).
53. Nosbaum, A. *et al.* Cutting Edge: Regulatory T Cells Facilitate Cutaneous Wound Healing. *J Immunol* **196**, 2010–2014 (2016).
54. Bielecki, P. *et al.* Skin-resident innate lymphoid cells converge on a pathogenic effector state. *Nature* **592**, 128–132 (2021).
55. Kobayashi, T., Ricardo-Gonzalez, R. R. & Moro, K. Skin-Resident Innate Lymphoid Cells - Cutaneous Innate Guardians and Regulators. *Trends Immunol* **41**, 100–112 (2020).
56. Teunissen, M. B. M. *et al.* Composition of innate lymphoid cell subsets in the human skin: enrichment of NCR(+) ILC3 in lesional skin and blood of psoriasis patients. *J Invest Dermatol* **134**, 2351–2360 (2014).
57. Salimi, M. & Ogg, G. Innate lymphoid cells and the skin. *BMC dermatology* **14**, 18 (2014).
58. Byrd, A. L., Belkaid, Y. & Segre, J. A. The human skin microbiome. *Nat Rev Microbiol* **16**, 143–155 (2018).
59. Iwase, T. *et al. Staphylococcus epidermidis* Esp inhibits *Staphylococcus aureus* biofilm formation and nasal colonization. *Nature* **465**, 346–349 (2010).
60. Prescott, S. L. *et al.* The skin microbiome: impact of modern environments on skin ecology, barrier integrity, and systemic immune programming. *World Allergy Organization Journal* **10**, 29 (2017).
61. Ziebuhr, W. *et al.* Nosocomial infections by *Staphylococcus epidermidis*: how a commensal bacterium turns into a pathogen. *Int J Antimicrob Agents* **28 Suppl 1**, S14-20 (2006).
62. Brown, M. M. & Horswill, A. R. *Staphylococcus epidermidis*—Skin friend or foe? *PLOS Pathogens* **16**, e1009026 (2020).
63. Cardona, A. F. & Wilson, S. E. Skin and soft-tissue infections: a critical review and the role of telavancin in their treatment. *Clin. Infect. Dis.* **61 Suppl 2**, S69-78 (2015).
64. Ramakrishnan, K., Salinas, R. C. & Agudelo Higuita, N. I. Skin and Soft Tissue Infections. *Am Fam Physician* **92**, 474–483 (2015).
65. Tun, K., Shurko, J. F., Ryan, L. & Lee, G. C. Age-based health and economic burden of skin and soft tissue infections in the United States, 2000 and 2012. *PLoS One* **13**, (2018).
66. Leong, H. N. *et al.* Management of complicated skin and soft tissue infections with a special focus on the role of newer antibiotics. *Infect Drug Resist* **11**, 1959–1974 (2018).
67. Mwangi, M. M. *et al.* Tracking the *in vivo* evolution of multidrug resistance in *Staphylococcus aureus* by whole-genome sequencing. *Proc Natl Acad Sci U S A* **104**, 9451–9456 (2007).

68. Taylor, T. A. & Unakal, C. G. *Staphylococcus aureus*. in *StatPearls* (StatPearls Publishing, 2021).
69. Sonesson, A. *et al.* Identification of bacterial biofilm and the *Staphylococcus aureus* derived protease, staphopain, on the skin surface of patients with atopic dermatitis. *Sci Rep* **7**, 8689 (2017).
70. Mottola, C. *et al.* Susceptibility patterns of *Staphylococcus aureus* biofilms in diabetic foot infections. *BMC Microbiol.* **16**, 119 (2016).
71. Khan, T. M. *et al.* Incidence of methicillin resistant *Staphylococcus aureus* (MRSA) in burn intensive care unit: a systematic review. *Germs* **8**, 113–125 (2018).
72. Lacey, K. A., Geoghegan, J. A. & McLoughlin, R. M. The Role of *Staphylococcus aureus* Virulence Factors in Skin Infection and Their Potential as Vaccine Antigens. *Pathogens* **5**, (2016).
73. Miller, L. G. *et al.* Incidence of skin and soft tissue infections in ambulatory and inpatient settings, 2005-2010. *BMC Infect. Dis.* **15**, 362 (2015).
74. Peacock, S. J. & Paterson, G. K. Mechanisms of Methicillin Resistance in *Staphylococcus aureus*. *Annu Rev Biochem* **84**, 577–601 (2015).
75. Turner, N. A. *et al.* Methicillin-resistant *Staphylococcus aureus*: an overview of basic and clinical research. *Nat Rev Microbiol* **17**, 203–218 (2019).
76. Uhlemann, A.C. *et al.* Molecular tracing of the emergence, diversification, and transmission of S. aureus sequence type 8 in a New York community. *Proc Natl Acad Sci U S A* **111**, 6738–6743 (2014).
77. Gellatly, S. L. & Hancock, R. E. W. *Pseudomonas aeruginosa* : new insights into pathogenesis and host defenses. *Pathogens and Disease* **67**, 159–173 (2013).
78. Wu, D. C., Chan, W. W., Metelitsa, A. I., Fiorillo, L. & Lin, A. N. *Pseudomonas* skin infection: clinical features, epidemiology, and management. *Am J Clin Dermatol* **12**, 157–169 (2011).
79. Veesenmeyer, J. L., Hauser, A. R., Lisboa, T. & Rello, J. *Pseudomonas aeruginosa* Virulence and Therapy: Evolving Translational Strategies. *Crit Care Med* **37**, 1777–1786 (2009).
80. Hancock, R. E. W. & Speert, D. P. Antibiotic resistance in *Pseudomonas aeruginosa*: mechanisms and impact on treatment. *Drug Resist. Updat.* **3**, 247–255 (2000).
81. Kostakioti, M., Hadjifrangiskou, M. & Hultgren, S. J. Bacterial Biofilms: Development, Dispersal, and Therapeutic Strategies in the Dawn of the Postantibiotic Era. *Cold Spring Harb Perspect Med* **3**, (2013).
82. Flemming, H.C. *et al.* Biofilms: an emergent form of bacterial life. *Nat Rev Microbiol* **14**, 563–575 (2016).
83. Ma, L. *et al.* Assembly and Development of the *Pseudomonas aeruginosa* Biofilm Matrix. *PLoS Pathog* **5**, (2009).
84. Ibáñez de Aldecoa, A. L., Zafra, O. & González-Pastor, J. E. Mechanisms and Regulation of Extracellular DNA Release and Its Biological Roles in Microbial Communities. *Front. Microbiol.* **8**, (2017).
85. Rumbaugh, K. P. & Sauer, K. Biofilm dispersion. *Nat Rev Microbiol* **18**, 571–586 (2020).
86. Chua, S. L. *et al.* Dispersed cells represent a distinct stage in the transition from bacterial biofilm to planktonic lifestyles. *Nat Commun* **5**, 4462 (2014).
87. Wille, J. *et al.* Does the mode of dispersion determine the properties of dispersed *Pseudomonas aeruginosa* biofilm cells? *International Journal of Antimicrobial Agents* **56**, 106194 (2020).
88. de la Fuente-Núñez, C., Reffuveille, F., Fernández, L. & Hancock, R. E. W. Bacterial biofilm development as a multicellular adaptation: antibiotic resistance and new therapeutic strategies. *Curr Opin Microbiol* **16**, 580–589 (2013).
89. Taylor, P. K., Yeung, A. T. Y. & Hancock, R. E. W. Antibiotic resistance in *Pseudomonas*

aeruginosa biofilms: Towards the development of novel anti-biofilm therapies. *Journal of Biotechnology* **191**, 121–130 (2014).
90. Poudyal, B. & Sauer, K. The ABC of Biofilm Drug Tolerance: the MerR-Like Regulator BrlR Is an Activator of ABC Transport Systems, with PA1874-77 Contributing to the Tolerance of *Pseudomonas aeruginosa* Biofilms to Tobramycin. *Antimicrob Agents Chemother* **62**, e01981-17 (2018).
91. Dostert, M., Trimble, M. J. & Hancock, R. E. W. Antibiofilm peptides: overcoming biofilm-related treatment failure. *RSC Adv.* **11**, 2718–2728 (2021).
92. Mah, T.F. *et al.* A genetic basis for *Pseudomonas aeruginosa* biofilm antibiotic resistance. *Nature* **426**, 306–310 (2003).
93. Anderl, J. N., Zahller, J., Roe, F. & Stewart, P. S. Role of nutrient limitation and stationary-phase existence in *Klebsiella pneumoniae* biofilm resistance to ampicillin and ciprofloxacin. *Antimicrob Agents Chemother* **47**, 1251–1256 (2003).
94. Mah, T.F. C. & O'Toole, G. A. Mechanisms of biofilm resistance to antimicrobial agents. *Trends in Microbiology* **9**, 34–39 (2001).
95. Irving, S. E., Choudhury, N. R. & Corrigan, R. M. The stringent response and physiological roles of (pp)pGpp in bacteria. *Nat Rev Microbiol* **19**, 256–271 (2021).
96. Nguyen, D. *et al.* Active Starvation Responses Mediate Antibiotic Tolerance in Biofilms and Nutrient-Limited Bacteria. *Science* **334**, 982–986 (2011).
97. Strugeon, E., Tilloy, V., Ploy, M.C. & Da Re, S. The Stringent Response Promotes Antibiotic Resistance Dissemination by Regulating Integron Integrase Expression in Biofilms. *mBio* **7**, (2016).
98. Du Toit, A. Persisters running out of energy. *Nat Rev Microbiol* **15**, 194–194 (2017).
99. Rani, S. A. *et al.* Spatial patterns of DNA replication, protein synthesis, and oxygen concentration within bacterial biofilms reveal diverse physiological states. *J Bacteriol* **189**, 4223–4233 (2007).
100. Wood, T. K., Knabel, S. J. & Kwan, B. W. Bacterial Persister Cell Formation and Dormancy. *Appl Environ Microbiol* **79**, 7116–7121 (2013).
101. Saxena, P., Joshi, Y., Rawat, K. & Bisht, R. Biofilms: Architecture, Resistance, Quorum Sensing and Control Mechanisms. *Indian J Microbiol* **59**, 3–12 (2019).
102. Hassett, D. J. *et al.* Quorum sensing in *Pseudomonas aeruginosa* controls expression of catalase and superoxide dismutase genes and mediates biofilm susceptibility to hydrogen peroxide. *Mol Microbiol* **34**, 1082–1093 (1999).
103. Zhao, X., Yu, Z. & Ding, T. Quorum-Sensing Regulation of Antimicrobial Resistance in Bacteria. *Microorganisms* **8**, 425 (2020).
104. Tseng, B. S. *et al.* The extracellular matrix protects *Pseudomonas aeruginosa* biofilms by limiting the penetration of tobramycin. *Environ Microbiol* **15**, 2865–2878 (2013).
105. Anderl, J. N., Franklin, M. J. & Stewart, P. S. Role of Antibiotic Penetration Limitation in *Klebsiella pneumoniae* Biofilm Resistance to Ampicillin and Ciprofloxacin. *Antimicrob Agents Chemother* **44**, 1818–1824 (2000).
106. Medzhitov, R. Origin and physiological roles of inflammation. *Nature* **454**, 428–435 (2008).
107. Heneka, M. T. *et al.* Neuroinflammation in Alzheimer's disease. *Lancet Neurol* **14**, 388–405 (2015).
108. Murdoch, J. R. & Lloyd, C. M. Chronic inflammation and asthma. *Mutat. Res.* **690**, 24–39 (2010).
109. Tuttolomondo, A. *et al.* Atherosclerosis as an inflammatory disease. *Curr. Pharm. Des.* **18**, 4266–4288 (2012).
110. Molfino, N. A. & Jeffery, P. K. Chronic obstructive pulmonary disease: histopathology,

inflammation and potential therapies. *Pulm Pharmacol Ther* **20**, 462–472 (2007).
111. Firestein, G. S. Evolving concepts of rheumatoid arthritis. *Nature* **423**, 356–361 (2003).
112. Amarante-Mendes, G. P. *et al.* Pattern Recognition Receptors and the Host Cell Death Molecular Machinery. *Front Immunol* **9**, (2018).
113. Mogensen, T. H. Pathogen recognition and inflammatory signaling in innate immune defenses. *Clin. Microbiol. Rev.* **22**, 240–273, Table of Contents (2009).
114. Loo, Y.M. & Gale, M. Immune signaling by RIG-I-like receptors. *Immunity* **34**, 680–692 (2011).
115. Geijtenbeek, T. B. H. & Gringhuis, S. I. Signalling through C-type lectin receptors: shaping immune responses. *Nat Rev Immunol* **9**, 465–479 (2009).
116. Zhong, Y., Kinio, A. & Saleh, M. Functions of NOD-Like Receptors in Human Diseases. *Front Immunol* **4**, (2013).
117. Caneparo, V., Landolfo, S., Gariglio, M. & De Andrea, M. The Absent in Melanoma 2-Like Receptor IFN-Inducible Protein 16 as an Inflammasome Regulator in Systemic Lupus Erythematosus: The Dark Side of Sensing Microbes. *Front Immunol* **9**, 1180 (2018).
118. Rock, K. L., Latz, E., Ontiveros, F. & Kono, H. The sterile inflammatory response. *Annu. Rev. Immunol.* **28**, 321–342 (2010).
119. Shen, H., Kreisel, D. & Goldstein, D. R. Processes of sterile inflammation. *J. Immunol.* **191**, 2857–2863 (2013).
120. Chen, Q., Guan, X., Zuo, X., Wang, J. & Yin, W. The role of high mobility group box 1 (HMGB1) in the pathogenesis of kidney diseases. *Acta Pharm Sin B* **6**, 183–188 (2016).
121. Gaskell, H., Ge, X. & Nieto, N. High-Mobility Group Box-1 and Liver Disease. *Hepatol Commun* **2**, 1005–1020 (2018).
122. Zindel, J. & Kubes, P. DAMPs, PAMPs, and LAMPs in Immunity and Sterile Inflammation. *Annu. Rev. Pathol. Mech. Dis.* **15**, 493–518 (2020).
123. Kawasaki, T. & Kawai, T. Toll-like receptor signaling pathways. *Front Immunol* **5**, 461 (2014).
124. Newton, K. & Dixit, V. M. Signaling in innate immunity and inflammation. *Cold Spring Harb Perspect Biol* **4**, (2012).
125. Zhang, H. & Sun, S.C. NF-κB in inflammation and renal diseases. *Cell Biosci* **5**, 63 (2015).
126. Chen, L. *et al.* Inflammatory responses and inflammation-associated diseases in organs. *Oncotarget* **9**, 7204–7218 (2018).
127. Liu, T., Zhang, L., Joo, D. & Sun, S.C. NF-κB signaling in inflammation. *Signal Transduct Target Ther* **2**, (2017).
128. Guo, H., Callaway, J. B. & Ting, J. P.Y. Inflammasomes: mechanism of action, role in disease, and therapeutics. *Nat Med* **21**, 677–687 (2015).
129. Zhang, P., Martin, M., Michalek, S. M. & Katz, J. Role of Mitogen-Activated Protein Kinases and NF-κB in the Regulation of Proinflammatory and Anti-Inflammatory Cytokines by *Porphyromonas gingivalis* Hemagglutinin B. *Infect Immun* **73**, 3990–3998 (2005).
130. Moens, U., Kostenko, S. & Sveinbjørnsson, B. The Role of Mitogen-Activated Protein Kinase-Activated Protein Kinases (MAPKAPKs) in Inflammation. *Genes (Basel)* **4**, 101–133 (2013).
131. Behnia, F., Sheller, S. & Menon, R. Mechanistic Differences Leading to Infectious and Sterile Inflammation. *Am J Reprod Immunol* **75**, 505–518 (2016).
132. Leonard, W. J. & Lin, J.X. Cytokine receptor signaling pathways. *Journal of Allergy and Clinical Immunology* **105**, 877–888 (2000).
133. Legler, D. F. & Thelen, M. New insights in chemokine signaling. *F1000Res* **7**, (2018).
134. Gray, R. D. *et al.* Activation of conventional protein kinase C (PKC) is critical in the generation of human neutrophil extracellular traps. *Journal of Inflammation* **10**, 12 (2013).
135. Capucetti, A., Albano, F. & Bonecchi, R. Multiple Roles for Chemokines in Neutrophil Biology. *Front Immunol* **11**, 1259 (2020).

136. Metzemaekers, M., Gouwy, M. & Proost, P. Neutrophil chemoattractant receptors in health and disease: double-edged swords. *Cell Mol Immunol* **17**, 433–450 (2020).
137. Ricciotti, E. & FitzGerald, G. A. Prostaglandins and inflammation. *Arterioscler Thromb Vasc Biol* **31**, 986–1000 (2011).
138. Abdulkhaleq, L. A. *et al.* The crucial roles of inflammatory mediators in inflammation: A review. *Vet World* **11**, 627–635 (2018).
139. Sherwood, E. R. & Toliver-Kinsky, T. Mechanisms of the inflammatory response. *Best Practice & Research Clinical Anaesthesiology* **18**, 385–405 (2004).
140. Chow, Z., Egawa, G. & Kabashima, K. Live Imaging of the Skin Immune Responses. in *Make Life Visible* (eds. Toyama, Y., Miyawaki, A., Nakamura, M. & Jinzaki, M.) 261–272 (Springer, 2020). doi:10.1007/978-981-13-7908-6_26.
141. Kolaczkowska, E. & Kubes, P. Neutrophil recruitment and function in health and inflammation. *Nat Rev Immunol* **13**, 159–175 (2013).
142. Mortaz, E., Alipoor, S. D., Adcock, I. M., Mumby, S. & Koenderman, L. Update on Neutrophil Function in Severe Inflammation. *Front Immunol* **9**, 2171 (2018).
143. Tecchio, C., Micheletti, A. & Cassatella, M. A. Neutrophil-derived cytokines: facts beyond expression. *Front Immunol* **5**, 508 (2014).
144. Tsuda, Y. *et al.* Three different neutrophil subsets exhibited in mice with different susceptibilities to infection by methicillin-resistant *Staphylococcus aureus*. *Immunity* **21**, 215–226 (2004).
145. Goh, C. C. *et al.* Real-time imaging of dendritic cell responses to sterile tissue injury. *J Invest Dermatol* **135**, 1181–1184 (2015).
146. Mbongue, J. C., Nieves, H. A., Torrez, T. W. & Langridge, W. H. R. The Role of Dendritic Cell Maturation in the Induction of Insulin-Dependent Diabetes Mellitus. *Front Immunol* **8**, 327 (2017).
147. Kabashima, K. *et al.* CXCL12-CXCR4 engagement is required for migration of cutaneous dendritic cells. *Am J Pathol* **171**, 1249–1257 (2007).
148. Serbina, N. V., Salazar-Mather, T. P., Biron, C. A., Kuziel, W. A. & Pamer, E. G. TNF/iNOS-producing dendritic cells mediate innate immune defense against bacterial infection. *Immunity* **19**, 59–70 (2003).
149. Musumeci, A., Lutz, K., Winheim, E. & Krug, A. B. What Makes a pDC: Recent Advances in Understanding Plasmacytoid DC Development and Heterogeneity. *Front Immunol* **10**, 1222 (2019).
150. Shi, C. & Pamer, E. G. Monocyte recruitment during infection and inflammation. *Nat Rev Immunol* **11**, 762–774 (2011).
151. Italiani, P. & Boraschi, D. From Monocytes to M1/M2 Macrophages: Phenotypical vs. Functional Differentiation. *Front Immunol* **5**, 514 (2014).
152. Sabat, R., Wolk, K., Loyal, L., Döcke, W.D. & Ghoreschi, K. T cell pathology in skin inflammation. *Semin Immunopathol* **41**, 359–377 (2019).
153. Ye, P. *et al.* Requirement of interleukin 17 receptor signaling for lung CXC chemokine and granulocyte colony-stimulating factor expression, neutrophil recruitment, and host defense. *J Exp Med* **194**, 519–527 (2001).
154. Acosta-Rodriguez, E. V. *et al.* Surface phenotype and antigenic specificity of human interleukin 17-producing T helper memory cells. *Nat Immunol* **8**, 639–646 (2007).
155. Eyerich, S. *et al.* Th22 cells represent a distinct human T cell subset involved in epidermal immunity and remodeling. *J Clin Invest* **119**, 3573–3585 (2009).
156. Bonecchi, R. & Graham, G. J. Atypical Chemokine Receptors and Their Roles in the Resolution of the Inflammatory Response. *Front Immunol* **7**, 224 (2016).

157. El Kebir, D. & Filep, J. G. Targeting neutrophil apoptosis for enhancing the resolution of inflammation. *Cells* **2**, 330–348 (2013).
158. El Kebir, D. & Filep, J. G. Modulation of Neutrophil Apoptosis and the Resolution of Inflammation through β2 Integrins. *Front Immunol* **4**, 60 (2013).
159. Headland, S. E. & Norling, L. V. The resolution of inflammation: Principles and challenges. *Semin Immunol* **27**, 149–160 (2015).
160. World Health Organization. The top 10 causes of death. https://www.who.int/news-room/fact-sheets/detail/the-top-10-causes-of-death (2020).
161. O'Connor, S. M., Taylor, C. E. & Hughes, J. M. Emerging infectious determinants of chronic diseases. *Emerg Infect Dis* **12**, 1051–1057 (2006).
162. Grant, S. S. & Hung, D. T. Persistent bacterial infections, antibiotic tolerance, and the oxidative stress response. *Virulence* **4**, 273–283 (2013).
163. Amorim, A. *et al.* Chronic Bacterial Infection Prevalence, Risk Factors, and Characteristics: A Bronchiectasis Population-Based Prospective Study. *J Clin Med* **8**, (2019).
164. Rendon, A. & Schäkel, K. Psoriasis Pathogenesis and Treatment. *Int J Mol Sci* **20**, (2019).
165. Feng, B.J. *et al.* Multiple Loci within the Major Histocompatibility Complex Confer Risk of Psoriasis. *PLoS Genet* **5**, (2009).
166. Morizane, S. & Gallo, R. L. Antimicrobial peptides in the pathogenesis of psoriasis. *J Dermatol* **39**, 225–230 (2012).
167. Nestle, F. O. *et al.* Plasmacytoid predendritic cells initiate psoriasis through interferon-alpha production. *J Exp Med* **202**, 135–143 (2005).
168. Ogawa, E., Sato, Y., Minagawa, A. & Okuyama, R. Pathogenesis of psoriasis and development of treatment. *J Dermatol* **45**, 264–272 (2018).
169. Kagami, S., Rizzo, H. L., Lee, J. J., Koguchi, Y. & Blauvelt, A. Circulating Th17, Th22, and Th1 Cells Are Increased in Psoriasis. *J Invest Dermatol* **130**, 1373–1383 (2010).
170. Benham, H. *et al.* Th17 and Th22 cells in psoriatic arthritis and psoriasis. *Arthritis Res Ther* **15**, R136 (2013).
171. Suárez-Fariñas, M., Fuentes-Duculan, J., Lowes, M. A. & Krueger, J. G. Resolved psoriasis lesions retain expression of a subset of disease-related genes. *J Invest Dermatol* **131**, 391–400 (2011).
172. Clark, R. A. Resident memory T cells in human health and disease. *Sci Transl Med* **7**, 269rv1 (2015).
173. Owczarczyk Saczonek, A., Krajewska-Włodarczyk, M., Kasprowicz-Furmańczyk, M. & Placek, W. Immunological Memory of Psoriatic Lesions. *Int J Mol Sci* **21**, (2020).
174. Silverberg, J. I. Public Health Burden and Epidemiology of Atopic Dermatitis. *Dermatol Clin* **35**, 283–289 (2017).
175. Kim, J., Kim, B. E. & Leung, D. Y. M. Pathophysiology of atopic dermatitis: Clinical implications. *Allergy Asthma Proc* **40**, 84–92 (2019).
176. O'Regan, G. M., Sandilands, A., McLean, W. H. I. & Irvine, A. D. Filaggrin in atopic dermatitis. *J Allergy Clin Immunol* **122**, 689–693 (2008).
177. Nakamura, Y. *et al. Staphylococcus* δ-toxin induces allergic skin disease by activating mast cells. *Nature* **503**, 397–401 (2013).
178. Salimi, M. *et al.* A role for IL-25 and IL-33-driven type-2 innate lymphoid cells in atopic dermatitis. *J Exp Med* **210**, 2939–2950 (2013).
179. Koga, C., Kabashima, K., Shiraishi, N., Kobayashi, M. & Tokura, Y. Possible pathogenic role of Th17 cells for atopic dermatitis. *J Invest Dermatol* **128**, 2625–2630 (2008).
180. Guttman-Yassky, E., Krueger, J. G. & Lebwohl, M. G. Systemic immune mechanisms in atopic dermatitis and psoriasis with implications for treatment. *Exp Dermatol* **27**, 409–417 (2018).

181. Armstrong, A. W. & Read, C. Pathophysiology, Clinical Presentation, and Treatment of Psoriasis: A Review. *JAMA* **323**, 1945–1960 (2020).
182. Feldman, S. R. *et al.* The Challenge of Managing Atopic Dermatitis in the United States. *Am Health Drug Benefits* **12**, 83–93 (2019).
183. Deleanu, D. & Nedelea, I. Biological therapies for atopic dermatitis: An update. *Exp Ther Med* **17**, 1061–1067 (2019).
184. Yasir, M., Goyal, A., Bansal, P. & Sonthalia, S. Corticosteroid Adverse Effects. in *StatPearls* (StatPearls Publishing, 2021).
185. Eichenfield, L. F. *et al.* Costs and Treatment Patterns Among Patients with Atopic Dermatitis Using Advanced Therapies in the United States: Analysis of a Retrospective Claims Database. *Dermatol Ther (Heidelb)* **10**, 791–806 (2020).
186. Mookherjee, N., Anderson, M. A., Haagsman, H. P. & Davidson, D. J. Antimicrobial host defence peptides: functions and clinical potential. *Nat Rev Drug Discov* **19**, 311–332 (2020).
187. Haney, E. F., Straus, S. K. & Hancock, R. E. W. Reassessing the Host Defense Peptide Landscape. *Front Chem* **7**, 43 (2019).
188. Wang, G., Li, X. & Wang, Z. APD3: the antimicrobial peptide database as a tool for research and education. *Nucleic Acids Research* **44**, D1087–D1093 (2016).
189. Wang, G. Human Antimicrobial Peptides and Proteins. *Pharmaceuticals* **7**, 545–594 (2014).
190. Schauber, J. & Gallo, R. L. Antimicrobial peptides and the skin immune defense system. *J Allergy Clin Immunol* **122**, 261–266 (2008).
191. Sørensen, O. E. *et al.* Human cathelicidin, hCAP-18, is processed to the antimicrobial peptide LL-37 by extracellular cleavage with proteinase 3. *Blood* **97**, 3951–3959 (2001).
192. Kenshi, Y. & Richard, L. G. Antimicrobial peptides in human skin disease. *Eur J Dermatol* **18**, 11–21 (2008).
193. Hilchie, A. L., Wuerth, K. & Hancock, R. E. W. Immune modulation by multifaceted cationic host defense (antimicrobial) peptides. *Nat. Chem. Biol.* **9**, 761–768 (2013).
194. Hancock, R. E. W., Haney, E. F. & Gill, E. E. The immunology of host defence peptides: beyond antimicrobial activity. *Nat. Rev. Immunol.* **16**, 321–334 (2016).
195. Niyonsaba, F., Kiatsurayanon, C., Chieosilapatham, P. & Ogawa, H. Friends or Foes? Host defense (antimicrobial) peptides and proteins in human skin diseases. *Experimental Dermatology* **26**, 989–998 (2017).
196. Dinulos, J. G. H., Mentele, L., Fredericks, L. P., Dale, B. A. & Darmstadt, G. L. Keratinocyte expression of human beta defensin 2 following bacterial infection: role in cutaneous host defense. *Clin Diagn Lab Immunol* **10**, 161–166 (2003).
197. Yang, D. *et al.* Beta-defensins: linking innate and adaptive immunity through dendritic and T cell CCR6. *Science* **286**, 525–528 (1999).
198. De Yang, null *et al.* LL-37, the neutrophil granule- and epithelial cell-derived cathelicidin, utilizes formyl peptide receptor-like 1 (FPRL1) as a receptor to chemoattract human peripheral blood neutrophils, monocytes, and T cells. *J Exp Med* **192**, 1069–1074 (2000).
199. Zheng, Y. *et al.* Cathelicidin LL-37 induces the generation of reactive oxygen species and release of human alpha-defensins from neutrophils. *Br J Dermatol* **157**, 1124–1131 (2007).
200. Pena, O. M. *et al.* Synthetic cationic peptide IDR-1018 modulates human macrophage differentiation. *PLoS ONE* **8**, e52449 (2013).
201. Niyonsaba, F. *et al.* Antimicrobial Peptides Human β-Defensins Stimulate Epidermal Keratinocyte Migration, Proliferation and Production of Proinflammatory Cytokines and Chemokines. *J Invest Dermatol* **127**, 594–604 (2007).
202. Haney, E. F., Mansour, S. C., Hilchie, A. L., de la Fuente-Núñez, C. & Hancock, R. E. W. High throughput screening methods for assessing antibiofilm and immunomodulatory activities of

synthetic peptides. *Peptides* **71**, 276–285 (2015).
203. Haney, E. F., Wu, B. C., Lee, K., Hilchie, A. L. & Hancock, R. E. W. Aggregation and Its Influence on the Immunomodulatory Activity of Synthetic Innate Defense Regulator Peptides. *Cell Chem Biol* **24**, 969-980.e4 (2017).
204. Rivas-Santiago, B. *et al.* Ability of innate defence regulator peptides IDR-1002, IDR-HH2 and IDR-1018 to protect against Mycobacterium tuberculosis infections in animal models. *PLoS ONE* **8**, e59119 (2013).
205. Tokumaru, S. *et al.* Induction of keratinocyte migration via transactivation of the epidermal growth factor receptor by the antimicrobial peptide LL-37. *J Immunol* **175**, 4662–4668 (2005).
206. Kahlenberg, J. M. & Kaplan, M. J. Little peptide, big effects: the role of LL-37 in inflammation and autoimmune disease. *J Immunol* **191**, 10.4049/jimmunol.1302005 (2013).
207. Mookherjee, N. *et al.* Modulation of the TLR-mediated inflammatory response by the endogenous human host defense peptide LL-37. *J Immunol* **176**, 2455–2464 (2006).
208. Tewary, P. *et al.* β-Defensin 2 and 3 promote the uptake of self or CpG DNA, enhance IFN-α production by human plasmacytoid dendritic cells, and promote inflammation. *J Immunol* **191**, 865–874 (2013).
209. Prysliak, T. & Perez-Casal, J. Immune responses to *Mycoplasma bovis* proteins formulated with different adjuvants. *Can J Microbiol* **62**, 492–504 (2016).
210. Mansour, S. C., Pena, O. M. & Hancock, R. E. W. Host defense peptides: front-line immunomodulators. *Trends Immunol.* **35**, 443–450 (2014).
211. Bowdish, D. M. E. *et al.* Impact of LL-37 on anti-infective immunity. *Journal of Leukocyte Biology* **77**, 451–459 (2005).
212. Cherkasov, A. *et al.* Use of artificial intelligence in the design of small peptide antibiotics effective against a broad spectrum of highly antibiotic-resistant superbugs. *ACS Chem Biol* **4**, 65–74 (2009).
213. Zhang, L., Scott, M. G., Yan, H., Mayer, L. D. & Hancock, R. E. Interaction of polyphemusin I and structural analogs with bacterial membranes, lipopolysaccharide, and lipid monolayers. *Biochemistry* **39**, 14504–14514 (2000).
214. Sass, V. *et al.* Human beta-defensin 3 inhibits cell wall biosynthesis in *Staphylococci*. *Infect Immun* **78**, 2793–2800 (2010).
215. Zhang, R. *et al.* Efficacy of Antimicrobial Peptide DP7, Designed by Machine-Learning Method, Against Methicillin-Resistant *Staphylococcus aureus*. *Front Microbiol* **10**, 1175 (2019).
216. Overhage, J. *et al.* Human host defense peptide LL-37 prevents bacterial biofilm formation. *Infect Immun* **76**, 4176–4182 (2008).
217. Hancock, R. E. W., Alford, M. A. & Haney, E. F. Antibiofilm activity of host defence peptides: complexity provides opportunities. *Nat Rev Microbiol* 1–12 (2021) doi:10.1038/s41579-021-00585-w.
218. Di Somma, A., Moretta, A., Canè, C., Cirillo, A. & Duilio, A. Antimicrobial and Antibiofilm Peptides. *Biomolecules* **10**, 652 (2020).
219. de la Fuente-Núñez, C. *et al.* D-enantiomeric peptides that eradicate wild-type and multi-drug resistant biofilms and protect against lethal *Pseudomonas aeruginosa* infections. *Chem Biol* **22**, 196–205 (2015).
220. Mansour, S. C. A novel peptide-based treatment for bacterial abscess infections. (University of British Columbia, 2018). doi:10.14288/1.0366132.
221. de la Fuente-Núñez, C., Reffuveille, F., Haney, E. F., Straus, S. K. & Hancock, R. E. W. Broad-spectrum anti-biofilm peptide that targets a cellular stress response. *PLoS Pathog.* **10**, e1004152 (2014).

222. Pletzer, D., Wolfmeier, H., Bains, M. & Hancock, R. E. W. Synthetic Peptides to Target Stringent Response-Controlled Virulence in a *Pseudomonas aeruginosa* Murine Cutaneous Infection Model. *Front Microbiol* **8**, 1867 (2017).
223. Brancatisano, F. L. *et al.* Inhibitory effect of the human liver-derived antimicrobial peptide hepcidin 20 on biofilms of polysaccharide intercellular adhesin (PIA)-positive and PIA-negative strains of *Staphylococcus epidermidis*. *Biofouling* **30**, 435–446 (2014).
224. Haney, E. F. & Hancock, R. E. W. Peptide design for antimicrobial and immunomodulatory applications. *Biopolymers* **100**, 572–583 (2013).
225. Vagner, J., Qu, H. & Hruby, V. J. Peptidomimetics, a synthetic tool of drug discovery. *Curr Opin Chem Biol* **12**, 292–296 (2008).
226. Hansen, A. M., Skovbakke, S. L., Christensen, S. B., Perez-Gassol, I. & Franzyk, H. Studies on acid stability and solid-phase block synthesis of peptide-peptoid hybrids: ligands for formyl peptide receptors. *Amino Acids* **51**, 205–218 (2019).
227. Bonke G, Vedel L, Witt M, Jaroszewski JW, Olsen CA, Franzyk H. Dimeric Building Blocks for SolidPhase Synthesis of α-Peptide-β-Peptoid Chimeras. Synthesis-Stuttgart. 2008; 2008:2381-2390. DOI: 2381-2390. 10.1055/s-2008-1067171.
228. van der Plas, M. J. A. *et al. Pseudomonas aeruginosa* elastase cleaves a C-terminal peptide from human thrombin that inhibits host inflammatory responses. *Nat Commun* **7**, 11567 (2016).
229. Centers for Disease Control and Prevention (CDC). Outbreaks of community-associated methicillin-resistant *Staphylococcus aureus* skin infections--Los Angeles County, California, 2002-2003. *MMWR Morb. Mortal. Wkly. Rep.* **52**, 88 (2003).
230. Plaut, R. D., Mocca, C. P., Prabhakara, R., Merkel, T. J. & Stibitz, S. Stably Luminescent *Staphylococcus aureus* Clinical Strains for Use in Bioluminescent Imaging. *PLOS ONE* **8**, e59232 (2013).
231. Hancock, R. E. & Carey, A. M. Outer membrane of *Pseudomonas aeruginosa*: heat- 2-mercaptoethanol-modifiable proteins. *J. Bacteriol.* **140**, 902–910 (1979).
232. Lewenza, S. *et al.* Construction of a mini-Tn5-luxCDABE mutant library in *Pseudomonas aeruginosa* PAO1: a tool for identifying differentially regulated genes. *Genome Res* **15**, 583–589 (2005).
233. Berry, C. L. *et al.* Chemical and biological characterization of sclerosin, an antifungal lipopeptide. *Can. J. Microbiol.* **58**, 1027–1034 (2012).
234. Schenk, S. & Laddaga, R. A. Improved method for electroporation of *Staphylococcus aureus*. *FEMS Microbiol. Lett.* **73**, 133–138 (1992).
235. Pletzer, D., Braun, Y. & Weingart, H. Swarming motility is modulated by expression of the putative xenosiderophore transporter SppR-SppABCD in *Pseudomonas aeruginosa* PA14. *Antonie van Leeuwenhoek* **109**, 737–753 (2016).
236. Schindelin, J. *et al.* Fiji: an open-source platform for biological-image analysis. *Nat Meth* **9**, 676–682 (2012).
237. den Reijer, P. M. *et al.* Detection of Alpha-Toxin and Other Virulence Factors in Biofilms of *Staphylococcus aureus* on Polystyrene and a Human Epidermal Model. *PLoS ONE* **11**, e0145722 (2016).
238. Ewels, P., Magnusson, M., Lundin, S. & Käller, M. MultiQC: summarize analysis results for multiple tools and samples in a single report. *Bioinformatics* **32**, 3047–3048 (2016).
239. Aken, B. L. *et al.* The Ensembl gene annotation system. *Database (Oxford)* **2016**, (2016).
240. Dobin, A. *et al.* STAR: ultrafast universal RNA-seq aligner. *Bioinformatics* **29**, 15–21 (2013).
241. Anders, S., Pyl, P. T. & Huber, W. HTSeq--a Python framework to work with high-throughput sequencing data. *Bioinformatics* **31**, 166–169 (2015).
242. Love, M. I., Huber, W. & Anders, S. Moderated estimation of fold change and dispersion for

RNA-seq data with DESeq2. *Genome Biol.* **15**, 550 (2014).
243. Foroushani, A. B. K., Brinkman, F. S. L. & Lynn, D. J. Pathway-GPS and SIGORA: identifying relevant pathways based on the over-representation of their gene-pair signatures. *PeerJ* **1**, e229 (2013).
244. Xia, J., Gill, E. E. & Hancock, R. E. W. NetworkAnalyst for statistical, visual and network-based meta-analysis of gene expression data. *Nat Protoc* **10**, 823–844 (2015).
245. Breuer, K. *et al.* InnateDB: systems biology of innate immunity and beyond--recent updates and continuing curation. *Nucleic Acids Res.* **41**, D1228-1233 (2013).
246. Andrews, Simon. Babraham Bioinformatics - FastQC A Quality Control tool for High Throughput Sequence Data. https://www.bioinformatics.babraham.ac.uk/projects/fastqc/ (2010).
247. Jassal, B. *et al.* The reactome pathway knowledgebase. *Nucleic Acids Res* **48**, D498–D503 (2020).
248. Hotamisligil, G. S. Inflammation and metabolic disorders. *Nature* **444**, 860–867 (2006).
249. Nijnik, A. *et al.* Synthetic cationic peptide IDR-1002 provides protection against bacterial infections through chemokine induction and enhanced leukocyte recruitment. *J. Immunol.* **184**, 2539–2550 (2010).
250. Turner-Brannen, E. *et al.* Modulation of interleukin-1β-induced inflammatory responses by a synthetic cationic innate defence regulator peptide, IDR-1002, in synovial fibroblasts. *Arthritis Res. Ther.* **13**, R129 (2011).
251. Huante-Mendoza, A., Silva-García, O., Oviedo-Boyso, J., Hancock, R. E. W. & Baizabal-Aguirre, V. M. Peptide IDR-1002 Inhibits NF-κB Nuclear Translocation by Inhibition of IκBα Degradation and Activates p38/ERK1/2-MSK1-Dependent CREB Phosphorylation in Macrophages Stimulated with Lipopolysaccharide. *Front Immunol* **7**, 533 (2016).
252. Niyonsaba, F. *et al.* The innate defense regulator peptides IDR-HH2, IDR-1002, and IDR-1018 modulate human neutrophil functions. *J. Leukoc. Biol.* **94**, 159–170 (2013).
253. Rutkowski, R., Pancewicz, S. A., Rutkowski, K. & Rutkowska, J. Reactive oxygen and nitrogen species in inflammatory process. *Pol. Merkur. Lekarski* **23**, 131–136 (2007).
254. Kielland, A. *et al. In vivo* imaging of reactive oxygen and nitrogen species in inflammation using the luminescent probe L-012. *Free Radic. Biol. Med.* **47**, 760–766 (2009).
255. Salinas-Sánchez, D. O., Herrera-Ruiz, M., Pérez, S., Jiménez-Ferrer, E. & Zamilpa, A. Anti-inflammatory activity of hautriwaic acid isolated from *Dodonaea viscosa* leaves. *Molecules* **17**, 4292–4299 (2012).
256. Mittal, M., Siddiqui, M. R., Tran, K., Reddy, S. P. & Malik, A. B. Reactive oxygen species in inflammation and tissue injury. *Antioxid. Redox Signal.* **20**, 1126–1167 (2014).
257. Xiao, L. *et al.* A novel near-infrared fluorescence imaging probe for *in vivo* neutrophil tracking. *Mol Imaging* **11**, 372–382 (2012).
258. Blanchard, C. *et al.* Periostin facilitates eosinophil tissue infiltration in allergic lung and esophageal responses. *Mucosal Immunol* **1**, 289–296 (2008).
259. Chen, G. Y. & Nuñez, G. Sterile inflammation: sensing and reacting to damage. *Nat. Rev. Immunol.* **10**, 826–837 (2010).
260. Rider, P. *et al.* IL-1α and IL-1β recruit different myeloid cells and promote different stages of sterile inflammation. *J. Immunol.* **187**, 4835–4843 (2011).
261. Hsieh, C.Y. *et al.* Inhibiting glycogen synthase kinase-3 decreases 12-O-tetradecanoylphorbol-13-acetate-induced interferon-γ-mediated skin inflammation. *J. Pharmacol. Exp. Ther.* **343**, 125–133 (2012).
262. Hsieh,C.Y. *et al.* Macrophage migration inhibitory factor triggers chemotaxis of CD74+CXCR2+ NKT cells in chemically induced IFN-γ-mediated skin inflammation. *J.*

Immunol. **193**, 3693–3703 (2014).
263. Zhang, G. *et al.* Resolution of PMA-induced skin inflammation involves interaction of IFN-γ and ALOX15. *Mediators Inflamm.* **2013**, 930124 (2013).
264. Salmela, M. *et al.* Tumor promoter PMA enhances kindlin-2 and decreases vimentin recruitment into cell adhesion sites. *Int. J. Biochem. Cell Biol.* **78**, 22–30 (2016).
265. Widelitz, R. B. Wnt signaling in skin organogenesis. *Organogenesis* **4**, 123–133 (2008).
266. Lim, X. & Nusse, R. Wnt signaling in skin development, homeostasis, and disease. *Cold Spring Harb Perspect Biol* **5**, (2013).
267. Sun, L. & Ye, R. D. Role of G protein-coupled receptors in inflammation. *Acta Pharmacol. Sin.* **33**, 342–350 (2012).
268. Chmielewski, S., Piaszyk-Borychowska, A., Wesoly, J. & Bluyssen, H. A. R. STAT1 and IRF8 in Vascular Inflammation and Cardiovascular Disease: Diagnostic and Therapeutic Potential. *Int. Rev. Immunol.* **35**, 434–454 (2016).
269. Simon, P. S. *et al.* The NF-κB p65 and p50 homodimer cooperate with IRF8 to activate iNOS transcription. *BMC Cancer* **15**, 770 (2015).
270. Kinoshita, T., Imamura, R., Kushiyama, H. & Suda, T. NLRP3 mediates NF-κB activation and cytokine induction in microbially induced and sterile inflammation. *PLoS ONE* **10**, e0119179 (2015).
271. Fritsche, G. *et al.* Modulation of macrophage iron transport by Nramp1 (Slc11a1). *Immunobiology* **212**, 751–757 (2007).
272. Holmdahl, R., Sareila, O., Olsson, L. M., Bäckdahl, L. & Wing, K. Ncf1 polymorphism reveals oxidative regulation of autoimmune chronic inflammation. *Immunol. Rev.* **269**, 228–247 (2016).
273. Hamilton, J. A. Colony-stimulating factors in inflammation and autoimmunity. *Nat. Rev. Immunol.* **8**, 533–544 (2008).
274. Alter-Koltunoff, M. *et al.* Innate immunity to intraphagosomal pathogens is mediated by interferon regulatory factor 8 (IRF-8) that stimulates the expression of macrophage-specific Nramp1 through antagonizing repression by c-Myc. *J. Biol. Chem.* **283**, 2724–2733 (2008).
275. Liu, J. & Ma, X. Interferon regulatory factor 8 regulates RANTES gene transcription in cooperation with interferon regulatory factor-1, NF-kappaB, and PU.1. *J. Biol. Chem.* **281**, 19188–19195 (2006).
276. Pedchenko, T. V., Park, G. Y., Joo, M., Blackwell, T. S. & Christman, J. W. Inducible binding of PU.1 and interacting proteins to the Toll-like receptor 4 promoter during endotoxemia. *Am. J. Physiol. Lung Cell Mol. Physiol.* **289**, L429-437 (2005).
277. Vila-del Sol, V., Punzón, C. & Fresno, M. IFN-gamma-induced TNF-alpha expression is regulated by interferon regulatory factors 1 and 8 in mouse macrophages. *J. Immunol.* **181**, 4461–4470 (2008).
278. Gábor, M. Models of acute inflammation in the ear. *Methods Mol. Biol.* **225**, 129–137 (2003).
279. Boardman, P. L. & Hart, F. D. Side-effects of indomethacin. *Ann Rheum Dis* **26**, 127–132 (1967).
280. Lövgren, O. & Allander, E. Side-effects of Indomethacin. *Br Med J* **1**, 118 (1964).
281. Naito, Y., Yoshikawa, T., Yoshida, N. & Kondo, M. Role of oxygen radical and lipid peroxidation in indomethacin-induced gastric mucosal injury. *Dig. Dis. Sci.* **43**, 30S-34S (1998).
282. Niyonsaba, F., Someya, A., Hirata, M., Ogawa, H. & Nagaoka, I. Evaluation of the effects of peptide antibiotics human beta-defensins-1/-2 and LL-37 on histamine release and prostaglandin D(2) production from mast cells. *Eur. J. Immunol.* **31**, 1066–1075 (2001).
283. Dinarello, C. A. Interleukin-1 in the pathogenesis and treatment of inflammatory diseases. *Blood* **117**, 3720–3732 (2011).
284. Turner, M. D., Nedjai, B., Hurst, T. & Pennington, D. J. Cytokines and chemokines: At the

crossroads of cell signalling and inflammatory disease. *Biochim. Biophys. Acta* **1843**, 2563–2582 (2014).
285. Bradley, J. R. TNF-mediated inflammatory disease. *J. Pathol.* **214**, 149–160 (2008).
286. Pollard, K. M., Cauvi, D. M., Toomey, C. B., Morris, K. V. & Kono, D. H. Interferon-γ and systemic autoimmunity. *Discov Med* **16**, 123–131 (2013).
287. Bralley, E. E., Hargrove, J. L., Greenspan, P. & Hartle, D. K. Topical anti-inflammatory activities of *Vitis rotundifolia* (muscadine grape) extracts in the tetradecanoylphorbol acetate model of ear inflammation. *J Med Food* **10**, 636–642 (2007).
288. Calou, I. B. F. *et al.* Topically applied diterpenoids from *Egletes viscosa* (Asteraceae) attenuate the dermal inflammation in mouse ear induced by tetradecanoylphorbol 13-acetate- and oxazolone. *Biol. Pharm. Bull.* **31**, 1511–1516 (2008).
289. Ozato, K., Tailor, P. & Kubota, T. The interferon regulatory factor family in host defense: mechanism of action. *J. Biol. Chem.* **282**, 20065–20069 (2007).
290. Taniguchi, T., Ogasawara, K., Takaoka, A. & Tanaka, N. IRF family of transcription factors as regulators of host defense. *Annu. Rev. Immunol.* **19**, 623–655 (2001).
291. Wang, H. & Morse, H. C. IRF8 regulates myeloid and B lymphoid lineage diversification. *Immunol. Res.* **43**, 109–117 (2009).
292. Marquis, J.F. *et al.* Interferon regulatory factor 8 regulates pathways for antigen presentation in myeloid cells and during tuberculosis. *PLoS Genet.* **7**, e1002097 (2011).
293. Tamura, T., Nagamura-Inoue, T., Shmeltzer, Z., Kuwata, T. & Ozato, K. ICSBP directs bipotential myeloid progenitor cells to differentiate into mature macrophages. *Immunity* **13**, 155–165 (2000).
294. Tamura, T., Thotakura, P., Tanaka, T. S., Ko, M. S. H. & Ozato, K. Identification of target genes and a unique cis element regulated by IRF-8 in developing macrophages. *Blood* **106**, 1938–1947 (2005).
295. Xiong, H. *et al.* Ubiquitin-dependent degradation of interferon regulatory factor-8 mediated by Cbl down-regulates interleukin-12 expression. *J. Biol. Chem.* **280**, 23531–23539 (2005).
296. Yan, M. *et al.* Cutting Edge: Expression of IRF8 in Gastric Epithelial Cells Confers Protective Innate Immunity against *Helicobacter pylori* Infection. *J. Immunol.* **196**, 1999–2003 (2016).
297. Berghout, J. *et al.* Irf8-regulated genomic responses drive pathological inflammation during cerebral malaria. *PLoS Pathog.* **9**, e1003491 (2013).
298. Yu, H. B. *et al.* Sequestosome-1/p62 is the key intracellular target of innate defense regulator peptide. *J. Biol. Chem.* **284**, 36007–36011 (2009).
299. Kim, J. Y. & Ozato, K. The Sequestosome 1/p62 Attenuates Cytokine Gene Expression in Activated Macrophages by Inhibiting IFN Regulatory Factor 8 and TNF Receptor-Associated Factor 6/NF-κB Activity. *J Immunol* **182**, 2131–2140 (2009).
300. He, H.Q. & Ye, R. D. The Formyl Peptide Receptors: Diversity of Ligands and Mechanism for Recognition. *Molecules* **22**, (2017).
301. Winther, M., Dahlgren, C. & Forsman, H. Formyl Peptide Receptors in Mice and Men: Similarities and Differences in Recognition of Conventional Ligands and Modulating Lipopeptides. *Basic Clin. Pharmacol. Toxicol.* **122**, 191–198 (2018).
302. Skovbakke, S. L., Holdfeldt, A., Forsman, H., Bylund, J. & Franzyk, H. The Role of Formyl Peptide Receptors for Immunomodulatory Activities of Antimicrobial Peptides and Peptidomimetics. *Curr. Pharm. Des.* **24**, 1100–1120 (2018).
303. Li, L. *et al.* New development in studies of formyl-peptide receptors: critical roles in host defense. *J. Leukoc. Biol.* **99**, 425–435 (2016).
304. Prevete, N., Liotti, F., Marone, G., Melillo, R. M. & de Paulis, A. Formyl peptide receptors at the interface of inflammation, angiogenesis and tumor growth. *Pharmacol. Res.* **102**, 184–191

(2015).
305. Chen, K. *et al.* Regulation of inflammation by members of the formyl-peptide receptor family. *J Autoimmun* **85**, 64–77 (2017).
306. Dufton, N. *et al.* Anti-inflammatory role of the murine formyl-peptide receptor 2: ligand-specific effects on leukocyte responses and experimental inflammation. *J. Immunol.* **184**, 2611–2619 (2010).
307. Dorward, D. A. *et al.* The Role of Formylated Peptides and Formyl Peptide Receptor 1 in Governing Neutrophil Function during Acute Inflammation. *Am J Pathol* **185**, 1172–1184 (2015).
308. Hemshekhar, M., Anaparti, V. & Mookherjee, N. Functions of Cationic Host Defense Peptides in Immunity. *Pharmaceuticals (Basel)* **9**, (2016).
309. Afacan, N. J., Yeung, A. T. Y., Pena, O. M. & Hancock, R. E. W. Therapeutic potential of host defense peptides in antibiotic-resistant infections. *Curr. Pharm. Des.* **18**, 807–819 (2012).
310. Molchanova, N., Hansen, P. R. & Franzyk, H. Advances in Development of Antimicrobial Peptidomimetics as Potential Drugs. *Molecules* **22**, (2017).
311. Rotem, S. & Mor, A. Antimicrobial peptide mimics for improved therapeutic properties. *Biochim. Biophys. Acta* **1788**, 1582–1592 (2009).
312. Zuckermann, R. N. & Kodadek, T. Peptoids as potential therapeutics. *Curr. Opin. Mol. Ther.* **11**, 299–307 (2009).
313. Olsen, C. A. Peptoid-Peptide hybrid backbone architectures. *Chembiochem* **11**, 152–160 (2010).
314. Skovbakke, S. L., Larsen, C. J., Heegaard, P. M. H., Moesby, L. & Franzyk, H. Lipidated α-peptide/β-peptoid hybrids with potent anti-inflammatory activity. *J. Med. Chem.* **58**, 801–813 (2015).
315. Skovbakke, S. L. *et al.* The proteolytically stable peptidomimetic Pam-(Lys-βNSpe)$_6$-NH$_2$ selectively inhibits human neutrophil activation via formyl peptide receptor 2. *Biochem. Pharmacol.* **93**, 182–195 (2015).
316. Skovbakke, S. L. *et al.* The peptidomimetic Lau-(Lys-βNSpe)$_6$-NH$_2$ antagonizes formyl peptide receptor 2 expressed in mouse neutrophils. *Biochem. Pharmacol.* **119**, 56–65 (2016).
317. Wu, B. C., Lee, A. H.Y. & Hancock, R. E. W. Mechanisms of the Innate Defense Regulator Peptide-1002 Anti-Inflammatory Activity in a Sterile Inflammation Mouse Model. *The Journal of Immunology* **199**, 3592–3603 (2017).
318. Jahnsen, R. D., Frimodt-Møller, N. & Franzyk, H. Antimicrobial activity of peptidomimetics against multidrug-resistant *Escherichia coli*: a comparative study of different backbones. *J. Med. Chem.* **55**, 7253–7261 (2012).
319. Mestas, J. & Hughes, C. C. W. Of mice and not men: differences between mouse and human immunology. *J. Immunol.* **172**, 2731–2738 (2004).
320. Bitschar, K., Wolz, C., Krismer, B., Peschel, A. & Schittek, B. Keratinocytes as sensors and central players in the immune defense against *Staphylococcus aureus* in the skin. *J. Dermatol. Sci.* **87**, 215–220 (2017).
321. Peschel, A. & Otto, M. Phenol-soluble modulins and *staphylococcal* infection. *Nat. Rev. Microbiol.* **11**, 667–673 (2013).
322. Kretschmer, D. *et al.* Human formyl peptide receptor 2 senses highly pathogenic *Staphylococcus aureus*. *Cell Host Microbe* **7**, 463–473 (2010).
323. Liu, M. *et al.* Formylpeptide Receptors Mediate Rapid Neutrophil Mobilization to Accelerate Wound Healing. *PLoS One* **9**, (2014).
324. Zhang, Q. *et al.* Circulating mitochondrial DAMPs cause inflammatory responses to injury. *Nature* **464**, 104–107 (2010).
325. McDonald, B. *et al.* Intravascular danger signals guide neutrophils to sites of sterile

inflammation. *Science* **330**, 362–366 (2010).
326. Hazeldine, J., Hampson, P., Opoku, F. A., Foster, M. & Lord, J. M. N-Formyl peptides drive mitochondrial damage associated molecular pattern induced neutrophil activation through ERK1/2 and P38 MAP kinase signalling pathways. *Injury* **46**, 975–984 (2015).
327. Aslam, B. *et al.* Antibiotic resistance: a rundown of a global crisis. *Infect Drug Resist* **11**, 1645–1658 (2018).
328. Jamal, M. *et al.* Bacterial biofilm and associated infections. *J Chin Med Assoc* **81**, 7–11 (2018).
329. Malone, M. *et al.* The prevalence of biofilms in chronic wounds: a systematic review and meta-analysis of published data. *J Wound Care* **26**, 20–25 (2017).
330. Wolcott, R. D. *et al.* Biofilm maturity studies indicate sharp debridement opens a time-dependent therapeutic window. *J Wound Care* **19**, 320–328 (2010).
331. Wu, H., Moser, C., Wang, H.Z., Høiby, N. & Song, Z.J. Strategies for combating bacterial biofilm infections. *Int J Oral Sci* **7**, 1–7 (2015).
332. Wang, D., Shen, Y., Hancock, R. E. W., Ma, J. & Haapasalo, M. Antimicrobial Effect of Peptide DJK-5 Used Alone or Mixed with EDTA on Mono- and Multispecies Biofilms in Dentin Canals. *J Endod* **44**, 1709–1713 (2018).
333. Crabbé, A. *et al.* Antimicrobial efficacy against *Pseudomonas aeruginosa* biofilm formation in a three-dimensional lung epithelial model and the influence of fetal bovine serum. *Sci Rep* **7**, 43321 (2017).
334. Pletzer, D., Mansour, S. C. & Hancock, R. E. W. Synergy between conventional antibiotics and anti-biofilm peptides in a murine, sub-cutaneous abscess model caused by recalcitrant ESKAPE pathogens. *PLoS Pathog.* **14**, e1007084 (2018).
335. Haney E.F., Pletzer D., Hancock R.E.W. (2018) Impact of Host Defense Peptides on Chronic Wounds and Infections. In: . Recent Clinical Techniques, Results, and Research in Wounds. Springer, Cham. in.
336. Hong, S. D. *et al.* Hematoxylin and Eosin Staining for Detecting Biofilms: Practical and Cost-Effective Methods for Predicting Worse Outcomes After Endoscopic Sinus Surgery. *Clin Exp Otorhinolaryngol* **7**, 193–197 (2014).
337. Daniel, R. A. & Errington, J. Control of cell morphogenesis in bacteria: two distinct ways to make a rod-shaped cell. *Cell* **113**, 767–776 (2003).
338. Iwaki, M., Noguchi, N., Nakaminami, H., Sasatsu, M. & Ito, M. Antimicrobial activity and frequency of spontaneous gentamicin-resistant mutants in bacteria related skin infections. *Yakugaku Zasshi* **131**, 1653–1659 (2011).
339. Fernandes, P. Fusidic Acid: A Bacterial Elongation Factor Inhibitor for the Oral Treatment of Acute and Chronic *Staphylococcal* Infections. *Cold Spring Harb Perspect Med* **6**, a025437 (2016).
340. Contopoulos-Ioannidis, D. G., Ntzani, E. & Ioannidis, J. P. A. Translation of highly promising basic science research into clinical applications. *Am. J. Med.* **114**, 477–484 (2003).
341. Hackam, D. G. & Redelmeier, D. A. Translation of research evidence from animals to humans. *JAMA* **296**, 1731–1732 (2006).
342. Choi, K.Y., Wu, B. C., Lee, A. H.Y., Baquir, Beverlie, & Hancock, Robert E.W. Utilizing Organoid and Air-Liquid Interface Models as a Screening Method in the Development of New Host Defense Peptides. *Frontiers in Cellular and Infection Microbiology* **10**, 228 (2020).
343. Sachs, N. *et al.* Long-term expanding human airway organoids for disease modeling. *EMBO J.* **38**, (2019).
344. Iakobachvili, N. & Peters, P. J. Humans in a Dish: The Potential of Organoids in Modeling Immunity and Infectious Diseases. *Front Microbiol* **8**, 2402 (2017).
345. Periasamy, S. *et al.* How *Staphylococcus aureus* biofilms develop their characteristic structure.

PNAS **109**, 1281–1286 (2012).
346. Alves, C. S. *et al. Escherichia coli* Cell Surface Perturbation and Disruption Induced by Antimicrobial Peptides BP100 and pepR. *J Biol Chem* **285**, 27536–27544 (2010).
347. Hilpert, K., Volkmer-Engert, R., Walter, T. & Hancock, R. E. W. High-throughput generation of small antibacterial peptides with improved activity. *Nat. Biotechnol.* **23**, 1008–1012 (2005).
348. Ward, A. & Campoli-Richards, D. M. Mupirocin. *Drugs* **32**, 425–444 (1986).
349. Koning, S. *et al.* Fusidic acid cream in the treatment of impetigo in general practice: double blind randomised placebo controlled trial. *BMJ* **324**, 203–206 (2002).
350. Haisma, E. M. *et al.* Antimicrobial Peptide P60.4Ac-Containing Creams and Gel for Eradication of Methicillin-Resistant *Staphylococcus aureus* from Cultured Skin and Airway Epithelial Surfaces. *Antimicrob. Agents Chemother.* **60**, 4063–4072 (2016).
351. Kifer, D., Mužinić, V. & Klarić, M. Š. Antimicrobial potency of single and combined mupirocin and monoterpenes, thymol, menthol and 1,8-cineole against *Staphylococcus aureus* planktonic and biofilm growth. *J. Antibiot.* **69**, 689–696 (2016).
352. Jin, Y. *et al.* Subinhibitory Concentrations of Mupirocin Stimulate *Staphylococcus aureus* Biofilm Formation by Upregulating cidA. *Antimicrob. Agents Chemother.* **64**, (2020).
353. Melchionna, M., Styan, K. E. & Marchesan, S. The Unexpected Advantages of Using D-Amino Acids for Peptide Self-Assembly into Nanostructured Hydrogels for Medicine. *Curr Top Med Chem* **16**, 2009–2018 (2016).
354. Du, W. *et al.* Rapid Isolation of Functional ex vivo Human Skin Tissue-Resident Memory T Lymphocytes. *Front. Immunol.* **12**, (2021).
355. He, X., de Oliveira, V. L., Keijsers, R., Joosten, I. & Koenen, H. J. P. N. Lymphocyte Isolation from Human Skin for Phenotypic Analysis and Ex Vivo Cell Culture. *J Vis Exp* e52564 (2016) doi:10.3791/52564.
356. O'Neill, A. T., Monteiro-Riviere, N. A. & Walker, G. M. Characterization of microfluidic human epidermal keratinocyte culture. *Cytotechnology* **56**, 197–207 (2008).
357. Agrawal, R. & Woodfolk, J. A. Skin Barrier Defects in Atopic Dermatitis. *Curr Allergy Asthma Rep* **14**, 433 (2014).
358. Kennedy, P., Brammah, S. & Wills, E. Burns, biofilm and a new appraisal of burn wound sepsis. *Burns* **36**, 49–56 (2010).
359. Metcalf, D. G. & Bowler, P. G. Biofilm delays wound healing: A review of the evidence. *Burns Trauma* **1**, 5–12 (2015).
360. Zhao, G. *et al.* Biofilms and Inflammation in Chronic Wounds. *Adv Wound Care (New Rochelle)* **2**, 389–399 (2013).
361. Mulcahy, L. R., Isabella, V. M. & Lewis, K. *Pseudomonas aeruginosa* biofilms in disease. *Microb. Ecol.* **68**, 1–12 (2014).
362. Seth, A. K. *et al. In vivo* modeling of biofilm-infected wounds: a review. *J. Surg. Res.* **178**, 330–338 (2012).
363. Abdullahi, A., Amini-Nik, S. & Jeschke, M. G. Animal models in burn research. *Cell. Mol. Life Sci.* **71**, 3241–3255 (2014).
364. Zomer, H. D. & Trentin, A. G. Skin wound healing in humans and mice: Challenges in translational research. *J. Dermatol. Sci.* **90**, 3–12 (2018).
365. Wei, J. C. J. *et al.* Allometric scaling of skin thickness, elasticity, viscoelasticity to mass for micro-medical device translation: from mice, rats, rabbits, pigs to humans. *Sci Rep* **7**, 15885 (2017).
366. Gerdts, V. *et al.* Large animal models for vaccine development and testing. *ILAR J* **56**, 53–62 (2015).
367. de la Fuente-Núñez, C. *et al.* Inhibition of bacterial biofilm formation and swarming motility by

a small synthetic cationic peptide. *Antimicrob. Agents Chemother.* **56**, 2696–2704 (2012).
368. Croyle, M. J. *et al.* Role of epidermal primary cilia in the homeostasis of skin and hair follicles. *Development* **138**, 1675–1685 (2011).
369. Ezratty, E. *et al.* A role for the primary cilium in Notch signaling and epidermal differentiation during skin development. *Cell* **145**, 1129–1141 (2011).
370. Coppé, J.P., Desprez, P.Y., Krtolica, A. & Campisi, J. The Senescence-Associated Secretory Phenotype: The Dark Side of Tumor Suppression. *Annu Rev Pathol* **5**, 99–118 (2010).
371. Tchkonia, T., Zhu, Y., van Deursen, J., Campisi, J. & Kirkland, J. L. Cellular senescence and the senescent secretory phenotype: therapeutic opportunities. *J Clin Invest* **123**, 966–972 (2013).
372. Häcker, G. Apoptosis in infection. *Microbes and Infection* **20**, 552–559 (2018).
373. Celli, J. & Tsolis, R. M. Bacteria, the ER and the Unfolded Protein Response: Friends or Foes? *Nat Rev Microbiol* **13**, 71–82 (2015).
374. Kalliolias, G. D. & Ivashkiv, L. B. TNF biology, pathogenic mechanisms and emerging therapeutic strategies. *Nat Rev Rheumatol* **12**, 49–62 (2016).
375. Kondo, S. & Sauder, D. N. Tumor necrosis factor (TNF) receptor type 1 (p55) is a main mediator for TNF-alpha-induced skin inflammation. *Eur J Immunol* **27**, 1713–1718 (1997).
376. Choi, J. H., Seo, H. S., Lim, S. Y. & Park, K. Cutaneous Immune Defenses Against *Staphylococcus aureus* Infections. *J Lifestyle Med* **4**, 39–46 (2014).
377. Nakatsuji, T. *et al. Staphylococcus aureus* exploits epidermal barrier defects in atopic dermatitis to trigger cytokine expression. *J Invest Dermatol* **136**, 2192–2200 (2016).
378. Watters, C., Fleming, D., Bishop, D. & Rumbaugh, K. P. Host Responses to Biofilm. *Prog Mol Biol Transl Sci* **142**, 193–239 (2016).
379. Lowy, F. D. Is *Staphylococcus aureus* an intracellular pathogen? *Trends in Microbiology* **8**, 341–343 (2000).
380. Haisma, E. M. *et al.* Inflammatory and Antimicrobial Responses to Methicillin-Resistant *Staphylococcus aureus* in an *In Vitro* Wound Infection Model. *PLOS ONE* **8**, e82800 (2013).
381. Pastar, I. *et al.* Interactions of Methicillin Resistant *Staphylococcus aureus* USA300 and *Pseudomonas aeruginosa* in Polymicrobial Wound Infection. *PLOS ONE* **8**, e56846 (2013).
382. Alphonse, N., Dickenson, R. E. & Odendall, C. Interferons: Tug of War Between Bacteria and Their Host. *Front Cell Infect Microbiol* **11**, 624094 (2021).
383. Parker, D. & Prince, A. Type I interferon response to extracellular bacteria in the airway epithelium. *Trends Immunol* **32**, 582–588 (2011).
384. Nakanishi, G., Fujimoto, W. & Arata, J. IRF-1 expression in normal human epidermal keratinocytes. *Arch Dermatol Res* **289**, 415–420 (1997).
385. Mercado, N. *et al.* IRF2 is a master regulator of human keratinocyte stem cell fate. *Nat Commun* **10**, 4676 (2019).
386. Klopfenstein, N. *et al.* SOCS-1 inhibition of type I interferon restrains *Staphylococcus aureus* skin host defense. *PLOS Pathogens* **17**, e1009387 (2021).
387. Watters, C., Fleming, D., Bishop, D. & Rumbaugh, K. P. Chapter Seven - Host Responses to Biofilm. in *Progress in Molecular Biology and Translational Science* (eds. San Francisco, M. & San Francisco, B.) vol. 142 193–239 (Academic Press, 2016).
388. Tankersley, A., Frank, M. B., Bebak, M. & Brennan, R. Early effects of *Staphylococcus aureus* biofilm secreted products on inflammatory responses of human epithelial keratinocytes. *J Inflamm (Lond)* **11**, 17 (2014).
389. Percoco, G. *et al.* Antimicrobial peptides and pro-inflammatory cytokines are differentially regulated across epidermal layers following bacterial stimuli. *Exp. Dermatol.* **22**, 800–806 (2013).
390. Al Kindi, A. *et al. Staphylococcus aureus* Internalized by Skin Keratinocytes Evade Antibiotic

Killing. *Front. Microbiol.* **0**, (2019).
391. Gutierrez Jauregui, R. *et al.* IL-1β Promotes *Staphylococcus aureus* Biofilms on Implants *in vivo*. *Front. Immunol.* **0**, (2019).
392. Stojadinovic, A., Carlson, J. W., Schultz, G. S., Davis, T. A. & Elster, E. A. Topical advances in wound care. *Gynecol. Oncol.* **111**, S70-80 (2008).
393. Zhao, R., Liang, H., Clarke, E., Jackson, C. & Xue, M. Inflammation in Chronic Wounds. *Int J Mol Sci* **17**, (2016).
394. Mezentsev, A., Nikolaev, A. & Bruskin, S. Matrix metalloproteinases and their role in psoriasis. *Gene* **540**, 1–10 (2014).
395. Parnham, A. & Bousfield, C. The influence of matrix metalloproteases and biofilm on chronic wound healing: a discussion. *Br J Community Nurs* **23**, S22–S29 (2018).
396. Josse, J., Laurent, F. & Diot, A. *Staphylococcal* Adhesion and Host Cell Invasion: Fibronectin-Binding and Other Mechanisms. *Front. Microbiol.* **8**, (2017).
397. Larjava, H., Koivisto, L. & Häkkinen, L. Keratinocyte Interactions with Fibronectin during Wound Healing. *Madame Curie Bioscience Database* (Landes Bioscience, 2013).
398. Fowler, T., Johansson, S., Wary, K. K. & Höök, M. Src kinase has a central role in *in vitro* cellular internalization of *Staphylococcus aureus*. *Cell Microbiol* **5**, 417–426 (2003).
399. Agerer, F. *et al.* Cellular invasion by *Staphylococcus aureus* reveals a functional link between focal adhesion kinase and cortactin in integrin-mediated internalisation. *J Cell Sci* **118**, 2189–2200 (2005).
400. Wang, J.H. *et al.* Involvement of phosphatidylinositol 3-Kinase/Akt signaling pathway in β1 integrin-mediated internalization of *Staphylococcus aureus* by alveolar epithelial cells. *J Microbiol* **51**, 644–650 (2013).
401. Shen, Y., Naujokas, M., Park, M. & Ireton, K. InlB-Dependent Internalization of Listeria Is Mediated by the Met Receptor Tyrosine Kinase. *Cell* **103**, 501–510 (2000).
402. Bou-Dargham, M. J., Khamis, Z. I., Cognetta, A. B. & Sang, Q.X. A. The Role of Interleukin-1 in Inflammatory and Malignant Human Skin Diseases and the Rationale for Targeting Interleukin-1 Alpha. *Med Res Rev* **37**, 180–216 (2017).
403. Li, H., Gade, P., Xiao, W. & Kalvakolanu, D. V. The Interferon Signaling Network and Transcription Factor C/EBP-β. *Cell Mol Immunol* **4**, 407–418 (2007).
404. Galien, R. & Garcia, T. Estrogen receptor impairs interleukin-6 expression by preventing protein binding on the NF-kappaB site. *Nucleic Acids Res* **25**, 2424–2429 (1997).
405. Madonna, S., Scarponi, C., Pallotta, S., Cavani, A. & Albanesi, C. Anti-apoptotic effects of suppressor of cytokine signaling 3 and 1 in psoriasis. *Cell Death Dis* **3**, e334–e334 (2012).
406. Duncan, S. A., Baganizi, D. R., Sahu, R., Singh, S. R. & Dennis, V. A. SOCS Proteins as Regulators of Inflammatory Responses Induced by Bacterial Infections: A Review. *Front Microbiol* **8**, 2431 (2017).
407. Stoiber, D., Stockinger, S., Steinlein, P., Kovarik, J. & Decker, T. Listeria monocytogenes modulates macrophage cytokine responses through STAT serine phosphorylation and the induction of suppressor of cytokine signaling 3. *J Immunol* **166**, 466–472 (2001).
408. Rozpędek, W. *et al.* The Role of the PERK/eIF2α/ATF4/CHOP Signaling Pathway in Tumor Progression During Endoplasmic Reticulum Stress. *Curr Mol Med* **16**, 533–544 (2016).
409. Li, W. *et al.* Crosstalk between ER stress, NLRP3 inflammasome, and inflammation. *Appl Microbiol Biotechnol* **104**, 6129–6140 (2020).
410. Chen, X. *et al.* ER Stress Activates the NLRP3 Inflammasome: A Novel Mechanism of Atherosclerosis. *Oxidative Medicine and Cellular Longevity* **2019**, e3462530 (2019).
411. Angel, P., Szabowski, A. & Schorpp-Kistner, M. Function and regulation of AP-1 subunits in skin physiology and pathology. *Oncogene* **20**, 2413–2423 (2001).

412. Sur, I., Ulvmar, M. & Toftgård, R. The Two-Faced NF-κB in the Skin. *International Reviews of Immunology* **27**, 205–223 (2008).
413. Syrovets, T. & Simmet, T. Novel aspects and new roles for the serine protease plasmin. *Cell Mol Life Sci* **61**, 873–885 (2004).
414. Jeong, S. H. *et al.* Egr-1 is a key regulator of IL-17A-induced psoriasin upregulation in psoriasis. *Exp Dermatol* **23**, 890–895 (2014).
415. Sevilla, L. M. & Pérez, P. Glucocorticoids and Glucocorticoid-Induced-Leucine-Zipper (GILZ) in Psoriasis. *Front Immunol* **10**, 2220 (2019).
416. Hvid, H., Teige, I., Kvist, P. H., Svensson, L. & Kemp, K. TPA induction leads to a Th17-like response in transgenic K14/VEGF mice: a novel *in vivo* screening model of psoriasis. *Int. Immunol.* **20**, 1097–1106 (2008).
417. Smits, J. P. H. *et al.* Immortalized N/TERT keratinocytes as an alternative cell source in 3D human epidermal models. *Sci Rep* **7**, 11838 (2017).
418. van den Bogaard, E. H. *et al.* Crosstalk between keratinocytes and T cells in a 3D microenvironment: a model to study inflammatory skin diseases. *J. Invest. Dermatol.* **134**, 719–727 (2014).
419. Engelhart, K., El Hindi, T., Biesalski, H.K. & Pfitzner, I. *In vitro* reproduction of clinical hallmarks of eczematous dermatitis in organotypic skin models. *Arch. Dermatol. Res.* **297**, 1–9 (2005).
420. Bracken, M. B. Why animal studies are often poor predictors of human reactions to exposure. *J R Soc Med* **102**, 120–122 (2009).

Appendices

A.1 Skin Permeability Assays

To investigate how long the N/TERT epidermal skin could endure biofilm growth, luminescence signals of skin biofilm were imaged using the ChemiDoc Imaging System (Bio-Rad) every 24 hours after infected skin with $1x10^6$ CFU MRSA-*lux* or PAO1-*lux*. Luminescence detected in the culture medium underneath the skin indicating that the skin barrier had been breached. To quantify skin permeability, skin samples with or without biofilm were rinsed once on both the apical and basolateral side of the filter insert in phenol red free DMEM/F12 medium (ThermoFisher Scientific). The medium was then decanted and the filter inserts were transferred to a fresh well in a sterile 12-well plate. One milliliter of phenol free DMEM/F12 medium was added to the apical and basolateral side of the filter insert. TEER across the skin layer was measured using a Millicell ERS Volt-Ohm meter (MilliporeSigma). The resistance across an empty filter membrane was subtracted from all sample measurements and TEER values (Ωcm^2) were calculated assuming a cell culture area corresponding to a filter area of 1.131 cm^2. Following TEER measurements, fluorescein isothiocyanate (FITC)-dextran 4000 (Sigma-Aldrich) was added to the medium on the apical side of the filter insert to a concentration of 500 µg/ml. The medium on the basolateral side of the filter insert was sampled (100 µl) at time intervals of 0, 10, 20, 30 and 60 minutes, replacing the equivalent volume removed with fresh medium at each time point. Samples were transferred to a black walled plate and FITC fluorescence was measured on a Synergy 2 Multi-Mode Microplate reader (BioTek) using an excitation wavelength of 487 nm and an emission wavelength of 528 nm. Data was recorded using optics at the top of the microplate at a read height of 7 mm. The concentration of FITC-dextran in each sample was determined based on a FITC-dextran standard curve that was prepared in parallel. All permeability assays were performed in duplicate.

A.2 Appendix Table

Table A1. Estimation of the changes in cell populations in response to IDR-1002 treatment in PMA-inflamed ear tissue.

Based on the RNA-Seq analysis performed on the ear tissue from 15 mice, 6 hours post-treatment (as reported in the main manuscript), a read count table was generated using HTSeq-count v0.6.1p1. The changes in immune cell populations were estimated by calculating the geometric mean of the fold change in cell surface markers Reads Per Kilobase of transcript per Million mapped reads (RPKM) for each cell type. Statistical analysis was performed using the One-sample t-test. Significantly altered values are indicated in bold ($P \leq 0.05$).

Cell type	Cell marker	RPKM ± SD		Average RPKM fold change (Range)
		PMA + 0.6mg IDR-1002	PMA	PMA + 0.6mg IDR-1002 vs. PMA
Macrophage/ Monocyte	CD11b	2.5 ± 0.5	5.8 ± 1.2	**0.6 (0.3-0.9)**
	CD14	77.4 ± 16.1	389.5 ± 78.6	
	CD64	3.1 ± 1.2	7.4 ± 5.0	
	CD68	30.8 ± 2.2	47.6 ± 4.6	
	CD115	29.2 ± 4.3	29.4 ± 5.5	
	CD163	16.3 ± 4.1	23.8 ± 6.5	
	CD204	11.6 ± 2.2	16.6 ± 4.4	
	F4/80	5.3 ± 0.7	7.1 ± 2.3	
Dendritic cell	CD11c	5.0 ± 0.8	11.3 ± 2.1	**0.6 (0.4-0.7)**
	CD83	19.5 ± 4.5	27.6 ± 0.7	
	CD207	44.2 ± 7.2	75.1 ± 21.1	
Neutrophil	CD11b	2.5 ± 0.5	5.8 ± 1.2	**0.3 (0.2-0.5)**
	CD114	24.6 ± 7.0	113.5 ± 32.1	
	CD177	1.4 ± 0.7	5.4 ± 4.2	
	Ly6c	9.3 ± 1.4	17.3 ± 6.3	
	Ly6g	0.3 ± 0.3	1.4 ± 1.0	
Eosinophil/ Basophil	CD123	4.5 ± 0.6	5.9 ± 2.3	1.0 (0.8-1.2)
	CD125	0.2 ± 0.1	0.2 ± 0.2	
	CD203c	1.2 ± 0.2	0.9 ± 0.1	
	CD294	0.1 ± 0.1	0.1 ± 0.1	
Mast cell	CD34	61.0 ± 7.9	45.8 ± 4.2	**1.4 (1.2-1.6)**
	CD117	5.3 ± 0.7	3.1 ± 1.0	
	CD203c	1.2 ± 0.2	0.9 ± 0.1	
	Fcer1a	1.8 ± 0.3	1.5 ± 0.2	
Natural killer cell	CD94	2.2 ± 1.0	3.2 ± 1.9	**0.5 (0.3-0.8)**
	CD244	3.4 ± 0.6	8.4 ± 0.9	
	CD314	0.9 ± 0.2	1.1 ± 0.5	
	CD335	0.4 ± 0.4	1.1 ± 0.7	
B cell	CD19	0.3 ± 0.2	0.1 ± 0.0	1.2 (0.6-2.3)
	CD20	> 0.1	> 0.1	
	CD22	0 .1 ± 0.1	0.1 ± 0.1	
	CD45R	15.2 ± 2.7	36.3 ± 3.7	
	CD267	1.0 ± 0.1	1.4 ± 0.5	

	CD268	0.3 ± 0.1	0.2 ± 0.2	
	CD269	0.1± 0.2	0.1 ± 0.1	
T cell	CD3d	1.4 ± 0.4	2.3 ± 0.1	0.5 (0.2-1.1)
	CD3e	3.5 ± 0.8	3.9 ± 1.1	
	CD3g	6.5 ± 2.6	6.0 ± 3.7	
	CD4	1.3 ± 0.3	1.5 ± 0.5	
	CD8a	0.0 ± 0.0	0.1 ± 0.1	
	CD8b	0.0 ± 0.0	0.1 ± 0.1	
Epithelial cell/ Fibroblast	CD111	37.1 ± 4.9	48.1 ± 1.5	0.9 (0.7-1.1)
	CD326	149.0 ± 10.1	202.7 ± 10.3	
	CD331	27.8 ± 2.2	25.4 ± 2.8	

A.3 Appendix Figures

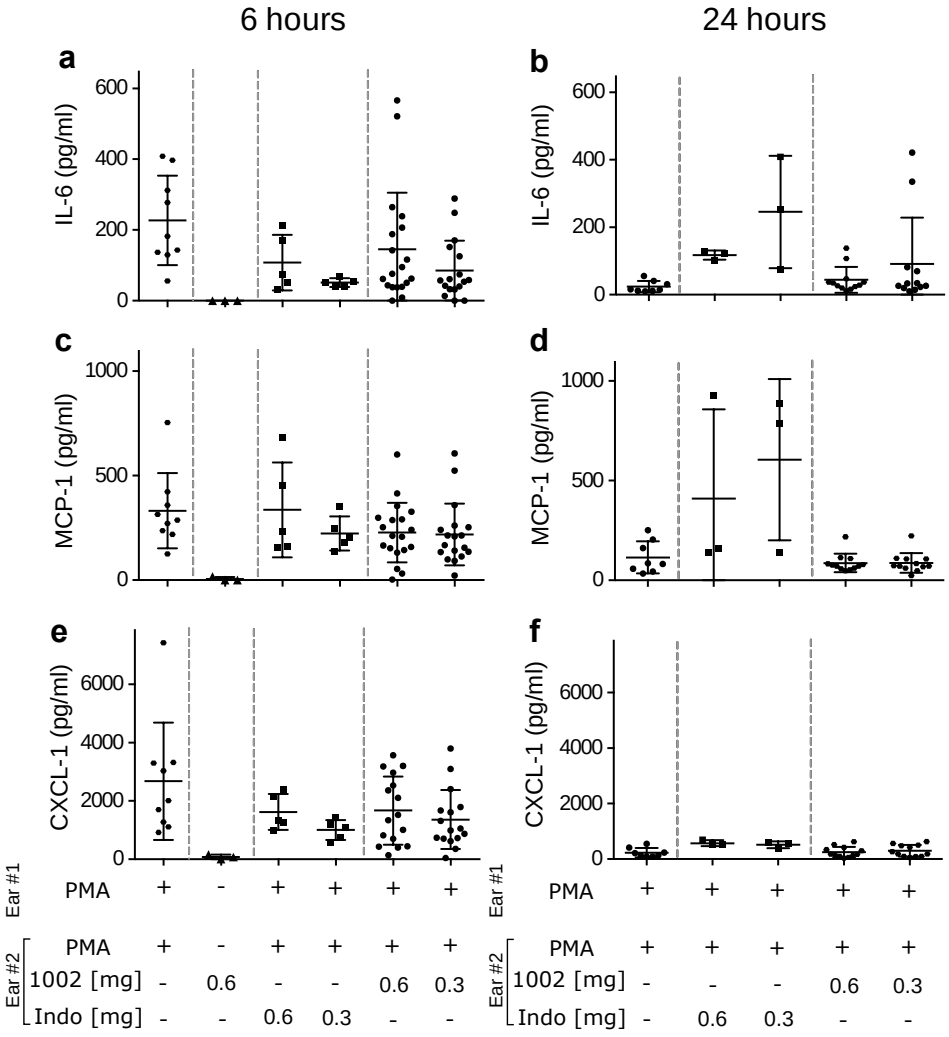

Figure A1. IDR-1002 did not significantly alter serum cytokine and chemokine levels in the PMA-treated mice.

The ears of CD-1 mice were treated topically with 20 μl of 125 μg/ml PMA. Either 0.6 mg/ear or 0.3 mg/ear IDR-1002 was administered onto one ear of each mouse immediately after PMA treatment. Indomethacin (Indo) at a dose of 0.6 mg/ear or 0.3 mg/ear, was used as the positive anti-inflammatory control and was also applied topically onto one ear of each mouse post PMA treatment. The contralateral ears were given the same volume of the vehicle/solvent. Mice were euthanized 6 hours (**a, c, e**) or 24 hours (**b, d, f**) post-PMA treatment and blood was collected by cardiac puncture. The production of serum IL-6 (**a**-**b**), MCP-1 (**c**-**d**) and CXCL-1 (**e**-**f**) was quantified by ELISA.

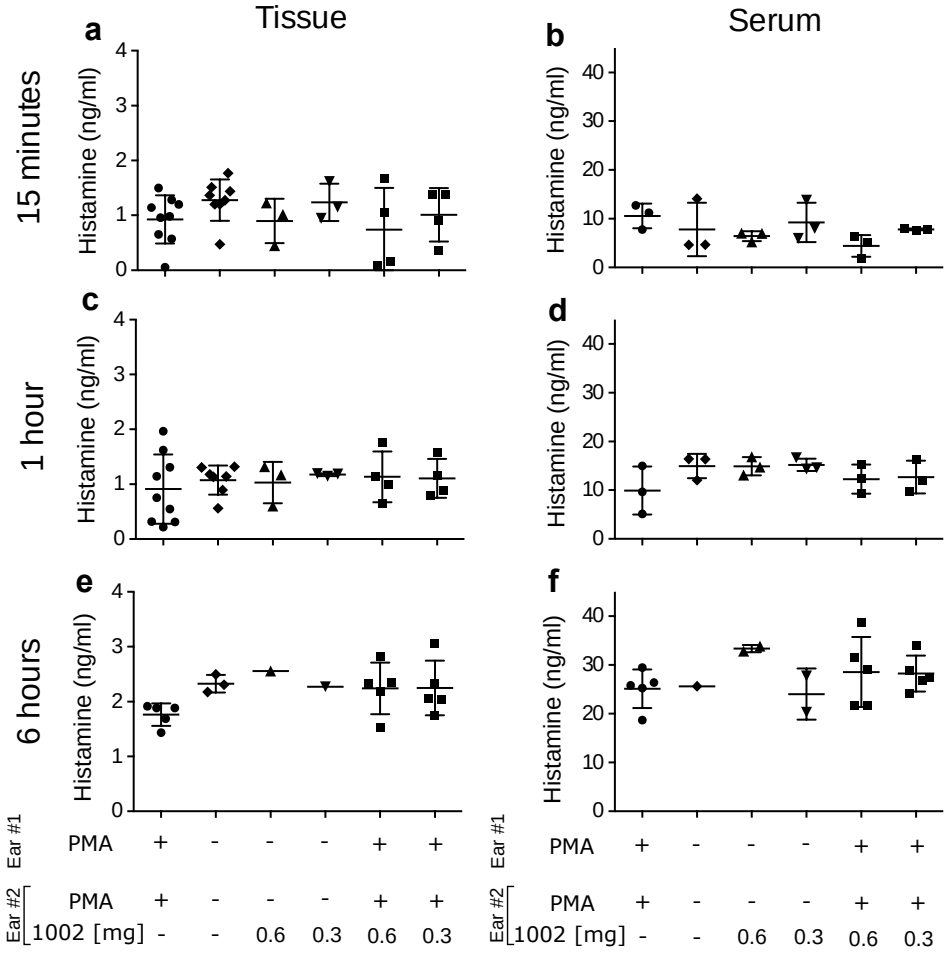

Figure A2. IDR-1002 did not significantly alter tissue or serum histamine concentrations in the PMA-treated mice.

Ears of CD-1 mice were treated topically with 20 μl of 125 μg/ml PMA. Either 0.6 mg/ear or 0.3 mg/ear IDR-1002 was administered onto one ear of each mouse immediately after PMA treatment. The contralateral ear was given the same volume of solvent (20 μl of 50% ethanol). Mice were euthanized 15 minutes (**a, b**), 1 hour (**c, d**) or 6 hours (**e, f**) post-PMA treatment. The production of histamine in ear tissue biopsy (**a, c, e**) and serum (**b, d, f**) was quantified by ELISA.

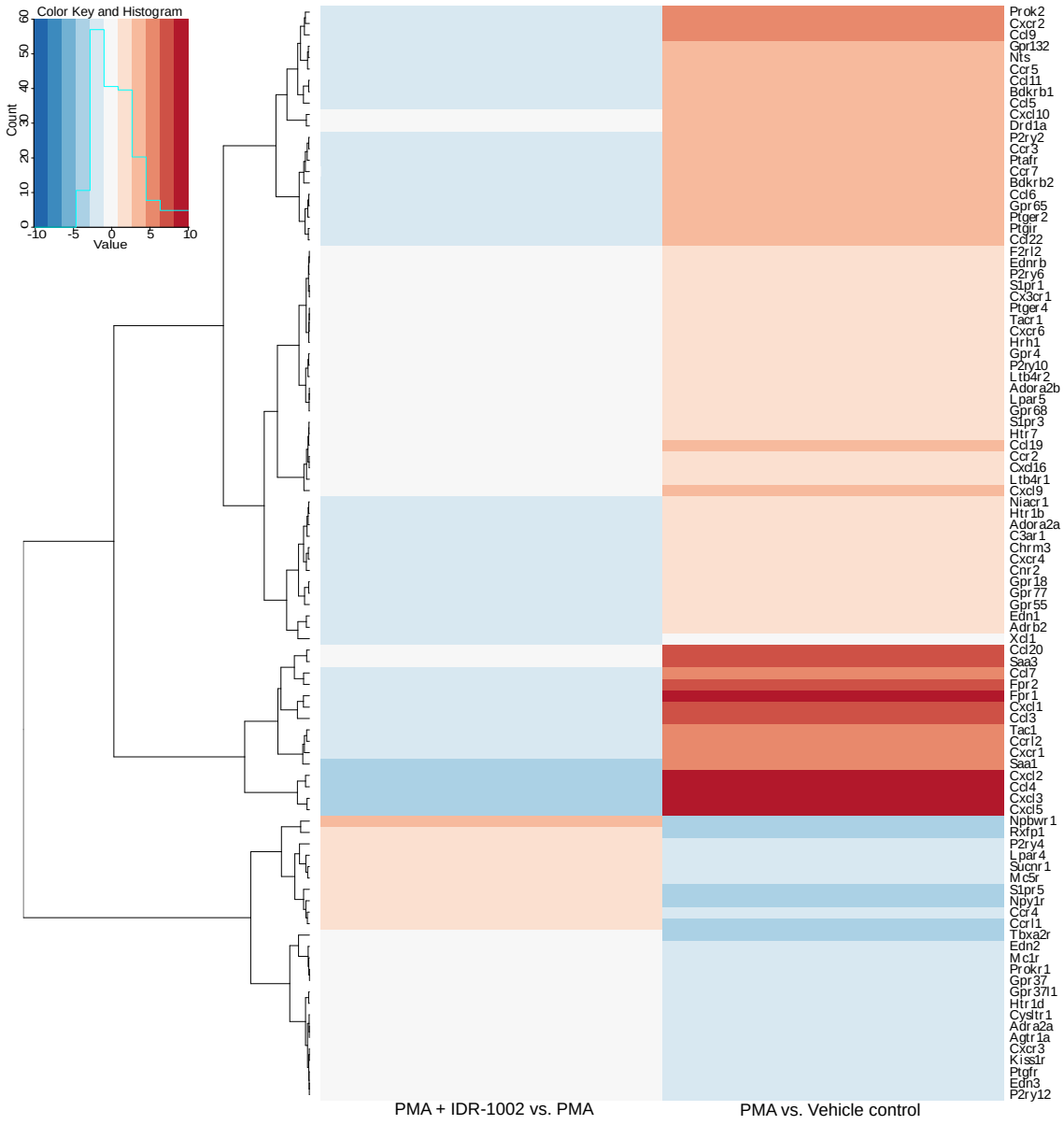

Figure A3. Heatmap of differentially expressed genes from the G-protein coupled receptor (class A/1 rhodopsin-like) pathway in response to PMA-induced inflammation with or without IDR-1002 treatment.

Genes was downloaded from InnateDB. The heatmap of differentially expressed genes (≥±2-fold change, adjusted p-value ≤0.05) was generated using R v.3.3.3, qplot package. Red indicates upregulation and blue indicates downregulation.

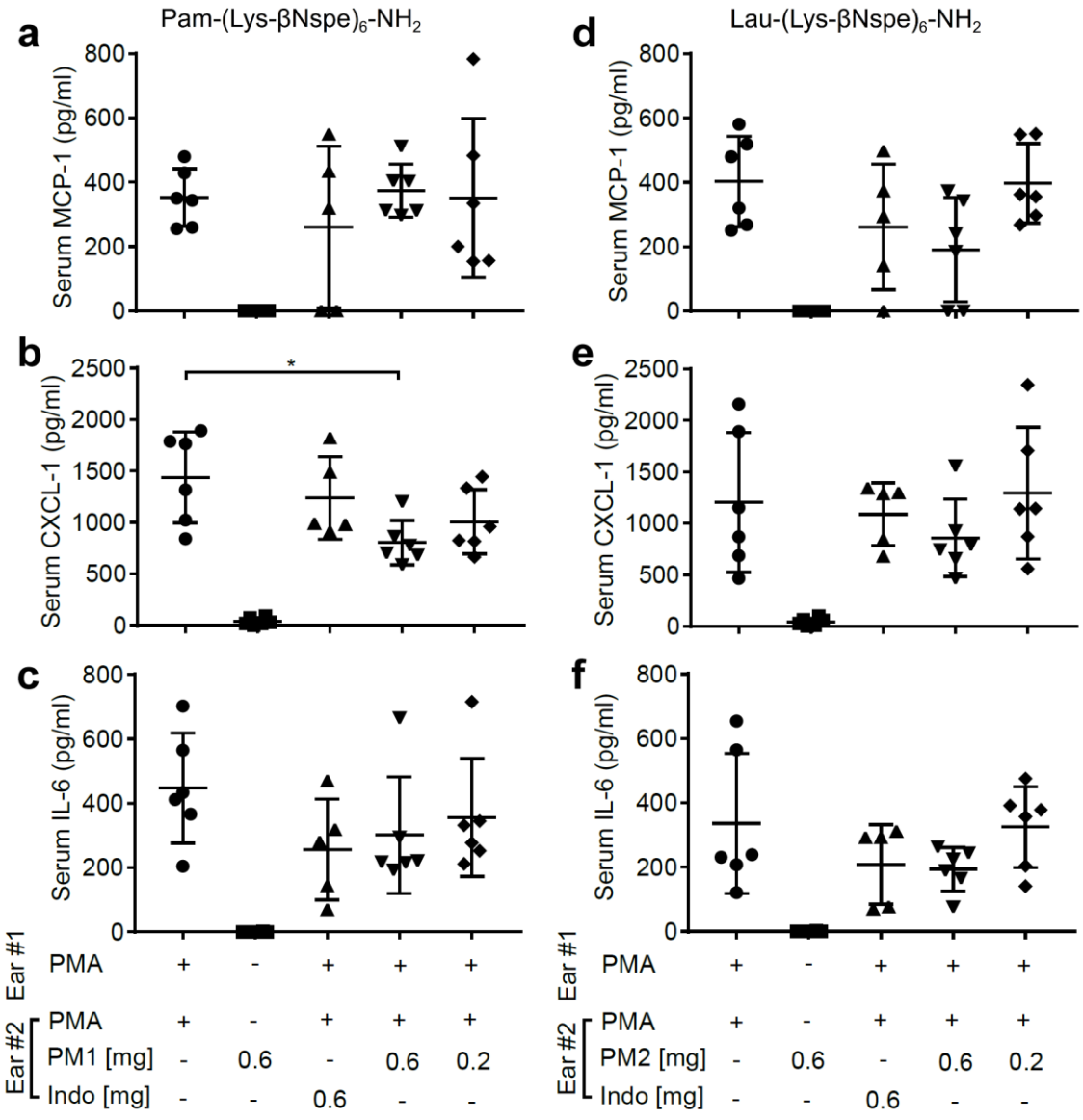

Figure A4. Peptidomimetics PM1 and PM2 only had minor effects on serum chemokine and cytokine levels.

PMA (20 µl of 125 µg/ml solution) was applied topically onto CD-1 female mice ears. Indomethacin (Indo) or peptidomimetic Pam-(Lys-βNspe)$_6$-NH$_2$ (PM1; **a-c**) or Lau-(Lys-βNspe)$_6$-NH$_2$ (PM2; **d-f**) at 0.6 or 0.2 mg/ear was given topically to one ear of each mouse after PMA being absorbed. The contralateral ear was given 20 µL of vehicle. Mice were euthanized 6 hours post-treatment and the levels of serum MCP-1, CXCL-1 and IL-6 were quantified by ELISA. Five to six biological replicates in four independent experiments were included per treatment group. Error bars indicate Mean ± SD. Statistics: *p ≤ 0.05, **p ≤ 0.01, ***p ≤ 0.001, ****p ≤ 0.0001, Student's unpaired *t*-test.

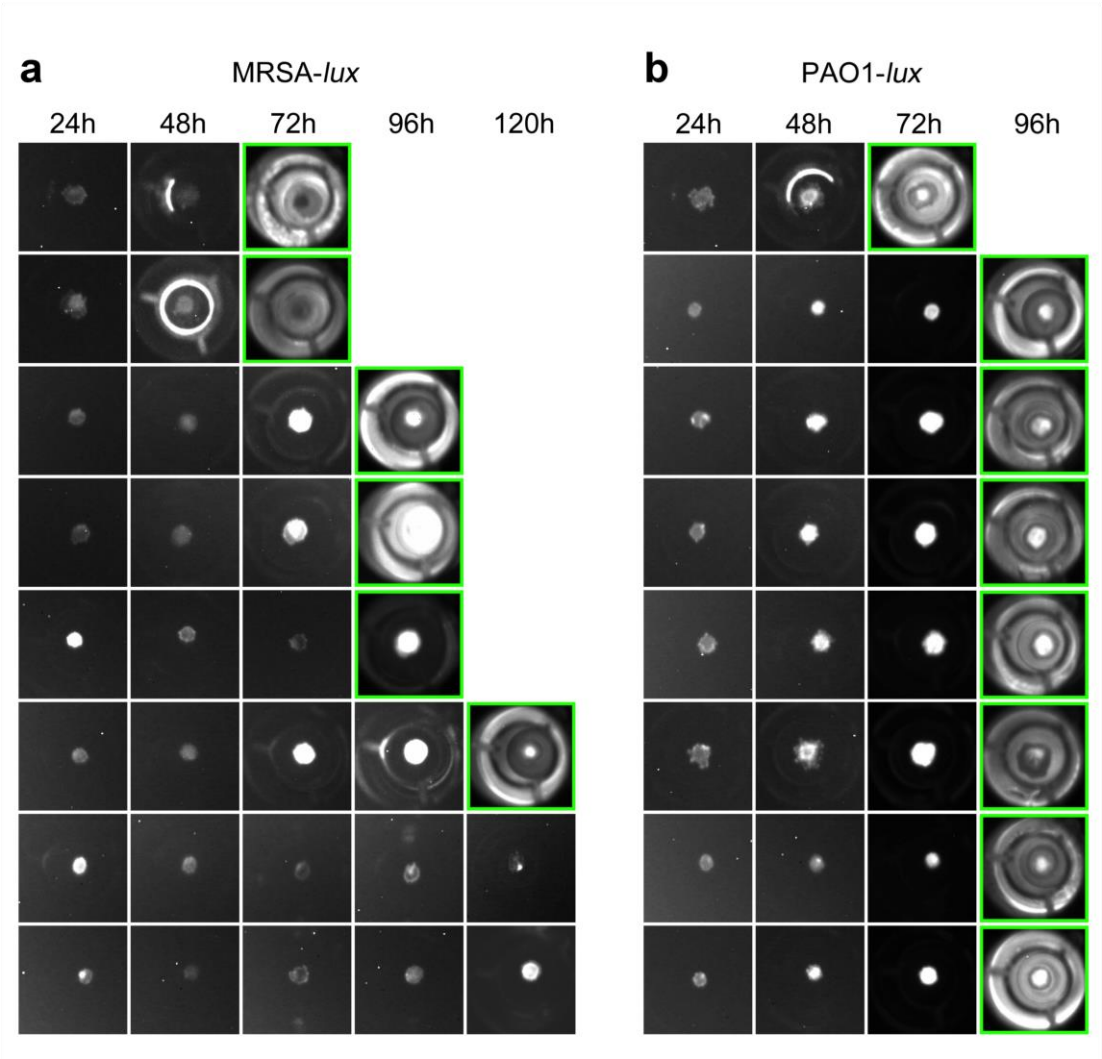

Figure A5. The N/TERT skin could endure MRSA and PAO1 biofilm for about 3 days.
MRSA-*lux* (**a**) or PAO1-*lux* (**b**) were seeded on top of skin and the resulting biofilms were imaged every 24 hours after seeding (n=8). Luminescence at the center of the filter insert indicated confined biofilm on the surface of the skin. In some cases, luminescence signals were detected in the growth medium in the wells below the skin filter inserts (labeled with green outline), which indicated that bacteria penetrated through the skin barrier.

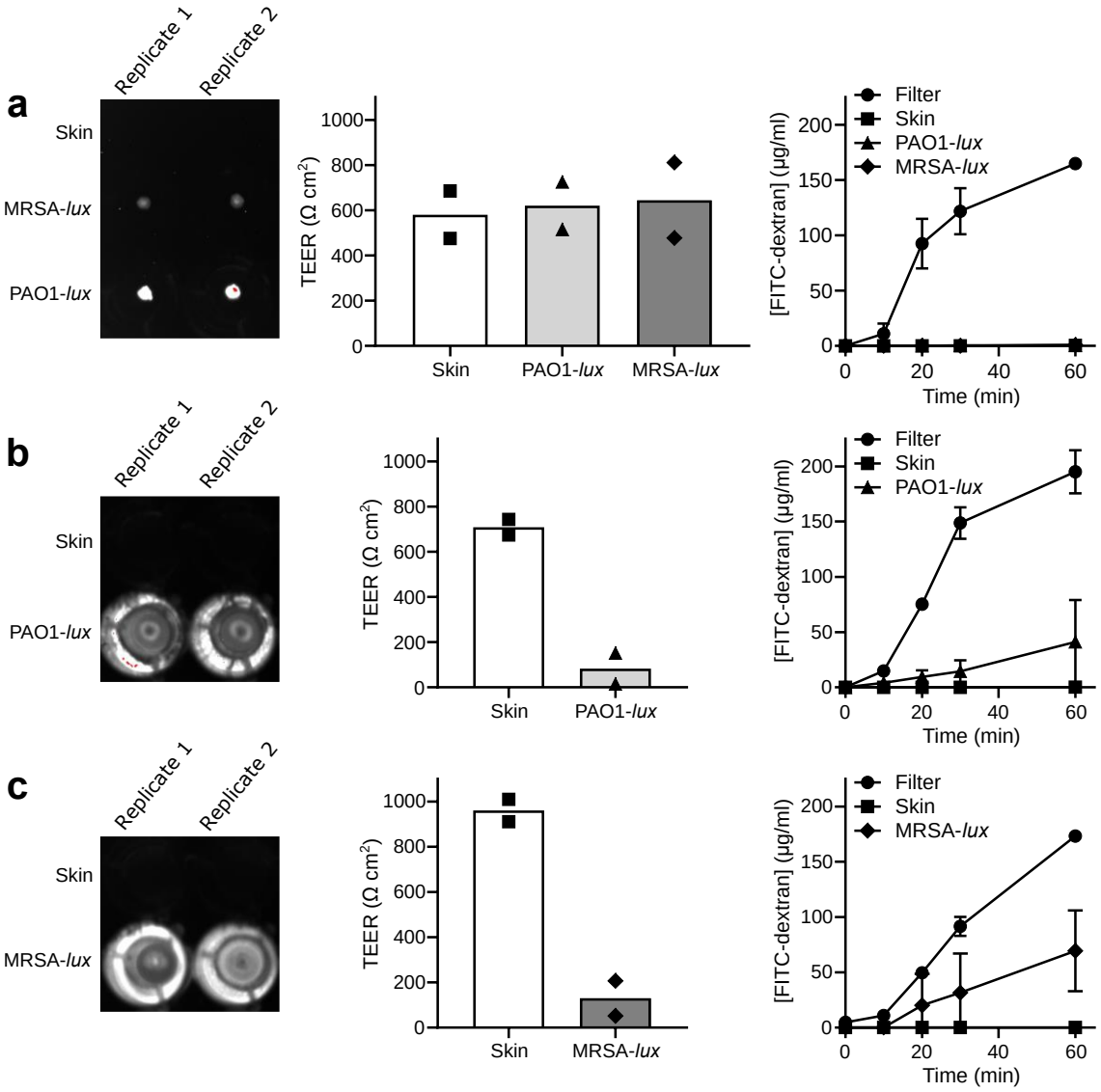

Figure A6. Permeability of skin barrier in response to biofilm infection by PAO1-*lux* and MRSA-*lux*.

Twenty-four hours post-infection (**a**), both MRSA-*lux* and PAO1-*lux* biofilms formed on the skin surface (left panel) but no large differences in TEER measurements (middle panel) or FITC-dextran permeability (right panel) were observed between samples, demonstrating that the skin barrier was intact in all samples. PAO1-*lux* bacteria penetrated through the skin after 48-hrs (**b**) resulting in reduced TEER values and increased permeability to FITC-dextran compared to uninfected skin samples. MRSA-*lux* bacteria penetrated the skin after 96 hours (**c**), again resulting in reduced TEER and increased FITC-dextran permeability compared to uninfected skin.

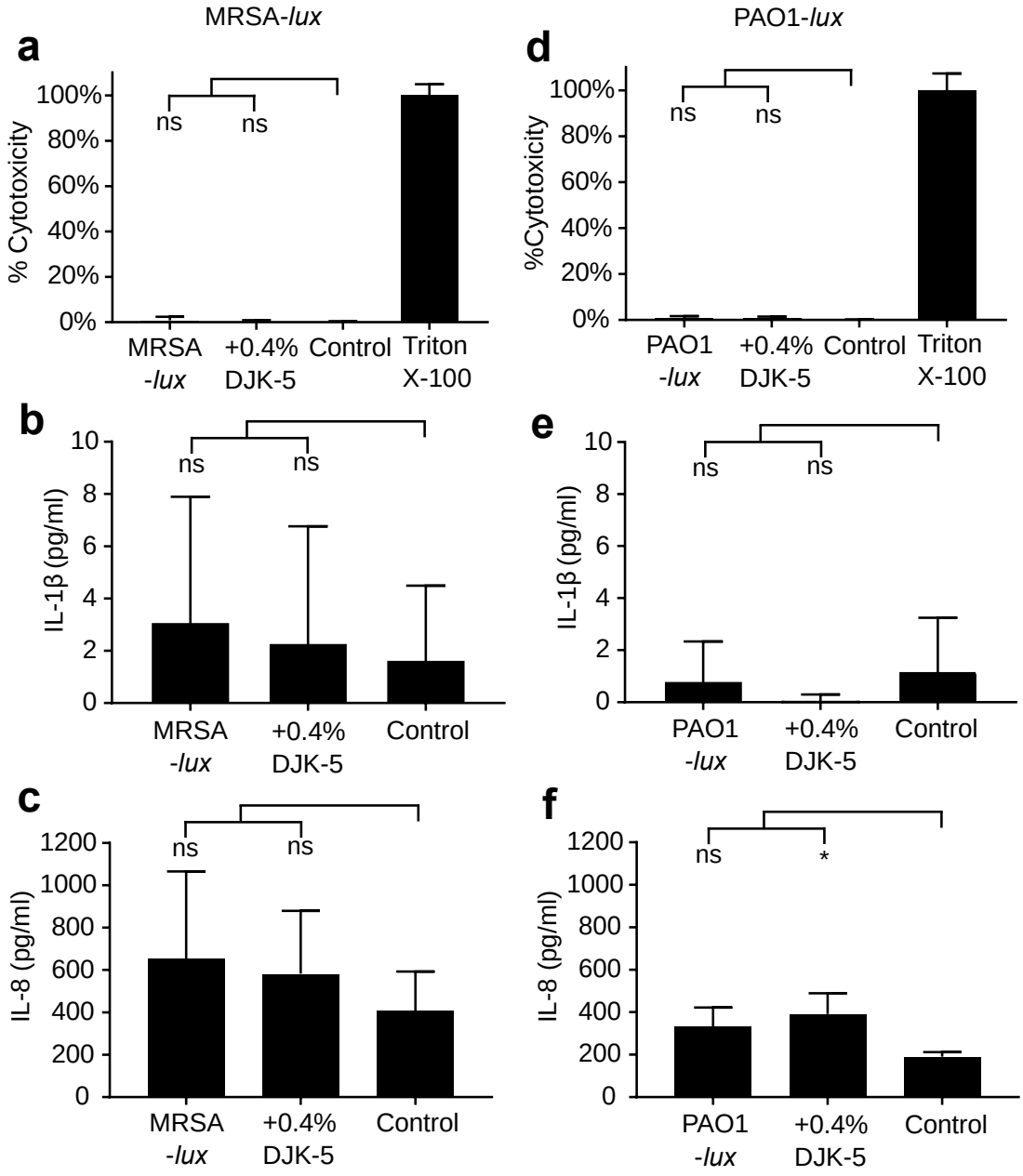

Figure A7. N/TERT skin with 3-day MRSA and PAO1 biofilm had no cytotoxicity and basal level cytokine production.

MRSA-*lux* (**a, b, c**) and PAO1-*lux* (**d, e, f**) biofilm were established on top of epidermal skin for 3 days followed by 4-hour 0.4% DJK-5 peptide treatment. Culture supernatants below the skin were used for measuring cytotoxicity by the Lactate dehydrogenase assay. Untreated skin samples and skin samples treated with 5% Triton X-100 were used as negative (0% toxicity) and positive (100% toxicity) control, respectively (**a, d**). The amount of IL-1β (**b, e**) and IL-8 (**c, f**) in the supernatant was quantified by ELISA. Error bars indicate mean with SD (n=6). Statistical significance was performed using the One-way ANOVA, Dunnett's multiple comparisons test (* $p \leq 0.05$).

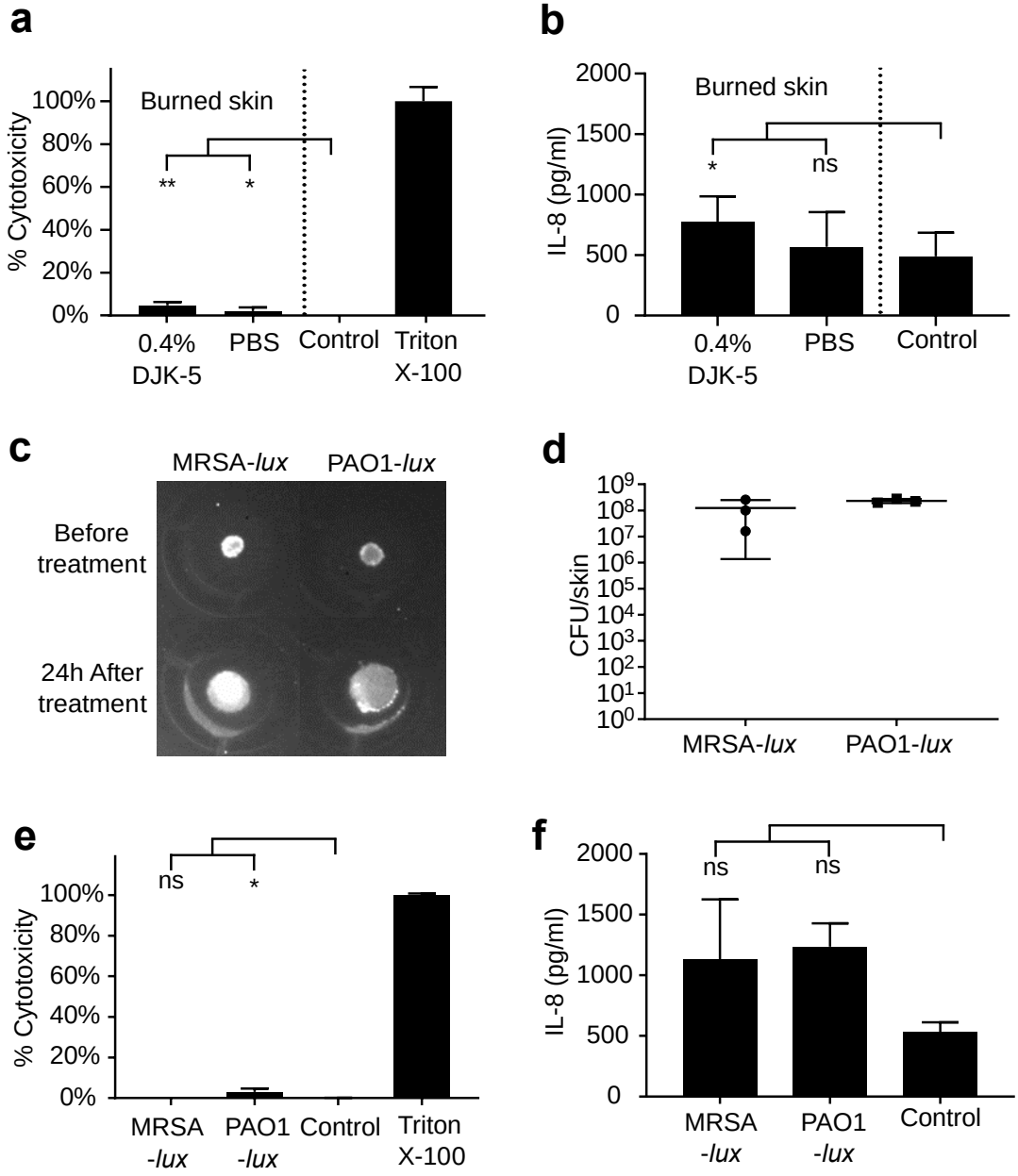

Figure A8. Burned skin without infection and 2-day biofilm on skin without thermal damage had minimal changes in cytotoxicity and cytokine production compared to skin control without infection and thermal damage.

Thermally damaged epidermal skin was mock infected with PBS for 24 hours, followed by 24 hours treatment with 0.4% DJK-5 or water (**a, b**). The cytotoxicity (**a**) and IL-8 production (**b**) from culture supernatant beneath skin was determined. One day pre-established MRSA-*lux* and PAO1-*lux* skin biofilm was treated with vehicle control-water for 24 hours, changes in luminescence signal (**c**), bacteria load (**d**), skin cytotoxicity (**e**) and IL-8 level (**f**) was quantified. Error bars indicate mean with SD (n=3). One-way ANOVA, Dunnett's multiple comparisons test (* $P \leq 0.05$; ** $P \leq 0.01$).